Quantenphasenübergänge: Grüneisen Parameter, dimensionaler Crossover und gekoppelte Störstellen

Zur Erlangung des akademischen Grades eines
DOKTORS DER NATURWISSENSCHAFTEN
von der Fakultät für Physik der
Universität Karlsruhe (TH)

vorgelegte

DISSERTATION

von

Dipl.-Phys. Markus Garst

aus Ludwigshafen am Rhein

Tag der mündlichen Prüfung:	12.12.2003
Hauptreferent:	Prof. Dr. P. Wölfle
Korreferent:	Prof. Dr. M. Vojta
Betreuer:	Dr. A. Rosch

Aspects of Quantum Phase Transitions: Grüneisen Parameter, Dimensional Crossover and Coupled Impurities

Zur Erlangung des akademischen Grades eines
DOKTORS DER NATURWISSENSCHAFTEN
von der Fakultät für Physik der
Universität Karlsruhe (TH)

vorgelegte

DISSERTATION

von

Dipl.-Phys. Markus Garst

aus Ludwigshafen am Rhein

Tag der mündlichen Prüfung:	12.12.2003
Hauptreferent:	Prof. Dr. P. Wölfle
Korreferent:	Prof. Dr. M. Vojta
Betreuer:	Dr. A. Rosch

Markus Garst

Addresse	Oberwaldstr. 16 76227 Karlsruhe Tel.: 0721-4908136
e-mail	markus@tkm.physik.uni-karlsruhe.de
Geburtsdatum	15. September 1973
Familienstand	ledig
Staatsangehörigkeit	deutsch

Ausbildung

1984 – 1993	Besuch des Theodor–Heuss Gymnasiums, Ludwigshafen am Rhein
1994 – 1999	Physikstudium an der Universität Karlsruhe (TH)
1999 – 2000	Diplomarbeit am Institut für Theorie der Kondensierten Materie von Prof. P. Wölfle unter Betreuung von Prof. T. Kopp mit dem Titel: "Mesoskopische Fluktuationen des Suprastromes in diffusiven Punktkontakten"
Februar 2000	Diplom in Physik
ab September 2000	Dissertation am Institut für Theorie der Kondensierten Materie von Prof. P. Wölfle unter der Betreuung von Dr. A. Rosch

Publikationen

- *Quantum phase transition of Ising–coupled Kondo impurities*
  M. Garst, S. Kehrein, T. Pruschke, A. Rosch, and M. Vojta, [cond-mat/0310222].
- *Universally diverging Grüneisen parameter and magnetocaloric effect close to quantum critical points*, L. Zhu, M. Garst, A. Rosch, Q. Si, Phys. Rev. Lett. **91**, 066404 (2003), [cond-mat/0212335]
- *Transport in a classical model of a one-dimensional Mott insulator: Influence of conservation laws*, M. Garst and A. Rosch, Europhys. Lett. **55**, 66 (2001), [cond-mat/0102109]
- *Random-Matrix Theory: Distribution of Mesoscopic Supercurrents through a Chaotic Cavity*, M. Garst and T. Kopp, J. of Low Temp. Phys. **126**, 1305 (2002), [cond-mat/0109520]

Zusammenfassung

Viele noch unerklärte Phänomene im Bereich der korrelierten Elektronensysteme werden mit den außergewöhnlichen Eigenschaften von Quantenphasenübergänge [1, 2] in Verbindung gebracht, dass heißt mit Phasenübergängen, die am absoluten Temperaturnullpunkt unter Variation eines äußeren Kontrollparameters wie z.B. des Druckes stattfinden. Das theoretische Verständnis von solchen Phasenübergängen und deren Auswirkung auf physikalische Eigenschaften bei endlichen Temperaturen sowie deren eingehenden experimentellen Untersuchung steht erst am Anfang und ist eines der aufregendsten Forschungsbereiche der heutigen Physik.

Diese Arbeit besteht aus zwei Teilen, die sich jeweils mit solchen quantenkritischen Phänomenen beschäftigen. Im ersten Teil wird vorwiegend der Quantenphasenübergang betrachtet, der mit einer magnetischen Instabilität in itineranten Elektronensystemen verbunden ist. Im zweiten Teil steht die Physik von gekoppelten Störstellen im Mittelpunkt. Im folgenden soll ein kurzer Überblick über die einzelnen Kapitel dieser Arbeit gegeben werden.

Im Vergleich zu den klassischen Phasenübergängen, die bei einer endlichen Temperatur stattfinden, sind Quantenphasenübergänge streng genommen experimentell nicht zugänglich, da sie nur am absoluten Temperaturnullpunkt vorkommen. Der Experimentator ist deswegen darauf beschränkt, deren Einfluss auf die physikalischen Eigenschaften bei endlichen Temperaturen zu analysieren. Physikalische Größen wie z.B. die spezifische Wärme, deren Divergenz an einem klassischen Phasenübergang üblicherweise wichtige Folgerungen auf dessen Universalitätsklasse ermöglichen, sind jedoch an einem Quantenphasenübergang nicht vergleichbar singulär. In Kapitel 1 wird erläutert, dass der Grüneisen Parameter, das Verhältnis zwischen thermischer Ausdehnung und spezifischer Wärme, an einem durch Druck kontrollierten Quantenphasenübergang notwendigerweise divergiert und deshalb eine wichtiges experimentelles Werkzeug für die Analyse von quantenkritischen Phänomenen darstellt vergleichbar mit der Rolle der spezifischen Wärme an einem klassischen Übergang. Durch eine Skalenanalyse wird gezeigt, dass die Divergenz des Grüneisen Parameters durch den kritischen Exponenten ν der Korrelationslänge charakterisiert wird. Erstaunlicherweise wird der Vorfaktor dieser Divergenz ausschließlich durch eine Kombination von kritischen Exponenten bestimmt und ist in diesem Sinne universell. Diese Universalität hat ihren Ursprung tatsächlich in der verschwindenden Restentropie bei Temperatur Null, d.h. im dritten Hauptsatz der Thermodynamik. Weiterhin wird darauf hingewießen, dass der magnetokalorische Effekt die analoge Größe zum Grüneisen Parameter ist im Falle eines durch das Magnetfeld kontrollierten Quantenphasenübergangs. Die Ergebnisse von Kapitel 1 sind in Ref. [3] publiziert.

Um die Vorhersagen der Skalenanalyse in einem bestimmten Modell zu überprüfen, wird in Kapitel 2 zunächst eine Theorie von J. A. Hertz [4] vorgestellt, die in einfachster Weise die magnetische Instabilität in itineranten Elektronensystemen bei Temperatur Null beschreibt. Weiterhin wird in die Renormierungsgruppe (RG) eingeführt, die A. J. Millis [5] auf das Hertz Modell angewendet hat, um dessen Temperaturverhalten zu untersuchen. In Kapitel

3 werden wir schließlich diese RG dazu verwenden, um zusätzlich zur spezifischen Wärme, die schon in den Refs. [5, 6] berechnet wurden, auch die thermische Ausdehnung und den Grüneisen Parameter des Hertz Modells zu bestimmen. Wir finden, dass die Korrekturen zur Skalenanalyse aus Kapitel 1 höchstens logarithmisch sind, und wir identifizieren deren Ursache.

In Kapitel 4 wird eine anisotrope Version des Hertz Modells betrachtet, um den theoretisch erwarteten dimensionalen Übergang in dem Schwerfermion–System $CeCu_{6-x}Au_x$ zu beschreiben. Um dessen außergewöhnliches thermodynamisches Verhalten zu erklären, wurde von A. Rosch [7] vorgeschlagen, dass zweidimensionale Spinfluktuationen das kritische Verhalten von $CeCu_{6-x}Au_x$ dominieren. Diese wurden dann in Neutronenstreuexperimenten [8] auch tatsächlich identifiziert. Die magnetische Ordnung, die unterhalb der Néel Temperatur beobachtet wird, hat jedoch dreidimensionalen Charakter, so dass die zweidimensionalen Spinfluktuationen nur ein Vorläufer zur tatsächlichen magnetischen Ordnung darstellen. Nahe des Phasenübergangs wird deswegen ein Crossover von zwei- zu dreidimensionalem kritischen Verhalten erwartet, den wir durch die anisotrope Hertz Theorie modellieren und verstehen wollen. Experimentell wurde der dimensionale Crossover im kritischen Verhalten jedoch noch nicht entdeckt weder in den Neutronenstreudaten noch in thermodynamischen Größen. Unsere theoretische Analyse sagt voraus, dass die Signaturen dieses Crossovers besonders ausgeprägt sind in der Temperaturabhängigkeit der thermodynamischen Ausdehnung. Diese Größe ist demnach gut geeignet, um den Crossover experimentell zu detektieren. Weiterhin bestimmen wir sämtliche Übergangslinien im Phasendiagramm. Dazu werden drei verschiedene Methoden verwendet. Die erste Methode ist eine Modifikation der Renormierungsgruppenmethode von A. J. Millis. Um den dimensionalen Crossover zu beschreiben, wird dabei der RG Fluss in zwei Phasen unterteilt. In der ersten Phase wird dieser Fluss von dem zweidimensionalen Fixpunkt und in der zweiten Phase von dem dreidimensionalen Fixpunkt dominiert. Der Parameter, der die Abweichung von dem isotropen Modell kontrolliert, ist während der ersten RG Phase eine relevante Größe im RG Sinne, was zu einem zusätzlichen singulären Beitrag in der thermischen Ausdehnung führt. Die zweite Methode, mit der das anisotrope Hertz Modell undersucht wird, ist bekannt unter dimensionaler Reduktion und besteht aus der Herleitung einer effektiven Theorie für die Matsubara Nullmode. Die dritte Methode schließlich ist eine Analyse, die im Limes $N \to \infty$ exakt wird, wobei N die Anzahl der Komponenten des Ordnungsparameters ist.

Im zweiten Teil der Arbeit beschäftigen wir uns mit der Physik von gekoppelten Störstellen. Es wird eine Variante des zwei-Störstellen Kondo Problems betrachtet, das in einfachster Weise den Wettbewerb zwischen Abschirmung der lokalen Momente durch den Kondo Effekt und magnetischer Ordnung beschreibt. Man geht davon aus, dass der Wettstreit zwischen diesen zwei Mechanismen den magnetischen Phasenübergang in den Schwerfermion-Systemen dominiert. Die meisten Studien haben sich auf das zwei-Störstellen Kondo Modell mit einer SU(2) symmetrischen Austauschwechselwirkung zwischen den Störstellen konzentriert. In dieser Arbeit soll jedoch eine anisotrope Kopplung zwischen den magnetischen Momenten im Mittelpunkt stehen. Dies ist unter anderem motiviert durch die anhaltende Kontroverse über die Rolle von Unordnung in der Nähe eines magnetischen Übergangs, worauf in Kapitel 5 eingegangen wird. Wir schlagen vor, dass dieses Modell die Dynamik von kleinsten magnetischen Clustern beschreibt, die generisch in der Nähe eines Quantenphasenübergangs in einem stark anisotropen itineranten Magnet mit Unordnung entstehen.

In Kapitel 6 wird gezeigt, dass das effektive Niederenergiemodell des stark anisotropen zwei-Störstellen Kondo Problems gegeben ist durch ein Zweikanal–Kondo Modell. Dies ist

deshalb so von Interesse, weil das Zweikanal–Kondo Modell zu einer der Universalitätsklassen gehört, die sich durch eine lokale Nicht-Fermiflüssigkeit auszeichnen. Sie bieten sich daher als alternativen Erklärungsversuch für das ungewöhnliche Verhalten in den Schwerfermion Systemen wie etwa $CeCu_{6-x}Au_x$ an. Wie auch in vielen anderen Modellen, die durch ein effektives Zweikanal–Kondo Modell beschrieben werden, ist auch hier ebenfalls ein effektives Magnetfeld vorhanden, das die interessante Nicht-Fermiflüssigkeitsphysik unterdrückt. Ein ausgeprägtes Nicht-Fermiflüssigkeitsverhalten wird deshalb nur in einem sehr engen Parameterbereich erwartet.

Im darauf folgenden Kapitel 7 schränken wir das betrachtete anisotrope zwei-Störstellen Kondo Problem weiter ein, indem wir annehmen, dass die lokalen Momenten jeweils an separate fermionische Bäder koppeln. Wie schon von N. Andrei *et al.* [9] erkannt wurde, werden gewisse Systeme von gekoppelten Quantenpunkten durch ein solches Modell beschrieben. Insbesondere wurde von diesen Autoren betont, dass dieses Modell einen Quantenphasenübergang von einer Singulett– zu einer Dublett–Phase zeigt. Die Universalitätsklasse als auch die Signaturen des Phasenübergangs in Transportgrößen blieb jedoch unbeantwortet. S. Kehrein und M. Vojta [10] erkannten, dass für bestimmte Werte der Parameter dieses Modell durch die Physik des Anderson Modells wiedergegeben wird. In Kapitel 7 wird gezeigt, dass die kritische Theorie des Quantenphasenübergangs tatsächlich durch die Niederenergietheorie eines verallgemeinerten Anderson Modells beschrieben wird. Diese kritische Theorie kann als ein effektives Cluster–Kondo Modell interpretiert werden. Wir erhalten das verallgemeinerte Anderson Modell durch Bosonisierung des anisotropen zwei-Störstellen Kondo Problems und Anwenden einer unitären Transformation mit anschließender Refermionisierung. Die universelle kritische Theorie wird durch eine Schrieffer–Wolff Transformation hergeleitet, wobei kollektive Anregungen im Hochenergiesektor berücksichtigt werden. Nachdem wir die kritische Theorie als Cluster–Kondo Modell identifiziert haben, können wir folgern, dass der Quantenphasenübergang zwischen der Singulett– und der Dublett–Phase der Kosterlitz–Thouless Universalitätsklasse angehört. Dies wird bestätigt durch eine Analyse mit der numerischen Renormierungsgruppe, die von M. Vojta und T. Pruschke durchgeführt wurde und deren Ergebnisse zusammen mit den hier vorgestellten in Ref. [11] publiziert wurden. Der Phasenübergang hinterlässt erstaunliche Signaturen in Transportgrößen. Je nach experimenteller Realisierung erwarten wir am Übergang einen universellen Sprung in der Leitfähigkeit von einem Wert $G = 2e/h \cos^2 \pi/(2\sqrt{2})$ nach $2e/h$ oder einer Anomalie in der Spannungsabhängigkeit $G \sim |V|^{-2(\sqrt{2}-1)}$.

Am Ende sei noch erwähnt, dass im Anhang B.6 die Anderson–Yuval–Hamann Renormierungsgruppengleichungen für das Kondo Modell im Rahmen der Bosonisierung hergeleitet werden. Dies ermöglicht eine Interpretation der RG Transformationen als Sequenz von infinitesimalen unitären Transformationen.

Contents

Introduction

Nowadays it is widely claimed that a route for understanding many open problems in the physics of correlated electrons is offered by the peculiarities of quantum critical phenomena [1, 2], i.e. phase transitions at zero temperature. The theoretical study of their influence on finite temperature properties and the corresponding experimental investigations are still in their infancy and constitute one of the most fascinating fields of physics today.

This thesis is divided into two parts each with several self-contained contributions to the physics of quantum critical phenomena. The first part mainly concerns quantum phase transitions in itinerant magnets such as the heavy fermion compounds, while the second part focuses on the physics of coupled impurities. Below we give a short overview of the different chapters.

In contrast to their classical finite temperature counterparts, quantum phase transitions (QPT) are in a strict sense not experimentally accessible since they occur at zero temperature, and the experimentalist is rather limited to analysing their traces at non-zero temperature. As a consequence, quantities such as the specific heat are not expected to be as singular near a QPT as they are close to classical finite temperature transitions. In Chapter 1 we show by a scaling analysis that the Grüneisen parameter (the ratio of the thermal expansion and specific heat) diverges close to a pressure tuned QPT, and similarly the magnetocaloric effect close to a magnetic field tuned QPT. This divergence is characterized by the correlation length exponent ν of the QPT, and due to the third law of thermodynamics the prefactor of this divergence is universal and solely given in terms of critical exponents. The Grüneisen parameter therefore plays an essential role in the pursuit of quantum critical phenomena, as important as, for example, the specific heat in classical phase transitions. The content of Chapter 1 is published in Ref. [3].

In order to confirm the above results for a specific model, we then in Chapter 2 review the standard theory for zero-temperature magnetic instabilities in itinerant magnetic systems due to J. A. Hertz [4] and rederive the renormalization group (RG) equations of A. J. Millis [5]. In Chapter 3 we calculate the thermal expansion and the Grüneisen parameter in addition to the specific heat, which has been previously obtained [5, 6], and we compare them to the results of the scaling analysis of Chapter 1. It is found that for this specific case the corrections to scaling are at most logarithmic, and their origin is identified.

In Chapter 4 an anisotropic Hertz theory is proposed in order to make predictions about the dimensional crossover expected to occur in the heavy fermion compound $CeCu_{6-x}Au_x$. In neutron scattering experiments [8] two-dimensional spin fluctuations have been observed, confirming a scenario proposed by A. Rosch [7] to account for the peculiar properties observed in the specific heat and the resistivity. However, the crystal structure of $CeCu_{6-x}Au_x$ is of a three-dimensional character, and it is believed that the dominance of two-dimensional spin fluctuations is only transient, eventually giving way to three-dimensional ones sufficiently

close to the phase transition. Experimentally this dimensional crossover has not yet been found either in neutron scattering or in thermodynamic quantities. We analyse it theoretically within the anisotropic Hertz theory of Chapter 4, and find that thermal expansion measurements are a likely candidate to detect the dimensional crossover in $CeCu_{6-x}Au_x$ experimentally. The crossover lines in the phase diagram are also identified and their signatures in thermodynamic quantities are determined. To this end three different methods are applied. The first method is a generalization of the Millis renormalization group of Chapter 3 adapted to the anisotropic Hertz theory. In order to account for the dimensional crossover a two-stage RG is used: in the first stage the theory flows to the primary, two-dimensional fixed point, and during the second stage the flow is governed by the secondary fixed point describing the three dimensional theory. The parameter controlling the anisotropy of the theory is a relevant quantity in the RG sense with respect to the three-dimensional fixed point, which results in an additional singular contribution to the thermal expansion. The second method applied to the anisotropic Hertz theory is known as dimensional reduction, which involves the derivation of an effective finite-temperature theory for the zero-Matsubara mode. Finally, the third method is a large N analysis.

The second part of this thesis is concerned with the physics of coupled local moments and considers a variant of the two-impurity Kondo model. This model has aroused interest since it provides a relatively accessible example of the competition between Kondo screening and magnetic alignment of local moments, which is believed to be at the origin of the magnetic phase transition in heavy fermion compounds. Most studies of this model have focused on an SU(2) invariant exchange coupling between the local moments. Here, however, we consider the strongly anisotropic version, i.e. an Ising-like coupling between the impurities, which is motivated by the controversy of the role of disorder effects near magnetic instabilities, as discussed in Chapter 5. This model is suggested to mimic the dynamics of small magnetic droplets, which are likely to be generated close to a quantum phase transition in strongly anisotropic itinerant magnets in the presence of disorder.

It is shown in Chapter 6 that the effective low-energy theory of strongly Ising-coupled local moments is given by a two-channel Kondo model. This is particularly interesting since the two-channel Kondo model belongs to one of the universality classes of impurity problems that are characterized by local non-Fermi liquid behavior. They thus offer an alternative route to explain the unusual physics observed in heavy fermion materials such as $CeCu_{6-x}Au_x$. It is argued that the magnetic droplets might provide a generic realization of two-channel Kondo physics. Unfortunately, as in other proposals of effective two-channel Kondo models, such as the quadrupolar Kondo effect [12], the effective model is invariably accompanied by an effective magnetic field that suppresses the interesting non-Fermi liquid physics, and fine-tuning is therefore required for it to develop.

In Chapter 7 the Ising-coupled two-impurity Kondo model is considered with each local moment coupled to its own fermionic bath, which is a crucial restriction on the model not present in the version of the preceding Chapter 6. Certain double quantum dot systems are naturally represented by this model, as was realized by N. Andrei *et al.* [9]. They pointed out the existence of a quantum phase transition within this model from an impurity doublet to a singlet phase. However, both the nature of the transition and its associated signatures in transport remained unresolved. A first step in this direction was provided by S. Kehrein and M. Vojta [10], who realized that for a certain parameter set this model exhibits the physics of the Anderson model. In Chapter 7 it is shown that the critical theory of the quantum phase transition of this impurity model is indeed given by the low-energy theory of

a generalized Anderson model and can be interpreted as an effective cluster Kondo model. The generalized Anderson model is obtained by bosonizing the original two-impurity model, applying a unitary transformation and refermionizing. The critical theory is derived via a Schrieffer–Wolff transformation that takes into account non-trivial excitation effects in the high-energy sector. After having identified the critical theory as a cluster Kondo model we can conclude that the quantum phase transition of the original model between the doublet and the singlet phase is in the Kosterlitz–Thouless universality class. These conclusions have been confirmed by a numerical renormalization group analysis carried out by M. Vojta and T. Pruschke [11]. We show that these results have interesting consequences for transport properties. Because the critical degrees of freedom of the electrons are complicated solitonic excitations of the Fermi seas, their phase shift undergoes a universal jump which is the analogue of the universal jump of the superfluid density in ^{4}He films at the vortex binding–unbinding transition [13]. Depending on the experimental set-up, this jump is reflected in either a universal jump in the dimensionless conductance from a value $g = \cos^2 \pi/(2\sqrt{2})$ to 1 at the transition or a characteristic zero-bias anomaly $g \sim |V|^{-2(\sqrt{2}-1)}$. The results of Chapter 7 have been published in Ref. [11].

Finally, we mention that Appendix B.6 is self-contained, and considers a re-derivation of the Anderson–Yuval–Hamann RG equations of the Kondo model within the bosonization approach. It is shown that within this formulation the RG transformations can be understood as a sequence of infinitesimal unitary transformations.

Part I

Grüneisen Parameter and Dimensional Crossover

Chapter 1

Universally Diverging Grüneisen Parameter

In section 1.1 we briefly review the concept of a quantum critical point. In Section 1.2 we introduce the Grüneisen parameter and the magnetocaloric effect, which are expected to reveal many characteristic features of a quantum phase transition. We investigate this in detail in the framework of a scaling analysis in Section 1.3. It is shown that the Grüneisen parameter and the magnetocaloric effect necessarily diverge near quantum critical points. We also explain that due to the third law of thermodynamics the form of this divergence is universal. For these reasons the Grüneisen parameter and the magnetocaloric effect are argued to be very important tools in the analysis of quantum criticality. In Section 1.4 we comment on experiments which have utilized the Grüneisen parameter to characterize the quantum critical point in certain heavy fermion compounds. The essence of this chapter is published in Ref. [3].

1.1 Introduction

A quantum mechanical system may possess different ground states depending on the values of its coupling constants. A transition between these ground states, i.e. phases, can be induced by varying a certain coupling constant. Since the ground state is a zero-temperature property of the system this phase transition is triggered by quantum fluctuations, in contrast to the thermal fluctuations which drive the familiar phase transitions at finite temperatures. Phenomenologically, the distance to such a quantum phase transition is described by the control parameter r, which is some complicated function of all the coupling constants and the applied fields. The quantum phase transition occurs when the control parameter r vanishes and the position $r = 0$ in parameter space is called the quantum critical point. Physically, the control parameter might be tuned by varying pressure p, doping x, magnetic field H or some other quantity. In the immediate vicinity of the quantum critical point the control parameter can be linearized in these physically accessible fields, e.g. in the case of pressure tuning $r \approx (p - p_c)/p_0$, where p_c is the critical pressure and p_0 a certain pressure scale, or in the case of magnetic field tuning $r \approx (H - H_c)/H_0$ with the critical field H_c and a certain field scale H_0.

Often the quantum critical point is the zero-temperature endpoint of a line of second order phase transitions in the control parameter–temperature plane (r,T). A generic phase diagram is shown in Fig. 1.1. It is important to understand that the quantum critical point which separates the two different phases at zero temperature $T = 0$ is *qualitatively* different from the rest of the phase boundary at finite T. Near the phase transition the physics will be dominated by the correlation length ξ, which diverges at the phase transition. The peculiarity at zero temperatures is that there is not only a divergent correlation volume in space, ξ^d, but also in (imaginary) time, $\tau_{cr} \propto \xi^z$, where d is the space dimension and z the so-called dynamical exponent. The phase transition at zero temperature — the quantum phase transition — is therefore characterized by a divergent correlation volume with an effective dimensionality $d + z$. The critical fluctuations at zero temperature are exclusively of a quantum mechanical nature. Their typical energy scale is given by $\hbar/\tau_{cr} \propto \xi^{-z}$ and vanishes as the phase transition is approached, $\xi \to \infty$, a phenomenon known as "critical slowing down". In terms of the zero-temperature control parameter the correlation length is given by

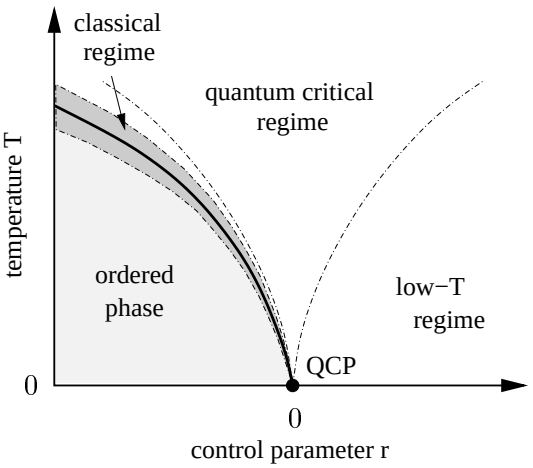

Figure 1.1: *Schematic phase diagram with order present at finite temperatures.*

$$\xi \propto |r|^{-\nu} \tag{1.1}$$

where ν is the correlation length exponent of the quantum phase transition.

How is the situation changed when the temperature T is finite? Then the quantum fluctuation are complemented by the thermal fluctuations with their characteristic energy scale of $k_B T$. They will have to compete with each other and the winner happens to be the one with the larger energy scale,

$$\begin{aligned} &\text{quantum fluctuations:} && \hbar/\tau_{cr} \propto \xi^{-z} \\ &\text{thermal fluctuations:} && k_B T\,. \end{aligned}$$

For low temperatures away from the quantum critical point the quantum fluctuations around the quantum ground state still prevail. Their dominance is however challenged when the temperature is comparable to their typical energy scale $\hbar/\tau_{cr}$,

$$k_B T \sim \hbar/\tau_{cr} \propto \xi^{-z} \propto |r|^{-\nu z}\,. \tag{1.2}$$

This identifies the crossover to the quantum critical regime, see Fig. 1.1. In the quantum critical regime the competition between quantum and thermal fluctuations are especially fierce and it is precisely the existence of this regime that makes the study of quantum phase transitions interesting. The fierce battle between fluctuations of thermal and quantum origin is reflected in unusual, exciting finite temperature properties, e.g. non-Fermi liquid behavior in metallic systems. Moreover, the quantum critical regime can extend to relatively high temperatures depending on the microscopic energy scales. Although the quantum phase transition only occurs at zero temperature it thus influences drastically the physics at finite temperatures.

Within both regimes there might exist additional sub-regimes which arise, for example, due to the presence of dangerously irrelevant operators. Such a case is discussed in Chapter 3.

Finally, the quantum fluctuations have to give in suffiently close to the finite temperature transition initiating a crossover to the classical regime. The phase transition at finite temperature is only triggered by thermal fluctuations and quantum mechanics is not of importance for the critical degrees of freedom: the system behaves classically in the classical regime. In particular, at the classical transition only the fluctuations in space are critical and the divergent correlation volume is thus confined to only d dimension, ξ^d. In this sense the quantum–classical crossover is analogous to a dimensional crossover of a system from $d+z$ to d dimensions. The classical finite temperature transition is therefore, as mentioned before, *qualitatively* different from the quantum phase transition. Technically speaking, they belong to different universality classes. Nevertheless, the portion of the phase diagram around the finite temperature phase boundary that can be described exclusively in terms of classical degrees of freedom is quite small near the quantum critical point. The classical regime shrinks quickly to zero as the temperature is lowered. In fact, the critical behavior associated with the classical phase transition is practically unobservable at low enough temperatures.

We know that the importance of fluctuations increase with decreasing dimensionality of the system. When the spatial dimensionality d of the physical system is sufficiently low, i.e. below the lower critical dimension, the thermal fluctuations will totally suppress the phase transition at finite temperatures, although the existence of the quantum phase transition might still be secured due to its enhanced dimensionality $d+z$. A phase diagram of such a system is depicted in Fig. 1.2. An example is the Heisenberg ferromagnet in two dimensions, whose magnetization has the internal symmetry $O(3)$. It possesses a quantum phase transition but the ordered state is destroyed at finite temperatures by the would-be Goldstone modes [14].

For a more comprehensive inroduction into quantum critical phenomena we refer the reader to Refs [2, 1].

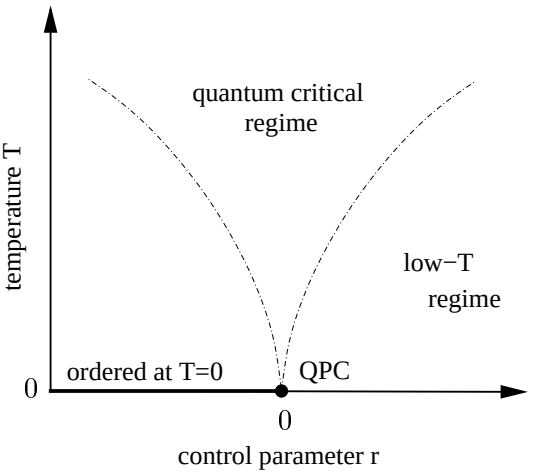

Figure 1.2: *Schematic phase diagram without order at finite temperatures.*

1.2 Great expectations: Grüneisen parameter

In the last section we stressed the fact that the phase boundary in the phase diagram Fig. 1.1 consists of a line of classical finite-temperature transitions ending in a quantum critical point. In the (r, T) plane there exists only a single preferred direction to approach the classical transition, namely the direction perpendicular to the phase boundary; however, there are two independent directions to approach the quantum critical point. We expect that the variations of, for example, the entropy along these two directions yield complementary information about the nature of the quantum phase transition. This has not been appreciated before. It is shown in the following that this basic observation leads to interesting and very useful results.

Consider the total differential of the entropy in the (r,T) plane

$$dS = \left.\frac{\partial S}{\partial T}\right|_r dT + \left.\frac{\partial S}{\partial r}\right|_T dr\,. \tag{1.3}$$

It is characterized by two derivatives specifying the sensitivity of entropy to changes in either temperature T or control parameter r, the two axes of the phase diagram in Fig. 1.1. The first derivative is the variation of entropy S with respect to variations in temperature. It is measured by the (molar) specific heat coefficient which is indeed often investigated in the pursuit of quantum criticality,

$$\gamma = \frac{\mathcal{N}_A}{\mathcal{N}} \left.\frac{\partial S}{\partial T}\right|_r . \tag{1.4}$$

where $\mathcal{N}_A$ is Avogadro's number and $\mathcal{N}$ is the number of particles in the system. The second derivative in (1.3) is the variation of the entropy with respect to variations in the control parameter and is the quantity complementary to the specific heat. Depending on the experimental realization this derivative can also be identified with well-known and experimentally accessible thermodynamic quantities. In the case of pressure tuning, $r \approx (p-p_c)/p_0$, it is proportional to the thermal expansion α,

$$\alpha = \frac{1}{V}\left.\frac{\partial V}{\partial T}\right|_p = \frac{1}{V}\frac{\partial^2 F}{\partial T \partial p} = -\frac{1}{V}\left.\frac{\partial S}{\partial p}\right|_T = -\frac{1}{V p_0}\left.\frac{\partial S}{\partial r}\right|_T \tag{1.5}$$

where F is the Gibbs free energy, $F = F(p,T)$, which depends on pressure p and temperature T. If the quantum phase transition is controlled by the magnetic field H, $r \approx (H-H_c)/H_0$, this is the derivative of the magnetization M with respect to temperature,

$$\left.\frac{\partial M}{\partial T}\right|_H = -\frac{\partial^2 F}{\partial T \partial H} = \left.\frac{\partial S}{\partial H}\right|_T = \frac{1}{H_0}\left.\frac{\partial S}{\partial r}\right|_T \tag{1.6}$$

where the free energy is now given by $F = F(H,T)$.

We will pay special attention to the constant entropy curves $T(r)|_S$ in the (r,T) plane. The derivative along these curves is related to the ratio between the two partial derivatives discussed above. We will discuss this constant-entropy derivative in the form of the parameter,

$$\Gamma = \frac{1}{T}\left.\frac{dT}{dr}\right|_S = -\frac{1}{T}\frac{(\partial S/\partial r)_T}{(\partial S/\partial T)_r}\,. \tag{1.7}$$

In the case of pressure tuning this combination is proportional to the Grüneisen parameter Γ_p [15, 16], the ratio of thermal expansion and (molar) specific heat $c_p = \gamma\, T$,

$$\Gamma_p = \frac{\alpha}{c_p} = \frac{\Gamma}{p_0 V_m}\,. \tag{1.8}$$

where V_m is the molar volume. For this reason we will often sloppily refer to the general relation (1.7) as the Grüneisen ratio irrespective of the actual physical controlling field. If the magnetic field is used to control the quantum phase transition the generalized Grüneisen ratio (1.7) can be identified as a magnetocaloric effect Γ_H,

$$\Gamma_H = \frac{\Gamma}{H_0} = \frac{1}{T}\left.\frac{\partial T}{\partial H}\right|_S = -\frac{1}{T}\frac{(\partial S/\partial H)_T}{(\partial S/\partial T)_H} = -\frac{(\partial M/\partial T)_H}{c_H}\,. \tag{1.9}$$

Whereas in the case of pressure tuning the thermal expansion and specific heat have to be measured separately in order to determine the Grüneisen parameter, in the case of magnetic field tuning the magnetocaloric effect can be directly obtained experimentally.

What do we know about the Grüneisen parameter? We now examine some classical arguments which suggest that unusual behavior occurs at the quantum critical point; this will be verified by a scaling analysis in Section 1.3.

If the system is dominated by a single energy scale E_0, such as the Fermi energy in the case of fermions or the Debye frequency in the case of phonons, the entropy can be cast into a simple scaling form [16]

$$S = \psi\left(\frac{T}{E_0}\right) \tag{1.10}$$

where ψ is some scaling function. Putting this scaling form into the formula for the Grüneisen parameter (1.8) we obtain,

$$\Gamma_p = \frac{\alpha}{c_p} = -\frac{1}{TV_m}\frac{(\partial S/\partial p)_T}{(\partial S/\partial T)_r} = \frac{1}{V_m E_0}\frac{\partial E_0}{\partial p}\,, \tag{1.11}$$

i.e. Γ_p is just given as the logarithmic derivative of the energy scale E_0 with respect to pressure[1]. In particular, the Grüneisen parameter is independent of temperature. This result is known as the Grüneisen law (see e.g. Ref. [16] §67). However, the physical situation we are interested in is quite unusual in the sense that the typical energy scale near a quantum phase transition, $E_0 \sim \xi^{-z}$, is about to vanish! Taking formula (1.11) literally, though naively, over to the scenario of quantum criticality would suggest a diverging Grüneisen parameter at the quantum critical point.

Another indication that interesting behavior is to be expected of the Grüneisen parameter in quantum critical systems comes from the theory of classical second order phase transitions. It is known that the specific heat, c_p, diverges at a classical second order phase transition with the same critical exponent as the thermal expansion, α (see Ref. [16] §148). In particular, in the ratio of thermal expansion and specific heat this divergence cancels. This can be understood by writing the molar entropy in the form [16]

$$S = S(T, p - p_c(T)) \tag{1.12}$$

where the function $p_c(T)$ identifies the phase boundary in the phase diagram of Fig. 1.1. The derivative of the entropy with respect to its second argument becomes infinite for a second order phase transition as $p \to p_c$. Retaining only the divergent terms we obtain for the specific heat near the transition

$$c_p = T_c \left.\frac{\partial S}{\partial T}\right|_p = -T_c \frac{\partial S(T, p - p_c(T))}{\partial p}\frac{dp_c}{dT} = V_m \alpha\, T_c \frac{dp_c}{dT}\,. \tag{1.13}$$

In the immediate vicinity of the finite-temperature phase boundary $T_c(p)$, i.e. in the classical regime of Fig. 1.1, we therefore expect the Grüneisen parameter to behave as

$$\Gamma_p = \frac{1}{V_m T_c}\frac{dT_c}{dp}\,. \tag{1.14}$$

[1] In the literature one often reads that the Grüneisen parameter equals the logarithmic derivative of the energy scale E_0 with respect to volume V instead of pressure p. This would result from considering the specific heat in the ratio (1.8) at constant volume and not at constant pressure. While the latter is more suitable for our purposes, the physical content of the Grüneisen law however remains unchanged.

The Grüneisen parameter is thus just given by the logarithmic derivative of the phase boundary $T_c(p)$. As the line of second order phase transitions approaches zero temperature, $T_c \to 0$, it follows from the above formula that the Grüneisen law is in a certain sense maximally violated at the quantum critical point: the Grüneisen parameter diverges! In the following section this prediction is borne out by a scaling analysis which will also specify the nature of this divergence.

1.3 Scaling theory

In this section we analyze the quantities introduced in the last section in the framework of scaling theory [17]. To this end we introduce the scaling dimensions of the parameters involved. Traditionally, the scaling dimension of the control parameter is given by $1/\nu$ and the temperature scales with the dynamical critical exponent z. Furthermore, we introduce the scaling dimension ϕ for the critical part of the free energy per mole, f_{cr}. When hyperscaling [17, 18] applies this scaling dimension is equal to the effective dimensionality, $\phi = d + z$. Upon rescaling the unit length by a factor l an interval in space Δx is changed to $\Delta x' = \Delta x\, l^{-1}$ and therefore has scaling dimension -1,

$$\begin{array}{lll} \Delta x & \longrightarrow \Delta x' & = \Delta x\, l^{-1} \\ r & \longrightarrow r' & = r\, l^{1/\nu} \\ \mathcal{T} & \longrightarrow \mathcal{T}' & = \mathcal{T}\, l^{z} \\ f_{cr} & \longrightarrow f'_{cr} & = f_{cr}\, l^{\phi}\,. \end{array} \tag{1.15}$$

Here we have introduced the dimensionless temperature $\mathcal{T} = T/T_0$, where T_0 is some temperature scale.

1.3.1 Scaling Ansatz

The scaling Ansatz we use is based on the assumption of scale invariance near the quantum critical point. This implies that as far as singular dependences are concerned the correlation length ξ is the only relevant length in the system: the quantum critical physics is independent of the microscopic details. Mathematically, the scale invariance at criticality is expressed by

$$l^{\phi}\, f_{cr}(r, \mathcal{T}) \stackrel{!}{=} f_{cr}(r\, l^{1/\nu}, \mathcal{T}\, l^{z})\,, \tag{1.16}$$

i.e. the scale transformation of the control parameter and the temperature in the arguments of the free energy per mole can be absorbed into the scale factor of the free energy itself. From equation (1.16) some remarkable properties of the Grüneisen parameter can be derived. First of all let us determine its scaling dimension. Putting the scaling Ansatz (1.16) into the definition of Γ, (1.7), we obtain

$$\begin{aligned} \Gamma_{cr}(r, \mathcal{T}) &= -\frac{1}{\mathcal{T}} \frac{\partial^2 f_{cr}(r, \mathcal{T})}{\partial r \partial \mathcal{T}} \left(\frac{\partial^2 f_{cr}(r, \mathcal{T})}{\partial \mathcal{T}^2} \right)^{-1} \\ &\stackrel{!}{=} -\frac{1}{\mathcal{T}} \frac{\partial^2 (l^{-\phi}\, f_{cr}(r\, l^{1/\nu}, \mathcal{T}\, l^{z}))}{\partial r \partial \mathcal{T}} \left(\frac{\partial^2 (l^{-\phi}\, f_{cr}(r\, l^{1/\nu}, \mathcal{T}\, l^{z}))}{\partial \mathcal{T}^2} \right)^{-1} \\ &= -l^{1/\nu} \frac{1}{\mathcal{T}\, l^{z}} \frac{\partial^2 f_{cr}(r\, l^{1/\nu}, \mathcal{T}\, l^{z})}{\partial (r\, l^{1/\nu}) \partial (\mathcal{T}\, l^{z})} \left(\frac{\partial^2 f_{cr}(r\, l^{1/\nu}, \mathcal{T}\, l^{z})}{\partial (\mathcal{T}\, l^{z})^2} \right)^{-1} = l^{1/\nu}\, \Gamma_{cr}(r\, l^{1/\nu}, \mathcal{T}\, l^{z})\,. \end{aligned} \tag{1.17}$$

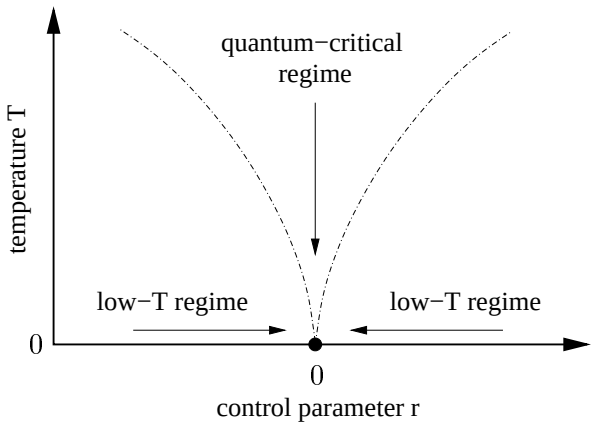

Figure 1.3: *Two regimes in the (r,T) plane. The crossover lines are defined by the condition $|r| \sim \mathcal{T}^{1/(\nu z)}$.*

That means that the Grüneisen parameter has the scaling dimension $-1/\nu$, i.e. minus the scaling dimension of the control parameter r,

$$\boxed{\dim[\Gamma_{cr}] = -\dim[r] = -1/\nu\,.} \tag{1.18}$$

This has some interesting consequences for the properties of Γ in quantum critical systems.

1.3.2 Divergent Grüneisen parameter

From (1.18) it follows that the Grüneisen parameter diverges upon approaching the quantum critical point. However, we have to distinguish how exactly the quantum critical point is approached. Depending on the relative values of control parameter and temperature there exist two different regimes, sketched in Fig. 1.3. The two regimes are separated by the crossover line at which the scale-invariant combination $|r|\,\mathcal{T}^{-1/(\nu z)}$ is of order one. In the quantum critical regime this combination is small, $|r|\,\mathcal{T}^{-1/(\nu z)} \ll 1$. To determine the behaviour of Γ in this regime we choose a definite value for the arbitrary scale l in equation (1.17), namely such that $\mathcal{T}\,l^z = 1$. The leading behaviour of the Grüneisen parameter is then given by

$$\Gamma_{cr}(r,\mathcal{T}) = \mathcal{T}^{-\frac{1}{\nu z}}\,\Gamma_{cr}(r\,\mathcal{T}^{-\frac{1}{\nu z}},1) \approx \mathcal{T}^{-\frac{1}{\nu z}}\,\Gamma_{cr}(0,1) \qquad \text{for} \quad |r|\,\mathcal{T}^{-\frac{1}{\nu z}} \ll 1\,, \tag{1.19}$$

i.e. the Grüneisen parameter diverges with decreasing temperature with an exponent $-1/(\nu z)$. In the other, low-temperature regime $|r|\,\mathcal{T}^{-1/(\nu z)} \gg 1$, we choose instead the scale such that $|r|\,l^{1/\nu} = 1$ and get

$$\Gamma_{cr}(r,\mathcal{T}) = \frac{1}{|r|}\,\Gamma_{cr}(\mathrm{sign}(r),\mathcal{T}\,|r|^{-\nu z}) \approx \frac{1}{|r|}\,\Gamma_{cr}(\mathrm{sign}(r),0) \qquad \text{for} \quad |r|\,\mathcal{T}^{-\frac{1}{\nu z}} \gg 1\,. \tag{1.20}$$

Hence, in the low-temperature regime the Grüneisen parameter also diverges with the inverse of the control parameter r, which is a direct consequence of (1.18).

The scaling analysis thus indeed confirms the conjecture of Section 1.2. The Grüneisen parameter (1.8) or the magnetocaloric effect (1.9) necessarily diverge algebraically near a quantum critical point driven by pressure or magnetic field, respectively. The quantity Γ therefore provides a tool to identify unambiguously the very existence of a quantum critical

point, because it carries the negative scaling dimension of the relevant operator, i.e. the control parameter r. If there is no such relevant operator r to which pressure or magnetic field couples, i.e. no quantum critical point, the Grüneisen parameter will not diverge algebraically. In particular, if the quantum critical point is washed out to a quantum critical line (see Fig. 1.4) by, say, disorder, the scaling dimension of the control parameter is at most marginal along this line, i.e. $\dim[r] = 0$. Accordingly, the Grüneisen parameter diverges at most logarithmically with temperature in the quantum critical regime

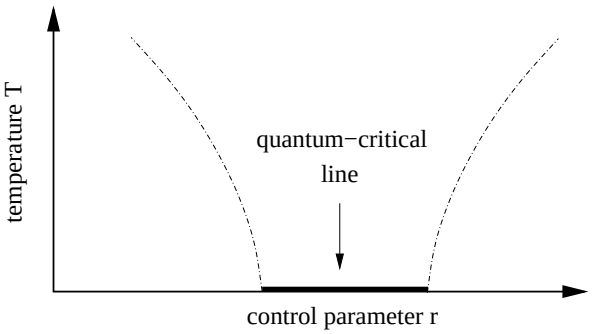

Figure 1.4: *Phase Diagram with a quantum critical line*

$$\Gamma_{cr} \sim \log \mathcal{T} \,. \tag{1.21}$$

The quantity Γ thus offers a criterion for determining the existence of a quantum critical point.

Furthermore, a divergent Γ_{cr} implies that the specific heat coefficient $\gamma = (\partial S/\partial T)_r$ is *less* singular than the quantity $(\partial S/\partial r)_T/T$, which is either proportional to α/T or $(\partial M/\partial T)_H/T$ for pressure or magnetic field tuning, respectively. As a consequence, the thermal expansion α and the temperature dependence of magnetization can be advocated to be the preferred quantities for the investigation of quantum critical phenomena.

1.3.3 Universality

We can learn more about the prefactors $\Gamma(0,1)$ and $\Gamma(1,0)$ appearing in Eqs. (1.19) and (1.20), respectively, by going back to the original scaling Ansatz (1.16) for the free energy per mole f_{cr}. Differentiating once with respect to temperature we obtain the scaling form for the molar entropy,

$$s_{cr}(r, \mathcal{T}) = l^{-\phi+z}\, s_{cr}(r\, l^{1/\nu}, \mathcal{T}\, l^z) \,. \tag{1.22}$$

Repeating the procedure of the last section it is convenient to rewrite the entropy by choosing certain scales in two different ways suitable for either the quantum critical or the low-temperature regime,

$$s_{cr}(r,\mathcal{T}) = \begin{cases} \mathcal{T}^{\frac{\phi-z}{z}}\, s_{cr}(r\,\mathcal{T}^{-1/(\nu z)}, 1) & = \left(\dfrac{T}{T_0}\right)^{\frac{\phi-z}{z}} \Psi_{\mathrm{QCR}}\left(r\,\left(\dfrac{T}{T_0}\right)^{-1/(\nu z)}\right) \\ |r|^{\nu(\phi-z)}\, s_{cr}(\mathrm{sign}(r), \mathcal{T}\, r^{-\nu z}) & = |r|^{\nu(\phi-z)}\, \Psi_{\mathrm{LT}}^{\mathrm{sign}(r)}\left(\dfrac{T}{T_0}\,|r|^{-\nu z}\right), \end{cases} \tag{1.23}$$

with the corresponding *a priori* unknown universal scaling functions Ψ_{QCR} and $\Psi_{\mathrm{LT}}^{\pm}$. Note that in the low-temperature regime we have had to introduce two scaling functions, Ψ_{LT}^{+} and Ψ_{LT}^{-}, for positive and negative values of the control parameter r respectively. Moreover, we traded the dimensionless temperature $\mathcal{T}$ for the dimensionful constant T_0 in order to make explicit that the scaling functions and their arguments have the engineering dimension zero. To obtain the leading behavior of the molar entropy in the two regimes we must expand the

scaling functions for small arguments. The function $\Psi_{\rm QCR}$ is expected to be regular for small arguments since there is no phase transition at $r = 0$ for finite T,

$$\Psi_{\rm QCR}(x) = \Psi_{\rm QCR}(0) + \Psi'_{\rm QCR}(0)\, x + \ldots \qquad \text{for} \quad x \to 0\,. \tag{1.24}$$

An important attribute of quantum phase transitions comes into play in the consideration of the other scaling function $\Psi^{\pm}_{\rm LT}$. This scaling function describes the low-temperature behavior of the phases to the left and right of the quantum critical point (see Fig. 1.1). Upon approaching zero temperature the entropy has to vanish according to the third law of thermodynamics. This requirement restricts the small argument behavior of $\Psi^{\pm}_{\rm LT}$ in an essential way. We will assume that the entropy vanishes algebraically so that the low-temperature expansion of $\Psi^{\pm}_{\rm LT}$ has the form

$$\Psi^{\pm}_{\rm LT}(x) = \mathcal{C}^{\pm}\, x^{y_0^{\pm}} + \ldots \qquad \text{for} \quad x \to 0\,, \tag{1.25}$$

where $\mathcal{C}^{\pm}$ are constants and the positive exponents $y_0^{\pm} > 0$ characterize the power-law behavior of the specific heat in the low-temperature regime, $c \sim T^{y_0}$. For example, if the low-energy excitations are bosons in d spatial dimension with a dispersion $\omega \sim k^p$ the exponent is given by $y_0 = d/p$, e.g. d and $d/2$ for an insulating antiferromagnet and ferromagnet, respectively. Gapped systems in which the entropy vanishes exponentially in the low-temperature regime are discussed in Appendix A.1. The limiting behavior of the two derivatives of the molar entropy with respect to either temperature or control parameter are easily obtained,

$$\gamma_{cr} = \frac{\partial s_{cr}}{\partial T} = \begin{cases} \dfrac{1}{T_0}\,\dfrac{\phi - z}{z}\,\Psi_{\rm QCR}(0)\,\left(\dfrac{T}{T_0}\right)^{\frac{\phi-2z}{z}} & \text{for} \quad |r|\,(T/T_0)^{-\frac{1}{\nu z}} \ll 1 \\ \dfrac{1}{T_0}\,y_0^{\pm}\,\mathcal{C}^{\pm}\,|r|^{\nu(\phi-z-zy_0)}\,\left(\dfrac{T}{T_0}\right)^{y_0^{\pm}-1} & \text{for} \quad |r|\,(T/T_0)^{-\frac{1}{\nu z}} \gg 1 \end{cases} \tag{1.26}$$

and

$$\frac{\partial s_{cr}}{\partial r} = \begin{cases} \Psi'_{\rm QCR}(0)\,\left(\dfrac{T}{T_0}\right)^{\frac{\phi-z}{z}-\frac{1}{\nu z}} & \text{for} \quad |r|\,(T/T_0)^{-\frac{1}{\nu z}} \ll 1 \\ \nu(\phi - z - zy_0^{\pm})\,\mathcal{C}^{\pm}\,|r|^{\nu(\phi-z-zy_0^{\pm})}\,\dfrac{1}{r}\left(\dfrac{T}{T_0}\right)^{y_0^{\pm}} & \text{for} \quad |r|\,(T/T_0)^{-\frac{1}{\nu z}} \gg 1\,. \end{cases} \tag{1.27}$$

The behavior of the general Grüneisen parameter (1.7) follows readily:

$$\Gamma_{cr} = \begin{cases} -\dfrac{z\,\Psi'_{\rm QCR}(0)}{(\phi - z)\,\Psi_{\rm QCR}(0)}\,\left(\dfrac{T}{T_0}\right)^{-\frac{1}{\nu z}} & \text{for} \quad |r|\,(T/T_0)^{-\frac{1}{\nu z}} \ll 1 \\ -\dfrac{\nu(\phi - z(1+y_0^{\pm}))}{y_0^{\pm}}\,r^{-1} & \text{for} \quad |r|\,(T/T_0)^{-\frac{1}{\nu z}} \gg 1\,. \end{cases} \tag{1.28}$$

Whereas in the quantum critical regime $|r|\,(T/T_0)^{-\frac{1}{\nu z}} \ll 1$ the unknown scaling function enters the prefactor of the divergence, it disappears completely in the low-temperature regime $|r|\,(T/T_0)^{-\frac{1}{\nu z}} \gg 1$. The prefactor is just given by a combination of critical exponents. To make this result manifest we give here the low-temperature behavior both of the Grüneisen

parameter, $\Gamma_{cr,p}$, for a pressure-tuned QCP and of the magnetocaloric effect, $\Gamma_{cr,H}$, for a magnetic-dield-tuned QCP, obtained using hyperscaling $\phi = d + z$:

$$\boxed{\begin{aligned} \Gamma_{cr,p} &= -\frac{\nu(d - zy_0^{\pm})}{y_0^{\pm}} \frac{1}{V_m(p - p_c)} \qquad \text{for} \quad |p - p_c|\, T^{-\frac{1}{\nu z}} \gg p_0 T_0^{-\frac{1}{\nu z}} \\ \Gamma_{cr,H} &= -\frac{\nu(d - zy_0^{\pm})}{y_0^{\pm}} \frac{1}{H - H_c} \qquad \text{for} \quad |H - H_c|\, T^{-\frac{1}{\nu z}} \gg H_0 T_0^{-\frac{1}{\nu z}} \, . \end{aligned}} \tag{1.29}$$

The exponent $y_0^{\pm}$ is understood to be either y_0^+ or y_0^- for positive or positive control parameters, $p - p_c$ and $H - H_c$, respectively. All the exponents ν, z, d and $y_0^{\pm}$ (and the molar volume V_m) can be determined by available means. When they are known the Grüneisen parameter is unambiguously determined. The scaling analysis is thus not only able to determine the divergence but also its prefactor. In this sense the behavior of the Grüneisen parameter is universal in the low-temperature regime. This is the main result of this chapter. The underlying reason why the scaling analysis is so powerful here is the third law of thermodynamics, i.e. the absence of a residual entropy, which requires the expansion (1.25).

A possible application of the universal result (1.29) is for example the determination of the location of a putative quantum critical point. In principle, a measurement of the Grüneisen parameter at different pressures p allows extrapolation to the critical pressure p_c. Alternatively, systems such as heavy fermion materials can often be tuned to their quantum critical point either by pressure p or doping x. Assuming that they are related, $p - p_c \propto x - x_c$, measurements at ambient pressure on samples with different doping levels could lead to the determination of the critical doping x_c.

In the quantum critical regime Γ_{cr} can also be put to important experimental use, although the prefactor is not universal: (using hyperscaling $\phi = d + z$)

$$\begin{aligned} \Gamma_{cr,p} &= -\frac{z\,\Psi'_{\mathrm{QCR}}(0)}{d\,\Psi_{\mathrm{QCR}}(0)} \frac{1}{V_m p_0 T_0^{-\frac{1}{\nu z}}} T^{-\frac{1}{\nu z}} \qquad \text{for} \quad |p - p_c|\, T^{-\frac{1}{\nu z}} \ll p_0 T_0^{-\frac{1}{\nu z}} \, , \\ \Gamma_{cr,H} &= -\frac{z\,\Psi'_{\mathrm{QCR}}(0)}{d\,\Psi_{\mathrm{QCR}}(0)} \frac{1}{H_0 T_0^{-\frac{1}{\nu z}}} T^{-\frac{1}{\nu z}} \qquad \text{for} \quad |H - H_c|\, T^{-\frac{1}{\nu z}} \ll H_0 T_0^{-\frac{1}{\nu z}} \, . \end{aligned} \tag{1.30}$$

The striking feature is obviously the divergence with falling temperature with the exponent $1/(\nu z)$. The most important application is therefore the determination of the combination of critical exponents νz by measuring Γ_{cr}. In addition, the prefactor of this divergence allows an estimate of the crossover line in the (p, T) or (H, T) plane between the quantum critical and low-temperature regimes because it is inversely proportional to $p_0 T_0^{-\frac{1}{\nu z}}$ and $H_0 T_0^{-\frac{1}{\nu z}}$, respectively. The numerical prefactor $\frac{z\,\Psi'_{\mathrm{QCR}}(0)}{d\,\Psi_{\mathrm{QCR}}(0)}$ is expected to be of order one.

1.3.4 Restrictions

There are several restrictions which should be mentioned. They are listed below.

1. In an experiment usually $\Gamma_p = \alpha/c_p$ is measured, rather than the ratio of the critical contributions $\Gamma_{cr,p} = \alpha_{cr}/c_{cr,p}$. There may be leading non-critical contribution which have to be carefully subtracted in order to extract the scaling behavior of the Grüneisen parameter. A specific example, the Grüneisen parameter of $CeNi_2Ge_2$, is presented below.

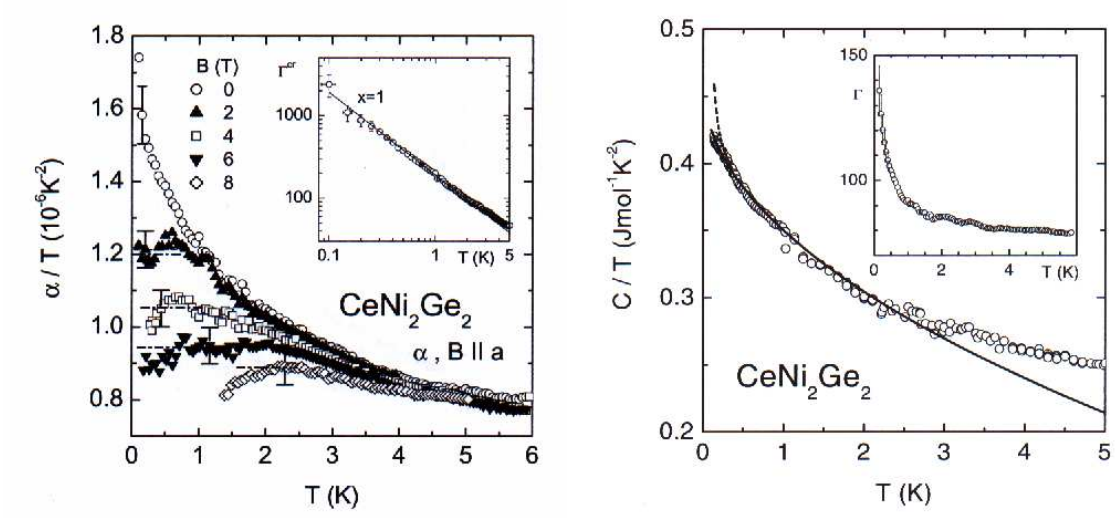

Figure 1.5: *Experimental data [22] showing thermal expansion and specific heat of $CeNi_2Ge_2$. They agree with the prediction of the scaling analysis for the quantum critical regime leading to a diverging Grüneisen parameter.*

2. There may be corrections to scaling. Generally, the scaling Ansatz (1.16) is expected to hold only below the upper critical dimension ($d+z < 4$ in ϕ^4 theories). Above the upper critical dimension corrections due to dangerously irrelevant operators may arise which can destroy scaling. In Chapter 2 it is shown for a particular case, the spin-density wave transition described by the Hertz model, that the corrections on the paramagnetic side are at most logarithmic. It is also worth mentioning that truly Gaussian theories also obey the scaling Ansatz (1.16).

3. The third caveat of our scaling treatment is of a more fundamental nature, and it concerns the underlying assumption of the scaling Ansatz (1.16). We assumed that at the quantum critical point only a single diverging time scale characterized by the dynamical exponent z plays a role. However, there might be scenarios where this assumption does not apply. For example, in a nearly magnetic metal there are two types of low-energy degrees of freedom, magnetic fluctuations and fermionic quasiparticles, both of which exhibit critical slowing down [19]. Furthermore, a local quantum critical point [20, 21], at which local degrees of freedom are driven critical by (critical) long-wavelength magnetic fluctuations in two dimensions, would also require a modification of the scaling Ansatz (1.16).

Nevertheless, for a wide class of quantum critical materials the considerations of the last section are applicable. Because of the many experimental possibilities it offers we expect that the Grüneisen parameter becomes a widely-used tool in the investigation of quantum criticality. Indeed, it has already been applied to two heavy fermion systems as outlined in the following.

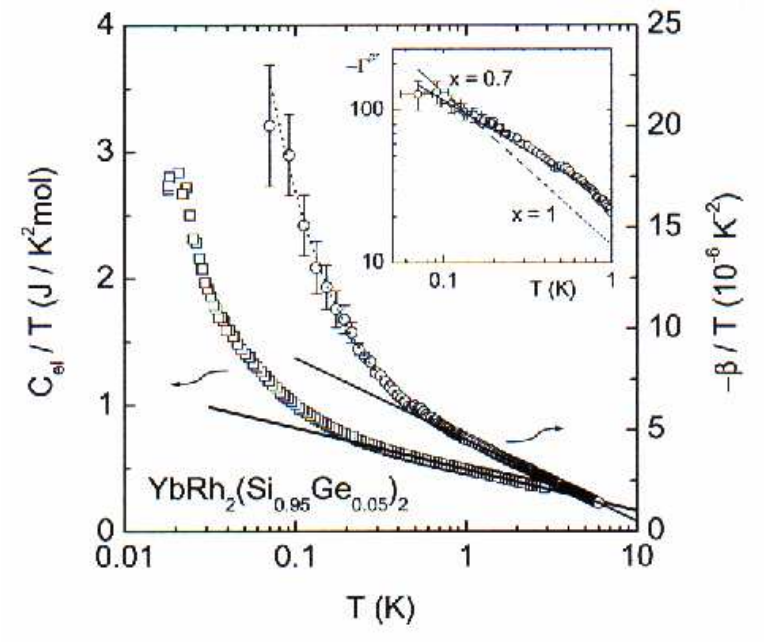

Figure 1.6: *Experimental data [22] showing thermal expansion and specific heat of* $YbRh_2(Si_{0.95}Ge_{0.05})_2$. *The Grüneisen parameter diverges,* $\Gamma_{cr} \propto T^{-x}$, *but the exponent* x *seems to be incompatible with the conventional spin-density wave scenario.*

1.4 Experiments

The theoretical prediction of a diverging Grüneisen parameter has already been tested experimentally by R. Küchler *et al.* [22] in two metallic heavy-fermion compounds exhibiting an antiferromagnetic quantum phase transition, $CeNi_2Ge_2$ and $YbRh_2Ge_2$. They are especially suited for studying quantum criticality since at ambient pressure they are located very near to the magnetic instability making them amenable to thermal expansion measurements. (Thermal expansion is rather difficult to measure under pressure.) Furthermore, they are stoichiometric and therefore clean with a low residual resistivity ensuring that the role of disorder is minimized.

In Fig. 1.5 the thermal expansion and the specific heat of a $CeNi_2Ge_2$ single crystal are shown. In zero magnetic field the thermal expansion divided by temperature is described by a non-Fermi liquid divergence $\alpha/T \sim 1/\sqrt{T}$ over more than two decades in temperature ranging from 6 K down to 50 mK. Only after applying a magnetic field does the divergence give way to the saturation expected for a Fermi liquid. This well-pronounced non-Fermi liquid behavior suggests that $CeNi_2Ge_2$ is quantum critical at ambient pressure, i.e. the critical pressure is $p_c \approx 0$. Below 3 K the specific heat coefficient can be well fitted with $c/T = \gamma_0 - c\sqrt{T}$, where the square root dependence on temperature is attributed to the quantum critical contribution. One has to be careful to subtract the non-critical contribution γ_0 in order to obtain the correct critical behavior of the Güneisen parameter Γ_{cr}. The inset of the graph showing the thermal expansion in Fig. 1.5 establishes that the exponent measured in the quantum critical regime for the Grüneisen parameter (1.30) is $1/(\nu z) = 1$. These experimental findings agree with a conventional three-dimensional antiferromagnetic spin-density wave scenario described by the Hertz model (see Chapter 2): $\nu = 1/2$, $z = 2$ and $\phi = d + z = 5$. Taking into account

for the molar volume V_m the dimensionful prefactor of the critical Güneisen parameter (1.30) has been determined [23] to be $T_0/p_0 \sim 1.5$ K/GPa. This identifies the crossover line in the pressure–temperature phase diagram between the quantum critical and the low-temperature, Fermi-liquid regime. It remains to be seen if this can be confirmed by directly measuring the pressure induced crossover to Fermi-liquid behavior in $CeNi_2Ge_2$.

Previous measurements [24] on the stoichiometric compound $YbRh_2Ge_2$ have revealed a very small Néel temperature T_N of about 65 mK, which can be further suppressed by doping it slightly with Ge. Fig. 1.6 shows the thermal expansion and specific heat of $YbRh_2(Si_{0.95}Ge_{0.05})_2$ of R. Küchler *et al.* [22]. It can be clearly seen that at an energy scale of about 300 mK the thermodynamic behavior changes. Up to now it is not yet clear which physical mechanism is associated with this energy scale. Nevertheless, the critical behavior is assumed to set in only below 300 mK. The Grüneisen parameter is again found to diverge. The extracted exponent $1/(\nu z) = 0.7$ however has to be taken with a pinch of salt since the fit included data points well *above* the existing temperature scale of 300 mK. Nevertheless, it seems that the divergence cannot be explained in the framework of an antiferromagnetic spin-density wave instability which would require an exponent $1/(\nu z) = 1$.

Chapter 2

Hertz Theory and Millis RG

In a seminal paper J. A. Hertz [4] pointed out the importance of quantum phase transitions for the physics at finite temperatures. After 30 years the model he considered has become the standard theory for magnetic instabilities in itinerant electronic systems at zero temperature. Its finite-temperature properties have been derived within a renormalization group treatment (RG) developed by A. J. Millis [5]. Its most prominent feature is the non-Fermi liquid behavior above the zero-temperature instability , and it is used to describe several experiments on heavy fermion compounds.

In Section 2.1 we shortly review the Hertz model. The RG treatment proposed by A. J. Millis will be presented in Section 2.2. Some subtle points in its derivation will be discussed and minor errors appearing in the original paper [5] corrected. The solution of the RG equations is given in the following chapter, where we compare the results for the thermal expansion and Grüneisen parameter with the scaling treatment of Chapter 1.

2.1 Hertz' effective action

The treatment of Hertz starts by considering the Hubbard interaction Hamiltonian. Its local density–density interaction can be separated into a charge- and spin-density part

$$H_{\text{Hubbard}} = U \sum_i n_{i\uparrow} n_{i\downarrow} = \frac{U}{2} \sum_i \left(n_{i\uparrow} + n_{i\downarrow}\right) - \frac{U}{2} \sum_i \left(n_{i\uparrow} - n_{i\downarrow}\right)^2 , \tag{2.1}$$

where i labels the number of sites. Near a spin-density wave transition the charge density fluctuations will be very fast in comparison to the critical slow modes and can be neglected. Furthermore, the spin-density part can be recast into a form where the spin rotation symmetry is manifest. This can be achieved by using the Fierz identity for Pauli matrices [25]

$$\boldsymbol{\sigma}_{\alpha\beta} \boldsymbol{\sigma}_{\gamma\delta} = \delta_{\alpha\beta}\delta_{\gamma\delta} - 2\,\epsilon_{\alpha\gamma}\epsilon_{\beta\delta} \tag{2.2}$$

where $\boldsymbol{\sigma}$ is the three-component vector of Pauli matrices and ϵ is the antisymmetric tensor. With this identity the spin-density part of the Hubbard interaction can be rewritten as

$$H_{\text{SDW}} = -\frac{U}{2} \sum_i \left(n_{i\uparrow} - n_{i\downarrow}\right)^2 = -J \sum_i \left(\sum_{\alpha\beta} \Psi^\dagger_{i\alpha} \frac{1}{2} \boldsymbol{\sigma}_{\alpha\beta} \Psi_{i\beta} \right)^2 \tag{2.3}$$

where Ψ is the electron operator and the exchange coupling $J = 2U/3$. In the continuum limit the corresponding partition function is given by $Z = \int \mathcal{D}\Psi^* \mathcal{D}\Psi \; e^{-\mathcal{S}}$ with the action

$$\begin{aligned} \mathcal{S} &= \int_0^\beta d\tau d\tau' \int d\mathbf{r} d\mathbf{r}' \sum_\sigma \Psi^*_\sigma(\tau,\mathbf{r}) g_0^{-1}(\tau-\tau',\mathbf{r}-\mathbf{r}') \Psi_\sigma(\tau',\mathbf{r}') \\ &\quad - J \int_0^\beta d\tau \int d\mathbf{r} \left(\sum_{\alpha\beta} \Psi^*_\alpha(\tau,\mathbf{r}) \frac{1}{2} \boldsymbol{\sigma}_{\alpha\beta} \Psi_\beta(\tau,\mathbf{r}) \right)^2 . \end{aligned} \tag{2.4}$$

The Fourier transform of the free electron Green function is $g_0(i\omega_n,\mathbf{k}) = [-i\omega_n + \xi_\mathbf{k}]^{-1}$, where $\xi_\mathbf{k}$ is the electron energy with respect to the chemical potential. The spin-density coupling of fourth order in the fermions can be decoupled by applying a Hubbard–Stratonovich transformation[1] on the real spin-density field $\sqrt{J/2}\sum_{\alpha\beta} \Psi^*_\alpha \boldsymbol{\sigma}_{\alpha\beta} \Psi_\beta$,

$$Z = Z_\Psi \left\langle \exp\left[-\int_0^\beta d\tau \int d\mathbf{r} \sum_{\alpha\beta} \Psi^*_\alpha(\tau,\mathbf{r}) \left[-\sqrt{\frac{J}{2}} \boldsymbol{\sigma}_{\alpha\beta} \Phi(\tau,\mathbf{r}) \right] \Psi_\beta(\tau,\mathbf{r}) \right] \right\rangle_{\Psi,\Phi} . \tag{2.5}$$

The average has to be taken with respect to the real bosonic Hubbard–Stratonovich field Φ, which is a three-component vector, and the fermionic field Ψ,

$$\langle \hat{\mathcal{O}} \rangle_\Phi \equiv \frac{1}{Z_\Phi} \int \mathcal{D}\Phi \; \hat{\mathcal{O}} \exp\left[-\frac{1}{2} \int_0^\beta d\tau \int d\mathbf{r} \, \Phi^2(\tau,\mathbf{r}) \right] \tag{2.6}$$

$$\langle \hat{\mathcal{O}} \rangle_\Psi \equiv \frac{1}{Z_\Psi} \int \mathcal{D}\Psi^* \mathcal{D}\Psi \; \hat{\mathcal{O}} \exp\left[-\int_0^\beta d\tau d\tau' \int d\mathbf{r} d\mathbf{r}' \sum_\sigma \Psi^*_\sigma(\tau,\mathbf{r}) g_0^{-1}(\tau-\tau',\mathbf{r}-\mathbf{r}') \Psi_\sigma(\tau',\mathbf{r}') \right] \tag{2.7}$$

with $Z_\Phi = \langle 1 \rangle_\Phi$ and $Z_\Psi = \langle 1 \rangle_\Psi$. The bosonic and the fermionic fields are coupled and it is *a priori* not clear to which category the critical degrees of freedom belong. In the Hertz theory it is *assumed* that the critical modes are well described by the bosonic field alone in the sense that an expansion of the effective action in Φ is well-behaved. In Section 2.1.1 we will shortly comment on the validity of this assumption. The fermions are integrated out and one ends up with a Ginzburg–Landau free energy functional Ω for the Hubbard–Stratonovich field Φ:

$$\frac{Z}{Z_\Psi} = \frac{1}{Z_\Phi} \int \mathcal{D}\Phi \; e^{-\Omega[\Phi]} \qquad \text{with} \quad \Omega[\Phi] = \int_0^\beta d\tau \int d\mathbf{r} \frac{1}{2} \Phi^2(\tau,\mathbf{r}) - \operatorname{tr} \log\{1 - \mathbf{V}\mathbf{G_0}\} . \tag{2.8}$$

[1] The Hubbard–Stratonovich transformation for a real field $\vec{x}$ uses the identity

$$\int \frac{dx_1 dx_2 \ldots dx_n}{(2\pi)^{n/2}} \exp\left[-\frac{1}{2} \vec{x}^T A \vec{x} + \vec{x}^T \vec{y} \right] = (\det A)^{-1/2} \exp\left[\frac{1}{2} \vec{y}^T A^{-1} \vec{y} \right]$$

where A is a matrix.

The matrices $\mathbf{V}$ and $\mathbf{G_0}$ are given by

$$\mathbf{V} = \delta_{\tau,\tau'}\delta_{\mathbf{r},\mathbf{r}'}\sqrt{\frac{J}{2}}\boldsymbol{\sigma}_{\sigma,\sigma'}\Phi(\tau,\mathbf{r}) \tag{2.9}$$

$$\mathbf{G_0} = \delta_{\tau,\tau'}\delta_{\mathbf{r},\mathbf{r}'}\delta_{\sigma,\sigma'}g_0(\tau-\tau',\mathbf{r}-\mathbf{r}')\,. \tag{2.10}$$

The trace is therefore meant to extend over time, space and spin variables. The Hertz theory assumes that the field Φ fluctuates around a vanishing expectation value, i.e. it describes only the disordered phase. Generally, there are two classes of magnetic instabilities to be distinguished. In the case of a ferromagnetic instability the magnetic order is homogenous and the Fourier components of the order parameter field only carry small momenta. The ferromagnetic order parameter in space is represented by a *real* field with three components, $\Phi(\tau,\mathbf{R})$. On the other hand, in an antiferromagnet the critical degrees of freedom carry a finite wave vector $\pm\mathbf{Q}$,

$$\Phi(\tau,\mathbf{R}) = e^{i\mathbf{QR}}\Phi_{\mathbf{Q}}(\tau,\mathbf{R}) + e^{-i\mathbf{QR}}\Phi^*_{\mathbf{Q}}(\tau,\mathbf{R})\,. \tag{2.11}$$

The fluctuations around the modulated magnetic structure are in general described by a *complex* field, $\Phi_{\mathbf{Q}}(\tau,\mathbf{R})$. An exception is the commensurate antiferromagnet where a multiple of the modulation vector $\mathbf{Q}$ coincides with a lattice vector, in particular $e^{i2\mathbf{QR}} = 1$. One can easily convince oneself that in this case $\Phi^*_{\mathbf{Q}}(\tau,\mathbf{R}) = \Phi_{\mathbf{Q}}(\tau,\mathbf{R})$ and a real field suffices to describe the critical modes. More generally, the system might be instable against a non-homogenous magnetic structure characterized by several different modulation vectors. Such a critical theory comprises several in general complex fields, each associated with the corresponding ordering wave vector.

In the magnetically disordered phase the logarithm in expression (2.8) arising from the functional determinant of the electrons can be expanded in the fluctuations $\Phi = (\phi^1,\phi^2,\phi^3)$ around the disordered ground state. The interesting lowest order terms are listed below[2].

- First order

$$= -\mathrm{tr}\,\{(\mathbf{VG_0})\} = 0 \tag{2.12}$$

  The contribution of this diagram vanishes trivially in the absence of a magnetic field since the trace over spin indices gives zero, $\mathrm{tr}\{\sigma^i\} = 0$.

- Second order

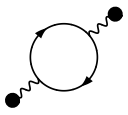

$$= -\frac{1}{2}\mathrm{tr}\left\{(\mathbf{VG_0})^2\right\} = \frac{J}{2}\frac{1}{\beta V}\sum_p \chi_{\mathrm{L}}(p)\Phi^T(p)\Phi(-p) \tag{2.13}$$

[2]The following spin traces are needed

$$\frac{1}{2}\mathrm{tr}\,\{\sigma^n\sigma^m\} = \delta^{nm}\,, \qquad \frac{1}{2}\mathrm{tr}\left\{\sigma^n\sigma^m\sigma^l\right\} = i\epsilon^{nml}\,, \qquad \frac{1}{2}\mathrm{tr}\left\{\sigma^n\sigma^m\sigma^l\sigma^k\right\} = \delta^{nm}\delta^{lk} - \delta^{nl}\delta^{mk} + \delta^{nk}\delta^{ml}\,.$$

We use the four-dimensional notation $p = (i\omega_n, \mathbf{k})$ for the fermionic Matsubara frequency and the momentum. The so-called Lindhard function χ_{L} is given by

$$\chi_{\mathrm{L}}(p) = \chi_{\mathrm{L}}(i\omega_n, \mathbf{k}) = -\frac{1}{\beta V} \sum_{\Omega_m, \mathbf{q}} g_0(i\Omega_m, \mathbf{q}) g_0(i\Omega_m + i\omega_n, \mathbf{q} + \mathbf{k}) \,. \tag{2.14}$$

where $\Omega_m = 2\pi m T$ is here and in the following always a bosonic Matsubara frequency. The Lindhard function is the basic fermionic vacuum loop and is also known as the polarization diagram [26].

- Third order

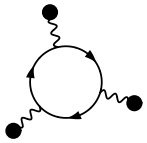

$$= -\frac{1}{3} \mathrm{tr} \left\{ (\mathbf{V}\mathbf{G}_\mathbf{0})^3 \right\} \tag{2.15}$$

$$= \frac{2}{3} \left(\frac{J}{2} \right)^{3/2} \frac{1}{\beta^3 V^3} \sum_{\substack{p_j \\ j=1,2,3}} \beta V \delta \left(\sum_{j=1}^{3} p_j \right) \chi^{(3)}(p_1, p_2, p_3)\, i\, \epsilon^{nml} \phi^n(p_1) \phi^m(p_2) \phi^l(p_3)$$

The three field components appear in an antisymmetric combination. As a consequence, the three-point correlation function $\chi^{(3)}(p_1, p_2, p_3)$ has to be antisymmetric with respect to each pair of its three arguments. This drastically restricts its behavior at large spatial and temporal distances, i.e. for small momenta and frequencies.

For a ferromagnetic instability a possible lowest-order term in a gradient expansion satisfying the antisymmetry conditions is

$$\chi^{(3)}(p_1, p_2, p_3) \approx \lambda \left((\mathbf{k}_1 - \mathbf{k}_2)(\mathbf{k}_3 - \mathbf{k}_1)(i\omega_{n2} - i\omega_{n3}) + \mathrm{cycl.\,perm.} \right) , \tag{2.16}$$

It leads to the following term in the Ginzburg–Landau functional for the field $\Phi(t, \mathbf{R})$:

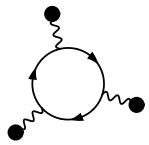

$$\approx \frac{2}{3} \left(\frac{J}{2} \right)^{3/2} 24\lambda \int d\mathbf{R}\, dt\, \nabla^2 \Phi(t, \mathbf{R}) \left(\frac{\partial}{\partial t} \Phi(t, \mathbf{R}) \times \Phi(t, \mathbf{R}) \right) . \tag{2.17}$$

However, according to power counting [27] this term is irrelevant in the renormalization group sense for the space dimensions of interest and can be neglected.

In the case of a non-homogenous magnetic instability the important critical degrees of freedom are the Fourier components of the field Φ with a momentum that fluctuates around finite ordering wave vectors. Depending on the symmetry of the non-homogenous magnetic structure there are two cases one has to distinguish. First let us assume that no three of the ordering wave vectors happen to add to zero. As a consequence, the fields Φ are required to carry collectively a rather large momentum fluctuation in order to fulfill the momentum conservation demanded by the delta function in (2.15). Such Fourier components of the fields do not however influence the critical behavior and the third-order term (2.15) can be discarded in the analysis of criticality. In particular,

this applies to the case of the antiferromagnet with a single ordering wavevector $\mathbf{Q}$. The second possibility is the special case of a magnetic modulation that allows for a combination of ordering wave vectors $\mathbf{Q}_1 + \mathbf{Q}_2 + \mathbf{Q}_3 = 0$. In such a case the third-order term (2.15) may be important.

- Fourth order

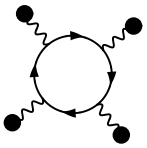

$$= -\frac{1}{4}\mathrm{tr}\left\{(\mathbf{V}\mathbf{G}_\mathbf{0})^4\right\} = \frac{1}{2}\left(\frac{J}{2}\right)^2 \frac{1}{\beta^4 V^4} \sum_{\substack{p_j \\ j=1,2,3,4}} \beta V \delta\left(\sum_{j=1}^{4} p_j\right) \tag{2.18}$$

$$\times \left(\delta^{nm}\delta^{kl} - \delta^{nk}\delta^{ml} + \delta^{nl}\delta^{mk}\right) \chi^{(4)}(p_1,p_2,p_3,p_4)\phi^n(p_1)\phi^m(p_2)\phi^k(p_3)\phi^l(p_4)$$

$$= \frac{1}{2}\left(\frac{J}{2}\right)^2 \frac{1}{\beta^4 V^4} \sum_{\substack{p_j \\ j=1,2,3,4}} \beta V \delta\left(\sum_{j=1}^{4} p_j\right) \chi_S^{(4)}(p_1,p_2,p_3,p_4)\phi^n(p_1)\phi^n(p_2)\phi^m(p_3)\phi^m(p_4)\,.$$

In the last line we introduced the symmetrized four-point correlation function, $\chi_S^{(4)}$, by incorporating the different contractions of the internal degrees of freedom of the fields. The unsymmetrized four-point correlation function is given by

$$\chi^{(4)}(p_1,p_2,p_3,p_4) = -\frac{1}{\beta V} \sum_{q=(i\Omega_n,\mathbf{q})} g_0(q)g_0(q+p_1)g_0(q+p_1+p_2)g_0(q+p_1+p_2+p_3)\,. \tag{2.19}$$

Its frequency and momentum dependence is irrelevant in the RG sense and can be neglected, reducing it to a local contact interaction. However, the resulting contribution to the Ginzburg–Landau functional depends on whether the magnetic structure is homogenous or not.

Up to irrelevant terms, for the ferromagnet we simply have

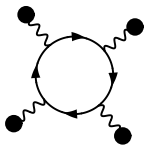

$$\approx \frac{1}{2}\left(\frac{J}{2}\right)^2 \chi^{(4)}(0,0,0,0) \int_0^\beta d\tau \int d\mathbf{R}\, \left(\Phi^T(\tau,\mathbf{R})\Phi(\tau,\mathbf{R})\right)^2\,. \tag{2.20}$$

Note that in contrast to the contribution of third order in the field Φ there are no symmetry restrictions which require the local contact interaction to vanish. (Loop and vertex corrections, however, lead to important corrections, see discussion of Section 2.1.1.) The situation is more elaborate in the case of an antiferromagnet. In order to satisfy the momentum conservation demanded by the delta function a field $\Phi_\mathbf{Q}$ of (2.11) is always accompanied by its complex conjugate $\Phi^*_\mathbf{Q}$. Taking into account all possible combination we finally arrive at the expression for the antiferromagnet

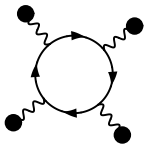

$$\approx \frac{1}{2}\left(\frac{J}{2}\right)^2 \frac{1}{\beta^4 V^4} \sum_{\substack{p_j \\ j=1,2,3,4}} \beta V \delta\left(\sum_{j=1}^{4} p_j\right) \tag{2.21}$$

$$\times \left(A\,\phi^{*n}_\mathbf{Q}(p_1)\phi^{*n}_\mathbf{Q}(p_2)\phi^m_\mathbf{Q}(p_3)\phi^m_\mathbf{Q}(p_4) + B\,\phi^{*n}_\mathbf{Q}(p_1)\phi^n_\mathbf{Q}(p_2)\phi^{*m}_\mathbf{Q}(p_3)\phi^m_\mathbf{Q}(p_4)\right)\,.$$

where we again neglected irrelevant terms. The constants, A and B, are given in terms of the four-point correlation function,

$$\begin{aligned} A =& \chi_S^{(4)}(\mathbf{Q},\mathbf{Q},-\mathbf{Q},-\mathbf{Q}) + \chi_S^{(4)}(-\mathbf{Q},-\mathbf{Q},\mathbf{Q},\mathbf{Q}) \\ B =& \chi_S^{(4)}(\mathbf{Q},-\mathbf{Q},\mathbf{Q},-\mathbf{Q}) + \chi_S^{(4)}(\mathbf{Q},-\mathbf{Q},-\mathbf{Q},\mathbf{Q}) + \chi_S^{(4)}(-\mathbf{Q},\mathbf{Q},-\mathbf{Q},\mathbf{Q}) \\ &+ \chi_S^{(4)}(-\mathbf{Q},\mathbf{Q},\mathbf{Q},-\mathbf{Q})\,. \end{aligned} \tag{2.22}$$

Only for the commensurate antiferromagnet does this fourth order interaction reduce to the simple form (2.20).

The theory originally proposed by Hertz considers only a real field Φ. It is therefore appropriate for the ferromagnet (with certain restrictions explained below) and the commensurate antiferromagnet. We extend the field to N components giving rise to an $O(N)$ internal symmetry and making the Hertz theory amenable to large N methods. Combining all important terms the Hertz theory reads[3]

$$Z_{\text{Hertz}} = \frac{Z}{Z_\Psi} = \frac{1}{Z_\Phi}\int \mathcal{D}\Phi\, e^{-S_{\text{Hertz}}[\Phi]} \tag{2.23}$$

$$S_{\text{Hertz}}[\Phi] = S^{(2)}[\Phi] + S^{(4)}[\Phi] \tag{2.24}$$

$$S^{(2)}[\Phi] = \frac{1}{\beta V}\sum_{\omega_n,\mathbf{k}} \frac{1}{2}\Phi^T(i\omega_n,\mathbf{k})\,\chi_0^{-1}(i\omega_n,\mathbf{k})\,\Phi(-i\omega_n,-\mathbf{k}) \tag{2.25}$$

$$S^{(4)}[\Phi] = g\int_0^\beta d\tau \int d\mathbf{R}\,\left(\Phi^T(\tau,\mathbf{R})\Phi(\tau,\mathbf{R})\right)^2\,. \tag{2.26}$$

The normalization $Z_\Phi = \sqrt{\det(\beta V)}$ in front of the path integral can alternatively be absorbed into a renormalization of the fields $\Phi(i\omega_n,\mathbf{k}) \to \sqrt{\beta V}\Phi(i\omega_n,\mathbf{k})$. In particular, this should be done in order to obtain the form of the Hertz theory as in Refs. [4] and [5]. We prefer not to do this final step and keep instead the familiar factors $1/(\beta V)$ in front of the Matsubara and momentum sums. The propagator in any case is given by χ_0 which derives from the low-frequency, low-momentum behavior of the Lindhard function (see Appendix A.2),

$$1 - J\chi_{\text{L}}(i\omega_n,\mathbf{k}) \approx \chi_0^{-1}(i\omega_n,\mathbf{k}) \equiv \delta_0 + \xi_0^2\,k^2 + \frac{|\omega_n|}{T_0 k^{z-2}} \tag{2.27}$$

where we introduce the dynamical scaling exponent z. For an antiferromagnetic instability the dynamical exponent is $z=2$ and for a ferromagnetic instability $z=3$. (Again, higher order corrections to the propagator are important, cf. Section 2.1.1.) The parameters δ_0, ξ_0, T_0 and the quartic coupling g depend on microscopic details. For the antiferromagnetic instability the exact correspondence between the bare parameters and the microscopic parameters depends

[3] For completeness we cite here the convention we use for the Fourier transform:

$$\begin{aligned} \Phi(\tau,\mathbf{R}) &= \frac{1}{\beta V}\sum_{\omega_n,\mathbf{k}} e^{i(\mathbf{k}\mathbf{R}-\omega_n\tau)}\,\Phi(i\omega_n,\mathbf{k}) \\ \Phi(i\omega_n,\mathbf{k}) &= \int d\mathbf{R}\int d\tau\, e^{-i(\mathbf{k}\mathbf{R}-\omega_n\tau)}\,\Phi(\tau,\mathbf{R}) \end{aligned}$$

on the specific band structure of the material under consideration. For a ferromagnetic instability, on the other hand they can be evaluated and are given by

$$\delta_0 = 1 - J\mathcal{N}_\mathrm{F} \tag{2.28}$$

$$\xi_0^2 = \frac{1}{12}\frac{\mathcal{N}_\mathrm{F}}{k_\mathrm{F}} \tag{2.29}$$

$$T_0 = \frac{2}{\pi}\frac{\mathrm{v}_\mathrm{F}}{\mathcal{N}_\mathrm{F}} \tag{2.30}$$

$$g = \frac{J^2}{8}\chi^{(4)}(0,0,0,0) = -\frac{J^2}{48}\int \frac{d\mathbf{q}}{(2\pi)^3}\frac{\partial^3}{\partial\xi_\mathbf{q}^3} f(\xi_\mathbf{q}) \approx \frac{J^2}{48}\mathcal{N}_\mathrm{F}'' \,. \tag{2.31}$$

The explicit value for ξ_0^2 has been obtained with the assumption of a quadratic energy dispersion $\epsilon_\mathbf{k} = \mathbf{k}^2/(2m^*)$. In the bare theory, i.e. on the level of perturbation theory, the ferromagnetic instability occurs if the mass vanishes, $\delta_0 = 1 - J\mathcal{N}_\mathrm{F} = 0$. This condition is just the well-known Stoner criterion.

2.1.1 Validity of the Hertz theory

In deriving the effective theory (2.23) we integrated out the electronic degrees of freedom and expanded in the magnetic order parameter Φ. We have already mentioned that in doing so we might have missed some important subtle physical features.

It was realized by D. Belitz, T. R. Kirkpatrick and and T. Vojta [28] that in the case of the ferromagnet in zero magnetic field this procedure is indeed doomed to fail. They pointed out that the Fermi liquid possesses soft particle–hole excitations that are distinct from the magnetic order parameter fluctuations but nevertheless might couple sufficiently strongly to the latter to influence their critical behavior. In the case of the ferromagnet these soft modes, which have been integrated out, show up as non-analyticities in higher order corrections to the polarization diagram [28, 29, 30] that have been neglected in the derivation of the last section. These non-analyticities render the resulting effective theory for the magnetic order parameter Φ non-local and hard to analyze. The Hertz theory in its simple form (2.23) therefore does not apply to the itinerant ferromagnet. However, in the presence of a magnetic field the SU(2)-spin rotational invariance is broken and, as a consequence, the non-analyticities are cut off. It is therefore believed that the Hertz theory with a dynamical scaling exponent $z = 3$ is the proper description for the quantum critical endpoint of magnetic first order transitions [31].

The antiferromagnet on the other hand has a non-homogenous order parameter and carries a non-zero ordering wavevector. The fermionic soft modes are only soft for a vanishing wavevector and their coupling to the antiferromagnetic fluctuations are not expected to spoil the Hertz theory. The effective theory (2.23) with a dynamical scaling exponent $z = 2$ therefore expected to describe correctly the quantum phase transition in itinerant (commensurate) antiferromagnets [32].

However, this issue remains contentious and is the subject of current research.

2.2 Millis' renormalization group treatment

In this section we review the renormalization group (RG) treatment of the Hertz action (2.23) introduced by A. J. Millis [5]. The main complication in the RG analysis of (2.23) is the inclusion of the Matsubara frequency dependence. Since the Matsubara frequency

at finite temperature is not a continuous variable like the momentum, the extension of for example Wilson's momentum shell RG to the dynamical, i.e., frequency-dependent part of the Hertz action is not straightforward. The solution of Millis was to perform the RG not on the Lagrangian level but rather directly on the free energy after converting all Matsubara sums into integrals.

2.2.1 Derivation of the RG equations

First consider the free energy due to the Gaussian part of (2.23) only. It is given by

$$\begin{aligned} e^{-\beta F_G} &= \frac{1}{Z_\Phi}\int \mathcal{D}\Phi\, e^{-S^{(2)}[\Phi]} = \left(\det \chi_0^{-1}\right)^{-1/2} \\ \Longrightarrow F_G &= \frac{N}{2\beta}\sum_{\omega_n,\mathbf{k}} \log \chi_0^{-1}(i\omega_n,\mathbf{k}) = \frac{N}{2\beta}\sum_{\omega_n,\mathbf{k}} \log\left\{\delta_0 + \xi_0^2\, k^2 + \frac{|\omega_n|}{T_0 k^{z-2}}\right\} \end{aligned} \tag{2.32}$$

The sum over Matsubara frequencies can be converted into an integral and (in the limit $V\to\infty$) is given by

$$F_G = -T_0\,\frac{N}{2}\,\frac{V}{\xi_0^d}\int^{\Lambda}\frac{d^d\mathbf{k}}{(2\pi)^d}\int_0^{\Gamma k^{z-2}}\frac{d\epsilon}{\pi}\coth\frac{T_0\epsilon}{2T}\arctan\frac{k^{2-z}\,\epsilon}{\delta_0+k^2} \tag{2.33}$$

where Λ and Γ are (dimensionless) cutoffs. The inclusion of the momentum in the upper limit of the energy integral in the case of a ferromagnet $z=3$ is not contained in the Hertz action as it stands (2.23). It is rather justified with hindsight, since we know that the natural cutoff for particle–hole excitations in the case of a ferromagnetic instability scales with momentum k (see Appendix A.2). Furthermore, the momentum and frequency integrals have been rescaled so that the parameters T_0 and ξ_0 can be absorbed in the measure of the free energy and the temperature. The microscopic length scale ξ_0 is presumably of the order k_{F}^{-1}. Note that the prefactor V/ξ_0^d in front of (2.33) is then basically the number of particle in the system, $Vk_{\mathrm{F}}^d \sim \mathcal{N}_A$. This implies that the free energy we are dealing with is not explicitly dependent on the volume. Its extensitivity is rather connected to the number of particles. Moreover, we can adopt the viewpoint that the mass is controlled by the pressure and we can identify the thermodynamic potential as the Gibbs free energy which is a function of temperature, pressure and particle number, $F = F(T,p,\mathcal{N})$. This will be important later when we analyze the thermal expansion. In the following it will be convenient to consider the dimensionless free energy density $\mathcal{F} = F\xi_0^d/(T_0 V)$ and the dimensionless temperature $\mathcal{T} = T/T_0$.

The correction to the Gaussian part of the free energy can be obtained with a linked cluster expansion in the quartic coupling g. Up to second order in u the result is (for details see Appendix A.3)

$$F = F_G + gN(N+2)I^2 + \frac{g^2}{2!}\left[8N(N+2)^2I^2J + 8N(N+2)K\right] + \mathcal{O}(g^3)\,, \tag{2.34}$$

where we have introduced the three functions

$$
\begin{aligned}
I =& \frac{1}{\beta V}\sum_{\omega_n,\mathbf{k}} \chi_0(i\omega_n,\mathbf{k})\,, \qquad J = -\frac{1}{\beta V}\sum_{\omega_n,\mathbf{k}} \chi_0(i\omega_n,\mathbf{k})\chi_0(-i\omega_n,-\mathbf{k})\,,\\
K =& -\frac{1}{(\beta V)^4}\sum_{\substack{\omega_{nj},\mathbf{k}_j\\ j=1,2,3,4}} V\delta\left(\sum_{i=1}^4 \mathbf{k}_i\right)\beta\delta\left(\sum_{i=1}^4 \omega_{in}\right)\\
&\times \chi_0(i\omega_{1n},\mathbf{k}_1)\chi_0(i\omega_{2n},\mathbf{k}_2)\chi_0(i\omega_{3n},\mathbf{k}_3)\chi_0(i\omega_{4n},\mathbf{k}_4)
\end{aligned}
\tag{2.35}
$$

expressed in terms of the propagator (2.27). The important point for the RG process is that the functions I and J are just derivatives of the Gaussian free energy (2.33) with respect to the bare mass δ_0, $I = (2/NV)\partial F_G/\partial\delta_0$ and $J = \partial I/\partial\delta_0$. At first sight the function K does not have this property. To understand its contribution in the Millis RG let us digress a moment to the usual momentum–shell RG. In the momentum-shell RG it is known [27, 18] that the second order diagram contributing to the renormalization of u,

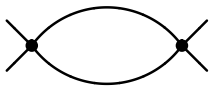

(2.36)

results in a momentum dependent quartic coupling. This means that the corresponding interaction in real space is non-local. However, this momentum dependence is known to be irrelevant [27] and only the momentum independent term is to be kept in the RG process. The contribution K now stems exactly from the diagram in the linked cluster expansion which is obtain by pairing the two open legs at one vertex of the above diagram with the legs of the other vertex,

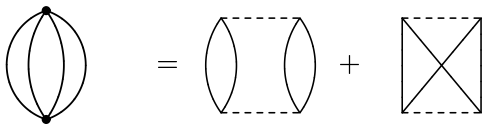

(2.37)

(It is actually a sum of two diagrams with different contractions of the internal indices of the fields involved; the dashed line represents the quartic interaction g. The first diagram on the right hand side of the equation is of order $\mathcal{O}(N^2)$ and the second diagram of order $\mathcal{O}(N)$ where N is the number of field components.) The momentum dependence which this diagram induces in the momentum-shell RG manifests itself in the structure of the function K: all four momenta and frequencies appear in the delta functions. The analogous step of neglecting the induced momentum dependence in the momentum-shell RG is to demand frequency- and momentum conservation, represented by the delta functions of K, only with respect to two frequencies and two momenta. However, there are $\binom{4}{2} = 6$ possibilities to choose two out of four,

$$
V\delta\left(\sum_{i=1}^4 \mathbf{k}_i\right)\beta\delta\left(\sum_{i=1}^4 \omega_{in}\right) \longrightarrow \binom{4}{2} V\delta\left(\mathbf{k}_1+\mathbf{k}_2\right)\beta\delta\left(\omega_{1n}+\omega_{2n}\right)\,. \tag{2.38}
$$

If we manipulate the delta functions in this way the function K collapses to $6I^2J$. Effectively, the function K thus leads to a contribution in the Millis RG process corresponding to $6I^2J$. The corrections are irrelevant in the RG sense. In Millis' original paper he swept these

subtleties under the carpet and as a starting point for the derivation of the RG equations used the expansion of the free energy with K substituted by $6I^2J$,

$$F = F_G + gN(N+2)I^2 + \frac{g^2}{2!}\,8N(N+2)(N+8)I^2J + \mathcal{O}(g^3) + \text{irrelevant terms}\,. \tag{2.39}$$

We do not want to dwell on the justification of the above statement but rather continue with the derivation of the RG equations. They are derived from (2.39) in the spirit of the momentum-shell RG but on the level of the free energy: a momentum shell $[\Lambda, \Lambda/b]$ is separated from the momentum integrals of the functions F_G, I and J. This shell will renormalize the bare mass δ_0 and the quartic coupling g. Afterwards the integrand is rescaled which, via the momentum dependence of the upper limit of the frequency integral, induces a second renormalization from the frequency shell. This finally yields the following RG equations[4]

$$\frac{\partial\,\mathcal{F}(b)}{\partial \log b} = (d+z)\,\mathcal{F}(b) - \frac{1}{2}\,N\,f_0(\delta(b),\mathcal{T}(b)) \tag{2.40}$$

$$\frac{\partial\,\mathcal{T}(b)}{\partial \log b} = z\,\mathcal{T}(b) \tag{2.41}$$

$$\frac{\partial\,\delta(b)}{\partial \log b} = 2\,\delta(b) + 4\,(N+2)\,u(b)\,f_2(\delta(b),\mathcal{T}(b)) \tag{2.42}$$

$$\frac{\partial\,u(b)}{\partial \log b} = (4-d-z)\,u(b) - 4\,(N+8)\,u^2(b)\,f_4(\delta(b),\mathcal{T}(b)) \tag{2.43}$$

where $\mathcal{F} = F\xi_0^d/(T_0V)$ is the dimensionless free energy (per particle), $u = g\xi_0^d/(T_0V)$ the dimensionless quartic coupling and $\mathcal{T} = T/T_0$ the dimensionless temperature. We have introduced the three functions

$$\begin{aligned} f_0(\delta,\mathcal{T}) &= K_d\Lambda^d \int_0^{\Gamma\Lambda^{z-2}} \frac{d\epsilon}{\pi}\,\coth\frac{\epsilon}{2\mathcal{T}}\arctan\frac{\Lambda^{2-z}\,\epsilon}{\delta+\Lambda^2} + \int^{\Lambda}\frac{d^dk}{(2\pi)^d}\,\frac{2\Gamma}{\pi}\,\coth\frac{\Gamma}{2\mathcal{T}}\arctan\frac{k^{2-z}\,\Gamma}{\delta+k^2} \\ f_2(\delta,\mathcal{T}) &= -\frac{\partial}{\partial\delta}\,f_0(\delta,\mathcal{T}) \\ f_4(\delta,\mathcal{T}) &= -\frac{\partial}{\partial\delta}\,f_2(\delta,\mathcal{T}) \end{aligned} \tag{2.44}$$

and

$$K_d = \int\frac{d\Omega}{(2\pi)^d} = \left(2^{d-1}\pi^{d/2}\Gamma(d/2)\right)^{-1} \tag{2.45}$$

is the surface of the d-dimensional sphere in momentum space. The first term of the function f_0 arises from the renormalization due to the separated momentum shell — momentum is set on shell $k = \Lambda$ — whereas the second term is the renormalization due to the frequency shell — frequency is set on shell $\epsilon = \Gamma$. It turns out that the main effect of the contribution of the

[4] The above RG equation differ from the equations in Millis' paper [5] in the following points. The factor $-N/2$ is missing in front of the function f_0. The minus sign stems from the transformation of the Matsubara sum to an integral in the expression for the Gaussian part of the free energy. The factor N comes from the summation over the internal degrees of freedom and the factor $1/2$ is due to the fact that the fields Φ are real and not complex. The inverse of the same factor $1/2$ is involved in the factor 4 in front of the function f_2 where Millis has only a factor of 2. Moreover, there is an additional factor of 2 in the function f_4 in comparison to Millis. Similar differences occur in the functions I and J defined above.

frequency shell is to renormalize zero temperature properties only. The additional corrections at finite temperatures due to the frequency shell are exponentially suppressed,

$$f_0(\delta,\mathcal{T}) - f_0(\delta,0) = K_d \Lambda^d \int_0^\infty \frac{d\epsilon}{\pi} \left(\coth\frac{\epsilon}{2\mathcal{T}} - 1\right) \arctan\frac{\Lambda^{2-z}\,\epsilon}{\delta+\Lambda^2} + \mathcal{O}(e^{-\Gamma/\mathcal{T}})\,. \tag{2.46}$$

The leading contribution to the thermodynamic quantities like specific heat and thermal expansion therefore comes from the temperature dependence due to the separated momentum-shell.

2.2.2 Classical limit

Technically speaking, the difference between the Hertz theory and the conventional "classical" ϕ^4-theory is the additional dependence on the Matsubara frequency of the Gaussian propagator (2.27). If we just neglect the non-zero Matsubara modes the remaining field corresponding to a Matsubara frequency $\omega_0 = 0$ is indeed governed by such a classical ϕ^4-theory. After rescaling this field by $\vec{\varphi}(\mathbf{k}) = \beta^{-1/2}\,\Phi(0,\mathbf{k})$ (cf. discussion after (2.23)), the action of the zero Matsubara mode reads

$$\begin{aligned} S_{\text{class}}[\varphi] &= \frac{1}{2V}\sum_{\mathbf{k}} \vec{\varphi}^T(\mathbf{k}) \left(\delta_0 + \xi_0^2 k^2\right) \vec{\varphi}(-\mathbf{k}) \\ &\quad + \frac{u}{\beta V^4} \sum_{\mathbf{k}_1,\mathbf{k}_2,\mathbf{k}_3,\mathbf{k}_4} V\delta\left(\sum_{i=1}^4 \mathbf{k}_i\right) \left(\vec{\varphi}^T(\mathbf{k}_1)\vec{\varphi}(\mathbf{k}_2)\right)\left(\vec{\varphi}^T(\mathbf{k}_3)\vec{\varphi}(\mathbf{k}_4)\right) \end{aligned} \tag{2.47}$$

with a "classical" quartic coupling which depends on temperature, $v \equiv u/\beta$. Formally, the Hertz theory thus reduces to the classical theory (2.47) when the influence of the non-zero Matsubara modes can be neglected. This is the case for temperatures larger than the energy cutoff , $\mathcal{T} \gg \Gamma\Lambda^{z-2}$. The Hertz theory and in particular the form of the propagator (2.27) is, of course, not justified in this limit and therefore should not be interpreted physically. (In its derivation we used the limiting behavior of the Lindhard function (2.14) for frequencies *less* than momentum, $\omega \ll k \ll 1$.) Nevertheless, in this limit the Millis RG equations should formally reduce to the well-known RG equations of the classical ϕ^4-theory. The consideration of this limit therefore provides a crosscheck for the validity of the Millis RG equations (2.40–2.43).

To reduce Millis' RG equations to the classical ones we substitute $u(b)$ by $v(b) = u(b)\,\mathcal{T}(b)$. Moreover, we have to take the high temperature limit of the f_n functions, which amounts to replacing the coth functions in the integrand by the inverse of their argument. After taking the limit $\Gamma \to \infty$ one ends up with the classical RG equations of ϕ^4 theory [18]

$$\frac{\partial\,\delta(b)}{\partial \log b} = 2\,\delta(b) + 4\,(N+2)\,v(b)\,\frac{K_d\Lambda^d}{\delta(b)+\Lambda^2}\,, \tag{2.48}$$

$$\frac{\partial\,v(b)}{\partial \log b} = (4-d)\,v(b) - 4\,(N+8)\,v^2(b)\,\frac{K_d\Lambda^d}{\left(\delta(b)+\Lambda^2\right)^2}\,. \tag{2.49}$$

As pointed out by S. Sachdev [2] for small but finite temperatures $0 < T \ll \Gamma\Lambda^{z-2}$ the effective theory is indeed given by (2.47), but with the *bare* parameters strongly renormalized by the non-zero Matsubara modes. This leads to a conceptually different point of view to the

Millis approach and we will refer the reader to Refs. [2, 33]. Nevertheless, if in the following the leading contribution of some quantity is due to the high-temperature limit of the f_n functions we will refer to it as resulting from "scaling into the classical regime".

2.2.3 Running mass and correlation length

The RG equation for the mass δ can formally be integrated. After separating the trivial scaling dimension of the mass $1/\nu = 2$ by substituting $\delta(b) = R(b)\, b^2$ we get

$$R(b) = \delta_0 + 4\,(N+2) \int_0^{\log b} dx\, e^{-2x}\, u(e^x)\, f_2(R(e^x)\, e^{2x}, \mathcal{T} e^{zx})\,, \tag{2.50}$$

where δ_0 is the bare mass appearing in the propagator χ_0 in (2.23). It is convenient to introduce the running mass at zero temperature,

$$\Delta(b) = \delta_0 + 4\,(N+2) \int_0^{\log b} dx\, e^{-2x}\, u(e^x)\, f_2(\Delta(e^x)\, e^{2x}, 0)\,. \tag{2.51}$$

Since we are interested only in the behavior of the theory in the vicinity of the quantum critical point we can expand in Δ,

$$\begin{aligned}\Delta(b) &\approx \delta_0 + 4\,(N+2)\; f_2(0,0) \int_0^{\log b} dx\, e^{-2x}\, u(e^x) - 4\,(N+2)\, f_4(0,0) \int_0^{\log b} dx\; u(e^x)\, \Delta(e^x) \\ &\sim (\delta_0 - \delta_c)\, \exp\left[-4\,(N+2)\, f_4(0,0) \int_0^{\log b} dx\, u(e^x)\right]\,. \end{aligned} \tag{2.52}$$

In the second line we already extracted the behavior of Δ for large scales b by solving the implicit equation of the first line, which can be identified with a first-order linear differential equation. In doing so, we introduced the critical bare mass δ_c, which identifies the position of the quantum critical point,

$$\delta_c = -4\,(N+2)\; f_2(0,0) \int_0^{\infty} dx\, e^{-2x}\, u(e^x)\,. \tag{2.53}$$

With the help of (2.51) we obtain the temperature correction to the running mass, which is of first order in the running quartic coupling u,

$$\begin{aligned} R(b) - \Delta(b) &= 4\,(N+2) \int_0^{\log b} dx\, e^{-2x}\, u(e^x)\; \big(f_2(R(e^x)\, e^{2x}, \mathcal{T} e^{zx}) - f_2(\Delta(e^x)\, e^{2x}, 0)\big) \\ &= R_T(b) + \delta R(b) = R_T(b) + \mathcal{O}(u^2)\,, \end{aligned} \tag{2.54}$$

where we have introduced the quantities

$$\delta R(b) = 4\,(N+2) \int_0^{\log b} dx\, e^{-2x}\, u(e^x)\; \big(f_2(R(e^x)\, e^{2x}, 0) - f_2(\Delta(e^x)\, e^{2x}, 0)\big)\,, \tag{2.55}$$

$$R_T(b) = 4\,(N+2) \int_0^{\log b} dx\, e^{-2x}\, u(e^x)\; \big(f_2(R(e^x)\, e^{2x}, \mathcal{T} e^{zx}) - f_2(R(e^x)\, e^{2x}, 0)\big)\,. \tag{2.56}$$

The contribution of the term δR is of higher order in u and has to be neglected. The running mass converges eventually for large scales to the correlation length,

$$R(b) = \Delta(b) + R_T(b) \simeq \xi^{-2}\,. \tag{2.57}$$

2.2.4 Quantum–classical crossover: Estimate of the critical temperature

It is tempting to determine the finite temperature phase transition in the (r, T) plane by the condition of a vanishing effective mass, $R(b) \simeq \xi^{-2}$,

$$\xi^{-2}(r, T) = 0 \qquad \text{at} \quad \mathcal{T} = \mathcal{T}_c(r)\,. \tag{2.58}$$

However, we will explain in the following why the parameter region where $\xi^{-2}(r, T) = 0$ is beyond the reach of the perturbative RG equations (2.40–2.43).

As we have already mentioned the phase transition at finite temperatures is governed by an effective *classical* ϕ^4 or Ginzburg–Landau theory. In such a theory the phase transition is identified with a sign change of the mass, $R \propto T - T_c$. Near the critical temperature T_c the thermodynamical quantities are very sensitive to variations in the mass. Hence, we can identify the quantum–classical crossover in the (r, T) plane by comparing different contributions to, for example, the specific heat: the quantum contribution which arises from the explicit temperature dependence of the Hertz propagator, and the classical contribution which arises from the sensitivity of the renormalized mass, R, to temperature variations. The RG trajectory of the running mass $R(b)$ itself depends on the temperature and it is this implicit temperature dependence which starts to dominate the thermodynamics at the quantum–classical crossover [34].

Below four space dimension, however, the finite temperature phase transition is not captured by the Gaussian fixed point, but is rather described by the Wilson–Fisher fixed point [35]. Therefore, there will be a further crossover in the $(r, \mathcal{T})$ plane from a Gaussian to the non–Gaussian behavior of the Wilson–Fisher fixed point. Since the physics embodied by the Wilson–Fisher fixed point is beyond the scope of the Millis RG analysis this crossover is associated with the breakdown of the perturbative Millis RG treatment. This Gaussian to non-Gaussian crossover is determined by the Ginzburg temperature (see below). So, strictly speaking, we are not able to locate the phase boundary since the region where $\xi^{-2}(r, T) = 0$ is beyond the applicability of the RG equations (2.40-2.43). Nevertheless, having pointed this out we still use the vanishing mass criterion in the following to get a first estimate of the location of the phase boundary.

2.2.5 Gaussian–non-Gaussian crossover: Ginzburg temperature

The Ginzburg temperature $\mathcal{T}_G(r)$ defines the Gaussian–non-Gaussian crossover in the (r, T) plane just alluded to. It is based on the Ginzburg criterion which can be formulated in several ways [18, 17]. It arises naturally when the effective classical Ginzburg–Landau theory in less than four space dimensions, which describes the finite temperature phase transition, is considered as a crossover phenomena. Upon approaching the phase boundary at a finite temperature the singular part of the free energy density will asymptotically satisfy the usual scaling form [16]

$$b^{-d} f_{\text{sing}}(R(b) b^{1/\nu}, v\, b^{y_v}) \sim [R(b)]^{\nu d}\, f_{\text{sing}}(1, v\, [R(b)]^{-\nu y_v}) \tag{2.59}$$

with the classical quartic coupling $v = u\,\mathcal{T}$ introduced in section 2.2.2. In the Gaussian region the exponents are given (up to logarithmic corrections) by the Landau values, $\nu = 1/2$ and $y_v = 4 - d$. The singular free energy exhibits a crossover depending on the size of the so-called Ginzburg parameter $v\, [R(b)]^{-\nu y_v}$. In the Gaussian region this parameter is small and can be treated perturbatively. In the non-Gaussian region, however, it becomes large and the

physics crosses over to the realm of the Wilson–Fisher fixed point. The crossover occurs at the Ginzburg temperature where the Ginzburg parameter attains a value of order one,

$$v\, R^{-\nu y_v} = u\, \mathcal{T}\, R^{\frac{d-4}{2}} \sim 1 \qquad \text{at} \quad \mathcal{T} = \mathcal{T}_G(r)\,. \tag{2.60}$$

The Ginzburg temperature $\mathcal{T}_G(r)$ defines a crossover line in the (r, T) plane of the phase diagram beyond which the Millis RG treatment breaks down. Consequently, in the non-Gaussian region beyond $\mathcal{T}_G(r)$ we cannot extract any reliable information from the perturbative RG treatment presented in this chapter.

2.2.6 Physical quantities

Free energy

Integrating the RG equation for the dimensionless free energy we can rewrite it as an integral along the RG trajectory, after accounting for the trivial scaling dimension $d + z$

$$\mathcal{F}(b)\, b^{-(d+z)} \overset{b\to\infty}{\longrightarrow} \mathcal{F} = -\frac{N}{2} \int_0^\infty dx\, e^{-(d+z)x}\, f_0(R(e^x)\, e^{2x}, \mathcal{T}\, e^{zx})\,. \tag{2.61}$$

Again we recall that $\mathcal{F}$ is the free energy measured in units of $T_0 V/\xi_0^d$. The important point to note is that the free energy $\mathcal{F}$ has an explicit temperature dependence via the second argument of the function f_0 and an implicit T dependence due to the running mass. The RG trajectory of $R(b)$ itself depends on T [cf. (2.50)] which has to be taken into account when computing the entropy.

Entropy

Correspondingly, there are two terms when the derivative with respect to temperature is taken (measuring the entropy in units of V/ξ_0^d),

$$S = -\frac{d\mathcal{F}}{d\mathcal{T}} = S_{\mathrm{QCP}} + S_{\mathrm{CL}}\,. \tag{2.62}$$

The first term is due to the partial derivative with respect to temperature,

$$S_{\mathrm{QCP}} = -\frac{\partial \mathcal{F}}{\partial \mathcal{T}} = \frac{N}{2} \int_0^\infty dx\, e^{-(d+z)x}\, \frac{\partial}{\partial \mathcal{T}} f_0(R(e^x)\, e^{2x}, \mathcal{T}\, e^{zx})\,, \tag{2.63}$$

and the subscript indicates that it is this term which leads to the peculiar temperature dependences typical for quantum critical phenomena. The second term stems from the implicit temperature dependence of the RG trajectory of the running mass,

$$S_{\mathrm{CL}} = -\frac{N}{2} \int_0^\infty dx\, e^{(2-d-z)x}\, f_2(R(e^x)\, e^{2x}, \mathcal{T}\, e^{zx}) \frac{dR_T(e^x)}{d\mathcal{T}}\,. \tag{2.64}$$

It is this term which is most singular near the phase boundary at finite T initiating the quantum–classical crossover.

Specific heat

We will consider here the specific heat coefficient $\gamma = C/T$, which is just the derivative of entropy with respect to temperature. We will measure the specific heat coefficient in units of $V/(\xi_0^d T_0)$ in the following. There are two important contributions to the specific heat. The quantum critical contribution is given by

$$\gamma_{\mathrm{QCP}} = \frac{\partial S_{\mathrm{QCP}}}{\partial \mathcal{T}} = \frac{N}{2} \int_0^\infty dx\, e^{-(d+z)x}\, \frac{\partial^2}{\partial \mathcal{T}^2} f_0(R(e^x)\, e^{2x}, \mathcal{T}\, e^{zx})\,. \tag{2.65}$$

Near the phase boundary the temperature sensitivity of the RG trajectory of the running mass takes over,

$$\gamma_{\mathrm{CL}} = \frac{N}{2} \int_0^\infty dx\, e^{(4-d-z)x}\, f_4(R(e^x)\, e^{2x}, \mathcal{T}\, e^{zx}) \left(\frac{dR_T(e^x)}{d\mathcal{T}} \right)^2 . \tag{2.66}$$

It should be noted that there is also another term, the partial derivative of S_{CL} with respect to temperature. However, the leading contribution in the quantum and classical regimes are γ_{QCP} and γ_{CL}, respectively. The quantum-classical crossover can be estimated by comparing these two contributions with each other.

Thermal expansion

The thermal expansion is defined as the change in volume as the system temperature is changed with pressure p and particle number $\mathcal{N}$ held constant:

$$\alpha = \frac{1}{V} \frac{\partial V}{\partial T}\bigg|_{p,\mathcal{N}} = \frac{1}{V} \frac{\partial^2 F}{\partial p\, \partial T} = -\frac{1}{V} \frac{\partial S}{\partial p}\bigg|_{T,\mathcal{N}} . \tag{2.67}$$

Using the Gibbs free energy, $F = F(T, p, \mathcal{N})$, we have rewritten the thermal expansion as a derivative of entropy with respect to pressure. Near a pressure tuned quantum critical point the control parameter is proportional to the distance to the critical pressure, $r = (p - p_c)/p_0$, where p_0 is an *a priori* unknown pressure scale. Up to a proportionality constant we recognize that the thermal expansion is actually the change of entropy upon variation of the control parameter r,

$$\alpha = -\frac{1}{V p_0} \frac{\partial S}{\partial r}\,. \tag{2.68}$$

From now on we will measure the thermal expansion in units of $1/(\xi_0^d p_0)$. Again we can distinguish between a contribution due to the quantum critical point,

$$\alpha_{\mathrm{QCP}} = -\frac{\partial S_{\mathrm{QPC}}}{\partial r} = \frac{N}{2} \int_0^\infty dx\, e^{(2-d-z)x}\, \frac{\partial R(e^x)}{\partial r} \frac{\partial}{\partial \mathcal{T}} f_2(R(e^x)\, e^{2x}, \mathcal{T}\, e^{zx})\,, \tag{2.69}$$

and a classical contribution dominating near the phase boundary,

$$\alpha_{\mathrm{CL}} = -\frac{\partial S_{\mathrm{CL}}}{\partial r} = -\frac{N}{2} \int_0^\infty dx\, e^{(4-d-z)x}\, f_4(R(e^x)\, e^{2x}, \mathcal{T}\, e^{zx}) \frac{dR_T(e^x)}{d\mathcal{T}} \frac{dR(e^x)}{dr}\,. \tag{2.70}$$

Grüneisen parameter

The thermodynamic Grüneisen parameter, Γ, is the ratio of the thermal expansion to the specific heat

$$\Gamma = \frac{\alpha}{T\gamma}\,. \tag{2.71}$$

In the following we will measure Γ in units $1/(Vp_0)$.

Chapter 3

Solution of Millis RG Equations

In this chapter the solution of the RG equations is obtained. The results obtained earlier by U. Zülicke and A. J. Millis [6] for the specific heat in three spatial dimensions are complemented by its calculation in 2D. The thermal expansion and the Grüneisen parameter presented here have not been calculated within Hertz' theory so far. We will compare the results with the prediction of the scaling treatment of Section 1.3.

The Hertz model can be successfully treated within a perturbative Millis RG treatment because for the physical systems of interest its effective dimension $d + z$ is above or at the upper critical dimension, $d + z \geq 4$, where the quartic coupling u is either an irrelevant or a marginal perturbation, respectively. In the Millis RG however not only the quartic coupling u is treated as a small parameter. We will also expand in the distance to the quantum critical point, which is measured by both the control parameter r and the temperature $\mathcal{T}$. In doing so we obtain universal finite temperature properties of the Hertz model associated with the fixed point of the quantum phase transition.

It turns out that space dimension $d = 2$ plays a special role. It is known from a theorem due to N. D. Mermin and H. Wagner [14] that generally in two space dimensions systems with a continuous symmetry and finite–range interactions do not show a spontaneous macroscopic magnetization at finite temperatures. The underlying reason is the existence of logarithmically divergent fluctuations of would-be Goldstone modes. Technically the divergence stems from the IR part of the momentum integral

$$\int dk\, k^{d-1} \frac{1}{m^2 + k^2} \sim -\log m \qquad \text{for} \quad m \to 0 \quad \text{in} \quad d = 2\,. \tag{3.1}$$

We will refer in the following to divergences of this kind as Mermin–Wagner divergences. In general, they appear in two space dimensions irrespective of the internal symmetry of the order parameter $O(N)$. The Mermin–Wagner divergence is reflected in logarithmic corrections to several thermodynamic quantities in $d = 2$.

For $N > 2$ there is indeed no magnetically ordered phase at finite temperatures in two space dimension, as one expects from the Mermin–Wagner theorem. However, the XY model has $N = 2$ and although in $d = 2$ there is no spontaneous macroscopic magnetization it does exhibit the peculiar Kosterlitz–Thouless transition, which is of topological nature. Finally, the infamous Ising model, $N = 1$, has only a $\mathbb{Z}_2$ symmetry and the Mermin–Wagner theorem does not apply. The continuous phase transition in two space dimension of the Ising model as well as the Kosterlitz–Thouless transition of the XY-model are, however, beyond the Millis RG approach and we will not perceive any signatures of the onset of order in these systems.

In order to familiarize the reader with the confusing number of crossovers in the (r, T) plane of the phase diagram we have sketched them in Fig. 3.1. The regime of applicability of the perturbative Millis RG is given by the region on the right-hand side of the Gaussian–non-Gaussian crossover line associated with the Ginzburg temperature $\mathcal{T}_G$. It will turn out that the quantum–classical crossover, where the leading behavior to the specific heat and the thermal expansion starts to stem from the sensitivity the effective mass [34], is located within the non-Gaussian region. Whereas for example in regions I, II and III the contribution $\alpha_{\rm QCP}$ (2.69) to the thermal expansion dominates, the contribution $\alpha_{\rm CL}$ (2.70) takes over only within region IV. The non-Gaussian region IV might be separated by the phase boundary from a magnetically ordered phase. We can only get an estimate for the phase boundary since it is located in a regime that is beyond the applicability of the perturbative RG. In particular, for space dimension $d = 2$ Mermin–Wagner divergences suppress this estimate to zero, suggesting that no ordered state exists at finite temperature. Regions II and III comprise the so–called quantum critical regime where the temperature dominates the thermodynamics, $\mathcal{T} \gg |r|^{\nu z}$. It is this regime which is associated with the peculiarity of the quantum critical point. The specific heat as well as the thermal expansion show here a pronounced non-Fermi liquid behavior. Region II and III are separated by a crossover in the behavior of the correlation length. Finally, the crossover to region I, $\mathcal{T} \ll |r|^{\nu z}$, is accompanied with a restoration of the usual Fermi liquid like dependences of the thermodynamics.

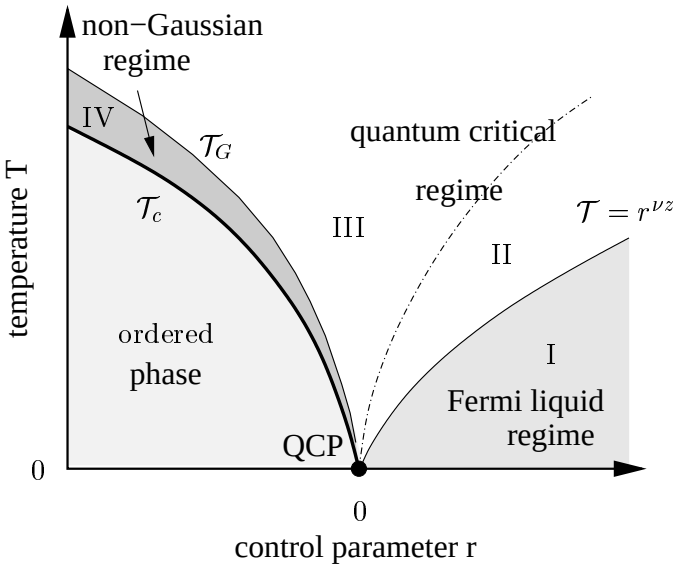

Figure 3.1: *Phase diagram of the Hertz model. I: Fermi liquid regime, II+III: quantum critical regime, IV: classical and non-Gaussian regime.*

The following sections are organized as follows. Initially, the quartic coupling, the correlation length and the Ginzburg temperature are calculated. First this is done for the system above its upper critical dimension, $d + z > 4$, and afterwards for $d + z = 4$, in which case additional logarithmic corrections to scaling are expected. After that thermodynamic quantities — specific heat, thermal expansion and the Grüneisen parameter — are determined in terms of the correlation length. In the final section the results are summarized and discussed.

3.1 Above the upper critical dimension: $d + z > 4$

3.1.1 Quartic coupling

Above the upper critical dimension, $d + z > 4$, the scaling dimension of the quartic coupling u is negative and the contribution of order $\mathcal{O}(u^2)$ in the RG equation (2.43) can be ignored.

The scale dependence of the quartic coupling is then given by

$$u(b) = u\, b^{4-d-z} \qquad \text{for} \quad d + z > 4\,, \tag{3.2}$$

where u is the bare quartic coupling of the theory.

3.1.2 Correlation length ξ

The expression for the running mass at zero temperature (2.52) can simply be integrated and yields,

$$\lim_{b\to\infty} \Delta(b) = (\delta_0 - \delta_c) \exp\left[\frac{4\,(N+2)\, f_4(0,0)\, u}{4-d-z}\right] \equiv r\,. \tag{3.3}$$

We introduced the control parameter $r \propto \delta_0 - \delta_c$ and absorbed the exponential factor into its units of measurements. The correlation length is given by equation (2.57),

$$\begin{aligned} \xi^{-2} \;&=\; \lim_{b\to\infty} \{\Delta(b) + R_T(b)\} = r + 4\,(N+2)\, K_d\, \Lambda^{d+z-4}\, \mathcal{T}^{\frac{2}{z}} \\ &\int_{\log \mathcal{T}^{1/z}/\Lambda}^{\infty} dx \int_0^{\infty} \frac{dv}{\pi} \frac{4\, v\, (\coth v - 1)\; e^{(-2+2z)x}\, u(e^x \Lambda \mathcal{T}^{-\frac{1}{z}})}{\left(R(e^x\Lambda\mathcal{T}^{-\frac{1}{z}})\mathcal{T}^{-2/z} e^{2x} + 1\right)^2 + (2\, e^{zx} v)^2}\,. \end{aligned} \tag{3.4}$$

We have made use of expression (2.46) for the f_n functions in deriving the leading contribution of the temperature dependent part R_T (2.56). The leading behavior of the remaining integral can be extracted in the two limits corresponding to the quantum critical regime, $r\,\mathcal{T}^{-2/z} \ll 1$, and the Fermi–liquid regime, $r\,\mathcal{T}^{-2/z} \gg 1$.

Quantum critical regime: $r\,\mathcal{T}^{-2/z} \ll 1$

We have to distinguish between the space dimensions $d = 2$ and $d > 2$.

$z > d - 2 > 0$: In the quantum critical regime for $d > 2$ we can neglect the dependence of the integrand in expression (3.4) on $R(.)\mathcal{T}^{-2/z}$. Moreover, we can extend the lower limit of the x-integral to minus infinity thereby neglecting contributions of order $\mathcal{O}\left(\Lambda\,\mathcal{T}^{-1/z}\right)^{(d-2)-z}$,

$$\xi^{-2} \;=\; r + 4\,(N+2)\, \frac{K_d}{z\, \cos\left(\frac{d-2}{2\,z}\pi\right)}\, \Gamma\left(1 + \frac{d-2}{z}\right)\, \zeta\left(1 + \frac{d-2}{z}\right) u\, \mathcal{T}^{\frac{d+z-2}{z}}\,. \tag{3.5}$$

where Γ is the Gamma function and ζ is the Zeta function[1]. We can subdivide the quantum critical regime further in two regimes where either the first or the second term dominates giving rise to the two sub-regimes II and III indicated in Fig. 3.1.

[1] The following integrals have been used:

$$\int_0^\infty dy \frac{(2y)^n}{\sinh^2 y} = 2\, n\Gamma(n)\, \zeta(n) \qquad \text{and} \qquad \int_0^\infty dy \frac{y^a}{1+y^2} = \frac{\pi}{2\, \cos(a\pi/2)}\,.$$

$d = 2$: As explained at length in the introduction, in two space dimension we have to struggle with Mermin–Wagner divergences (3.1). These divergences are associated with the effective classical theory and correspondingly we expect them to originate from the scaling into the classical regime, i.e. from the IR-part of the v-integral of (3.4) (cf. discussion in Section 2.2.2).

Consider only the double integral in (3.4) with the running coupling constant (3.2). In $d = 2$ the combination $R\,\mathcal{T}^{-2/z}$ acts as an IR-cutoff for the v-integral. Without this term the integral would diverge logarithmically. We can extract this logarithmic divergence by integrating by parts with respect to x,

$$-\int\limits_{\log \mathcal{T}^{1/z}/\Lambda}^{\infty} dx\, x\, \frac{d}{dx} \int\limits_{0}^{\infty} \frac{dv}{\pi} \frac{4\, v\, (\coth v - 1)\; e^{zx}}{\left(R(e^x \Lambda \mathcal{T}^{-\frac{1}{z}}) \mathcal{T}^{-2/z} e^{2x} + 1\right)^2 + (2\, e^{zx} v)^2}$$

where we set explicitly $d = 2$. The surface term is of order $\mathcal{O}(\mathcal{T}/\Lambda^z \log \mathcal{T}/\Lambda^z)$ and has been neglected. We expand the hyperbolic function for small v, evaluate the v-integral and obtain in leading order

$$-\int\limits_{\log \mathcal{T}^{1/z}/\Lambda}^{\infty} dx\, x\, \frac{d}{dx} \frac{1}{1 + R(e^x \Lambda \mathcal{T}^{-\frac{1}{z}}) \mathcal{T}^{-2/z} e^{2x}}\,.$$

To evaluate the remaining integral we will use a trick which proves to be useful throughout the rest of this chapter, and so we now explain it in some detail. After taking the derivative and multiplying both numerator and denominator with $\left(1 + \xi^{-2} \mathcal{T}^{-2/z} e^{2x}\right)^2$ we get,

$$\int\limits_{\log \mathcal{T}^{1/z}/\Lambda}^{\infty} dx\, \frac{x\, e^{2x}}{\left(1 + \xi^{-2} \mathcal{T}^{-2/z} e^{2x}\right)^2} \tag{3.6}$$

$$\times \left\{ \frac{\left(1 + \xi^{-2} \mathcal{T}^{-2/z} e^{2x}\right)^2}{\left(1 + R(e^x \Lambda \mathcal{T}^{-\frac{1}{z}}) \mathcal{T}^{-2/z} e^{2x}\right)^2} \left(2R(e^x \Lambda \mathcal{T}^{-\frac{1}{z}}) \mathcal{T}^{-2/z} + R'(e^x \Lambda \mathcal{T}^{-\frac{1}{z}}) e^x \Lambda \mathcal{T}^{-\frac{3}{z}}\right) \right\}.$$

The term in front of the curly brackets is a strongly peaked function with a maximum located at $x_{\max} \approx \log \xi \mathcal{T}^{1/z}$. Around this maximum the remaining term in the bracket is only slowly varying and the argument of the running mass at the maximum, $e^{x_{\max}} \Lambda \mathcal{T}^{-\frac{1}{z}} = \xi \Lambda \to \infty$, tends to infinity in the universal limit $\Lambda \to \infty$. That means that around the maximum the running mass has almost converged to its limiting value ξ^{-2}. The leading contribution can therefore be obtained by a saddle point approximation which in the universal limit $\Lambda \to \infty$ amounts to taking the slowly varying term in the bracket at the maximum value $x_{\max}$, giving

$$\int\limits_{-\infty}^{\infty} dx\, \frac{2\; x\; \xi^{-2} \mathcal{T}^{-2/z} e^{2x}}{\left(1 + \xi^{-2} \mathcal{T}^{-2/z} e^{2x}\right)^2} = \log \xi\, \mathcal{T}^{1/z}\,.$$

Putting this result in the formula for the correlation length we obtain for $d = 2$

$$\xi^{-2} \sim r + 4\,(N+2)\, \frac{K_d}{2}\, u\, \mathcal{T} \log \frac{1}{\xi^{-2}\, \mathcal{T}^{-2/z}} \tag{3.7}$$

Above the quantum critical point, $r=0$, we can solve the implicit equation for the correlation length iteratively and obtain in leading order

$$\xi^{-2}(r=0) = 4\,(N+2)\,\frac{K_d}{2}\,u\,\mathcal{T}\log\frac{1}{u\,\mathcal{T}^{1-2/z}} + \mathcal{O}\left(u\,\mathcal{T}\log\log\frac{1}{u\,\mathcal{T}^{1-2/z}}\right). \tag{3.8}$$

Fermi liquid regime: $r\,\mathcal{T}^{-2/z} \gg 1$

In the Fermi–liquid regime up to sub-leading temperature corrections the running mass in the integrand can be replaced for low temperatures by the control parameter r. The leading contribution of the remaining integral can then be evaluated,

$$\begin{aligned}\xi^{-2} &\approx r + 4\,(N+2)\,K_d\,u\,\mathcal{T}^{\frac{d+z-2}{z}} \int\limits_{\log \mathcal{T}^{1/z}/\Lambda}^{\infty} dx \int\limits_0^\infty \frac{dv}{\pi} \frac{4\,v\,(\coth v-1)\;e^{(2-d+z)x}}{\left(r\,\mathcal{T}^{-2/z}e^{2x}+1\right)^2+\left(2\,e^{zx}v\right)^2} \\ &= r + 4\,(N+2)\,K_d\,u\,\mathcal{T}^2\,r^{\frac{d-z-2}{2}} \int\limits_{\log r^{1/2}/\Lambda}^{\infty} dx \int\limits_0^\infty \frac{dv}{\pi} \frac{4\,v\,(\coth v-1)\;e^{(2-d+z)x}}{\left(e^{2x}+1\right)^2+\left(2\,\mathcal{T}r^{-z/2}e^{zx}v\right)^2}\end{aligned} \tag{3.9}$$

To lowest order the term $\mathcal{T}r^{-z/2}$ can be neglected in the denominator of the integrand. Moreover, for $2-d+z>0$ the lower limit of the x-integral can be extended to minus infinity inducing an error of order $\mathcal{O}\left(r^{1/2}/\Lambda\right)^{2-d+z}$. For $2-z+d>0$ the remaining x-integral is convergent and we obtain

$$\begin{aligned}\xi^{-2} &\approx r + 4\,(N+2)\,K_d\,u\,\mathcal{T}^2\,r^{\frac{d-z-2}{2}} \int\limits_{-\infty}^{\infty} dx \int\limits_0^\infty \frac{dv}{\pi} \frac{4\,v\,(\coth v-1)\;e^{(2-d+z)x}}{\left(e^{2x}+1\right)^2} \\ &= r + 4\,(N+2)\,\frac{\pi^2}{12}\,\frac{d-z}{\sin\left(\frac{d-z}{2}\,\pi\right)}\,K_d\,u\,\mathcal{T}^2\,r^{\frac{d-z-2}{2}}\end{aligned} \tag{3.10}$$

where the temperature dependent contribution is sub-leading.

3.1.3 Estimate of the critical temperature

We can obtain an estimate for the critical temperature $\mathcal{T}_c(r)$ from the criterion (2.58) that the correlation length is infinite at $\mathcal{T}_c$. We find that this can only be fulfilled for negative values of the control parameter, $r<0$. As explained in detail in Section 2.2.4, the value of $\mathcal{T}_c$ determined in this way is only an estimate since it falls into regime beyond the applicability of the Millis RG approach. We will distinguish between the cases $d>2$ and $d=2$.

Critical temperature for $d>2$

Using the expression for the correlation length (3.5) we obtain the critical temperature

$$r = -\frac{4\,(N+2)\,K_d}{z\,\cos\left(\frac{d-2}{2\,z}\,\pi\right)}\,\Gamma\left(1+\frac{d-2}{z}\right)\,\zeta\left(1+\frac{d-2}{z}\right)\,u\,\mathcal{T}_c^{\frac{d+z-2}{z}}. \tag{3.11}$$

Critical temperature for $d = 2$

The Mermin–Wagner divergencies (3.1) in two space dimensions prohibit a solution of $\xi^{-2} = 0$ at finite temperatures. It appears that no ordered phase exists at finite temperatures. According to (3.7) the effective mass ξ^{-2} decreases exponentially for $r < 0$ upon lowering the temperature but never vanishes at finite temperatures,

$$\xi^{-2} \propto \mathcal{T}^{2/z} e^{-\frac{\pi |r|}{(N+2)u\mathcal{T}}} . \tag{3.12}$$

3.1.4 Ginzburg temperature

The Ginzburg temperature (2.60) determines the crossover line between Gaussian to non-Gaussian behavior, see Fig. 3.1. With the results for the correlation length (3.5) and (3.7) we can determine $\mathcal{T}_G(r)$. Again we distinguish between the cases $d = 2$ and $d > 2$.

$d > 2$: Putting the expression (3.5) for the correlation length into the definition (2.60) we get an equation which implicitly defines $\mathcal{T}_G(r)$,

$$u\,\mathcal{T}_G = \left(r + \frac{4\,(N+2)\,K_d}{z\,\cos\left(\frac{d-2}{2\,z}\pi\right)} \Gamma\left(1+\frac{d-2}{z}\right) \zeta\left(1+\frac{d-2}{z}\right) u\,\mathcal{T}_G^{\frac{d+z-2}{z}} \right)^{\frac{4-d}{2}} . \tag{3.13}$$

The Ginzburg temperature differs from the critical temperature (3.11) by

$$\frac{\mathcal{T}_G - \mathcal{T}_c}{\mathcal{T}_c} \approx \frac{\frac{z^2}{d+z-2}\,\cos\left(\frac{d-2}{2\,z}\pi\right)}{4\,(N+2)\,K_d\,\Gamma\left(1+\frac{d-2}{z}\right)\,\zeta\left(1+\frac{d-2}{z}\right)} \left(u\mathcal{T}_c\right)^{\frac{d-2}{4-d}} \mathcal{T}_c^{\frac{2-d}{z}} . \tag{3.14}$$

$d = 2$: Putting the definition of the Ginzburg temperature for $d = 2$, $\xi^{-2} = u\mathcal{T}_G(r)$, into the expression for the correlation length (3.7) we obtain

$$r = u\,\mathcal{T}_G \left(1 - 4\,(N+2)\,K_d\,\frac{1}{2}\log\frac{1}{u\,\mathcal{T}_G^{\frac{z-2}{z}}} \right) . \tag{3.15}$$

3.2 At the upper critical dimension: $d + z = 4$

This section considers two-dimensional spin fluctuations in a antiferromagnetic metal, $d = z = 2$. The corresponding Hertz theory is at its upper critical dimension, and it is plagued by logarithmic corrections of different origin.

3.2.1 Quartic coupling

At the upper critical dimension the quartic coupling is marginal and we have to take into account the u^2-term in its differential equation (2.43). The solution reads

$$u(b) = \frac{u}{1 + 4(N+8)\,u\,g(b)} \qquad \text{for} \quad d+z=4 \tag{3.16}$$

$$g(b) = \int_0^{\log b} dx\, f_4(R(e^x)e^{2x}, Te^{zx}) . \tag{3.17}$$

In the vicinity of the quantum critical point, i.e. for small temperatures and small running mass, the quartic coupling is given approximately by

$$u(b) \approx \frac{u}{1+4(N+8)\,u\,f_4\,\log b} = \frac{1}{4(N+8)\,f_4}\left(\log b\; e^{\frac{1}{4(N+8)\,f_4\,u}}\right)^{-1}, \tag{3.18}$$

where

$$f_4 \equiv f_4(0,0) = \frac{K_2}{\pi}. \tag{3.19}$$

Note that f_4 is independent of the cutoffs Λ and Γ, i.e. it is universal. It is the product of the surface of the two-dimensional sphere in momentum space, K_2 (2.45), and the surface of the sphere in frequency space, $1/\pi$.

3.2.2 Correlation length ξ

In contrast to the case $d+z>4$, the exponential factor in the expression for the running mass at zero temperature (2.52) now does not converge leading to a scale dependent mass gap,

$$\Delta(b) = \frac{r}{\left(\log\left[b^2\; e^{\frac{2}{4(N+8)\,f_4\,u}}\right]\right)^{\frac{N+2}{N+8}}} \qquad \text{with} \quad r \equiv \frac{\delta_0-\delta_c}{(2(N+8)f_4u)^{\frac{N+2}{N+8}}}. \tag{3.20}$$

The logarithmic dependence of the zero-temperature mass Δ on the scale b is characteristic for a ϕ^4 theory at the upper critical dimension, $d+z=4$. For $\epsilon = 4-d+z>0$ the correlation length exponent ν will deviate from its Landau value $1/2$ and the leading correction is known to be linear in ϵ, see e.g. Ref. [36]. At the upper critical dimension, $\epsilon=0$, logarithmic corrections to scaling occur and are materialized in the scale dependence of Δ. In particular, that means that we cannot simply take the limit $b\to\infty$ neither in the expression for the rescaled quartic coupling (3.18) nor in the expression for the mass gap Δ. Choosing the scale $\Delta(b)b^2=\Lambda^2$ we obtain the following correction to the correlation length exponent ν

$$\Delta(b) = \frac{r}{\left(\log\frac{\bar\Lambda^2}{\Delta(b)}\right)^{\frac{N+2}{N+8}}} \qquad \Longrightarrow \qquad 2\nu \equiv \frac{\partial\log\Delta}{\partial\log r} = \left[1-\frac{\frac{N+2}{N+8}}{\log\frac{\bar\Lambda^2}{\Delta(b)}}\right]^{-1} \tag{3.21}$$

where we have introduced a "renormalized" cutoff $\bar\Lambda$, which depends on the bare quartic coupling constant u,

$$\bar\Lambda \equiv \Lambda\, e^{\frac{\pi}{4(N+8)\,K_2\,u}}. \tag{3.22}$$

The expression for ν agrees with the result of the epsilon expansion of the ϕ^4 theory [36] if we identify $\epsilon = 1/\log\frac{\bar\Lambda}{\sqrt{\Delta(b)}}$. At finite temperature we will instead choose the scale $R(b)b^2=\Lambda^2$ and identify the correlation length with

$$\xi^{-2}b^2 \simeq R(b)b^2 = \Lambda^2 \qquad \Longrightarrow \qquad R(\xi\Lambda)\simeq\xi^{-2}. \tag{3.23}$$

In the following the limiting behavior of the temperature correction (2.56) will be evaluated, ($R_T = \lim_{b\to\infty} R_T(b)$),

$$R_T = 4\,(N+2)\,K_2\,\mathcal{T}\int\limits_{\log\mathcal{T}^{1/2}/\Lambda}^{\infty} dx \int\limits_0^\infty \frac{dv}{\pi}\frac{4\,v\,(\coth v-1)\;e^{2x}\,u(e^x\Lambda\mathcal{T}^{-\frac12})}{\left(R(e^x\Lambda\mathcal{T}^{-\frac12})\mathcal{T}^{-1}e^{2x}+1\right)^2+(2\,e^{2x}v)^2}. \tag{3.24}$$

Quantum critical regime: $r\left(\log\frac{\bar\Lambda^2}{r}\right)^{-\frac{N+2}{N+8}} \ll \mathcal{T}$

The same arguments as in the analysis above the upper critical dimension in $d=2$ lead to the leading behavior,

$$\begin{aligned} R_T &\sim -4\,(N+2)\,K_2\,\mathcal{T}\int\limits_{\log\mathcal{T}^{1/2}/\Lambda}^{\infty} dx\,x\,\frac{d}{dx}\frac{u(e^x\Lambda\mathcal{T}^{-\frac{1}{2}})}{1+R(e^x\Lambda\mathcal{T}^{-\frac{1}{2}})\mathcal{T}^{-1}e^{2x}} \\ &\sim 4\,(N+2)\,K_2\,\mathcal{T}\int\limits_{\log\mathcal{T}^{1/2}/\Lambda}^{\infty} dx\,\frac{2x\;u(e^x\Lambda\mathcal{T}^{-\frac{1}{2}})R(e^x\Lambda\mathcal{T}^{-\frac{1}{2}})\mathcal{T}^{-1}e^{2x}}{\left(1+R(e^x\Lambda\mathcal{T}^{-\frac{1}{2}})\mathcal{T}^{-1}e^{2x}\right)^2}\,. \end{aligned} \tag{3.25}$$

In contrast to what happens above the upper critical dimension, the running quartic coupling constant now is only logarithmically varying. The integrand can thus be separated into a product of a strongly peaked function at the position $x_{\max}=\log\xi\mathcal{T}^{1/z}$ and a slowly varying part which includes the quartic coupling u. Applying a saddle point approximation we obtain

$$R_T \sim 4\,(N+2)\,K_2\,\mathcal{T}u(e^{x_{\max}}\Lambda\mathcal{T}^{-\frac{1}{2}})x_{\max}\,. \tag{3.26}$$

Using the expression (3.18) for the running quartic coupling we obtain the implicit equation for the correlation length

$$\xi^{-2} \simeq \Delta(\xi\Lambda)+\pi\,\frac{N+2}{N+8}\,\mathcal{T}\,\frac{\log\left(\xi^2\mathcal{T}\right)}{\log\left(\xi^2\bar\Lambda^2\right)} = \frac{r}{\left(\log\left(\xi^2\bar\Lambda^2\right)\right)^{\frac{N+2}{N+8}}}+\pi\,\frac{N+2}{N+8}\,\mathcal{T}\,\frac{\log\left(\xi^2\mathcal{T}\right)}{\log\left(\xi^2\bar\Lambda^2\right)}\,. \tag{3.27}$$

There exist a sub-regime II (see Fig. 3.1) where the control parameter still governs the correlation length,

$$\xi^{-2}\sim\begin{cases} \dfrac{r}{\left(\log\frac{\bar\Lambda^2}{r}\right)^{\frac{N+2}{N+8}}} & \text{if} \quad \text{II:} \qquad \mathcal{T}^{\frac{\log\log\frac{\bar\Lambda^2}{\mathcal{T}}}{\log\frac{\bar\Lambda^2}{\mathcal{T}}}} \ll r\left(\log\frac{\bar\Lambda^2}{r}\right)^{-\frac{N+2}{N+8}} \\ \pi\,\dfrac{N+2}{N+8}\mathcal{T}\dfrac{\log\log\frac{\bar\Lambda^2}{\mathcal{T}}}{\log\frac{\bar\Lambda^2}{\mathcal{T}}} & \text{if} \quad \text{III:} \qquad r\left(\log\frac{\bar\Lambda^2}{r}\right)^{-\frac{N+2}{N+8}} \ll \mathcal{T}^{\frac{\log\log\frac{\bar\Lambda^2}{\mathcal{T}}}{\log\frac{\bar\Lambda^2}{\mathcal{T}}}}\,. \end{cases} \tag{3.28}$$

Note that the asymptotic expansion in the regime III is not very revealing since the convergence is very slow. It is only meaningful in the negligible small sub-region of III where $\log\log\frac{\bar\Lambda^2}{\mathcal{T}}\gg 1$.

Fermi liquid regime: $r\left(\log\frac{\bar\Lambda^2}{r}\right)^{-\frac{N+2}{N+8}} \ll \mathcal{T}$

In the Fermi liquid regime the correlation length will be dominated by the zero temperature contribution $\xi^{-2}\sim\Delta\sim r\left(\log\frac{\bar\Lambda^2}{\Delta}\right)^{-\frac{N+2}{N+8}}$. After a convenient substitution we can extract the temperature correction from expression (3.24)

$$R_T \sim 4\,(N+2)\,K_2\,\mathcal{T}^2\,\xi^2\int\limits_{-\log(\xi\Lambda)}^{\infty} dx\int\limits_0^{\infty}\frac{dv}{\pi}\,\frac{4\,v\,(\coth v-1)\;e^{2x}\;u(e^x\xi\Lambda)}{\left(R(e^x\xi\Lambda)\xi^2e^{2x}+1\right)^2+\left(2\,\mathcal{T}\,\xi^2\,e^{2x}v\right)^2}\,. \tag{3.29}$$

In the Fermi liquid regime we can neglect the term $\mathcal{T}\,\xi^2$ in the denominator of the integrand. This leads to

$$R_T \sim 4\,(N+2)\,\frac{\pi K_2}{3}\,\mathcal{T}^2\,\xi^2 \int\limits_{-\log \xi\Lambda}^{\infty} dx\,\frac{e^{2x}}{\left(R(e^x\xi\Lambda)\xi^2 e^{2x}+1\right)^2}\,u(e^x\xi\Lambda)\,. \tag{3.30}$$

The remaining integral can again be evaluated with a saddle point approximation. Taking the running quartic coupling at the saddle point, $x_{\max}=0$, we obtain for the correlation length

$$\xi^{-2} \simeq \Delta + \frac{\pi^2}{6}\,\frac{N+2}{N+8}\,\frac{\mathcal{T}^2}{\Delta\,\log\frac{\bar\Lambda^2}{\Delta}} \sim \frac{r}{\left(\log\frac{\bar\Lambda^2}{r}\right)^{\frac{N+2}{N+8}}} + \frac{\pi^2}{6}\,\frac{N+2}{N+8}\,\frac{\mathcal{T}^2}{r}\left(\log\frac{\bar\Lambda^2}{r}\right)^{\frac{N+2}{N+8}-1}\,. \tag{3.31}$$

The temperature dependent correction is characteristic of a Fermi liquid.

3.2.3 Ginzburg temperature

At the upper critical dimension the quartic coupling, u, as well as the correlation length are scale dependent. Choosing the scale $b=\xi/\Lambda$ we obtain the Ginzburg temperature $u\mathcal{T}_G(r)\sim\xi^{-2}$ as a set of two equations parameterized by ξ,

$$\left\{\begin{array}{lcl} \mathcal{T}_G &=& \dfrac{N+8}{\pi^2}\xi^{-2}\log\left(\xi^2\bar\Lambda^2\right) \\ r &=& \xi^{-2}\left(\log\xi^2\bar\Lambda^2\right)^{\frac{N+2}{N+8}}\left(1-\dfrac{N+2}{\pi}\,\log\left(\dfrac{N+8}{\pi^2}\log\left(\xi^2\bar\Lambda^2\right)\right)\right)\,. \end{array}\right. \tag{3.32}$$

The asymptotic behavior of the Ginzburg temperature can be obtained by solving these equations iteratively,

$$r \sim -\frac{\pi}{N+8}\,\frac{\mathcal{T}_G\left(\log\frac{\bar\Lambda^2}{\mathcal{T}_G}\right)^{\frac{N+2}{N+8}}}{\log\frac{\bar\Lambda^2}{\mathcal{T}_G}}\left((N+2)\log\log\frac{\bar\Lambda^2}{\mathcal{T}_G}-\pi\right)\,. \tag{3.33}$$

3.3 Thermodynamics

3.3.1 Specific heat

In the following the expressions (2.65) and (2.66) are evaluated. Using the leading-temperature contribution of the f_n functions (2.46) we get for expression (2.65) (after two convenient substitutions)

$$\gamma_{\rm QCP} = \frac{N}{2}K_d\,\mathcal{T}^{\frac{d-z}{z}} \int\limits_{\log\mathcal{T}^{1/z}/\Lambda}^{\infty} dx \int_0^\infty \frac{dv}{\pi}\,\left(\frac{2\,v}{\sinh v}\right)^2 \frac{\left(R(e^x\Lambda\mathcal{T}^{-\frac{1}{z}})\mathcal{T}^{-2/z}e^{2x}+1\right)\,e^{(z-d)x}}{\left(R(e^x\Lambda\mathcal{T}^{-\frac{1}{z}})\mathcal{T}^{-2/z}e^{2x}+1\right)^2+\left(2\,e^{zx}\,v\right)^2}\,. \tag{3.34}$$

Quantum critical regime: $r\,\mathcal{T}^{-1/(\nu z)} \ll 1$

$z > d$: We can neglect the $RT^{-2/z}$ terms and extend the lower limit of the x-integral to zero, neglecting contributions of order $\mathcal{O}\left(T^{1/z}/\Lambda\right)^{z-d}$. The leading behavior reads

$$\gamma_{\rm QCP} = \frac{N}{2}\,\frac{K_d}{z\,\cos\left(\frac{d}{2z}\pi\right)}\,\Gamma\left(2+\frac{d}{z}\right)\,\zeta\left(1+\frac{d}{z}\right)\,\mathcal{T}^{\frac{d-z}{z}}\,. \tag{3.35}$$

$z = d$: In the case $z = d$ the leading contribution of the specific heat will depend on the cutoff Λ. We approximate the x-integral by $\log\Lambda/T^{1/z}$ and we get

$$\gamma_{\rm QCP} \;=\; \frac{N}{2}\frac{2\pi\,K_d}{3}\,\log\frac{\Lambda}{\mathcal{T}^{1/z}}\,. \tag{3.36}$$

$z < d < 3z$: In this case the leading contribution is given by the cutoff.

$$\begin{aligned}\gamma_{\rm QCP} &= \frac{N}{2}\frac{2\pi\,K_d}{3\,(d-z)}\,\Lambda^{d-z} - \frac{N}{2}K_d\,T^{\frac{d-z}{z}}\int_0^\infty dx\,x^{z-d-1}\int_0^\infty\frac{dv}{\pi}\,\left(\frac{2\,v}{\sinh v}\right)^2\frac{(2\,x^z\,v)^2}{1+(2\,x^z\,v)^2}\\ &= \frac{N}{2}\,\frac{2\pi\,K_d}{3\,(d-z)}\,\Lambda^{d-z} + \frac{N}{2}\,\frac{K_d}{z\,\cos\left(\frac{d}{2z}\pi\right)}\,\Gamma\left(2+\frac{d}{z}\right)\,\zeta\left(1+\frac{d}{z}\right)\,\mathcal{T}^{\frac{d-z}{z}}\end{aligned} \tag{3.37}$$

We have neglected contributions of order $\mathcal{O}\left(\mathcal{T}^{1/z}/\Lambda\right)^{3z-d}$. Note that the temperature dependent part is negative due to the fact that $\cos\left(\frac{d}{2z}\pi\right) = -\left|\cos\left(\frac{d}{2z}\pi\right)\right|$.

Fermi liquid regime: $r\,\mathcal{T}^{-1/(\nu z)} \gg 1$

Substituting the running mass $R(.)$ by the correlation length, ξ^{-2}, in the integrand we obtain for the leading contribution

$$\begin{aligned}\gamma_{\rm QCP} &= \frac{N}{2}K_d\,(\xi^{-2})^{\frac{d-z}{2}}\int_{-\log\xi\Lambda}^\infty dx\int_0^\infty\frac{dv}{\pi}\,\left(\frac{2\,v}{\sinh v}\right)^2\frac{\left(e^{2x}+1\right)\,e^{(z-d)x}}{\left(e^{2x}+1\right)^2+\left(2\,\mathcal{T}\,\xi^z\,e^{zx}\,v\right)^2}\\ &\approx \frac{N}{2}\frac{2\pi\,K_d}{3}\,(\xi^{-2})^{\frac{d-z}{2}}\int_{-\log\xi\Lambda}^\infty dx\,\frac{e^{(z-d)x}}{1+e^{2x}}\,.\end{aligned} \tag{3.38}$$

In the second line the term $\mathcal{T}\,\xi^z$ in the integrand has been neglected and the v-integral performed.

$z > d$: Neglecting contributions of order $\mathcal{O}\,(\xi\Lambda)^{d-z}$ we get

$$\gamma_{\rm QCP} = \frac{N}{2}\,\frac{\pi^2\,K_d}{3\,\sin\left(\frac{z-d}{2}\pi\right)}\,(\xi^{-2})^{\frac{d-z}{2}}\,. \tag{3.39}$$

$z = d$: As in the quantum critical regime the integral over x leads to a logarithmic dependence on the cutoff, $\log\xi\Lambda$:

$$\gamma_{\rm QCP} = \frac{N}{2}\frac{2\pi\,K_d}{3}\,\log\xi\Lambda\,. \tag{3.40}$$

$d-2<z<d$: The leading contribution stems from the cutoff

$$\begin{aligned}\gamma_{\mathrm{QCP}} &\approx \frac{N}{2}\frac{2\pi\,K_d}{3\,(d-z)}\,\Lambda^{d-z} - \frac{N}{2}\frac{2\pi\,K_d}{3}\,(\xi^{-2})^{\frac{d-z}{2}}\int_{-\infty}^{\infty} dx\, e^{(z-d)x}\,\frac{e^{2x}}{1+e^{2x}} \\ &= \frac{N}{2}\frac{2\pi\,K_d}{3\,(d-z)}\,\Lambda^{d-z} + \frac{N}{2}\frac{\pi^2\,K_d}{3\,\sin\left(\frac{z-d}{2}\pi\right)}\,(\xi^{-2})^{\frac{d-z}{2}}\,. \end{aligned} \tag{3.41}$$

We neglected contributions of order $\mathcal{O}\,(\xi\Lambda)^{d-z-2}$. Note that the temperature dependent part corresponds to a negative correction, since $\sin\left(\frac{z-d}{2}\pi\right)<0$.

These results for the specific heat differ from the results obtained by U. Zülicke *et al.* [6] by a factor of 2. This factor can be traced back to the factor 1/2 in the RG equation for the free energy (2.40) which originates from the fact that the fields Φ in the Hertz model (2.23) are real. This factor was missing in Millis' original paper [5] (compare also footnote on page 28).

Classical regime

Near a classical phase transition the specific heat diverges with diminishing distance to the phase boundary according to $C\sim R^{-\alpha}$, where R is the effective mass of the classical theory. The exponent α is given by hyperscaling [17], $\alpha=2-d\nu$. In the vicinity of the finite temperature transition the specific heat coefficient is therefore dominated by (2.66) which gives the most diverging contribution for a vanishing running mass $R(.)$. Using the leading behavior of the f_n functions (2.46) the expression (2.66) becomes

$$\gamma_{\mathrm{CL}} = \frac{N}{2}K_d\Lambda^d\int_0^\infty dx\,\left(\frac{\partial R(e^x)}{\partial\mathcal{T}}\right)^2\int_0^\infty\frac{d\epsilon}{\pi}\,\coth\left(\frac{\epsilon}{2\mathcal{T}e^{zx}}\right)\frac{2\,\Lambda^{2-z}\,\epsilon\,e^{(4-d-z)x}\,\left(R(e^x)\,e^{2x}+\Lambda^2\right)}{\left(\left(R(e^x)\,e^{2x}+\Lambda^2\right)^2+\left(\Lambda^{2-z}\,\epsilon\right)^2\right)^2}\,.$$

It is convenient to perform two substitutions, first $\epsilon/(2\mathcal{T}e^{zx})\to v$ and then $e^x\to\Lambda\xi e^x$,

$$\gamma_{\mathrm{CL}} = \frac{N}{2}K_d\mathcal{T}^2\xi^{4-d+z}\int_{-\log(\Lambda\xi)}^\infty dx\,\left(\frac{\partial R(\Lambda\xi e^x)}{\partial\mathcal{T}}\right)^2\int_0^\infty\frac{dv}{\pi}\,\frac{8\,v\,\coth v\,e^{(4-d+z)x}\,\left(R(\Lambda\xi e^x)\,e^{2x}\xi^2+1\right)}{\left(\left(R(\Lambda\xi e^x)\,\xi^2e^{2x}+1\right)^2+\left(2\xi^z\,\mathcal{T}e^{zx}v\right)^2\right)^2}\,.$$

The leading contribution will come from the scaling into the classical regime, so we expand the hyperbolic function for small arguments keeping only the leading contribution. Afterwards we can perform the v-integral,

$$\gamma_{\mathrm{CL}} = \frac{N}{2}K_d\mathcal{T}\xi^{4-d}\int_{-\log(\Lambda\xi)}^\infty dx\,\left\{\left(\frac{\partial R(\Lambda\xi e^x)}{\partial\mathcal{T}}\right)^2\frac{\left(e^{2x}+1\right)^2}{\left(R(\Lambda\xi e^x)\,\xi^2e^{2x}+1\right)^2}\right\}\frac{e^{(4-d)x}}{\left(e^{2x}+1\right)^2}\,.$$

This integral can be evaluated with a saddle point approximation. The integrand consists of a product of a slowly varying term in the curly brackets and a strongly peaked function with the peak located at $x_{\max}=\frac{1}{2}\log\frac{4-d}{d}$. The argument of the running mass at the peak maximum is already very large, $\Lambda\xi e^{x_{\max}}$, and the running mass therefore varies only slowly at the peak position. Taking the value of the curly bracket at the peak maximum we can

evaluate the remaining integral. In the universal limit $\Lambda \to \infty$ the corrections to this saddle point approximation vanish (compare also Appendix D of Ref. [6]),

$$\gamma_{\rm CL} = \frac{N}{2} K_d \mathcal{T} \xi^{4-d} \left(\frac{\partial \xi^{-2}}{\partial \mathcal{T}} \right)^2 \int_{-\infty}^{\infty} dx \, \frac{e^{(4-d)x}}{\left(e^{2x}+1\right)^2} = \frac{N}{2} \frac{(2-d)\pi K_d}{4 \sin \frac{d\pi}{2}} \mathcal{T} \, \left(\xi^{-2}\right)^{-2+d/2} \left(\frac{\partial \xi^{-2}}{\partial \mathcal{T}} \right)^2 . \tag{3.42}$$

The specific heat diverges when the correlation length grows to infinity. The divergence is consistent with the above mentioned hyperscaling relationship with the Landau value $\nu = 1/2$, $\alpha = 2 - d/2$. The crossover to the actual classical, Wilson–Fisher fix-point value $\nu_{\rm WF} \neq 1/2$ occurs at the Ginzburg temperature $\mathcal{T}_G$. Let us estimate the quantum–classical crossover at which the classical contribution to the specific heat, $\gamma_{\rm CL}$, starts to dominate over the quantum contribution $\gamma_{\rm QCP}$. Using the expression for the correlation length (3.5) we find that the classical part is of order $\gamma_{\rm CL} \sim \mathcal{O}(\xi^{4-d} u^2 \mathcal{T}^{(z+2d-4)/z})$ whereas the quantum part $\gamma_{\rm QCP} \sim \mathcal{O}(\mathcal{T}^{(d-z)/z})$. The classical contribution takes over if the correlation length is of order,

$$\xi^{-2} \sim u^{\frac{4}{4-d}} \mathcal{T}^{\frac{2\,(d+2z-4)}{z\,(4-d)}} . \tag{3.43}$$

Since the temperature is very small we can conclude that the classical contribution $\gamma_{\rm CL}$ is only important in the immediate vicinity of the finite-temperature phase transition. In particular, the condition (3.43) should be compared with the definition of the Ginzburg criterion, $\xi^{-2} = (u\mathcal{T}_G)^{2/(4-d)}$; the latter will always be fulfilled first as the phase transition is approached. This means that the quantum–classical crossover of the specific heat is located within the non-Gaussian region, see Fig. 3.1.

3.3.2 Thermal expansion

In this section we will evaluate the expressions (2.69) and (2.70) for the thermal expansion. Again we start with the contribution due to the quantum critical point. Using the leading-temperature contribution of the f_n functions (2.46) we get (after two convenient substitutions)

$$\alpha_{\rm QCP} = \frac{N}{2} K_d \, \mathcal{T}^{\frac{d-2}{z}} \tag{3.44}$$
$$\times \int_{\log \mathcal{T}^{1/z}/\Lambda}^{\infty} dx \, \frac{\partial R(e^x \Lambda \mathcal{T}^{-\frac{1}{z}})}{\partial r} \int_0^{\infty} \frac{dv}{\pi} \, \left(\frac{2\,v}{\sinh v} \right)^2 \frac{e^{(2+z-d)\,x}}{\left(R(e^x \Lambda \mathcal{T}^{-\frac{1}{z}})\, \mathcal{T}^{-\frac{2}{z}} e^{2x} + 1 \right)^2 + \left(2\, e^{zx}\, v\right)^2} .$$

Quantum critical regime: $r\,\mathcal{T}^{-1/(\nu z)} \ll 1$

$z > d-2 > 0$: For space dimension $d > 2$ the running mass in the denominator of the integrand can be neglected in the quantum critical regime,

$$\alpha_{\rm QCP} = \frac{N}{2} K_d \, \mathcal{T}^{\frac{d-2}{z}} \int_{\log \mathcal{T}^{1/z}/\Lambda}^{\infty} dx \, \frac{\partial R(e^x \Lambda \mathcal{T}^{-\frac{1}{z}})}{\partial r} \int_0^{\infty} \frac{dv}{\pi} \, \left(\frac{2\,v}{\sinh v} \right)^2 \frac{e^{(2+z-d)\,x}}{1 + \left(2\, e^{zx}\, v\right)^2} .$$

Proceeding as before we take the argument of the running mass at the saddle point value of the double integral and obtain for $\Lambda \to \infty$

$$\alpha_{\rm QCP} = \frac{N}{2} \, \frac{K_d}{z \, \cos\left(\frac{d-2}{2\,z}\pi\right)} \, \Gamma\left(2 + \frac{d-2}{z}\right) \, \zeta\left(1 + \frac{d-2}{z}\right) \, \frac{\partial \xi^{-2}}{\partial r} \mathcal{T}^{\frac{d-2}{z}} . \tag{3.45}$$

$d = 2:$ As was the case for the correlation length in two space dimension we have to expect logarithmic corrections from scaling into the classical regime. Before expanding the hyperbolic function we perform the trick of integrating by parts (setting $d = 2$)

$$\alpha_{\rm QCP} = -\frac{N}{2} K_d \int\limits_{\log \mathcal{T}^{1/z}/\Lambda}^{\infty} dx\, x \times \frac{d}{dx} \frac{\partial R(e^x \Lambda \mathcal{T}^{-\frac{1}{z}})}{\partial r} \int_0^\infty \frac{dv}{\pi} \left(\frac{2\,v}{\sinh v}\right)^2 \frac{e^{z\,x}}{\left(R(e^x \Lambda \mathcal{T}^{-\frac{1}{z}})\, \mathcal{T}^{-\frac{2}{z}} e^{2x} + 1\right)^2 + (2\, e^{zx}\, v)^2}\,, \tag{3.46}$$

where the surface term is sub-leading. Expanding the hyperbolic function to leading order and performing the v-integral we obtain

$$\alpha_{\rm QCP} \simeq -\frac{N}{2} K_d \int\limits_{\log \mathcal{T}^{1/z}/\Lambda}^{\infty} dx\, x\, \frac{d}{dx} \frac{\partial R(e^x \Lambda \mathcal{T}^{-\frac{1}{z}})}{\partial r} \frac{1}{R(e^x \Lambda \mathcal{T}^{-\frac{1}{z}})\, \mathcal{T}^{-\frac{2}{z}} e^{2x} + 1}\,. \tag{3.47}$$

The saddle point approximation leads to ($\Lambda \to \infty$)

$$\alpha_{\rm QCP} \simeq -\frac{N}{2} K_d \frac{\partial \xi^{-2}}{\partial r} \int\limits_{-\infty}^{\infty} dx\, x\, \frac{d}{dx} \frac{1}{\xi^{-2}\, \mathcal{T}^{-\frac{2}{z}} e^{2x} + 1} \simeq \frac{N}{2} \frac{K_d}{2} \frac{\partial \xi^{-2}}{\partial r} \log \frac{1}{\xi^{-2}\, \mathcal{T}^{-\frac{2}{z}}}\,. \tag{3.48}$$

Fermi liquid regime: $r\, \mathcal{T}^{-1/(\nu z)} \gg 1$

Proceeding in the same way as for the correlation length we obtain for the leading behavior in the Fermi liquid regime

$$\alpha_{\rm QCP} = \frac{N}{2} \frac{\pi^2}{6} \frac{(d-z)\, K_d}{\sin\left(\frac{d-z}{2}\,\pi\right)} \mathcal{T}\, (\xi^{-2})^{\frac{d-z-2}{2}} \frac{\partial \xi^{-2}}{\partial r}\,. \tag{3.49}$$

Classical regime

Proceeding similarly as for the specific heat in the classical regime we obtain

$$\alpha_{\rm CL} = -\frac{N}{2} \frac{(2-d)\pi K_d}{4\, \sin\frac{d\pi}{2}} \mathcal{T}\, \xi^{4-d} \frac{\partial \xi^{-2}}{\partial \mathcal{T}} \frac{\partial \xi^{-2}}{\partial r}\,. \tag{3.50}$$

The thermal expansion shows the same divergence in the classical as the specific heat. This holds generally for a phase transition of the second kind (see Ref. [16] §148). In the following we consider the quantum–classical crossover for the thermal expansion. Using the expression for the correlation length (3.5) we find that the classical contribution is of order $\alpha_{\rm CL} \sim \mathcal{O}(\xi^{4-d} u \mathcal{T}^{(d+z-2)/z})$ and the quantum one of order $\alpha_{\rm QCP} \sim \mathcal{O}(\mathcal{T}^{(d-2)/z})$. Comparing these two we find the condition for the quantum–classical crossover to be

$$\xi^{-2} \sim (u\mathcal{T})^{\frac{2}{4-d}}\,, \tag{3.51}$$

which coincides with the Ginzburg criterion. As for the specific heat, the classical regime is located within the non–Gaussian region, see Fig. 3.1.

3.3.3 Grüneisen parameter

In this section we list the ratios between the critical contributions to the thermal expansion and specific heat.

Quantum critical regime: $r\,\mathcal{T}^{-1/(\nu z)} \ll 1$

$$z = d = 2: \qquad \Gamma_{\mathrm{cr}} = \frac{3}{4\pi} \frac{\log \frac{1}{\xi^{-2}\mathcal{T}^{-2/z}}}{\mathcal{T} \log \frac{\Lambda}{\mathcal{T}^{1/z}}} \frac{\partial \xi^{-2}}{\partial r} \tag{3.52}$$

$$z \neq d = 2: \qquad \Gamma_{\mathrm{cr}} = \frac{z \cos\left(\frac{d}{2z}\pi\right)}{2\Gamma\left(2+\frac{d}{z}\right)\zeta\left(1+\frac{d}{z}\right)} \mathcal{T}^{-\frac{d}{z}} \log \frac{1}{\xi^{-2}\mathcal{T}^{-2/z}} \frac{\partial \xi^{-2}}{\partial r} \tag{3.53}$$

$$d = z \neq 2: \qquad \Gamma_{\mathrm{cr}} = \frac{3\,\Gamma\left(2+\frac{d-2}{z}\right)\zeta\left(1+\frac{d-2}{z}\right)}{2\pi\, z \cos\left(\frac{d-2}{2\,z}\pi\right)} \mathcal{T}^{\frac{d-2-z}{z}} \left(\log \frac{\Lambda}{\mathcal{T}^{1/z}}\right)^{-1} \frac{\partial \xi^{-2}}{\partial r} \tag{3.54}$$

$$\text{otherwise}: \qquad \Gamma_{\mathrm{cr}} = \frac{\cos\left(\frac{d}{2z}\pi\right)}{\cos\left(\frac{d-2}{2\,z}\pi\right)} \frac{\Gamma\left(2+\frac{d-2}{z}\right)\zeta\left(1+\frac{d-2}{z}\right)}{\Gamma\left(2+\frac{d}{z}\right)\zeta\left(1+\frac{d}{z}\right)} \mathcal{T}^{-\frac{2}{z}} \frac{\partial \xi^{-2}}{\partial r} \tag{3.55}$$

Fermi liquid regime: $r\,\mathcal{T}^{-1/(\nu z)} \gg 1$

$$d = z: \qquad \Gamma_{\mathrm{cr}} = \frac{1}{2}\,(\xi^{-2})^{-1}\,(\log \xi\Lambda)^{-1} \frac{\partial \xi^{-2}}{\partial r} \tag{3.56}$$

$$d \neq z: \qquad \Gamma_{\mathrm{cr}} = \frac{z-d}{2}\,(\xi^{-2})^{-1} \frac{\partial \xi^{-2}}{\partial r}\,. \tag{3.57}$$

Classical regime

In the Grüneisen parameter the divergences of specific heat and thermal expansion cancel, and it measures essentially the pressure dependence of the critical temperature,

$$\Gamma_{\mathrm{CL}} = \frac{\alpha_{\mathrm{CL}}}{T\gamma_{\mathrm{CL}}} = -\frac{\frac{\partial \xi^{-2}}{\partial r}}{\mathcal{T}\frac{\partial \xi^{-2}}{\partial \mathcal{T}}}\,. \tag{3.58}$$

With the restrictions mentioned in Section 2.2.3 we can define a critical temperature by setting $\xi^{-2}(\mathcal{T}_c(r), r) = 0$. With the help of this definition we can rewrite the Grüneisen parameter in the vicinity of the phase boundary as

$$\Gamma_{\mathrm{CL}} = \frac{d \log \mathcal{T}_c(r)}{dr}\,. \tag{3.59}$$

The Grüneisen parameter in the classical region near the phase boundary essentially measures the pressure dependence of the critical temperature T_c [16].

3.4 Summary of results and discussion

The results of the rather lengthy derivations of the last sections are summarized in the following. We list explicitly the results for $d, z = 2, 3$ and show the resulting phase diagrams for $z = 2$ and $d = 2, 3$.

The regime of applicability of the perturbative Millis RG is confined to the right-hand side of the Ginzburg line $\mathcal{T}_G(r)$ in the $(r, \mathcal{T})$ plane of the phase diagram, see following Figs. 3.2 and 3.3. Depending on the spatial dimension and the internal symmetry of the order parameter $O(N)$ there might exist a finite temperature phase boundary originating in the quantum critical point and extending to higher temperatures. However, it will be located in the non-Gaussian region not accessible with the approach of this chapter. Nevertheless, a critical temperature $\mathcal{T}_c(r)$ can be estimated in space dimensions $d > 2$.

The scale invariant combination $r\mathcal{T}^{-1/\nu z}$ of the control parameter and the temperature defines an important crossover line that separates the phase diagram into a Fermi liquid regime, $r\mathcal{T}^{-1/\nu z} \gg 1$, and a quantum critical regime, $r\mathcal{T}^{-1/\nu z} \ll 1$. As the name suggests, in the Fermi liquid regime the thermodynamics is that of a conventional Fermi liquid. The quantum critical regime on the other hand is characterized by peculiar temperature dependencies of the correlation length, specific heat and the thermal expansion — the thermodynamics at finite temperatures is strongly influenced by the presence of a quantum phase transition.

The thermal expansion divided by temperature, α/T, which approaches a constant in a Fermi liquid at low temperatures, exhibits a distinct divergence in the quantum critical regime in agreement with the scaling treatment of Chapter 1. For example, it diverges as $\alpha/T \sim T^{-1/2}$ in the three dimensional (commensurate) antiferromagnet ($d = 3, z = 2$). This should be contrasted with the temperature dependence of the specific heat divided by temperature, $C/T = \gamma$, which also saturates towards a constant in a Fermi liquid at low temperatures. Its behavior in the quantum critical regime however is less spectacular than that of the thermal expansion. It either approaches a constant with peculiar temperature corrections for $d = 3, z = 2$ or it diverges rather slowly, e.g. logarithmically for $d = 2, z = 2$.

As a consequence, the ratio of these two quantities, the Grüneisen parameter, diverges as a function of temperature in the quantum critical regime. This bears out the prediction made in Chapter 1. In particular, we can now compare the properties of the Grüneisen parameter of a specific model, the Hertz theory, with the general scaling predictions (1.30) and (1.29). The (zero-temperature) Hertz model is above or at its upper critical dimension for $d, z = 2, 3$ and scaling is not necessarily expected to apply due to the quartic coupling u, which is a dangerously irrelevant operator. Nevertheless, we observe that the results agree to within logarithmic corrections. These logarithmic corrections abound and it is interesting to examine their origin. Firstly, for $d + z = 4$ the zero-temperature theory is at its upper critical dimension which leads to a logarithmic temperature dependence of the denominator of Γ_{cr} in the quantum critical regime. Secondly, for $d = 2$ the effective finite temperature theory is at its lower critical dimension resulting in a logarithmic temperature dependence of the numerator of Γ_{cr} in the quantum critical regime that can be traced to a Mermin–Wagner divergence (3.1). Thirdly, for $d = z$ the universal prefactor in the Fermi liquid regime (1.29) expected from the scaling treatment is supposed to vanish. This is reflected in a further logarithmic dependence of Γ_{cr} for $d = z$.

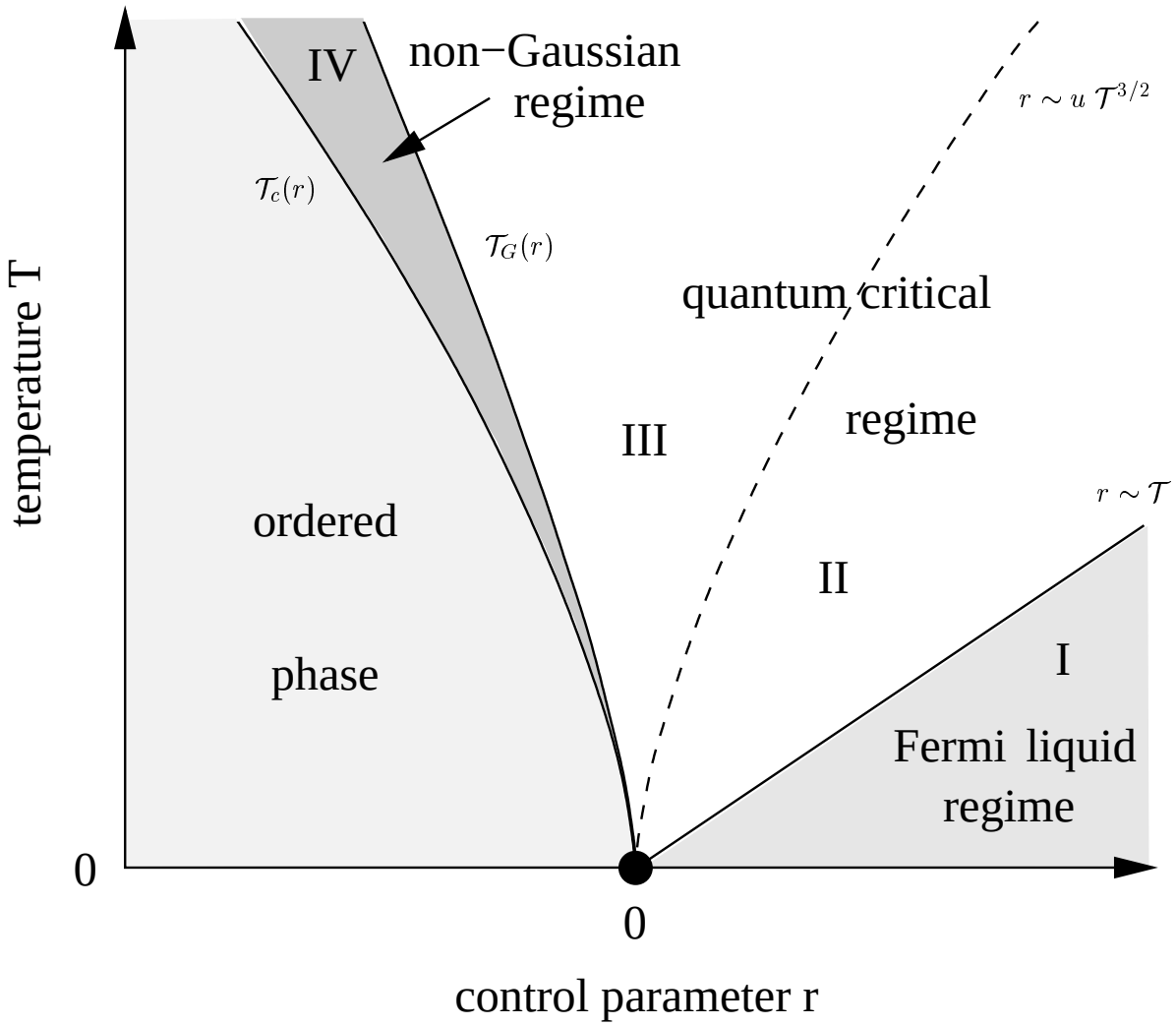

Figure 3.2: *Phase diagram of the Hertz' model for $d = 3$ and $z = 2$. In regime I Fermi liquid behavior is observed in all thermodynamic quantities. The quantum critical regime consists of regime II and III which are separated by a crossover in the behavior of the correlation length. The Ginzburg line $\mathcal{T}_G(r)$ identifies the breakdown of the perturbative RG and gives the crossover line to the non-Gaussian regime. The critical temperature $\mathcal{T}_c(r)$ is an estimate for the Néel temperature. Units: ξ^{-2} is measured in units of ξ_0^{-2}, $\mathcal{T}$ in T_0, γ in $V/(\xi_0^d T_0)$, α in $1/(\xi_0^d p_0)$ and Γ in $1/(V p_0)$. The control parameter is given by $r = (p - p_c)/p_0$.*

$d=3; z=2$	formula
quantum critical regime II+III: $r\,\mathcal{T}^{-1} \ll 1$	
$\xi^{-2} = \begin{cases} r & \text{for II:} \quad r \gg u\,\mathcal{T}^{\frac{3}{2}} \\ \frac{(N+2)\,\zeta\left(\frac{3}{2}\right)}{\sqrt{2}\,\pi^{3/2}}\,u\,\mathcal{T}^{\frac{3}{2}} & \text{for III:} \quad r \ll u\,\mathcal{T}^{\frac{3}{2}} \end{cases}$	(3.5)
$\gamma_{cr} = -\dfrac{\sqrt{2\pi}\,15\,\zeta\left(\frac{5}{2}\right) N}{64\,\pi^2}\,\mathcal{T}^{\frac{1}{2}} = -0.0798\,N\,\mathcal{T}^{\frac{1}{2}}$	(3.37)
$\alpha_{cr} = \dfrac{\sqrt{2\pi}\,3\,\zeta\left(\frac{3}{2}\right) N}{32\pi^2}\,\mathcal{T}^{\frac{1}{2}} = 0.0622\,N\,\mathcal{T}^{\frac{1}{2}}$	(3.45)
$\Gamma_{\rm cr} = -\dfrac{2\,\zeta\left(\frac{3}{2}\right)}{5\,\zeta\left(\frac{5}{2}\right)}\,\mathcal{T}^{-1} = -0.7789\,\mathcal{T}^{-1}$	(3.55)
Fermi liquid regime I: $r\,\mathcal{T}^{-1} \gg 1$	
$\xi^{-2} = r$	(3.10)
$\gamma_{cr} = -\dfrac{N}{12}\,r^{\frac{1}{2}}$	(3.41)
$\alpha_{cr} = \dfrac{N}{24}\,\mathcal{T}\,r^{-\frac{1}{2}}$	(3.49)
$\Gamma_{\rm cr} = -\dfrac{1}{2}r^{-1}$	(3.57)
Ginzburg temperature	
$r = u^2\mathcal{T}_G^2 - \dfrac{(N+2)\zeta(3/2)}{\sqrt{2}\pi^{3/2}}\,u\,\mathcal{T}_G^{3/2}$	(3.13)
Estimate of the critical temperature	
$r = -\dfrac{(N+2)\zeta(3/2)}{\sqrt{2}\pi^{3/2}}\,u\,\mathcal{T}_c^{3/2}$	(3.11)

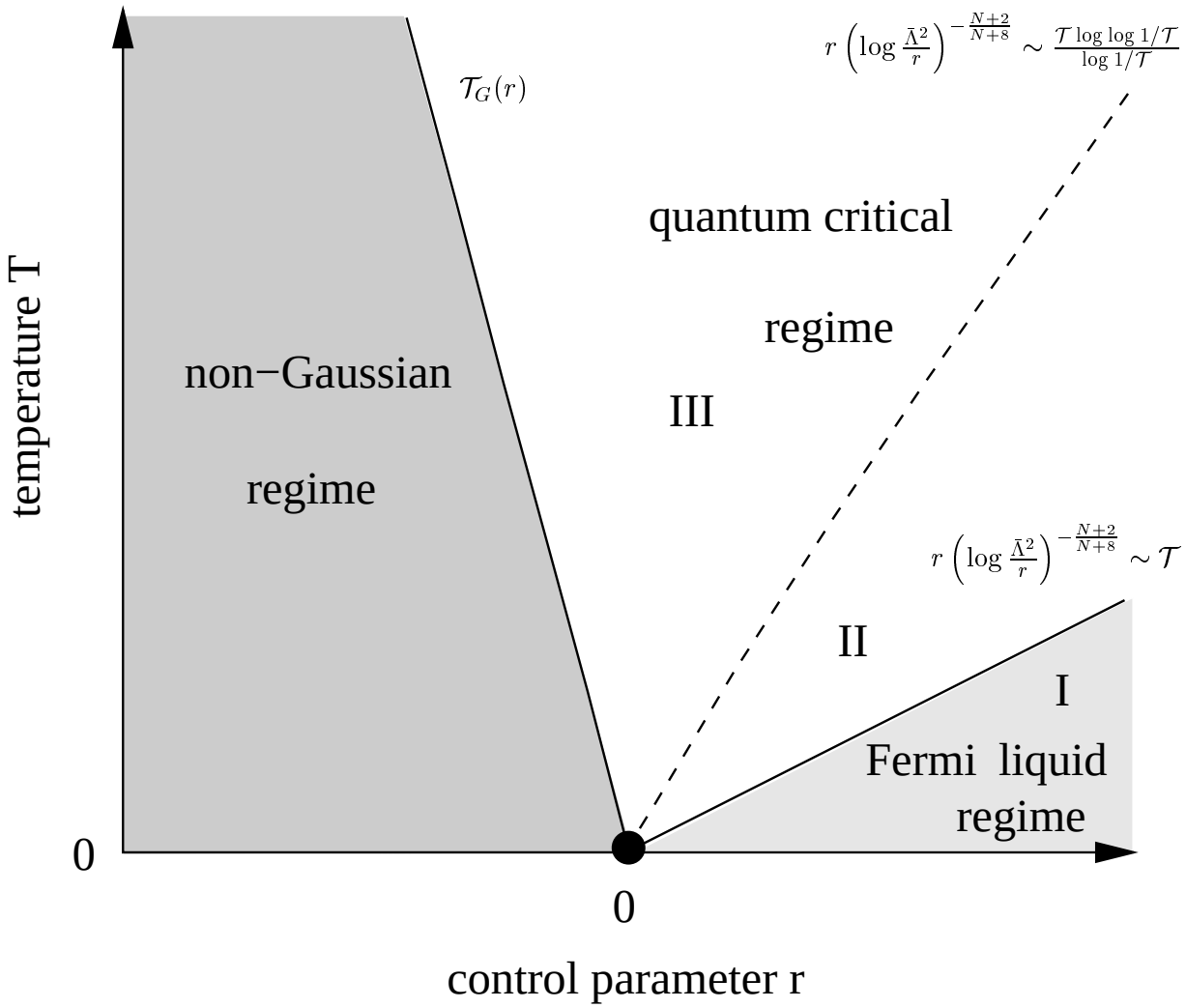

Figure 3.3: *Phase diagram of the Hertz' model for $d = 2$ and $z = 2$. Fermi liquid behavior is seen in regime I. Region II and III form the quantum critical regime. They are distinguished by different logarithmic corrections to thermodynamic quantities. Beyond the Ginzburg temperature $\mathcal{T}_G(r)$ starts the non-Gaussian regime where the perturbative RG breaks down. In two space dimension an estimate for the critical boundary could not be obtained due to the Mermin–Wagner divergence (3.1). Units: ξ^{-2} is measured in units of ξ_0^{-2}, $\mathcal{T}$ in T_0, γ in $V/(\xi_0^d T_0)$, α in $1/(\xi_0^d p_0)$ and Γ in $1/(V p_0)$. The control parameter is given by $r = (p - p_c)/p_0$.*

$d=2; z=2$	formula
quantum critical regime III: $r\left(\log\frac{\bar\Lambda^2}{r}\right)^{-\frac{N+2}{N+8}} \ll \mathcal{T}\frac{\log\log\frac{\bar\Lambda^2}{\mathcal{T}}}{\log\frac{\bar\Lambda^2}{\mathcal{T}}}$	
$\xi^{-2} \sim \pi\,\frac{N+2}{N+8}\mathcal{T}\frac{\log\log\frac{\bar\Lambda^2}{\mathcal{T}}}{\log\frac{\bar\Lambda^2}{\mathcal{T}}}$	(3.27)
$\gamma_{\rm cr} = \frac{N}{12}\,\log\frac{\Lambda^2}{\mathcal{T}}$	(3.36)
$\alpha_{\rm cr} \sim \frac{N}{8\pi}\frac{\log\log\frac{\bar\Lambda^2}{\mathcal{T}}}{\left(\log\frac{\bar\Lambda^2}{\mathcal{T}}\right)^{\frac{N+2}{N+8}}}$	(3.48)
$\Gamma_{\rm cr} \sim \frac{3}{2\pi}\frac{\log\log\frac{\bar\Lambda^2}{\mathcal{T}}}{\mathcal{T}\log\frac{\Lambda^2}{\mathcal{T}}\left(\log\frac{\bar\Lambda^2}{\mathcal{T}}\right)^{\frac{N+2}{N+8}}}$	(3.52)
quantum critical regime II: $\mathcal{T}\frac{\log\log\frac{\bar\Lambda^2}{\mathcal{T}}}{\log\frac{\bar\Lambda^2}{\mathcal{T}}} \ll r\left(\log\frac{\bar\Lambda^2}{r}\right)^{-\frac{N+2}{N+8}} \ll \mathcal{T}$	
$\xi^{-2} \sim \frac{r}{\left(\log\frac{\bar\Lambda^2}{r}\right)^{\frac{N+2}{N+8}}}$	(3.27)
$\gamma_{\rm cr} = \frac{N}{12}\,\log\frac{\Lambda^2}{\mathcal{T}}$	(3.36)
$\alpha_{\rm cr} \sim \frac{N}{8\pi}\frac{\log\frac{\mathcal{T}}{r}}{\left(\log\frac{\bar\Lambda^2}{r}\right)^{\frac{N+2}{N+8}}}$	(3.48)
$\Gamma_{\rm cr} \sim \frac{3}{2\pi}\frac{\log\frac{\mathcal{T}}{r}}{\mathcal{T}\log\frac{\Lambda^2}{\mathcal{T}}\left(\log\frac{\bar\Lambda^2}{r}\right)^{\frac{N+2}{N+8}}}$	(3.52)
Fermi liquid regime I: $r\left(\log\frac{\bar\Lambda^2}{r}\right)^{-\frac{N+2}{N+8}} \ll \mathcal{T}$	
$\xi^{-2} \sim \frac{r}{\left(\log\frac{\bar\Lambda^2}{r}\right)^{\frac{N+2}{N+8}}}$	(3.31)
$\gamma_{\rm cr} \sim \frac{N}{12}\,\log\frac{\Lambda^2}{r}$	(3.40)
$\alpha_{\rm cr} \sim \frac{N}{12}\,\frac{\mathcal{T}}{r}$	(3.49)
$\Gamma_{\rm cr} = \frac{1}{2}\,\frac{1}{r\,\log\frac{\Lambda}{\sqrt{r}}}$	(3.56)
Ginzburg temperature	
$r \sim -\frac{\pi}{N+8}\frac{\mathcal{T}_G\left(\log\frac{\bar\Lambda^2}{\mathcal{T}_G}\right)^{\frac{N+2}{N+8}}}{\log\frac{\bar\Lambda^2}{\mathcal{T}_G}}\left((N+2)\log\log\frac{\bar\Lambda^2}{\mathcal{T}_G} - \pi\right)$	(3.32)

$d=2; z=3$	formula
quantum critical regime: $r\,\mathcal{T}^{-2/z} \ll 1$	
$\xi^{-2} \sim r + \dfrac{N+2}{\pi}\, u\,\mathcal{T} \log \dfrac{1}{u\,\mathcal{T}^{1/3}}$	(3.8)
$\gamma = \dfrac{N}{6\pi}\,\Gamma\left(\dfrac{8}{3}\right)\zeta\left(\dfrac{5}{3}\right)\,\mathcal{T}^{-\frac{1}{3}}$	(3.35)
$\alpha \sim \dfrac{N}{8\pi} \log \dfrac{1}{u\,\mathcal{T}^{1/3}}$	(3.48)
$\Gamma_{\rm cr} \sim \dfrac{3}{4\,\Gamma\left(\frac{8}{3}\right)\zeta\left(\frac{5}{4}\right)}\,\mathcal{T}^{-\frac{2}{3}} \log \dfrac{1}{u\mathcal{T}^{1/3}}$	(3.53)
Fermi liquid regime: $r\,\mathcal{T}^{-2/z} \gg 1$	
$\xi^{-2} = r + \mathcal{O}\left(u\,\mathcal{T}^2\, r^{-\frac{3}{2}}\right)$	(3.10)
$\gamma = \dfrac{N\,\pi}{12}\, r^{-\frac{1}{2}}$	(3.39)
$\alpha = \dfrac{N\,\pi}{24}\,\mathcal{T}\, r^{-\frac{3}{2}}$	(3.49)
$\Gamma_{\rm cr} = \dfrac{1}{2}\, r^{-1}$	(3.57)

$d=3; z=3$	formula
quantum critical regime $r\,\mathcal{T}^{-2/z} \ll 1$	
$\xi^{-2} = r + \dfrac{4\,(N+2)}{3\sqrt{3}\,\pi^2}\,\Gamma\left(\dfrac{4}{3}\right)\,\zeta\left(\dfrac{4}{3}\right) u\,\mathcal{T}^{\frac{4}{3}}$	(3.5)
$\gamma = \dfrac{N}{6\pi}\,\log \dfrac{\Lambda}{\mathcal{T}^{1/3}}$	(3.36)
$\alpha = \dfrac{N}{6\sqrt{3}\,\pi^2}\,\Gamma\left(\dfrac{7}{3}\right)\,\zeta\left(\dfrac{4}{3}\right)\,\mathcal{T}^{\frac{1}{3}}$	(3.45)
$\Gamma_{\rm cr} = \dfrac{\Gamma\left(\frac{7}{3}\right)\,\zeta\left(\frac{4}{3}\right)}{\sqrt{3}\pi}\,\dfrac{\mathcal{T}^{-\frac{2}{3}}}{\log \frac{\Lambda}{\mathcal{T}^{1/3}}}$	(3.54)
Fermi liquid regime $r\,\mathcal{T}^{-2/z} \gg 1$	
$\xi^{-2} = r + \mathcal{O}\left(u\,\mathcal{T}^2\, r^{-1}\right)$	(3.10)
$\gamma = \dfrac{N}{6\pi}\,\log \dfrac{\Lambda}{r^{1/2}}$	(3.40)
$\alpha = \dfrac{N}{12\,\pi}\,\mathcal{T}\, r^{-1}$	(3.49)
$\Gamma_{\rm cr} = \dfrac{1}{2}\, r^{-1}\,\left(\log \dfrac{\Lambda}{r^{1/2}}\right)^{-1}$	(3.56)

Chapter 4

Anisotropic Hertz Theory

The work of this chapter was motivated by the observation of quasi two-dimensional antiferromagnetic spin fluctuations in neutron scattering experiments on the heavy fermion compound $CeCu_{6-x}Au_x$ [7, 8]. The crystal structure of this system is essentially of a three-dimensional character and the two-dimensional spin fluctuations are only a precursor to the three-dimensional magnetic ordering observed below the Néel temperature. Why two-dimensional fluctuations dominate an intrinsically 3D alloy is, however, only poorly understood. At sufficiently low temperatures one expects that the apparently very small coupling of the spin fluctuations in the third dimension becomes important leading to a dimensional crossover in the thermodynamic quantities, although the experimental confirmation of such a crossover has so far proved to be elusive.

The presumed scenario of a 2D–3D crossover in the vicinity of the quantum critical point in $CeCu_{6-x}Au_x$ is sketched in Fig. 4.1. The quantum critical point is housed in a pocket where 3D spin fluctuations dominate the quantum critical dynamics. From the measured phase diagram of $CeCu_{6-x}Au_x$ (right panel of Fig. 4.1) the quantum critical point has been associated with a doping level of $x = 0.1$ after extrapolating linearly the Néel temperature

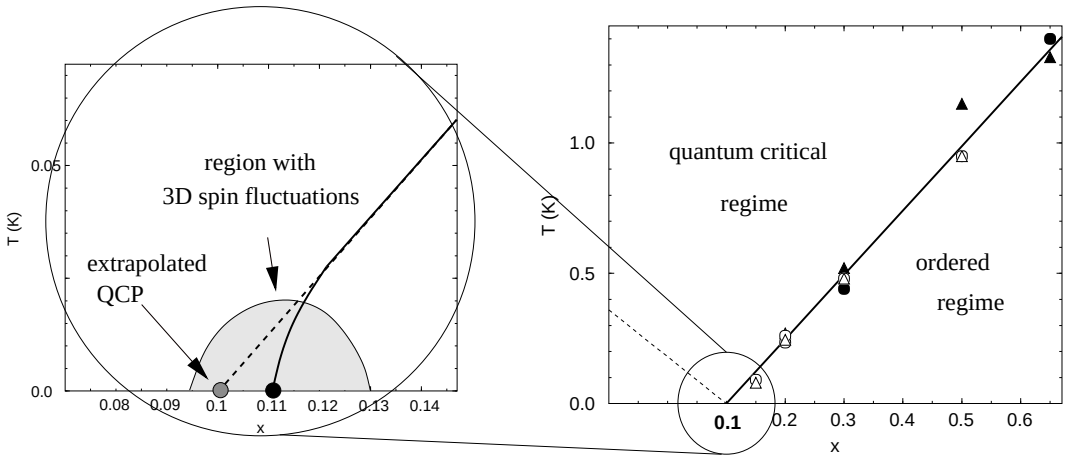

Figure 4.1: *The right panel shows the phase diagram of $CeCu_{6-x}Au_x$ [37] as a function of doping x. The zoom in the left panel is a sketch of the presumed 2D–3D dimensional crossover scenario.*

for various doping levels $x > 0.1$. Thermodynamic measurements [7] as well as neutron scattering experiments [8] on $CeCu_{5.9}Au_{0.1}$ have not observed any signatures of 3D spin fluctuations at the lowest temperatures. One could argue that the temperatures reached were still not low enough to detect the tiny coupling between the two-dimensional planes. Another line of argument suggests that the extrapolated quantum critical point at a doping level of $x = 0.1$ may not coincide with the actual location. In the three-dimensional pocket the functional dependence of the Néel temperature on doping might deviate from the linear behavior observed for higher doping levels, as indicated in the left panel of Fig. 4.1. As a consequence, the alloy $CeCu_{5.9}Au_{0.1}$ might not be located well inside the 3D pocket or might even fall outside it which would serve as a simple explanation of why 3D spin fluctuations have not been seen at lowest temperatures. The error in the location of the quantum critical point determined from an extrapolation of the experimental data can, however, be estimated theoretically. This is one of the purposes of this chapter. We will further clarify how the dimensional crossover is reflected in thermodynamic quantities: correlation length, specific heat, thermal expansion and the Grüneisen parameter.

Local quantum criticality

Apart from the specific questions posed by experiment the 2D–3D dimensional crossover scenario is also of interest for the notion of locally critical phase transitions in metals. Q. Si *et al.* [20, 21] have proposed a scenario for heavy fermion systems where the critical fluctuations of the local magnetic moments coexists with the extended two-dimensional spin fluctuations of the conduction electrons. They are interwoven and nurture each other in such a way that they become critical together. In contrast to, for example, the Hertz theory where the critical fluctuation modes are all extended the important feature of this new scenario is the inclusion of locally critical modes, which is the reason why this scenario has been dubbed a local quantum phase transition.

The scenario of a local quantum phase transition has also been proposed for $CeCu_{6-x}Au_x$ in order to explain the infamous ω/T scaling of the susceptibility [38].

A necessary condition for the development of local quantum criticality is the existence of two-dimensional spin fluctuations. The associated local spin susceptibility is characterized by a logarithmic divergence of the Mermin–Wagner type (3.1). This singularity feeds back into the coupling to the local moments giving rise to important nonlinear effects that are eventually responsible for why the extended and local modes become critical in a coordinated fashion. In three dimensions, however, the susceptibility is non-singular and such feedback is harmless: the conventional scenario of the Hertz model is expected to apply. Accordingly, in a material with a non-vanishing coupling in the third dimension the local quantum criticality should pass away when the 2D to 3D crossover occurs. All the predictions of local quantum criticality are therefore restricted to a regime where the two-dimensional spin fluctuations prevail, i.e. to high temperatures, and do not apply to the immediate vicinity of the quantum critical point. The position of the dimensional crossover in the phase diagram will therefore also clarify where the scenario of local quantum criticality is expected to break down.

Model

We are interested in the limit when the spin fuctuations are almost two-dimensional, i.e. when they prefer to propagate in two-dimensional planes and their mobility between the planes

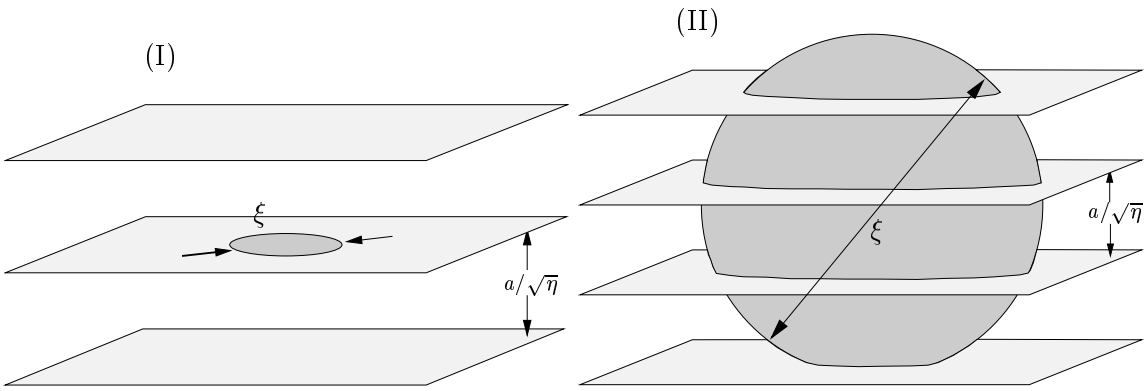

Figure 4.2: *Sketch of a fluctuation mode with (I) high momentum corresponding to a correlation length ξ smaller than the stretched distance between the planes $\xi \ll 1/\sqrt{\eta\Lambda^2} \sim a/\sqrt{\eta}$, where a is a lattice constant and η is the anisotropy parameter, and (II) low momentum that extends over several planes and is effectively three dimensional, $\xi \gg 1/\sqrt{\eta\Lambda^2} \sim a/\sqrt{\eta}$.*

is restricted. In a tight-binding picture we can associate a hopping amplitude t with the movement of the spin fluctuations in the planes and an amplitude t' describing their hopping between the planes. Their two dimensional character is reflected in the ratio of these hopping amplitudes, $\eta \equiv t'/t \ll 1$. The resulting energy–momentum dispersion is given by

$$\epsilon(\mathbf{k}) = t\,(2 - \cos k_x a - \cos k_y a) + t'\,(1 - \cos k_\perp a) \approx \xi_0^2\,\left(k_{\shortparallel}^2 + \eta\, k_\perp^2\right) \quad \text{for} \quad k_{\shortparallel}, k_\perp < \Lambda \sim 1/a\,. \tag{4.1}$$

where $\xi_0 = a\sqrt{t/2}$ and a is a lattice constant. The momentum component $k_\perp$ is perpendicular to the planes and k_x, k_y and $k_{\shortparallel}$ are the components in the plane. The approximation is valid for small momenta with the inverse lattice constant as a momentum cutoff, $\Lambda \sim 1/a$, and it describes the long-distance behavior that controls the critical behavior. The contribution of the perpendicular momentum component is weighted with the small number $\eta = t'/t$. In the limit $\eta \to 0$ the perpendicular component of momentum does not contribute and true two-dimensional physics is recovered. With an appropriate substitution of the perpendicular momentum we can rewrite the above dispersion relation as

$$\epsilon(\mathbf{k}) = \xi_0^2\,\left(k_{\shortparallel}^2 + k_\perp^2\right) \quad \text{for} \quad k_{\shortparallel} < \Lambda \sim \frac{1}{a} \quad \text{and} \quad k_\perp < \sqrt{\eta\Lambda^2} \sim \frac{\sqrt{\eta}}{a}\,. \tag{4.2}$$

The dispersion now *seems* to be isotropic in momentum space, but the cutoff for the perpendicular component now corresponds to an inverse stretched lattice constant of $a/\sqrt{\eta}$. This provides an alternative physical picture that will be suitable for an intuitive understanding of the dimensional crossover in criticality. By incorporating the anisotropy parameter in a new stretched lattice constant $a/\sqrt{\eta} = a\sqrt{t/t'}$ the approach to the two-dimensional limit $\eta \to 0$ can be interpreted as an increased separation of the two-dimensional planes; for $\eta = 0$ the planes have an infinite separation and therefore do not communicate with each other. The crossover from 2D to 3D criticality occurs when the correlation length ξ has increased such that it starts to extend over several stretched distances $a/\sqrt{\eta}$, see Fig. 4.2.

We are going to describe the dynamics of the antiferromagnetic spin fluctutions with the Hertz theory (2.23) with a dynamical exponent $z = 2$. The above considerations motivate the modifications of the Gaussian propagator (2.27),

$$\chi_0^{-1}(i\omega_n, \mathbf{k}) \;\; = \;\; \delta_0 + \xi_0^2\,\left(k_{\shortparallel}^2 + \eta\, k_\perp^2\right) + |\omega_n|/T_0\,. \tag{4.3}$$

The action of the three-dimensional anisotropic Hertz theory then reads (compare with (2.23))

$$\begin{aligned} S_{\mathrm{AH}}[\Phi] &= \frac{1}{\beta V}\sum_{\omega_n,\mathbf{k}} \frac{1}{2}\Phi^T(i\omega_n,\mathbf{k})\,\chi_0^{-1}(i\omega_n,\mathbf{k})\,\Phi(-i\omega_n,-\mathbf{k}) + S^{(4)}[\Phi] \\ S^{(4)}[\Phi] &= g\frac{1}{\beta^4 V^4}\sum_{\substack{\omega_{nj},\mathbf{k}_j \\ j=1,2,3,4}} V\delta\left(\sum_{j=1}^4 \mathbf{k}_j\right)\,\beta\,\delta\left(\sum_{j=1}^4 \omega_{nj}\right) \\ &\quad\times\left(\Phi^T(i\omega_{n1},\mathbf{k}_1)\Phi(i\omega_{n2},\mathbf{k}_2)\right)\left(\Phi^T(i\omega_{n3},\mathbf{k}_3)\Phi(i\omega_{n4},\mathbf{k}_4)\right)\,. \end{aligned} \tag{4.4}$$

We have just explained that for momenta in the range between $[\sqrt{\eta}\Lambda,\Lambda]$ the spin fluctuations are effectively two dimensional; they do not extend over a distance of the stretched lattice constant $1/\sqrt{\eta\Lambda^2}$. In particular, for such momenta the perpendicular component of momentum becomes a dead label of the fluctuation modes Φ. The dead label can be absorbed by introducing effective two dimensional fields,

$$\Phi_{\mathrm{2D}}(i\omega_n,\mathbf{k}_{\shortparallel}) \equiv \frac{V_{\mathrm{2D}}}{V}\sum_{\mathbf{k}_\perp}\Phi(i\omega_n,\mathbf{k}_{\shortparallel}) = \int_{-\Lambda}^{\Lambda}\frac{dk_\perp}{2\pi}\Phi(i\omega_n,\mathbf{k}_{\shortparallel}) = \frac{\Lambda}{\pi}\Phi(i\omega_n,\mathbf{k}_{\shortparallel}) \quad \text{for } \mathbf{k}_\perp\in[\sqrt{\eta}\Lambda,\Lambda]\,. \tag{4.5}$$

For high momenta the action will only be a functional of Φ_{2D} and the effective theory is therefore a two-dimensional one. It is instructive to relate the quartic coupling of the effective 2D theory to the quartic coupling g appearing in (4.4),

$$\begin{aligned} S^{(4)}[\Phi_{\mathrm{2D}}] &= \frac{\pi g}{\Lambda}\frac{1}{\beta^4 V_{\mathrm{2D}}^4}{\sum_{\substack{\omega_{nj},\mathbf{k}_{\shortparallel j} \\ j=1,2,3,4}}}' V_{\mathrm{2D}}\delta\left(\sum_{j=1}^4 \mathbf{k}_{\shortparallel j}\right)\,\beta\,\delta\left(\sum_{j=1}^4 \omega_{nj}\right) \\ &\quad\times\left(\Phi_{\mathrm{2D}}^T(i\omega_{n1},\mathbf{k}_{\shortparallel 1})\Phi_{\mathrm{2D}}(i\omega_{n2},\mathbf{k}_{\shortparallel 2})\right)\left(\Phi_{\mathrm{2D}}^T(i\omega_{n3},\mathbf{k}_{\shortparallel 3})\Phi_{\mathrm{2D}}(i\omega_{n4},\mathbf{k}_{\shortparallel 4})\right)\,. \end{aligned} \tag{4.6}$$

The prime on the summation indicates that the momenta are restricted to the intervall $\mathbf{k}_{\shortparallel j}\in[\sqrt{\eta}\Lambda,\Lambda]$. We can read off the effective two-dimensional quartic coupling

$$g_{\mathrm{2D}} = \frac{\pi g}{\Lambda} \quad\Longleftrightarrow\quad g_{\mathrm{2D}}\int_{-\Lambda}^{\Lambda}\frac{dk_\perp}{2\pi} = g\,. \tag{4.7}$$

We are mostly interested in the almost two-dimensional limit, i.e. in the case where the anisotropy parameter η is small. The anisotropic Hertz theory is then effectively two-dimensional except for the small momentum range $[0,\sqrt{\eta\Lambda^2}]$. We will see that for high temperatures $\mathcal{T} > \eta\Lambda^2$ this momentum range leads only to small corrections to the thermodynamics. In the following we will adopt the point of view of high temperatures: we will measure all quantities in units appropriate for the effective high-temperature, high-momentum two dimensional theory.

Particularities

To what extend does the anisotropic Hertz model differs from its true 2D and 3D counterparts analyzed in Chapter 3? Are there any qualitatively new features to be expected?

The most significant difference is the presence of the anisotropy parameter η which tunes between the 2D and 3D limits. It will turn out that the anisotropy parameter η is a relevant

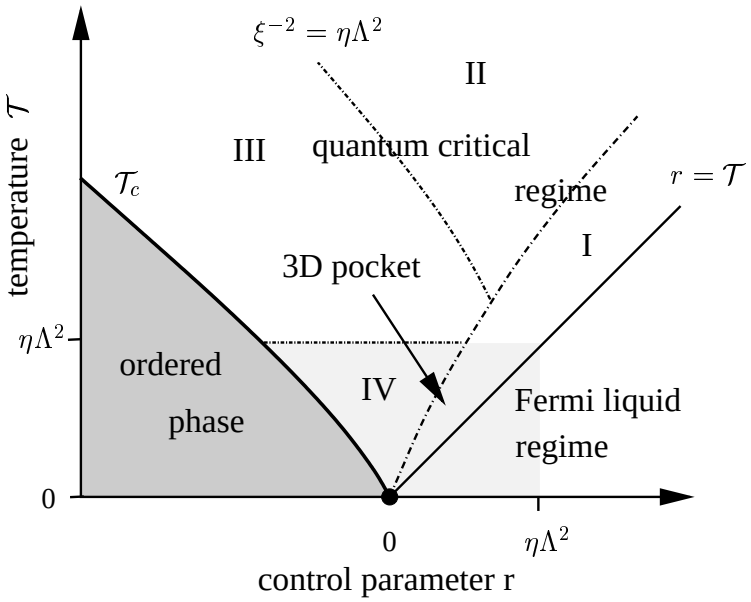

Figure 4.3: *Phase diagram of the anisotropic Hertz model. Three-dimensional spin fluctuations dominate in the shaded pocket around the quantum critical point. Two-dimensional spin fluctuations prevail in the non-shaded part of the phase diagram. The quantum critical regime inside the fan spanned by the solid lines is divided into four sub-regimes with different behaviors of the correlation length. In particular the crossover from sub-region II to sub-region III happens for* $\xi^{-2} \sim \eta\Lambda^2$.

quantity with respect to the two-dimensional fixed point. We will show that it carries the same scaling dimension as the control parameter r. In Chapter 1 we explained in detail that the thermal expansion is sensitive to relevant operators to which the pressure couples. If it is possible to vary not only the control parameter but also the anisotropy parameter with pressure, both will contribute to the thermal expansion. Moreover, since they carry the same scaling dimension both contributions will be equally important when the flow is governed by the two-dimensional fixed point. In particular, the additional contribution to the thermal expansion stemming from a pressure dependence of the anisotropy parameter η is

$$\Delta\alpha = -\frac{1}{V}\frac{dS}{d\eta}\,\frac{\partial\eta}{\partial p}\,. \tag{4.8}$$

This additional contribution constitutes a new feature of the anisotropic Hertz model.

In Fig. 4.3 we offer the reader a glimpse of the phase diagram of the anisotropic Hertz model which we will derive in detail in the forthcoming sections. It should be compared to the diagrams displayed in Section 3.4 for $d = 2, 3$ and $z = 2$. To avoid a clutter of lines we have omitted the crossover to the non-Gaussian regime. As before, the physics of the ordered regime (dark gray area) is beyond the scope of the Hertz theory and will not be discussed here. Around the quantum critical point (indicated by the light gray area) the physics is dominated by the 3D fixed point. In this regime the crossover lines as well as the leading thermodynamic behavior coincides with the isotropic Hertz model of Chapter 3. The dimensional crossover to the 2D regime occurs upon increasing the temperature or the control parameter above the inverse stretched lattice constant $\sqrt{\eta\Lambda^2}$. Interesting new features emerge in the 2D regime,

which are all linked to the cutting off of the Mermin–Wagner divergence (3.1) present in the true 2D Hertz model. In particular, this divergence prevented an estimate for the critical ordering temperature $\mathcal{T}_c$. As was explained in detail in Chapter 3 these divergences are associated with the effective classical theory. In the anisotropic Hertz model the associated logarithmic divergence is cut off by the anisotropy parameter η and an estimate for the critical temperature can be obtained. The location in the phase diagram where these logarithmic Mermin–Wagner divergencies are neutralized is given by the condition $\xi^2 = \eta\Lambda^2$, and it is associated with a dimensional 2D–3D crossover of the effective classical theory.

Methods

We are going to apply three different methods to investigate the properties of the anisotropic Hertz model. In Section 4.1 we apply a Millis RG treatment. We modify the solution already presented in Chapter 3 to the anisotropic case. It turns out that we have to apply a two-step RG process. In the first stage the anisotropic Hertz theory is rescaled with respect to the 2D fixed point. During this first stage the anisotropy parameter η is a relevant quantity in the RG sense: it will grow. At a certain RG scale it will have reached the isotropic 3D limit $\eta = 1$ and the RG flow stops. In the second stage the resulting effective isotropic 3D Hertz theory is treated within the standard approach of Chapter 3. In Section 4.2 we use the method of dimensional reduction put forward by S. Sachdev [33, 2], which will allow us to compute the crossover functions for the correlation length as a function of temperature, anisotropy parameter η and control parameter r. Finally, in Section 4.3 we apply the large N method which provides reliable information about the functional dependence of the Néel temperature on η and r.

4.1 Millis' RG analysis

In this section we will modify the RG method of Section 2.2 to take into account the anisotropy in momentum space of the propagator (4.3). The idea is to use a two-step RG process. First the theory is scaled towards the fixed point in space dimension $d = 2$. Under this scaling the anisotropy parameter η will grow and the model will flow toward an isotropic Hertz theory. The anisotropy parameter is therefore a relevant operator during the first stage. The RG equations which will govern this flow will be derived in the following sections. At some scale however the isotropic limit $\eta = 1$ will be reached and the theory can be treated with the usual isotropic RG equations of Chapter 2. In this second stage the model flows towards the 3D fixed point.

Cutoff procedure

In order to derive the RG equations we have to specify the cutoff procedure we are going to apply. We will choose an anisotropic cutoff procedure which interpolates between the pure two-dimensional and the pure three-dimensional case. For the perpendicular component of the momentum we take Λ as a cutoff: $-\Lambda \leq k_\perp \leq \Lambda$. For the radial part of the parallel component we choose the bound: $0 \leq k_\shortparallel \leq \sqrt{\Lambda^2 - \eta k_\perp^2}$. The momentum-space volume then becomes

$$\frac{1}{\Lambda^3}\int d^3k = \frac{1}{\Lambda^3}\int_{-\Lambda}^{\Lambda} dk_\perp \int_0^{\sqrt{\Lambda^2-\eta k_\perp^2}} dk_\shortparallel \, 2\pi k_\shortparallel = 2\pi\left(1 - \frac{\eta}{3}\right) \tag{4.9}$$

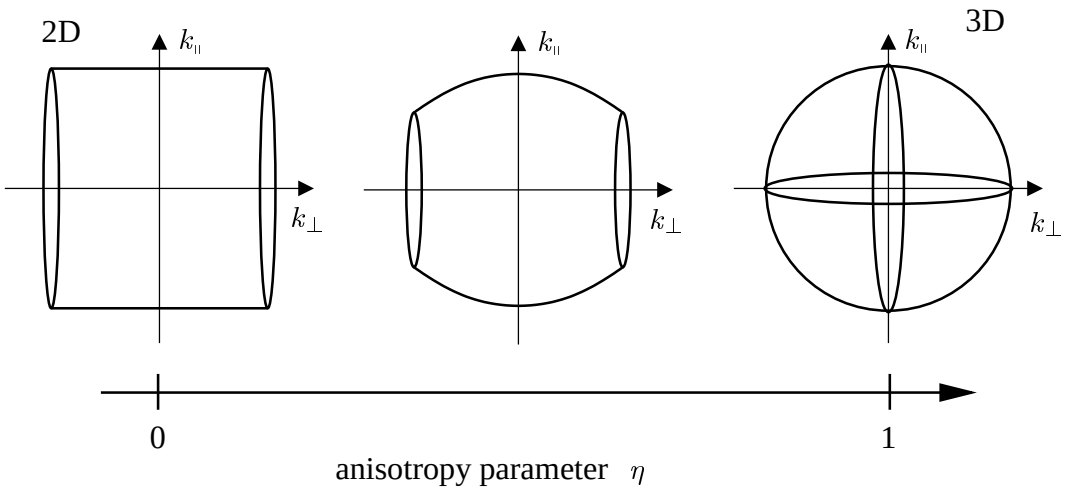

Figure 4.4: *Evolution of the sphere in momentum space during the flow towards the isotropic 3D limit according according to the cutoff procedure (4.9).*

which interpolates nicely between the value $4\pi/3$ for the 3D limit, $\eta = 1$, and the value 2π of the 2D limit, $\eta = 0$. Fig. 4.4 represents the evolution of the momentum-sphere and its enclosed volume as the anisotropy parameter, η, increases under the RG flow. In the isotropic 3D limit the usual three-dimensional sphere in momentum space is recovered.

Gaussian contribution

It is instructive to consider first the Gaussian contribution only. The Gaussian free energy (2.33) modified for the three-dimensional anisotropic Hertz model with the above cutoff scheme applied reads ($z = 2$)

$$\frac{\pi\xi_0^d}{VT_0\Lambda}\Delta F_G = -\frac{N}{2}\,\frac{\pi}{\Lambda}\int_{-\Lambda}^{\Lambda}\frac{dk_\perp}{2\pi}\int_0^{\sqrt{\Lambda^2-\eta k_\perp^2}}\frac{dk_{\shortparallel}}{(2\pi)^2}\,2\pi k_{\shortparallel}\int_0^\infty\frac{d\epsilon}{\pi}\left(\coth\frac{\epsilon}{2\mathcal{T}}-1\right)\arctan\frac{\epsilon}{\delta_0+k_{\shortparallel}^2+\eta k_\perp^2}$$

$$= -\frac{N}{2}\left(\underbrace{K_2\int_{\sqrt{\eta\Lambda^2}}^{\Lambda}dk\,k}_{\text{2D part}}+\underbrace{\frac{K_2}{\sqrt{\eta\Lambda^2}}\int_0^{\sqrt{\eta\Lambda^2}}dk\,k^2}_{\text{3D part}}\right)\times\int_0^\infty\frac{d\epsilon}{\pi}\left(\coth\frac{\epsilon}{2\mathcal{T}}-1\right)\arctan\frac{\epsilon}{\delta_0+k^2}\,. \tag{4.10}$$

We have subtracted the zero temperature contribution and introduced the dimensionless temperature $\mathcal{T} = T/T_0$. The surface of the d-dimensional momentum sphere K_d was defined in (2.45). In the second line after performing an integration by parts with respect to the perpendicular momentum component $k_\perp$ the Gaussian energy separated into two parts. We can interpret the part associated with a high momentum k as the two-dimensional contribution and the low momentum part as the three-dimensional contribution. The modes with a high momentum probe only a small region in space and therefore do not perceive the coupling between the two-dimensional planes. These high-momentum modes are effectively

two-dimensional. The modes with sufficiently small momenta, however, cannot resolve the spatial distances between the planes and therefore live in three-dimensional space, see Fig. 4.2.

4.1.1 Flow to the isotropic limit

RG equations

During the flow towards the isotropic limit the two-dimensional fluctuations are integrated out step by step leading to a renormalization of the coupling constants. The RG equations are derived in the spirit of Millis' original treatment, described in Chapter 2. In particular, we will always measure the free energy and the quartic coupling in two (!) dimensional units $\mathcal{F} = F\pi\xi_0^3/(T_0 V\Lambda)$, $u = g\pi\xi_0^3/(T_0 V\Lambda)$ and temperature $\mathcal{T} = T/T_0$, where V is the three dimensional volume. Using the same conventions the RG equations for the flow to the isotropic limit read

$$\begin{aligned}
\frac{\partial \mathcal{F}(b)}{\partial \log b} &= (d+z)\,\mathcal{F}(b) - \frac{1}{2}\,N\,a_0(\delta(b),\mathcal{T}(b),\eta(b)) \\
\frac{\partial \eta(b)}{\partial \log b} &= 2\,\eta(b) \\
\frac{\partial \mathcal{T}(b)}{\partial \log b} &= z\,\mathcal{T}(b) \\
\frac{\partial \delta(b)}{\partial \log b} &= 2\,\delta(b) + 4\,(N+2)\,u(b)\,a_2(\delta(b),\mathcal{T}(b),\eta(b)) \\
\frac{\partial u(b)}{\partial \log b} &= (4-d-z)\,u(b) - 4\,(N+8)\,u^2(b)\,a_4(\delta(b),\mathcal{T}(b),\eta(b))
\end{aligned} \tag{4.11}$$

where $d = z = 2$ is implied. The four RG equations are now supplemented by an additional one for the anisotropy parameter η, which has the scaling dimension 2 and is therefore a relevant quantity. The functions a_n are given by

$$\begin{aligned}
a_0(\delta,T,\eta) &= K_2\Lambda^2 \int_0^\Gamma \frac{d\epsilon}{\pi}\,\coth\frac{\epsilon}{2T}\arctan\frac{\epsilon}{\delta+\Lambda^2} \\
&\quad + \frac{\pi}{\Lambda}\int_{-\Lambda}^{\Lambda}\frac{dk_\perp}{2\pi}\int_0^{\sqrt{\Lambda^2-\eta k_\perp^2}}\frac{k_\shortparallel dk_\shortparallel}{2\pi}\,\frac{2\Gamma}{\pi}\,\coth\frac{\Gamma}{2T}\arctan\frac{\Gamma}{\delta+k_\shortparallel^2+\eta\,k_\perp^2} \\
a_2(\delta,T,\eta) &= -\frac{\partial}{\partial\delta}\,a_0(\delta,T,\eta) \\
a_4(\delta,T,\eta) &= -\frac{\partial}{\partial\delta}\,a_2(\delta,T,\eta)
\end{aligned} \tag{4.12}$$

and K_d is defined in (2.45). The leading correction at finite temperatures stems from the contribution due to the renormalization of momentum

$$a_0(\delta,T,\eta) - a_0(\delta,0,\eta) = K_2\Lambda^2\int_0^\infty\frac{d\epsilon}{\pi}\,\left(\coth\frac{\epsilon}{2T}-1\right)\arctan\frac{\epsilon}{\delta+\Lambda^2} + \mathcal{O}\left(e^{-\Gamma/\mathcal{T}}\right). \tag{4.13}$$

4.1.2 Crossover parameters

The solution of the RG equation for the anisotropy parameter is $\eta(b) = \eta b^2$. The scale b^* where the theory reaches the isotropic limit, $\eta(b^*) = 1$, can therefore be identified as

$$b^* \equiv \frac{1}{\sqrt{\eta}}. \tag{4.14}$$

In this section we are concerned with the values the parameters attain at this crossover scale. These rescaled parameters then act as the initial or effective parameters for the isotropic 3D flow. The derivation of the crossover values follows along the lines of the calculations presented in chapter 2 and the presentation will therefore be kept concise.

Quartic coupling

During the flow to the isotropic limit the theory is at its upper critical dimension: the quartic coupling is marginal. The RG equation for the quartic coupling u can be rewritten as an integral

$$u(b) = \frac{u}{1+4(N+8)\,u\,g(b)} \tag{4.15}$$

$$g(b) = \int_0^{\log b} dx\, a_4(R(e^x)e^{2x}, \mathcal{T}e^{zx}, \eta e^{2x})\,. \tag{4.16}$$

In the vicinity of the quantum critical point the quartic coupling is given by

$$u(b) \approx \frac{u}{1+4(N+8)\,u\,a_4\,\log b} = \frac{1}{4(N+8)\,a_4}\left(\log b\; e^{\frac{1}{4(N+8)\,a_4\,u}}\right)^{-1}, \tag{4.17}$$

where

$$\begin{aligned} a_4 \equiv a_4(0,0,\eta) &= \frac{K_2\sqrt{\Gamma}}{\sqrt{32}\pi\sqrt{\eta\Lambda^2}}\left(2\arctan\left(1+\sqrt{\frac{2\,\eta\Lambda^2}{\Gamma}}\right) - 2\arctan\left(1-\sqrt{\frac{2\,\eta\Lambda^2}{\Gamma}}\right)\right. \\ &\left. + \log\frac{\Gamma+\eta\Lambda^2+\sqrt{2\Gamma\eta\Lambda^2}}{\Gamma+\eta\Lambda^2-\sqrt{2\Gamma\eta\Lambda^2}}\right) = \frac{K_2}{\pi}\left(1+\mathcal{O}\left(\frac{\eta\Lambda^2}{\Gamma}\right)^2\right). \end{aligned}$$

At the crossover scale $b^* = 1/\sqrt{\eta}$ the quartic coupling takes the value

$$u^* \equiv u(b^*) = \frac{1}{4(N+8)\,a_4}\left(\log \eta^{-1/2}\; e^{\frac{1}{4(N+8)\,a_4\,u}}\right)^{-1}. \tag{4.18}$$

Effective mass

As in Section 2.2.3 we separate the trivial scaling dimension of the running mass, $\delta(b) = R(b)\,b^2$. The result for the zero-temperature running mass, $\Delta(b)$, follows the derivation of (3.20),

$$\Delta(b) \simeq \frac{r^*}{\left(\log\left[b^2\; e^{\frac{2}{4(N+8)\,a_4\,u}}\right]\right)^{\frac{N+2}{N+8}}}. \tag{4.19}$$

The control parameter r^* of the primary, two-dimensional fixed point reads

$$r^* \equiv \frac{1}{(2(N+8)a_4u)^{\frac{N+2}{N+8}}}\left(\delta_0 + 4\,(N+2)\;a_2(0,0)\int_0^{-\log\sqrt{\eta}} dx\, e^{-2x}\,u(e^x)\right). \tag{4.20}$$

The temperature correction $R_T(b)$ (2.56) to the running mass, $R(b) = \Delta(b) + R_T(b)$, at the crossover scale $b^* = 1/\sqrt{\eta}$ is given by

$$R_T(b^*) = 4\,(N+2)\,K_2\mathcal{T} \tag{4.21}$$
$$\times \int\limits_{\log \mathcal{T}^{1/2}/\Lambda}^{\log \mathcal{T}^{1/2}/(\sqrt{\eta}\Lambda)} dx\, e^{2x}\, u(\Lambda\mathcal{T}^{-\frac{1}{2}}\, e^x) \int\limits_0^\infty \frac{dv}{\pi} \frac{4\,v\,(\coth v - 1)}{\left(R(\Lambda\mathcal{T}^{-\frac{1}{2}}\, e^x)\mathcal{T}^{-1}e^{2x}+1\right)^2 + (2\,e^{2x}v)^2}\,.$$

The temperature correction depends on two parameters. In the quantum critical regime the magnitude of the parameter $\mathcal{T}/(\eta\Lambda^2)$ appearing in the upper limit of the x-integral determines whether the contribution from the RG trajectory towards the isotropic limit is significant. Similarly, the Fermi liquid regime is divided into two sub-regimes by the parameter $r^*/(\eta\Lambda^2)$. In the 3D regime the contributions from the 2D flow can be neglected to leading order. The interesting case here is the 2D regime which we will consider in the following.

Temperature correction in the quantum critical 2D regime: $\mathcal{T} \gg \eta\Lambda^2$ and $\Delta \ll \mathcal{T}$

As in the case of the 2D isotropic theory a logarithmic divergence is expected in the 2D regime from scaling into the classical region. In the isotropic case this divergence was cut off by the running mass in the denominator of the integrand of the temperature correction (3.24). In the anisotropic case the divergence for the effective mass at the crossover scale is either cut off by the combination $R(.)/\mathcal{T}$ in the denominator or by the upper limit of the x-integral in (4.21). The result will therefore depend on the combination $R^*/(\eta\Lambda^2)$.

We will proceed as in the case of the isotropic theory in $d = 2$. After integrating by parts with respect to the x-integral expression (4.21) becomes

$$R_T(b^*) = 4\,(N+2)\,K_2\mathcal{T} \tag{4.22}$$
$$\times \left\{ \left[x\, u(\Lambda\mathcal{T}^{-\frac{1}{2}}\, e^x) \int\limits_0^\infty \frac{dv}{\pi} \frac{4\,e^{2x}v\,(\coth v - 1)}{\left(R(\Lambda\mathcal{T}^{-\frac{1}{2}}\, e^x)\mathcal{T}^{-1}e^{2x}+1\right)^2 + (2\,e^{2x}v)^2} \right]_{x=\log \mathcal{T}^{1/2}/\Lambda}^{x=\log \mathcal{T}^{1/2}/(\sqrt{\eta}\Lambda)} \right.$$
$$\left. - \int\limits_{\log \mathcal{T}^{1/2}/\Lambda}^{\log \mathcal{T}^{1/2}/(\sqrt{\eta}\Lambda)} dx\, x\, \frac{d}{dx} \left[u(\Lambda\mathcal{T}^{-\frac{1}{2}}\, e^x) \int\limits_0^\infty \frac{dv}{\pi} \frac{4\,e^{2x}v\,(\coth v - 1)}{\left(R(\Lambda\mathcal{T}^{-\frac{1}{2}}\, e^x)\mathcal{T}^{-1}e^{2x}+1\right)^2 + (2\,e^{2x}v)^2} \right] \right\}\,.$$

First let us consider the surface term,

$$\left[x\, u(\Lambda\mathcal{T}^{-\frac{1}{2}}\, e^x) \int\limits_0^\infty \frac{dv}{\pi} \frac{4\,e^{2x}v\,(\coth v - 1)}{\left(R(\Lambda\mathcal{T}^{-\frac{1}{2}}\, e^x)\mathcal{T}^{-1}e^{2x}+1\right)^2 + (2\,e^{2x}v)^2} \right]_{x=\log \mathcal{T}^{1/2}/\Lambda}^{x=\log \mathcal{T}^{1/2}/(\sqrt{\eta}\Lambda)}$$
$$= \log\frac{\mathcal{T}^{1/2}}{\sqrt{\eta}\Lambda}\, u(\eta^{-1/2}) \int\limits_0^\infty \frac{dv}{\pi} \frac{4\,\frac{\mathcal{T}}{\eta\Lambda^2}v\,(\coth v - 1)}{(R^*/(\eta\Lambda^2)+1)^2 + \left(2\,\frac{\mathcal{T}}{\eta\Lambda^2}v\right)^2} + \mathcal{O}\left(u\frac{\mathcal{T}}{\Lambda^2}\log\frac{\mathcal{T}}{\Lambda^2}\right) \tag{4.23}$$
$$= \log\frac{\mathcal{T}^{1/2}}{\sqrt{\eta}\Lambda}\, u(\eta^{-1/2}) \left(\frac{1}{1+R^*/(\eta\Lambda^2)} + \mathcal{O}\left(\frac{\eta\Lambda^2}{\mathcal{T}}\log\frac{\eta\Lambda^2}{\mathcal{T}}\right)\right) + \mathcal{O}\left(u\frac{\mathcal{T}}{\Lambda^2}\log\frac{\mathcal{T}}{\Lambda^2}\right)$$

In the last line we extracted the leading contribution in the 2D regime $\mathcal{T} \gg \eta\Lambda^2$. It stems from small arguments of the hyperbolic function, i.e. from scaling into the classical regime. The integral of (4.22) can be treated along the lines of the derivation of the correlation length at the upper critical dimension in the isotropic theory of Section 3.2.2. The origin of the leading contribution lies in the fluctuations which lead to the logarithmic Mermin–Wagner divergences (3.1) and which come from small arguments of the hyperbolic function. Expanding the hyperbolic function the integral of (4.22) becomes in leading order [cf. (3.25)],

$$\int\limits_{\log \mathcal{T}^{1/2}/\Lambda}^{\log \mathcal{T}^{1/2}/(\sqrt{\eta}\Lambda)} dx \, \frac{2x \; u(e^x \Lambda \mathcal{T}^{-\frac{1}{2}}) R(e^x \Lambda \mathcal{T}^{-\frac{1}{2}}) \mathcal{T}^{-1} e^{2x}}{\left(1 + R(e^x \Lambda \mathcal{T}^{-\frac{1}{2}}) \mathcal{T}^{-1} e^{2x}\right)^2} \,. \tag{4.24}$$

This can be evaluated with a saddle point approximation. The integrand consists of a function strongly peaked at $x_{\max} = \log \mathcal{T}^{1/2}/{R^*}^{1/2}$ and a slowly varying part. The leading behavior of the integral then depends on whether the position of this peak is located within the integration region or not.

Sub-regime $R^* \gg \eta\Lambda^2$: In this sub-regime the peak lies in the integration region and the integral can be approximated by the saddle point contribution,

$$x_{\max} \, u(e^{x_{\max}} \Lambda \mathcal{T}^{-\frac{1}{2}}) \int\limits_{\log \mathcal{T}^{1/2}/\Lambda}^{\log \mathcal{T}^{1/2}/(\sqrt{\eta}\Lambda)} dx \, \frac{2 \, R(e^{x_{\max}} \Lambda \mathcal{T}^{-\frac{1}{2}}) \mathcal{T}^{-1} \, e^{2x}}{\left(1 + R(e^{x_{\max}} \Lambda \mathcal{T}^{-\frac{1}{2}}) \mathcal{T}^{-1} e^{2x}\right)^2}$$
$$= x_{\max} \, u(e^{x_{\max}} \Lambda \mathcal{T}^{-\frac{1}{2}}) \left(1 + \mathcal{O}\left(\frac{\eta\Lambda^2}{R^*}\right)\right)$$

The surface term is negligible in the subregion $R^* \gg \eta\Lambda^2$. Using the expression (4.17) for the running quartic coupling constant the effective mass at the crossover scale becomes in leading order [cf. (3.27)]

$$R^* = \Delta + \pi \, \frac{N+2}{N+8} \, \mathcal{T} \, \frac{\log \frac{\mathcal{T}}{R^*}}{\log \frac{\bar{\Lambda}^2}{R^*}} \tag{4.25}$$

where we have introduced the "renormalized" cutoff

$$\bar{\Lambda} \equiv \Lambda \, e^{\frac{1}{4(N+8) \, a_4 \, u}} \,. \tag{4.26}$$

Sub-regime $R^* \ll \eta\Lambda^2$: When the peak is beyond the integration region the integral is subleading and the contribution from the surface term dominates. In leading order we obtain,

$$R^* = \Delta + \pi \, \frac{N+2}{N+8} \, \mathcal{T} \, \frac{\log \frac{\mathcal{T}}{\eta\Lambda^2}}{\log \left[e^{\frac{2}{4(N+8) \, a_4 \, u}} / \eta \right]} \,. \tag{4.27}$$

Temperature correction in the 2D Fermi liquid regime: $\Delta \gg \eta\Lambda^2$ and $\Delta \gg \mathcal{T}$

Following the derivation of (3.31) we obtain in leading order for the temperature correction

$$R^* = \Delta + \frac{\pi^2}{6} \, \frac{N+2}{N+8} \, \frac{\mathcal{T}^2}{\Delta \, \log\left(\bar{\Lambda} \Delta^{-\frac{1}{2}}\right)} \,, \tag{4.28}$$

4.1.3 Flow towards the 3D fixed point

After the theory has reached the isotropic limit at the scale $b^* = 1/\sqrt{\eta}$ the flow is governed by a new set of RG equations: the RG equations of the 3D isotropic Hertz model (2.40-2.43) for a dynamical exponent $z = 2$. However, since we have chosen units of measurements with respect to the two-dimensional theory the function f_n of Eqs. (2.44) should be multiplied by π/Λ, so that effectively the surface of the three dimensional momentum sphere K_3 appearing in the f_n functions (2.44) gets replaced by $K_3\pi/\Lambda = K_2/\Lambda$. Furthermore, the initial conditions for the 3D flow are given by the 2D running parameters at the crossover scale $b^* = 1/\sqrt{\eta}$,

$$\begin{aligned} \mathcal{F}(b^*) &= \mathcal{F}^* \\ \delta(b^*) &= \delta^* = R^* b^{*2} \\ u(b^*) &= u^* \,, \end{aligned} \tag{4.29}$$

Solving the new RG equation for example for the quartic coupling (2.43) we obtain

$$u(b) = u^* b^* b^{-1} \qquad \text{for} \quad b > b^* \,. \tag{4.30}$$

i.e. the quartic coupling decreases for scales larger than b^*. The quartic coupling is irrelevant with respect to the three-dimensional fixed point.

4.1.4 Correlation length

Following the derivation of (3.4) the correlation length is given by the expression

$$\begin{aligned} \xi^{-2} &= \Delta + R_T(b^*) + 4\,(N+2)\,K_2\,u^* \frac{\mathcal{T}^{\frac{3}{2}}}{\sqrt{\eta\Lambda^2}} \\ &\quad \times \int\limits_{\log \mathcal{T}^{1/2}/(\sqrt{\eta}\Lambda)}^{\infty} dx \int\limits_0^{\infty} \frac{dv}{\pi} \frac{4\,v\,(\coth v - 1)\; e^x}{\left(R(e^x\Lambda\mathcal{T}^{-\frac{1}{2}})\mathcal{T}^{-1}e^{2x} + 1\right)^2 + (2\,e^{2x}v)^2} \,. \end{aligned} \tag{4.31}$$

The zero temperature gap Δ is to be taken at the scale set by the correlation length $b = \xi\Lambda$ (compare with Section 3.2),

$$\Delta \simeq \begin{cases} \dfrac{r^*}{\left(\log \frac{\bar{\Lambda}^2}{\xi^{-2}}\right)^{\frac{N+2}{N+8}}} & \text{if} \qquad \eta\Lambda^2 \ll \xi^{-2} \\ \left(\dfrac{r^*}{\left(\log \frac{\bar{\Lambda}^2}{\eta\Lambda^2}\right)^{\frac{N+2}{N+8}}} + \frac{N+2}{N+8}\frac{\pi^2 f_2(0,0)}{3\,\Lambda K_2}\dfrac{\eta}{\log \frac{\bar{\Lambda}}{\sqrt{\eta\Lambda^2}}}\right)\left(1 - \frac{N+2}{N+8}\frac{1}{\Lambda}\dfrac{1}{\log \frac{\bar{\Lambda}}{\sqrt{\eta\Lambda^2}}}\right) & \text{if} \qquad \eta\Lambda^2 \gg \xi^{-2} \end{cases} \tag{4.32}$$

Note that $f_2(0,0)$ is non-universal and depends on the cut-off.

In the following we list the results for the different regimes of Fig. 4.3.

Quantum critical 2D regime: $\mathcal{T} \gg \eta\Lambda^2$ and $\Delta \ll \mathcal{T}$

Up to corrections of order $\mathcal{O}(\mathcal{T}/(\eta\Lambda^2))^{-3/2}$ the correlation length is given by the effective mass R^*. Using the results obtained in Section 4.1.2 we get in leading order

$$\xi^{-2} = \Delta + \pi \frac{N+2}{N+8} \mathcal{T} \begin{cases} \dfrac{\log \mathcal{T}/\xi^{-2}}{\log \bar{\Lambda}^2/\xi^{-2}} & \text{for} \quad \xi^{-2} \gg \eta\Lambda^2 \\ \dfrac{\log \mathcal{T}/(\eta\Lambda^2)}{\log \bar{\Lambda}^2/(\eta\Lambda^2)} & \text{for} \quad \xi^{-2} \ll \eta\Lambda^2 \,. \end{cases} \tag{4.33}$$

where the "renormalized" cutoff $\bar{\Lambda}$ was defined in (4.26). Solving this implicit equation iteratively as in the derivation of (3.28) and discarding (logarithmic) corrections we obtain three different sub-regimes denoted as I, II and III in Fig. 4.3

$$\xi^{-2} = \begin{cases} \Delta & \text{for I:} \quad \eta\Lambda^2 \ll \pi \dfrac{N+2}{N+8} \dfrac{\mathcal{T} \log\log\left(\bar{\Lambda}^2/\mathcal{T}\right)}{\log\left(\bar{\Lambda}^2/\mathcal{T}\right)} \ll \Delta \\ \pi \dfrac{N+2}{N+8} \dfrac{\mathcal{T} \log\log\left(\bar{\Lambda}^2/\mathcal{T}\right)}{\log\left(\bar{\Lambda}^2/\mathcal{T}\right)} & \text{for II:} \quad |\Delta|, \eta\Lambda^2 \ll \pi \dfrac{N+2}{N+8} \dfrac{\mathcal{T} \log\log\left(\bar{\Lambda}^2/\mathcal{T}\right)}{\log\left(\bar{\Lambda}^2/\mathcal{T}\right)} \\ \pi \dfrac{N+2}{N+8} \mathcal{T} \dfrac{\log\left(\mathcal{T}/(\eta\Lambda^2)\right)}{\log\left(\bar{\Lambda}^2/(\eta\Lambda^2)\right)} & \text{for III:} \quad |\Delta| \ll \pi \dfrac{N+2}{N+8} \dfrac{\mathcal{T} \log\log\left(\bar{\Lambda}^2/\mathcal{T}\right)}{\log\left(\bar{\Lambda}^2/\mathcal{T}\right)} \ll \eta\Lambda^2 \end{cases} \tag{4.34}$$

Upon approaching the phase boundary in the quantum critical 2D regime the temperature dependence of the correlation length involves some complicated logarithmic corrections, which can be traced back to the fact that (a) the effective zero-temperature theory is at its upper critical dimension $d+z = 4$ and (b) the effective finite temperature theory is at its lower critical dimension $d = 2$ leading to Mermin–Wagner divergences (3.1). When the crossover between regions II and III is reached for $\xi^{-2} = \eta\Lambda^2$ the fluctuations start to notice the small coupling in the third dimension, ultimately allowing a classical finite-temperature phase transition which would be prohibited in 2D. Accordingly, the logarithmic temperature corrections are modified upon entering region III.

Quantum critical 3D regime: $\mathcal{T} \ll \eta\Lambda^2$ and $\Delta \ll \mathcal{T}$

Now the flow towards the isotropic limit is negligible and the correlation length is given by (3.5),

$$\xi^{-2} \;=\; \Delta + 4(N+2)\, K_2 \frac{\Gamma\left(\frac{3}{2}\right) \zeta\left(\frac{3}{2}\right)}{\sqrt{2}} u^* \frac{\mathcal{T}^{3/2}}{\sqrt{\eta\Lambda^2}} \,. \tag{4.35}$$

with u^* given by (4.18). With the limiting expression (4.17) for the coefficient a_4 this formula simplifies to

$$\xi^{-2} \;=\; \Delta + \sqrt{2}\pi\, \Gamma\left(\frac{3}{2}\right) \zeta\left(\frac{3}{2}\right) \frac{N+2}{N+8} \frac{\mathcal{T}^{3/2}}{\sqrt{\eta\Lambda^2}\, \log\left(\bar{\Lambda}^2/(\eta\Lambda^2)\right)} \,. \tag{4.36}$$

Depending on their relative values either the control parameter r via Δ or the temperature dominates the correlation length, indicated by the shaded part of regions I and region IV respectively in Fig. 4.3.

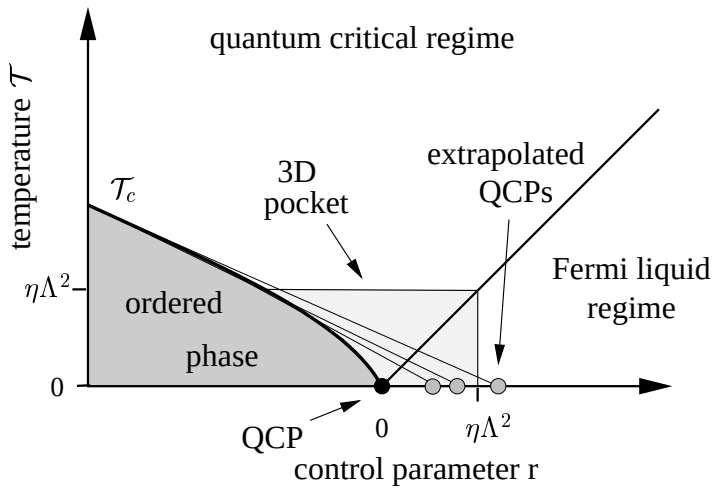

Figure 4.5: *The location of the extrapolated QCP is ambiguous because of logarithmic corrections in the functional dependence (4.39) of the critical temperature on r.*

2D Fermi liquid regime: $\Delta \gg \eta\Lambda^2$ and $\Delta \gg \mathcal{T}$

The mass R^*, now given by expression (4.28), again determines the correlation length,

$$\xi^{-2} = \Delta + \frac{\pi^2}{3}\,\frac{N+2}{N+8}\,\frac{\mathcal{T}^2}{\Delta\,\log\left(\bar{\Lambda}^2/\Delta\right)}\,. \tag{4.37}$$

3D Fermi liquid regime: $\Delta \ll \eta\Lambda^2$ and $\Delta \gg \mathcal{T}$

The leading contribution to the correlation length is given by expression (3.10),

$$\xi^{-2} = \Delta + \frac{N+2}{N+8}\frac{\pi^3}{6}\,\frac{1}{\log\left(\bar{\Lambda}^2/(\eta\Lambda^2)\right)}\,\frac{\mathcal{T}^2}{\sqrt{\Delta}\,\sqrt{\eta\Lambda^2}}\,. \tag{4.38}$$

In both Fermi liquid regimes the temperature dependence is sub-leading.

4.1.5 Estimate of the phase boundary

Strictly speaking the position of the phase boundary cannot reliably be determined within the RG analysis of this section, as was explained in detail in Section 2.2.4. Upon approaching the phase boundary from the disordered side higher order interactions increase in importance since the effective finite-temperature theory is below its upper critical dimension, and so the Ginzburg criterion is fulfilled before the phase boundary is reached. However, we will nevertheless use the results of the correlation length to get an estimate of the position of the finite-temperature phase transition. The result obtained will be confirmed by Sachdev's method of dimensional reduction in Section 4.2 as well as the large N analysis in Section 4.3.

Setting the correlation length in expressions (4.33) and (4.36) to infinity we obtain

$$\frac{r}{\eta\Lambda^2} \simeq \begin{cases} -\pi\,\dfrac{N+2}{N+8}\,\dfrac{\mathcal{T}_c}{\eta\Lambda^2}\,\dfrac{\log\left[\mathcal{T}_c/(\eta\Lambda^2)\right]}{\left(\log\frac{\bar{\Lambda}^2}{\eta\Lambda^2}\right)^{1-\frac{N+2}{N+8}}} & \text{for} \quad \eta\Lambda^2 \ll \mathcal{T}_c \\ -\dfrac{\pi^{3/2}\,\zeta\,(3/2)}{\sqrt{2}}\,\dfrac{N+2}{N+8}\,\dfrac{1}{\left(\log\frac{\bar{\Lambda}^2}{\eta\Lambda^2}\right)^{1-\frac{N+2}{N+8}}}\left(\dfrac{\mathcal{T}_c}{\eta\Lambda^2}\right)^{3/2} & \text{for} \quad \mathcal{T}_c \ll \eta\Lambda^2\,. \end{cases} \tag{4.39}$$

The corrections to the control parameter from the scaling towards the secondary, 3D fixed point are subleading and have been neglected, $r \simeq r^*$, see Eq. (4.32). The phase boundary in the 2D regime, $\eta\Lambda^2 \ll \mathcal{T}_c$, depends on temperature as $\mathcal{T}_c \log \mathcal{T}_c/(\eta\Lambda^2)$, i.e. the linear dependence of the critical temperature on the control parameter has logarithmic corrections. This implies that one cannot unambiguously extrapolate the phase boundary from high temperatures. The location of the extrapolated quantum critical point depends sensitively on the range of critical temperatures used in the extrapolation process; this is indicated by the thin lines in Fig. 4.5. In particular, this prevents us from using the extrapolated QCP of $CeCu_{6-x}Au_x$ (see Fig. 4.1) to draw any conclusions about the value of the anisotropy parameter $\eta\Lambda^2$.

The phase boundary is logarithmically suppressed in comparison with the crossover line between the quantum critical to the Fermi liquid regime, $\Delta \sim \mathcal{T}$. The logarithmic suppression is rooted in the Mermin–Wagner divergence (3.1) which prohibits a phase transition for a truely two dimensional system (with $N > 2$). The asymmetry between the slopes of the Néel temperature and the quantum critical-Fermi liquid crossover line is therefore a qualitative measure of the anisotropy present in the material.

4.1.6 Thermal expansion

It is reasonable to assume that the coupling between the 2D dimensional planes is affected when pressure is applied, which means that the anisotropy parameter η is generally dependent on pressure. This leads to an additional contribution to the thermal expansion,

$$\Delta\alpha = -\frac{1}{V}\frac{dS}{d\eta}\,\frac{\partial\eta}{\partial p}\,, \tag{4.40}$$

where the derivative $(\partial\eta/\partial p)$ is approximately constant for weak pressure dependence. This is a novel effect not encountered in the isotropic Hertz model.

Solving the RG equations we obtain for the interesting part of the entropy [cf. (2.63)]

$$\begin{aligned} S_{\mathrm{QCP}} = {} & \frac{N}{2}K_2\,\mathcal{T}\int_{\log\mathcal{T}^{1/2}/\Lambda}^{\log\mathcal{T}^{1/2}/(\sqrt{\eta}\Lambda)} dx \int_0^\infty \frac{dv}{\pi}\,\frac{2v\,e^{-2x}}{\sinh^2 v}\arctan\left(\frac{2\,e^{2x}\,v}{R(e^x\Lambda\mathcal{T}^{-\frac{1}{2}})\,\mathcal{T}^{-1}e^{2x}+1}\right) \\ & + \frac{N}{2}K_2\,\frac{\mathcal{T}^{\frac{3}{2}}}{\sqrt{\eta\Lambda^2}}\int_{\log\mathcal{T}^{1/2}/(\sqrt{\eta}\Lambda)}^{\infty} dx \int_0^\infty \frac{dv}{\pi}\,\frac{2v\,e^{-3x}}{\sinh^2 v}\arctan\left(\frac{2\,e^{2x}\,v}{R(e^x\Lambda\mathcal{T}^{-\frac{1}{2}})\,\mathcal{T}^{-1}e^{2x}+1}\right). \end{aligned} \tag{4.41}$$

The first term is due to the scaling process towards the isotropic limit and it will dominate in the 2D regimes. The second term results from the RG flow of the effective 3D isotropic

model and therefore dominates in the 3D regimes. From the isotropic model we are already familiar with the contribution $\alpha_{\rm QCP}$, which measures the pressure dependence of the control parameter r [cf. (3.44)]

$$\alpha_{\rm QCP} = \frac{N}{2} K_2 \int_{\log \mathcal{T}^{1/2}/\Lambda}^{\log \mathcal{T}^{1/2}/(\sqrt{\eta}\Lambda)} dx \, \frac{\partial R(e^x \Lambda \mathcal{T}^{-\frac{1}{2}})}{\partial r} \int_0^\infty \frac{dv}{\pi} \, \frac{4v^2 \, e^{2\,x} \, \sinh^{-2} v}{\left(R(e^x \Lambda \mathcal{T}^{-\frac{1}{2}}) \, \mathcal{T}^{-1} e^{2x} + 1 \right)^2 + (2\, e^{2x}\, v)^2} + \frac{N}{2} K_2 \frac{\sqrt{\mathcal{T}}}{\sqrt{\eta \Lambda^2}} \int_{\log \mathcal{T}^{1/2}/(\sqrt{\eta}\Lambda)}^{\infty} dx \, \frac{\partial R(e^x \Lambda \mathcal{T}^{-\frac{1}{2}})}{\partial r} \int_0^\infty \frac{dv}{\pi} \, \frac{4v^2 \, e^{x} \, \sinh^{-2} v}{\left(R(e^x \Lambda \mathcal{T}^{-\frac{1}{2}}) \, \mathcal{T}^{-1} e^{2x} + 1 \right)^2 + (2\, e^{2x}\, v)^2} \, . \tag{4.42}$$

In addition, we now have to consider the derivative of the entropy (4.41) with respect to η. There is an explicit dependence of the entropy $S_{\rm QCP}$ on the anisotropy parameter appearing in the limits of the x-integral. Moreover, there is an implicit η dependence hidden in the running mass $R(.)$, whose RG trajectory itself depends on the choice of η. However, the contribution due to the implicit dependence is always sub-leading, since it is at most of order $d\xi^{-2}/d\eta \sim \mathcal{O}(u)$, and it can be neglected. The new contribution to the thermal expansion in the anisotropic Hertz model therefore reads

$$\begin{aligned} \alpha_\eta &= -\frac{\partial S_{\rm QCP}}{\partial(\eta \Lambda^2)} \\ &= \frac{N}{2} \frac{K_2}{2} \left(\frac{\mathcal{T}}{\eta \Lambda^2} \right)^{3/2} \int_{\log \mathcal{T}^{1/2}/(\sqrt{\eta}\Lambda)}^{\infty} dx \int_0^\infty \frac{dv}{\pi} \, \frac{2v \, e^{-3x}}{\sinh^2 v} \arctan \left(\frac{2\, e^{2x}\, v}{R(e^x \Lambda \mathcal{T}^{-\frac{1}{2}}) \, \mathcal{T}^{-1} e^{2x} + 1} \right) . \end{aligned} \tag{4.43}$$

where α_η is measured in units of $(\partial(\eta\Lambda^2)/\partial p)\Lambda/(\pi \xi_0^3)$. Interestingly the contributions of the derivative with respect to the arguments in the limits of integral in expression (4.41) for the entropy cancel each other.

The behavior of the thermal expansion can be classified according to the four regimes already encountered above for the correlation length. The analysis of expression (4.42) closely follows the derivation of Section 3.3.2, except in the quantum critical 2D regime which will be presented in some detail.

Quantum critical 2D regime: $\mathcal{T} \gg \eta\Lambda^2$ and $\Delta \ll \mathcal{T}$

In the quantum critical 2D regime we can neglect the sub-leading second term in the expression for the thermal expansion $\alpha_{\rm QCP}$ (4.42). The following analysis will resemble that of the

correlation length in this regime. Following Section 3.3.2 we perform an integration by parts

$$\alpha_{\mathrm{QCP}} = \frac{N}{2} K_2 \tag{4.44}$$
$$\times \left\{ \left[x \frac{\partial R(e^x \Lambda \mathcal{T}^{-\frac{1}{2}})}{\partial r} \int_0^\infty \frac{dv}{\pi} \frac{4v^2\, e^{2\,x}\, \sinh^{-2} v}{\left(R(e^x \Lambda \mathcal{T}^{-\frac{1}{2}})\, \mathcal{T}^{-1} e^{2x} + 1 \right)^2 + (2\, e^{2x}\, v)^2} \right]_{\log \mathcal{T}^{1/2}/\Lambda}^{\log \mathcal{T}^{1/2}/(\sqrt{\eta}\Lambda)} \right.$$
$$\left. - \int_{\log \mathcal{T}^{1/2}/\Lambda}^{\log \mathcal{T}^{1/2}/(\sqrt{\eta}\Lambda)} dx\, x \frac{d}{dx} \left[\frac{\partial R(e^x \Lambda \mathcal{T}^{-\frac{1}{2}})}{\partial r} \int_0^\infty \frac{dv}{\pi} \frac{4v^2\, e^{2\,x}\, \sinh^{-2} v}{\left(R(e^x \Lambda \mathcal{T}^{-\frac{1}{2}})\, \mathcal{T}^{-1} e^{2x} + 1 \right)^2 + (2\, e^{2x}\, v)^2} \right] \right\} .$$

The lower limit of the surface term yields a negligible non-universal contribution of order $\mathcal{O}(\mathcal{T}/\Lambda^2 \log \mathcal{T}/\Lambda^2)$. After substituting the effective mass $R^* = R(1/\sqrt{\eta})$ by the correlation length, which is permissible in the 2D regime, the upper limit gives

$$\log \left(\frac{\mathcal{T}^{1/2}}{\sqrt{\eta}\Lambda} \right) \frac{\partial \xi^{-2}}{\partial r} \int_0^\infty \frac{dv}{\pi} \frac{4v^2\, \mathcal{T}/(\eta\Lambda^2)\, \sinh^{-2} v}{(\xi^{-2}/(\eta\Lambda^2) + 1)^2 + (2\, \mathcal{T}/(\eta\Lambda^2)\, v)^2}$$
$$= \log \left(\frac{\mathcal{T}^{1/2}}{\sqrt{\eta}\Lambda} \right) \frac{\partial \xi^{-2}}{\partial r} \left(\frac{1}{1 + \xi^{-2}/(\eta\Lambda^2)} + \mathcal{O}\left(\frac{\eta\Lambda^2}{\mathcal{T}} \log \frac{\eta\Lambda^2}{\mathcal{T}} \right) \right) . \tag{4.45}$$

The leading contribution of the integral which remains after integrating by parts can be extracted in a similar manner to that for the thermal expansion in Section 3.3.2 in 2D. The hyperbolic function is expanded to leading order and the v-integral is performed to yield

$$\int_{\log \mathcal{T}^{1/z}/\Lambda}^{\log \mathcal{T}^{1/2}/(\sqrt{\eta}\Lambda)} dx\, x \frac{d}{dx} \frac{\partial R(e^x \Lambda \mathcal{T}^{-\frac{1}{z}})}{\partial r} \frac{1}{R(e^x \Lambda \mathcal{T}^{-\frac{1}{z}})\, \mathcal{T}^{-\frac{2}{z}} e^{2x} + 1} . \tag{4.46}$$

This expression is evaluated with a saddle point approximation. The maximum of the peaked function is located at $x_{\max} = \log \xi \mathcal{T}^{1/2}$. As for the correlation length the behavior depends on whether this maximum is located within the integration region or not.

Sub-regime $\xi^{-2} \gg \eta\Lambda^2$: For this sub-regime the maximum is located within the integration region and the saddle point gives the leading contribution. Furthermore, the surface term is sub-leading. The thermal expansion is given to leading order by

$$\alpha_{\mathrm{QCP}} = \frac{N}{8\pi} \frac{\partial \xi^{-2}}{\partial r} \log \frac{\mathcal{T}}{\xi^{-2}} . \tag{4.47}$$

Sub-regime $\xi^{-2} \ll \eta\Lambda^2$: Now the saddle point is beyond the integration region and the leading contribution to the thermal expansion results from the surface term,

$$\alpha_{\mathrm{QCP}} = \frac{N}{8\pi} \frac{\partial \xi^{-2}}{\partial r} \log \frac{\mathcal{T}}{\eta\Lambda^2} . \tag{4.48}$$

Using the formulae for the correlation length of Section 4.1.4 in the quantum critical 2D regime and its iterative solution (compare Section 3.3.2) the leading behavior can be summarized as

$$\alpha_{\rm QCP} \sim \frac{N}{8\pi} \begin{cases} \dfrac{\log \frac{\mathcal{T}}{\eta\Lambda^2}}{\left(\log \frac{\bar{\Lambda}^2}{\eta\Lambda^2}\right)^{\frac{N+2}{N+8}}} & \text{for III:} \quad \xi^{-2} \ll \eta\Lambda^2 \\ \dfrac{\log\log \frac{\bar{\Lambda}^2}{\mathcal{T}}}{\left(\log \frac{\bar{\Lambda}^2}{\mathcal{T}}\right)^{\frac{N+2}{N+8}}} & \text{for II:} \quad \eta\Lambda^2 \ll \xi^{-2} \quad \text{and} \quad \Delta \ll \frac{T \log\log \frac{\bar{\Lambda}^2}{\mathcal{T}}}{\log \frac{\bar{\Lambda}^2}{\mathcal{T}}} \\ \dfrac{\log \frac{\mathcal{T}}{r}}{\left(\log \frac{\bar{\Lambda}^2}{r}\right)^{\frac{N+2}{N+8}}} & \text{for I:} \quad \eta\Lambda^2 \ll \xi^{-2} \quad \text{and} \quad \Delta \gg \frac{T \log\log \frac{\bar{\Lambda}^2}{\mathcal{T}}}{\log \frac{\bar{\Lambda}^2}{\mathcal{T}}} . \end{cases} \tag{4.49}$$

For the anisotropic contribution α_η we obtain the leading contribution from the scaling into the classical regime, i.e. for small arguments of the hyberbolic function,

$$\alpha_\eta = \frac{N}{2}\frac{K_2}{2}\left(\frac{\mathcal{T}}{\eta\Lambda^2}\right)^{3/2} \int\limits_{\log \mathcal{T}^{1/2}/(\sqrt{\eta}\Lambda)}^{\infty} dx\, e^{-3x} \left(\log \frac{2\, e^{2x}}{R(e^x \Lambda \mathcal{T}^{-\frac{1}{2}})\, \mathcal{T}^{-1} e^{2x} + 1} + \mathcal{O}(1) \right) \tag{4.50}$$

$$\approx \frac{N}{2}\frac{K_2}{6} \log \frac{\mathcal{T}}{\xi^{-2} + \eta\Lambda^2} \approx \frac{N}{2}\frac{K_2}{6} \begin{cases} \log \frac{\mathcal{T}}{\eta\Lambda^2} & \text{for III:} \quad \xi^{-2} \ll \eta\Lambda^2 \\ \log\log \frac{\bar{\Lambda}^2}{\mathcal{T}} & \text{for II:} \quad \eta\Lambda^2 \ll \xi^{-2} \text{ and } \Delta \ll \frac{T \log\log \frac{\bar{\Lambda}^2}{\mathcal{T}}}{\log \frac{\bar{\Lambda}^2}{\mathcal{T}}} \\ \log \frac{\mathcal{T}}{r} & \text{for I:} \quad \eta\Lambda^2 \ll \xi^{-2} \text{ and } \Delta \gg \frac{T \log\log \frac{\bar{\Lambda}^2}{\mathcal{T}}}{\log \frac{\bar{\Lambda}^2}{\mathcal{T}}} \end{cases}$$

The derivation of the leading behavior in the other regimes follows Section 3.3.2 and we simply present the results below.

Quantum critical 3D regime: $\mathcal{T} \ll \eta\Lambda^2$ and $\Delta \ll \mathcal{T}$

$$\alpha_{\rm QCP} = \frac{\sqrt{2\pi}\, 3\, \zeta\left(\frac{3}{2}\right) N}{32\pi} \left(\log \frac{\bar{\Lambda}^2}{\eta\Lambda^2}\right)^{-\frac{N+2}{N+8}} \frac{\sqrt{\mathcal{T}}}{\sqrt{\eta\Lambda^2}} \quad \text{and} \quad \alpha_\eta = \frac{N}{2}\frac{\pi K_2}{3}\frac{\mathcal{T}}{\eta\Lambda^2} \tag{4.51}$$

2D Fermi liquid regime: $\Delta \gg \eta\Lambda^2$ and $\Delta \gg \mathcal{T}$

$$\alpha_{\rm QCP} \simeq \frac{N}{12}\frac{\mathcal{T}}{r} \quad \text{and} \quad \alpha_\eta = \frac{N}{2}\frac{\pi K_2}{9}\frac{\mathcal{T}}{r} \tag{4.52}$$

3D Fermi liquid regime: $\Delta \ll \eta\Lambda^2$ and $\Delta \gg \mathcal{T}$

$$\alpha_{\rm QCP} \simeq \frac{N\pi}{24} \left(\log \frac{\bar{\Lambda}^2}{\eta\Lambda^2}\right)^{-\frac{N+2}{2(N+8)}} \frac{\mathcal{T}}{\sqrt{\eta\Lambda^2}\sqrt{r}} \quad \text{and} \quad \alpha_\eta = \frac{N}{2}\frac{\pi K_2}{3}\frac{\mathcal{T}}{\eta\Lambda^2} \tag{4.53}$$

As anticipated in the introduction the additional contribution α_η due to the anisotropy parameter is as important as $\alpha_{\rm QCP}$ in the 2D regimes. In the 3D regimes, on the other hand, it gives only a sub-leading contribution.

4.1.7 Specific heat

The leading contributions of the specific heat in the 2D and 3D regimes conform with the isotropic theory with the corresponding space dimensions. Following the derivation of (3.34) for the specific heat we get

$$\gamma_{\rm QCP} = \frac{N}{2} K_2 \int\limits_{\log \mathcal{T}^{1/2}/\Lambda}^{\log \mathcal{T}^{1/2}/(\sqrt{\eta}\Lambda)} dx \int_0^\infty \frac{dv}{\pi} \left(\frac{2\,v}{\sinh v}\right)^2 \frac{\left(R(e^x \Lambda \mathcal{T}^{-\frac{1}{2}})\mathcal{T}^{-1} e^{2x} + 1\right)}{\left(R(e^x \Lambda \mathcal{T}^{-\frac{1}{2}})\mathcal{T}^{-1} e^{2x} + 1\right)^2 + (2\,e^{2x}\,v)^2}$$
$$+ \frac{N}{2} K_2 \frac{\sqrt{\mathcal{T}}}{\sqrt{\eta\Lambda^2}} \int\limits_{\log \mathcal{T}^{1/2}/(\sqrt{\eta}\Lambda)}^{\infty} dx \int_0^\infty \frac{dv}{\pi} \left(\frac{2\,v}{\sinh v}\right)^2 \frac{\left(R(e^x \Lambda \mathcal{T}^{-\frac{1}{2}})\mathcal{T}^{-1} e^{2x} + 1\right) e^{-x}}{\left(R(e^x \Lambda \mathcal{T}^{-\frac{1}{2}})\mathcal{T}^{-1} e^{2x} + 1\right)^2 + (2\,e^{2x}\,v)^2}. \tag{4.54}$$

The leading contributions are given below

Quantum critical 2D regime: $\mathcal{T} \gg \eta\Lambda^2$ and $\Delta \ll \mathcal{T}$

$$\gamma_{\rm QCP} = \frac{N}{12} \log \frac{\Lambda^2}{\mathcal{T}} \tag{4.55}$$

Quantum critical 3D regime: $\mathcal{T} \ll \eta\Lambda^2$ and $\Delta \ll \mathcal{T}$

$$\gamma_{\rm QCP} = \frac{N}{12} \log \frac{1}{\eta} + \frac{N}{6} - \frac{\sqrt{2\pi}\, 15\, \zeta\left(\frac{5}{2}\right) N}{64\,\pi} \frac{\sqrt{\mathcal{T}}}{\sqrt{\eta\Lambda^2}} \tag{4.56}$$

2D Fermi liquid regime: $\Delta \gg \eta\Lambda^2$ and $\Delta \gg \mathcal{T}$

$$\gamma_{\rm QCP} = \frac{N}{6} \log \frac{\Lambda}{\Delta^{1/2}} \sim \frac{N}{6} \log \frac{\Lambda}{r^{1/2}} \tag{4.57}$$

3D Fermi liquid regime: $\Delta \ll \eta\Lambda^2$ and $\Delta \gg \mathcal{T}$

$$\gamma_{\rm QCP} = \frac{N}{12} \log \frac{1}{\eta} + \frac{N}{6} - \frac{N\pi}{12} \frac{\sqrt{r}}{\sqrt{\eta\Lambda^2}} \tag{4.58}$$

In the 3D regimes the critical contribution is sub-leading. The background is universal in the sense that it depends only on the anisotropy parameter η.

4.1.8 Effective critical exponents

The scaling analysis for quantum critical points of Chapter 1 predicted critical exponents for the specific heat and thermal expansion. These exponents depend on the scaling dimension, ϕ, of the free energy (1.15). When the so-called hyperscaling hypothesis is obeyed this scaling dimension is simply given by the dimensionality of the zero-temperature theory, i.e. $\phi = d+z$.

In the anisotropic Hertz model where we observe a dimensional crossover between two- and three-dimensional behavior hyperscaling is trivially violated since the effective spatial dimensionality varies between $d = 2$ and $d = 3$.. Accordingly, there exist no well-defined critical exponents characterizing the whole critical regime. However, we can consider effective

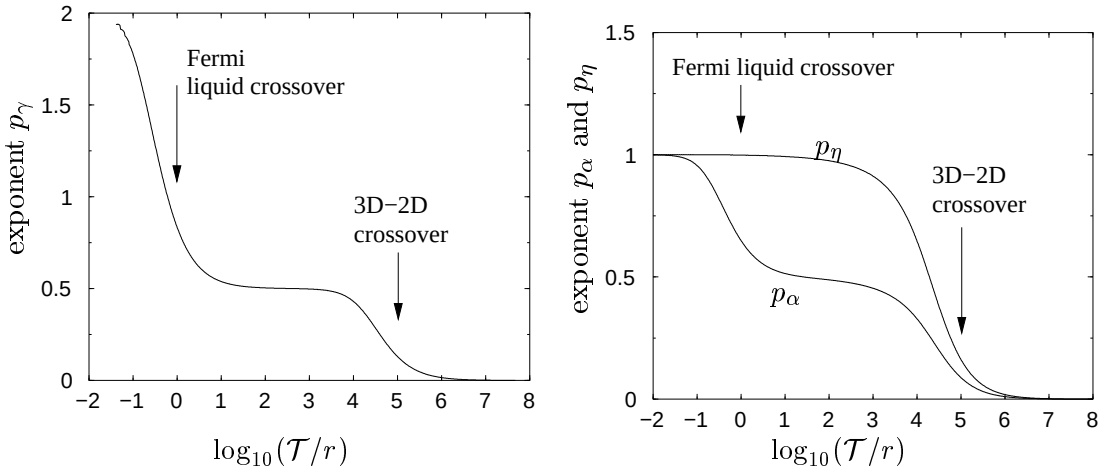

Figure 4.6: *Effective critical exponents for the specific heat (left panel), $\gamma = \gamma_0 + T^{p_\gamma}$, and the two contributions to the thermal expansion (right panel), $\alpha_{\rm QCP} = T^{p_\alpha}$ and $\alpha_\eta = T^{p_\eta}$. The crossover shown corresponds to the line $\eta\Lambda^2 = 10^5\, r$ in the phase diagram of Fig. 4.3.*

exponents which in turn lead to the concept of the effective dimension $d_{\rm eff}$ when applying (effective) hyperscaling with $\phi = d_{\rm eff} + z$. In the quantum critical regime the scaling analysis yields for the specific heat (1.26) and the thermal expansion (1.27) (using $y_0 = 1$, $z = 2$ and $\nu = 1/2$)

$$\gamma_{cr} \sim \mathcal{T}^{(d_{\rm eff}-2)/2} \qquad \text{and} \qquad \alpha_{cr} \sim \mathcal{T}^{(d_{\rm eff}-2)/2}\,. \tag{4.59}$$

In Fig. 4.6 the effective exponents of specific heat and thermal expansion are plotted, as calculated from the Gaussian part of the anisotropic Hertz model. The quartic coupling will only induce logarithmic corrections to the thermal expansion in the quantum critical 2D regime II of Fig. 4.3, see (4.49) and (4.50); for an analysis of the effective exponents these corrections will be neglected. Three different exponents p_γ, p_α and p_η are shown, corresponding to the critical part of the specific heat $\gamma_{\rm QCP}$ and the two contributions to the thermal expansion $\alpha_{\rm QCP}$ and α_η, respectively. They were determined with the formula

$$p = \frac{d}{d\log\mathcal{T}} \log\left(\frac{df(\mathcal{T})}{d\log\mathcal{T}}\right) \tag{4.60}$$

where $f(\mathcal{T})$ represents the quantity of interest. The formula is constructed in such a way that it automatically eliminates a constant background contribution. For example, the specific heat coefficient for a Fermi liquid at low temperatures is given by $\gamma = \gamma_0 + A\,T^2$, which yields a temperature exponent of $p = 2$.

For high temperature both the specific heat and the thermal expansion depend only logarithmically on temperature, leading to vanishing effective exponents. Upon entering the quantum critical 3D regime the exponents of $\gamma_{\rm QCP}$ and $\alpha_{\rm QCP}$ increase as expected to 1/2. The exponent of α_η however grows to 1 and is therefore only sub-leading. At even lower temperatures the quantities reach their Fermi liquid values.

4.2 Dimensional reduction analysis

In this section we apply a method proposed by S. Sachdev [33, 2] to the anisotropic Hertz model. It is based on concepts originally developed to describe critical phenomena in finite-size systems, and can be naturally transfered to the theory of quantum criticality. The quantum phase transition occurs at zero temperature and its critical properties are characterized by an effective dimensionality $d + z$. When the temperature is finite, however, the dynamics along the imaginary-time dimension is restricted by the inverse temperature $\beta = 1/T$. Whereas the critical fluctuations can still extend to infinity in d spatial dimensions they are now limited in the other z dimensions attributed to imaginary time. This means that we can think of quantum criticality at finite temperatures as the critical behavior in a system which is infinite in d dimensions and finite in z dimensions.

This method offers the possibility of deriving crossover functions in closed form. It is therefore especially suitable for the investigation of the anisotropic Hertz model, in which the finite-temperature crossover is complemented by the dimensional crossover triggered by the anisotropy parameter η. The method consists of two steps. First, applying a standard renormalization group the Hertz theory is scaled towards the zero-temperature fixed point. An effective theory is then derived which describes the finite temperature properties.

4.2.1 Flow to the zero-temperature fixed point

In order to derive the RG equations governing the zero-temperature flow we apply the following cutoff procedure. We introduce a single cutoff Λ for the integral over Matsubara frequencies, which are dense at zero temperature, and the three momentum integrals,

$$\begin{aligned}\int^{\Lambda} \chi &\equiv \frac{\pi}{\Lambda} \int_{-\Lambda^2}^{\Lambda^2} \frac{d\omega}{2\pi} \int_{-\sqrt{\Lambda^2-\omega}}^{\sqrt{\Lambda^2-\omega}} \frac{dk_\perp}{2\pi} \int_0^{\sqrt{\Lambda^2-\eta k_\perp^2-\omega}} \frac{dk_{\shortparallel}}{(2\pi)^2}\, 2\pi k_{\shortparallel} \frac{1}{\delta + k_{\shortparallel}^2 + \eta\, k_\perp^2 + |\omega|} \\ &= \frac{1}{4\pi^2\Lambda} \int_0^{\Lambda} dk_\perp \int_{\eta k_\perp^2}^{\Lambda^2} dy \int_y^{\Lambda^2} dx \frac{1}{\delta + x}\,. \end{aligned} \tag{4.61}$$

The susceptibility χ is given by (4.3) with the bare mass δ_0 replaced with the running mass δ. Moreover, we assume that the theory has been rescaled appropriately to eliminate the scales ξ_0 and T_0. As in the Millis' RG treatment of the last section, the theory is initially rescaled with respect to the $d = 2$ fixed point. Under this scaling the anisotropy parameter η grows with the scaling dimension 2, $\eta(b) = \eta\, b^2$. The RG flow is governed by the standard RG equations of ϕ^4 theory [18] which for a finite cutoff renormalization $\Lambda \to \Lambda/b$ read

$$\delta' = b^2 \left(\delta + 4(N+2)u \int_{\Lambda/b}^{\Lambda} \chi \right) \tag{4.62}$$

$$u' = b^{4-d-z} \left(u - 4(N+8)u^2 \int_{\Lambda/b}^{\Lambda} \chi^2 \right), \tag{4.63}$$

where $d = z = 2$. The primed values on the right hand side are the renormalized quantities. In the limit of an infinitesimal scale transformation, $\log b \ll 1$, these equations simplify to

$$\frac{\partial\,\delta(b)}{\partial \log b} = 2\,\delta(b) + 4(N+2)\,\frac{1}{2\pi^2}\,u(b)\,\frac{\Lambda^4}{\delta(b)+\Lambda^2}\left(1-\frac{\eta(b)}{3}\right) \tag{4.64}$$

$$\frac{\partial\,u(b)}{\partial \log b} = -4(N+8)\,\frac{1}{2\pi^2}\,u^2(b)\,\left(1-\frac{\eta(b)}{3}\right). \tag{4.65}$$

The running quartic coupling is readily obtained

$$u(b) = \frac{u}{1+4\,(N+8)\,\frac{1}{2\pi^2}\,u\,(\ln b + \frac{1}{6}\eta\,(1-b^2))} \sim \frac{4\pi^2}{4\,(N+8)}\,\frac{1}{\log\left[b^2 e^{\frac{4\pi^2}{4\,(N+8)\,u}}\right]}. \tag{4.66}$$

At the upper critical dimension the limiting behavior of the running mass $\Delta(b) = \delta(b) b^{-2}$ is given by the differential equation

$$\frac{\partial \Delta(b)}{\partial \log b} \approx \frac{2(N+2)}{\pi^2} u(b)\left(b^{-2}\Lambda^2 - \Delta(b)\right)\left(1-\frac{\eta(b)}{3}\right) \tag{4.67}$$

which has the solution [cf. (4.19)]

$$\Delta(b) \sim \frac{r}{\left(\log\left[b^2\; e^{\frac{\pi^2}{(N+8)\;u}}\right]\right)^{\frac{N+2}{N+8}}}, \tag{4.68}$$

where we introduced the control parameter r.

We will now consider now the theory at a certain scale b chosen in such a way that the quartic coupling constant $u(b)$ can be treated perturbatively. To do so either the scale must be sufficiently large so that the running coupling constant is sufficiently small, or the theory must have reached its isotropic limit, i.e. $\eta(b) = 1$ for $b = b^* \equiv 1/\sqrt{\eta}$. At the isotropic limit the zero-temperature Hertz theory is above its upper critical dimension, $d + z > 4$ for $d = 3$ and $z = 2$, and is therefore well described by mean field theory. The essence of Sachdev's method is that in the vicinity of the quantum critical point the *finite* temperature properties can also be derived by treating the quartic coupling as a perturbation.

4.2.2 Effective theory for the zero Matsubara mode

At finite temperatures the critical fluctuations are restricted in imaginary time but can still develop in the three spatial dimensions. In the language of Matsubara and momentum space this means that the available momenta are still continuous but the Matsubara frequencies are gapped. The critical finite-temperature properties will be determined by the gapless, zero Matsubara mode. In the following an effective model for this zero Matsubara mode is derived by perturbatively taking into account the influence of the gapped modes. It has been pointed out by S. Sachdev [33, 2] that all ultraviolet divergences, i.e. all cutoff dependences, of the zero temperature theory can be absorbed by appropriate *counterterms* (see also e.g. Ref. [25], Chapter 10.2), resulting in a universal T dependence of the correlation length.

We will start from the anisotropic Hertz theory whose parameters have been scaled according to the zero-temperature RG equations above,

$$S[\Phi] = \frac{1}{2}\mathcal{T}(b)\sum_{\omega_n}\int\frac{d^3\mathbf{k}}{(2\pi)^3}\Phi^T(i\omega_n,\mathbf{k})\,\left[\Delta(b)\,b^2+k_{\shortparallel}^2+\eta(b)\,k_\perp^2+|\omega_n|\right]\,\Phi(-i\omega_n,-\mathbf{k}) + u(b)\int_0^{1/\mathcal{T}(b)}d\tau\int d\mathbf{R}\,\left(\Phi^T(\tau,\mathbf{R})\Phi(\tau,\mathbf{R})\right)^2\,. \tag{4.69}$$

The scale b is understood to be fixed and smaller than the crossover scale $b^* = 1/\sqrt{\eta}$. It is important to note that under scaling the temperature $\mathcal{T}$ has also grown with the dynamical exponent z, $\mathcal{T}(b) = \mathcal{T}\,b^z$. The effective finite-temperature action for the zero Matsubara modes $\vec{\varphi}(\mathbf{k}) = (\mathcal{T}(b))^{1/2}\,\Phi(0,\mathbf{k})$ reads (compare also the discussion of Section 2.2.2)

$$\begin{aligned} S_{\text{eff}}[\vec{\varphi}] &= \frac{1}{2}\int\frac{d^3\mathbf{k}}{(2\pi)^3}\,\vec{\varphi}^T(\mathbf{k})\left[R(b)+k_{\shortparallel}^2+\eta(b)\,k_\perp^2\right]\vec{\varphi}(-\mathbf{k}) \\ &\quad + U(b)\,\mathcal{T}(b)\int\prod_{i=1}^4\frac{d^3\mathbf{k}_i}{(2\pi)^3}\,\delta\left(\textstyle\sum_{i=1}^4\mathbf{k}_i\right)\,\left(\vec{\varphi}^T(\mathbf{k}_1)\vec{\varphi}(\mathbf{k}_2)\right)\,\left(\vec{\varphi}^T(\mathbf{k}_3)\vec{\varphi}(\mathbf{k}_4)\right)\,. \end{aligned} \tag{4.70}$$

The effective parameters $U(b)$ and $R(b)$ result from integrating out the gapped Matsubara modes. To lowest order the effective quartic coupling $U(b)$ is just given by the rescaled coupling $u(b)$,

$$U(b) = u(b) + \mathcal{O}(u^2(b))\,. \tag{4.71}$$

The effective mass $R(b)$, however, is modified in first order in $u(b)$ by the gapped modes,

$$\begin{aligned} R(b) &= \Delta(b)b^2 + 4(N+2)\,u(b)\int\frac{d^3k}{(2\pi)^3}\,\left\{\mathcal{T}(b)\sum_{\omega_n\neq 0}\frac{1}{\Delta(b)b^2+k_{\shortparallel}^2+\eta(b)\,k_\perp^2+|\omega_n|}\right. \\ &\quad \left. -\int\frac{d\omega}{2\pi}\frac{1}{\Delta(b)b^2+k_{\shortparallel}^2+\eta(b)\,k_\perp^2+|\omega|}\right\} + \mathcal{O}(u^2(b))\,. \end{aligned} \tag{4.72}$$

The last term is an appropriate counterterm chosen in such a way that for zero temperature the running mass reduces to $R(b) = \Delta(b)b^2$.

4.2.3 Correlation length

Within the effective theory (4.70) we can again apply perturbation theory in order to evaluate the correlation length ξ. To lowest order it is given by

$$\xi^{-2}b^2 \equiv \xi^{-2}(b) = R(b) + 4(N+2)\,U(b)\,\mathcal{T}(b)\int\frac{d^3k}{(2\pi)^3}\,\frac{1}{\xi^{-2}(b)+k_{\shortparallel}^2+\eta(b)\,k_\perp^2}\,. \tag{4.73}$$

where the factor b^2 again accounts for the trivial scaling dimension. Using expression (4.72) we can express the correlation length in terms of the zero temperature mass gap $\Delta(b)$,

$$\begin{aligned} \xi^{-2}(b) &= \Delta(b)b^2 + 4(N+2)\,u(b)\int\frac{d^3k}{(2\pi)^3}\,\left\{\sum_{\omega_n\neq 0}\frac{\mathcal{T}(b)}{\Delta(b)b^2+k_{\shortparallel}^2+\eta(b)\,k_\perp^2+|\omega_n|}\right. \\ &\quad \left. -\int\frac{d\omega}{2\pi}\frac{1}{\Delta(b)b^2+k_{\shortparallel}^2+\eta(b)\,k_\perp^2+|\omega|}+\frac{\mathcal{T}(b)}{\xi^{-2}(b)+k_{\shortparallel}^2+\eta(b)\,k_\perp^2}\right\}\,. \end{aligned} \tag{4.74}$$

Following Refs. [33, 2] we separate this expression into three terms

$$\xi^{-2}(b) \;=\; \Delta(b)b^2 + 4(N+2)\,u(b)\,(R_1(b)+R_2(b)+R_3(b))\;, \tag{4.75}$$

where

$$\begin{aligned}
R_1(b) &= \int \frac{d^3k}{(2\pi)^3}\left(\sum_{\omega_n}\frac{\mathcal{T}(b)}{\Delta(b)b^2+k_{\shortparallel}^2+\eta(b)\,k_\perp^2+|\omega_n|}-\int\frac{d\omega}{2\pi}\frac{1}{\Delta(b)b^2+k_{\shortparallel}^2+\eta(b)\,k_\perp^2+|\omega|}\right)\\
R_2(b) &= -\int\frac{d^3k}{(2\pi)^3}\left(\frac{\mathcal{T}(b)}{\Delta(b)b^2+k_{\shortparallel}^2+\eta(b)\,k_\perp^2}-\frac{\mathcal{T}(b)}{k_{\shortparallel}^2+\eta(b)\,k_\perp^2}\right)\\
R_3(b) &= \int\frac{d^3k}{(2\pi)^3}\left(\frac{\mathcal{T}(b)}{\xi^{-2}(b)+k_{\shortparallel}^2+\eta(b)\,k_\perp^2}-\frac{\mathcal{T}(b)}{k_{\shortparallel}^2+\eta(b)\,k_\perp^2}\right).
\end{aligned} \tag{4.76}$$

To evaluate these we have to specify a cutoff procedure for the remaining momentum integrals. This seems to contradict the claim of S. Sachdev [33, 2] that we should obtain a universal temperature dependence for the correlation length. However, as we will see, the cutoff Λ only enters in combination with the anisotropy parameter, $\eta\Lambda^2$, to give a scaling parameter of dimension 2 which tunes the dimensional crossover. We will apply the same cutoff scheme as outlined in Section 4.1.1. After converting the Masubara sum into an integral (using $\mathcal{T}(b)/(\Delta(b)b^2)=\mathcal{T}/\Delta(b)$ and $\mathcal{T}(b)/\eta(b)=\mathcal{T}/\eta$) we get for $R_1(b)$

$$\begin{aligned}
R_1(b) &= \int^{\Lambda}\frac{d^3k}{(2\pi)^3}\int_0^\infty\frac{dz}{\pi}\left(\coth\frac{z\mathcal{T}(b)}{2}-1\right)\frac{z}{\left(\Delta(b)b^2+k_{\shortparallel}^2+\eta(b)\,k_\perp^2\right)^2+z^2}\\
&= \frac{\Lambda}{2\pi^2}\mathcal{T}(b)\int_0^1 dk_{\shortparallel}\int_{\frac12\log\mathcal{T}(b)/\Lambda^2}^{\frac12\log\mathcal{T}/(\eta\Lambda^2k_{\shortparallel}^2)}dx\int_0^\infty\frac{dv}{\pi}\frac{e^{2x}\,4v\,(\coth v-1)}{\left(\Delta(b)\mathcal{T}^{-1}e^{2x}+1\right)^2+\left(2ve^{2x}\right)^2}
\end{aligned} \tag{4.77}$$

The lower limit of the x-integral can be extended to minus infinity in the universal limit $\Lambda\to\infty$. Furthermore,

$$R_2(b)=\frac{\Lambda}{2\pi^2}\mathcal{T}(b)\left(\sqrt{\frac{\Delta(b)}{\eta\Lambda^2}}\arctan\sqrt{\frac{\eta\Lambda^2}{\Delta(b)}}+\frac12\log\left(1+\frac{\Delta(b)}{\eta\Lambda^2}\right)\right) \tag{4.78}$$

and similarly for $R_3(b)$. Now it is apparent that for $z=2$ the three functions R_n have the same scaling dimension, 2. The trivial scaling factors therefore drop out in the expression (4.75) and only the scale dependence of the running quartic coupling constant $u(b)$ and the mass gap $\Delta(b)$ remains. The reason is that the zero-temperature theory is at the upper critical dimension where logarithmic corrections occur. These are reflected in the remaining scale dependence of the zero-temperature parameters. If the anisotropy parameter η is the smallest scale in the problem, the scale b of $u(b)$ and $\Delta(b)$ is set by the correlation length ξ. However, for $\xi^{-2}<\eta\Lambda^2$ the zero-temperature parameters can be taken at $b=1/\sqrt{\eta}$.

We finally obtain for the correlation length the quasi-scaling form

$$\boxed{\frac{\xi^{-2}}{\eta\Lambda^2}=\frac{\Delta(b)}{\eta\Lambda^2}+\pi\frac{N+2}{N+8}\frac{\mathcal{T}}{\eta\Lambda^2}\;\log^{-1}\left[b\,e^{\frac{\pi^2}{2\,(N+8)u}}\right]\Psi\left(\frac{\mathcal{T}}{\eta\Lambda^2},\frac{\Delta(b)}{\eta\Lambda^2},\frac{\xi^{-2}}{\eta\Lambda^2}\right)} \tag{4.79}$$

where we have introduced the scaling function,

$$\Psi\left(a,b,c\right) \equiv \sqrt{b}\arctan\frac{1}{\sqrt{b}} - \sqrt{c}\arctan\frac{1}{\sqrt{c}} + \frac{1}{2}\log\left(\frac{1+b}{1+c}\right) + \Upsilon(a,b) \tag{4.80}$$

$$\Upsilon(a,b) \equiv \int_0^1 dk_{\shortparallel} \int_{-\infty}^{\frac{1}{2}\log(a\,k_{\shortparallel}^{-2})} dx \int_0^\infty \frac{dv}{\pi} \frac{e^{2x}\,4v\left(\coth v - 1\right)}{\left(ba^{-1}e^{2x}+1\right)^2 + \left(2ve^{2x}\right)^2}\,. \tag{4.81}$$

This result should be compared to (4.21) and (4.31) derived within the framework of the Millis RG.

In the following we will analyze the scaling function Ψ and determine its behavior in different regimes. It will be convenient to perform an integration by parts with respect to $k_{\shortparallel}$ in the definition of Υ,

$$\Upsilon\left(a,b\right) = \tag{4.82}$$
$$\int_{-\infty}^{\frac{1}{2}\log a} dx \int_0^\infty \frac{dv}{\pi} \frac{e^{2x}\,4v\left(\coth v - 1\right)}{\left(ba^{-1}e^{2x}+1\right)^2 + \left(2ve^{2x}\right)^2} + \sqrt{a}\int_{\frac{1}{2}\log a}^{\infty} dx \int_0^\infty \frac{dv}{\pi} \frac{e^{x}\,4v\left(\coth v - 1\right)}{\left(ba^{-1}e^{2x}+1\right)^2 + \left(2ve^{2x}\right)^2}\,.$$

The first integral is due to the boundary contribution and it will dominate for large a whereas the second integral dominates for small a. The derivation of the leading behavior closely follows the treatment of the correlation length of Section 4.1.4 and gives

$$\Psi\left(a,b,c\right) = \frac{1}{2}\left\{\begin{array}{lll} \pi\sqrt{b} & \text{if} & b \ll 1 \\ \log b & \text{if} & b \gg 1 \end{array}\right\} + \frac{1}{2}\left\{\begin{array}{lll} \pi\sqrt{c} & \text{if} & c \ll 1 \\ \log c & \text{if} & c \gg 1 \end{array}\right\} + \Upsilon(a,b) \tag{4.83}$$

$$\Upsilon(a,b) = \begin{cases} \frac{1}{2}\log\frac{a}{b} & \text{if} \quad a \gg b,\ a \gg 1,\ b \gg 1 \\ \frac{1}{2}\log a & \text{if} \quad a \gg b,\ a \gg 1,\ b \ll 1 \\ \frac{\Gamma\left(\frac{3}{2}\right)\zeta\left(\frac{3}{2}\right)}{\sqrt{2}}\sqrt{a} & \text{if} \quad a \gg b,\ a \ll 1 \\ \frac{\pi}{6}\frac{a}{b} & \text{if} \quad a \ll b,\ a \gg 1 \\ \frac{\pi^2}{12}\frac{a}{\sqrt{b}} & \text{if} \quad a \ll b,\ a \ll 1\,. \end{cases} \tag{4.84}$$

This results in the same crossover lines and the same leading behaviors for the correlation length as obtained within the Millis RG treatment in Section 4.1.4. However, it is interesting to note that the logarithmic Mermin–Wagner divergence (3.1) enters in the form of the one–loop correction (4.73) to the effective theory. It is encoded in the logarithmic dependence of the scaling function on the combination $\xi^{-2}/(\eta\Lambda^2)$. Upon approaching the phase boundary the divergence is cutoff by the anisotropy parameter $\eta\Lambda^2$, which in turn leads to the two sub-regions in the quantum critical 2D-regime already found in Section 4.1.4.

4.2.4 Phase boundary

The perturbative analysis of the effective theory for the zero Matsubara mode (4.70) suffers from the same drawbacks as the Millis RG analysis as far as the estimate of the phase boundary

is concerned. The perturbative one-loop treatment will break down at the Ginzburg criterion before the critical temperature is reached. As before, we will nevertheless use the above results to obtain an estimate for the Néel temperature $\mathcal{T}_c(r)$.

The estimate of the phase boundary $\mathcal{T}_c(r)$ depends crucially on the order of limits taken in the anisotropic Hertz model. Whereas we find a finite temperature solution for the phase boundary for a finite anisotropy parameter η, this solution vanishes for $\eta = 0$ due to the presence of a Mermin–Wagner divergence (3.1). In the 2D limit, $\eta = 0$, we find that the correlation length is implicitly given in the limit $\xi^{-2} \to 0$ by

$$\eta = 0: \qquad \xi^{-2} = \Delta(b) + \frac{\pi}{2}\frac{N+2}{N+8}\,\log^{-1}\left[b\,e^{\frac{\pi^2}{2\,(N+8)u}}\right]\mathcal{T}\log\left(\frac{\mathcal{T}}{\xi^{-2}}\right) \tag{4.85}$$

which possesses no solution with a diverging correlation length. This contrasts with the situation with a finite value for η: consider the limit $\xi^{-2} \to 0$ in (4.79) for finite $\eta > 0$,

$$\frac{\Delta(1/\sqrt{\eta})}{\eta\Lambda^2} = -\pi\frac{N+2}{N+8}\frac{\mathcal{T}_c}{\eta\Lambda^2}\,\log^{-1}\left[\frac{1}{\sqrt{\eta}}\,e^{\frac{\pi^2}{2\,(N+8)u}}\right]\Psi\left(\frac{\mathcal{T}_c}{\eta\Lambda^2}, \frac{\Delta(1/\sqrt{\eta})}{\eta\Lambda^2}, 0\right). \tag{4.86}$$

The expression can be simplified for high and low critical temperatures $\mathcal{T}_c$.

2D regime: $\mathcal{T}_c \gg \eta\Lambda^2$

In the 2D regime the phase boundary is located in the region of the phase diagram where $\Delta(1/\sqrt{\eta}) \gg \eta\Lambda^2$ and $\mathcal{T} \gg \eta\Lambda^2$. Using the appropriate limiting behavior of the scaling function Ψ we get

$$\frac{r}{\eta\Lambda^2} = -\pi\frac{N+2}{N+8}\frac{\mathcal{T}_c}{\eta\Lambda^2}\frac{\log\left(\frac{\mathcal{T}_c}{\eta\Lambda^2}\right)}{\left(\log\frac{\bar{\Lambda}^2}{\eta\Lambda^2}\right)^{1-\frac{N+2}{N+8}}}. \tag{4.87}$$

3D regime: $\mathcal{T}_c \ll \eta\Lambda^2$

$$\frac{r}{\eta\Lambda^2} = -\frac{\pi^{3/2}\zeta\left(\frac{3}{2}\right)}{\sqrt{2}}\frac{N+2}{N+8}\frac{1}{\left(\log\frac{\bar{\Lambda}^2}{\eta\Lambda^2}\right)^{1-\frac{N+2}{N+8}}}\left(\frac{\mathcal{T}_c}{\eta\Lambda^2}\right)^{3/2} \tag{4.88}$$

This is in agreement with the estimate obtained in Section 4.1.5.

4.3 Large N analysis

The third method with which we shall tackle the anisotropic Hertz model is large N analysis (see e.g. Ref. [36]). It is a systematic expansion in $1/N$ where N is the number of components of the field Φ. The Millis RG treatment as well as the analysis of Sachdev's effective theory have the drawback that they break down when the Ginzburg criterion is fulfilled. As a consequence the classical region, which always covers the phase boundary (cf. Fig. 3.1), cannot be addressed within these two approaches. The large N analysis on the other hand yields reliable information about the classical regime, since it only relies on $1/N$ as a small parameter. In particular, it will confirm the functional dependence of the critical temperature on the control parameter r obtained with the former methods.

We will briefly sketch the derivation of the equations which will become exact in the limit $N \to \infty$. We introduce a Hubbard–Stratonovich field λ decoupling the quartic term in the Hertz action (2.23),

$$Z = \int \mathcal{D}\lambda \mathcal{D}\Phi \, e^{-S[\Phi,\lambda]} \tag{4.89}$$

where S is now given by

$$S[\Phi,\lambda] = \frac{1}{2}\frac{1}{\beta}\sum_{\omega_n,\mathbf{k}} \left(\delta_0 + \lambda + k_{\shortparallel}^2 + \eta\, k_\perp^2 + |\omega_n|\right) \Phi(i\omega_n,\mathbf{k})\Phi(-i\omega_n,-\mathbf{k}) - \frac{\Lambda}{16\pi u}\,\lambda^2 \,. \tag{4.90}$$

We have again used the two-dimensional quartic coupling u, giving rise to the additional factor of Λ/π (compare the discussion preceding (4.7)). Integrating out the Φ fields yields an action solely dependent on λ:

$$S[\lambda] = -\frac{\Lambda}{16\pi u}\,\lambda^2 + \frac{N}{2}\mathrm{tr}\,\log\left(\delta_0 + \lambda + k_{\shortparallel}^2 + \eta\, k_\perp^2 + |\omega_n|\right) \,. \tag{4.91}$$

Again we assume that the theory has been appropriately rescaled to absorb the parameters ξ_0 and T_0. Applying a saddle point approximation to the remaining functional integral over λ leads to the condition

$$\lambda = \frac{4N\pi\, u}{\Lambda}\,\mathrm{tr}\,\frac{1}{\delta_0 + \lambda + k_{\shortparallel}^2 + \eta\, k_\perp^2 + |\omega_n|} \,. \tag{4.92}$$

The saddle point approximation can be justified in the limit of a large number of components N while treating the quartic coupling u as of order $1/N$.

By calculating the susceptibility we can identify $\delta_0 + \lambda$ with ξ^{-2}, where ξ is the correlation length,

$$\chi^{-1}(\mathbf{k}, i\omega_n) = \delta_0 + \lambda + k_{\shortparallel}^2 + \eta\, k_\perp^2 + |\omega_n| \,. \tag{4.93}$$

4.3.1 Zero-temperature mass gap

At zero temperature the saddle point condition becomes

$$\Delta = \delta_0 + \frac{4N\pi u}{\Lambda}\int \frac{d^3k}{(2\pi)^3}\int \frac{d\omega}{2\pi}\,\frac{1}{\Delta + k_{\shortparallel}^2 + \eta\, k_\perp^2 + |\omega|} \,. \tag{4.94}$$

We can identify the position of the quantum critical point with the condition that the mass gap Δ vanishes at the quantum phase transition,

$$\delta_c = -\frac{4N\pi u}{\Lambda}\int \frac{d^3k}{(2\pi)^3}\int \frac{d\omega}{2\pi}\,\frac{1}{k_{\shortparallel}^2 + \eta\, k_\perp^2 + |\omega|} \,. \tag{4.95}$$

Introducing the control parameter

$$r \equiv \frac{\delta_0 - \delta_c}{Nu/\pi^2} \tag{4.96}$$

that measures the distance to the quantum critical point we obtain for the mass gap

$$\Delta = \frac{Nu}{\pi^2}r + \frac{4N\pi u}{\Lambda}\int \frac{d^3k}{(2\pi)^3}\int \frac{d\omega}{2\pi}\left\{\frac{1}{\Delta + k_{\shortparallel}^2 + \eta\, k_\perp^2 + |\omega|} - \frac{1}{k_{\shortparallel}^2 + \eta\, k_\perp^2 + |\omega|}\right\} \,. \tag{4.97}$$

With the help of the scaling function

$$\Xi\left(\frac{\Delta}{\eta\Lambda^2}\right) \equiv \frac{2\pi^3}{\Delta\Lambda}\int\frac{d^3k}{(2\pi)^3}\int\frac{d\omega}{2\pi}\left\{\frac{1}{k_{\shortparallel}^2+\eta\,k_\perp^2+|\omega|}-\frac{1}{\Delta+k_{\shortparallel}^2+\eta\,k_\perp^2+|\omega|}\right\}-\log\frac{1}{\sqrt{\eta\Lambda^2}}$$
$$=\frac{2}{3}\left(1+\sqrt{\frac{\Delta}{\eta\Lambda^2}}\arctan\sqrt{\frac{\eta\Lambda^2}{\Delta}}\right)-\frac{1}{2}\left(1+\frac{\eta\Lambda^2}{3\Delta}\right)\log\left(1+\frac{\Delta}{\eta\Lambda^2}\right), \tag{4.98}$$

where we applied the cutoff scheme of Section 4.1.1, this can be rewritten as

$$\boxed{\frac{Nu}{\pi^2}r=\Delta\left\{1+\frac{4Nu}{2\pi^2}\left(\log\frac{1}{\sqrt{\eta\Lambda^2}}+\Xi\left(\frac{\Delta}{\eta\Lambda^2}\right)\right)\right\}.} \tag{4.99}$$

The function Ξ has the limiting behavior

$$\Xi(x)=\begin{cases}\dfrac{1}{2}\log\dfrac{1}{x}+\dfrac{4}{3}+\mathcal{O}\left(\dfrac{1}{x}\log\dfrac{1}{x}\right) & \text{for}\quad x\gg 1\\[2ex] \dfrac{1}{2}+\dfrac{\pi}{3}\sqrt{x}+\mathcal{O}\left(x\right) & \text{for}\quad x\ll 1\,.\end{cases} \tag{4.100}$$

In the 3D regime, $\Delta\ll\eta\Lambda^2$, the relation (4.99) simplifies to

$$r=\Delta\log\left(\frac{e\,e^{\frac{\pi^2}{Nu}}}{\eta\Lambda^2}\right)\qquad\text{for}\quad\Delta\ll\eta\Lambda^2\,, \tag{4.101}$$

which means that the mass gap is simply proportional to the control parameter r. In the 2D regime, $\Delta\gg\eta\Lambda^2$, we obtain

$$r=\Delta\log\left(\frac{e^{8/3}e^{\frac{\pi^2}{Nu}}}{\Delta}\right)\qquad\text{for}\quad\Delta\gg\eta\Lambda^2\,. \tag{4.102}$$

As expected, at the upper critical dimension, $d+z=4$, the correlation length exponent ν deviates from its Landau value $\nu=1/2$ by logarithmic corrections, $\Delta\sim r/\log\frac{1}{r}$.

4.3.2 Correlation length

The correlation length as a function of control parameter r and temperature $\mathcal{T}$ is given by

$$\xi^{-2}=\frac{Nu}{\pi^2}r+\frac{4N\pi u}{\Lambda}\int\frac{d^3k}{(2\pi)^3}\left\{\mathcal{T}\sum_{\omega_n}\frac{1}{\xi^{-2}+k_{\shortparallel}^2+\eta\,k_\perp^2+|\omega_n|}-\int\frac{d\omega}{2\pi}\frac{1}{k_{\shortparallel}^2+\eta\,k_\perp^2+|\omega|}\right\}. \tag{4.103}$$

Rearranging terms and applying the cutoff scheme of Section 4.1.1 this can be rewritten as

$$\boxed{\xi^{-2}\left\{1+\frac{4Nu}{2\pi^2}\left(\log\frac{1}{\sqrt{\eta\Lambda^2}}+\Xi\left(\frac{\xi^{-2}}{\eta\Lambda^2}\right)\right)\right\}=\frac{Nu}{\pi^2}r+\frac{4Nu}{2\pi}\mathcal{T}\,\Upsilon\left(\frac{\mathcal{T}}{\eta\Lambda^2},\frac{\xi^{-2}}{\eta\Lambda^2}\right),} \tag{4.104}$$

where the scaling function Υ is defined in (4.81).

4.3.3 Phase boundary

Setting $\xi^{-2} = 0$ in expression (4.104) yields for the critical temperature $\mathcal{T}_c$

$$r = -2\pi \mathcal{T}_c \, \Upsilon \left(\frac{\mathcal{T}_c}{\eta \Lambda^2}, 0 \right) . \tag{4.105}$$

In the following we will use the limiting behavior (4.84) of the scaling function Υ to distinguish again between the 2D and the 3D regime.

2D regime: $\mathcal{T}_c \gg \eta \Lambda^2$

In the 2D regime we can approximate $\Upsilon(x, 0) \approx \log \sqrt{x}$ and obtain

$$r = -\pi \mathcal{T}_c \, \log \frac{\mathcal{T}_c}{\eta \Lambda^2} . \tag{4.106}$$

3D regime: $\mathcal{T}_c \ll \eta \Lambda^2$

In the 3D regime, $\Upsilon(x, 0) \approx \Gamma\left(\frac{3}{2}\right) \, \zeta\left(\frac{3}{2}\right) \sqrt{x/2}$, we get

$$r = -\frac{\pi^{3/2} \, \zeta\,(3/2)}{\sqrt{2}} \, \frac{\mathcal{T}_c^{3/2}}{\sqrt{\eta \Lambda^2}} . \tag{4.107}$$

This again confirms the result (4.39) obtained in the framework of the Millis RG.

4.4 Discussion

We have investigated the anisotropic Hertz model (4.4) with a special emphasis on the dimensional crossover. We applied three different methods — the Millis RG, the method of dimensional reduction and the large N method — in order to determine the crossover lines.

In comparison with the solution of the isotropic Hertz theory presented in Chapter 3 we found three new crossover lines associated with the dimensional crossover, see Fig. 4.3. These are determined by comparing the squared inverse correlation length ξ^{-2}, the temperature $\mathcal{T}$ and the control parameter r with the squared inverse stretched lattice constant $\eta \Lambda^2$, see Fig. 4.2. The parameter $\eta \Lambda^2$ determines the extent of the 3D pocket around the quantum critical point where the three-dimensional spin fluctuations dominate. Furthermore, the crossover line $\xi^{-2} \sim \eta \Lambda^2$ signifies that close to the classical finite temperature transition the three-dimensional character of the theory dominates. It is associated with the cutoff of the logarithmic Mermin–Wagner divergence (3.1) present in two space dimension. As a consequence, the Néel temperature (4.39) is logarithmically suppressed by a factor $\log \mathcal{T}_c/(\eta \Lambda^2)$ and vanishes in the limit $\eta \Lambda^2 \to 0$, in agreement with the Mermin–Wagner theorem (for $N > 2$). The logarithmic suppression of the Néel temperature can be estimated by comparing with the quantum critical–Fermi liquid crossover line, and the difference between their slopes yields a qualitative estimate of the anisotropy present in the system.

Moreover, we have shown that the anisotropy parameter η is a relevant quantity in the RG sense in the regime where the two-dimensional spin fluctuations dominate, i.e. when the RG flow is still towards the primary, 2D fixed point. Sufficiently close to the quantum critical point, i.e. within the 3D pocket (see Fig. 4.3), the RG flow is eventually dominated

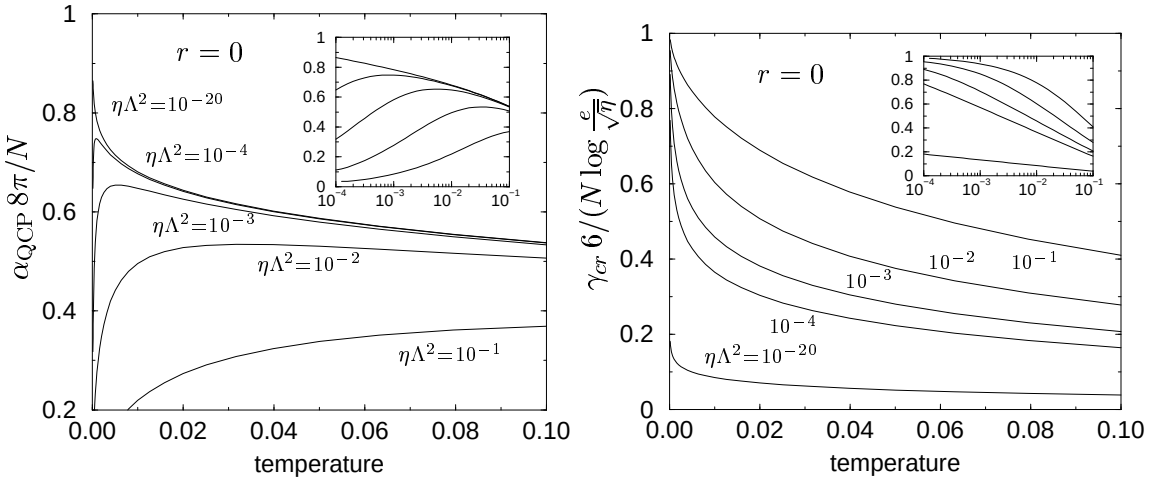

Figure 4.7: *Thermal expansion (left panel) and specific heat coefficient (right panel) in the quantum critical regime $r = 0$ for different anisotropies $\eta\Lambda$. The inset in each graph shows a logarithmic plot of the same curves. The dimensional crossover at a temperature $\mathcal{T} \sim \eta\Lambda^2$ is clearly seen as a knee in the temperature dependence of the thermal expansion whereas there are only small signatures in the specfic heat. In both graphs dimensionless units have been chosen.*

by the secondary, 3D fixed point. Within the 3D pocket all physical quantities exhibit scaling behavior with the scaling variables: anisotropy $\eta\Lambda^2$, temperature $\mathcal{T}$ and zero-temperature gap Δ. The relevance of the anisotropy parameter η with respect to the primary fixed point is particularly important when considering the thermal expansion, which in the 2D regime is composed of two equally important contributions: $\alpha_{\rm QCP}$ (4.42) arising from the pressure sensitivity of the control parameter r, and α_η (4.43) stemming from the pressure sensitivity of the anisotropy parameter η. However, within the 3D pocket the additional contribution α_η is only sub-leading in comparison to $\alpha_{\rm QCP}$.

We expect that the experimental identification of the dimensional crossover in the compound $CeCu_{6-x}Au_x$ is more easily achieved by measuring the thermal expansion than the specific heat. The underlying reason has already been discussed in detail in Chapter 1: the thermal expansion is more singular than the specific heat which makes it also easier to detect crossover behavior. In Fig. 4.7 theoretical curves of the thermal expansion and the specfic heat are shown at the critical value $r = 0$ for different anisotropies. Whereas there are only weak signatures at the dimensional crossover in the specific heat, a pronounced knee is visible in the thermal expansion initiating the crossover from a logarithmic divergence to a square root suppression as a function of temperature, see Section 4.1.6. It should be noted that the specific heat coefficient smoothly crosses over from a logarithmic temperature dependence to a square root dependence at $r = 0$. In particular, the slope decreases monotonically at the dimensional crossover and no Schottky-like anomaly is expected.

In outlook we mention that it seems promising to consider a further quantity likely to be even more sensitive to the dimensional crossover than the thermal expansion: the elastic constant [39, 40] which can be obtained by measuring sound velocities. Taking only the pressure sensitivity of the control parameter into account the elastic constant c is proportional to the second derivative of the free energy with respect to the control parameter, $c \propto d^2F/dr^2$,

and it is therefore the quantum critical counterpart of the specific heat at the classical finite temperature transition. The elastic constant is expected to be very sensitive to changes in the scaling behavior, and it is therefore a possible candidate for the detection of the dimensional crossover in $CeCu_{6-x}Au_x$.

Appendix A

A.1 Grüneisen parameter for gapped systems — QCP of non-interacting bosons

In this section we modify the expansion (1.24) of the scaling function $\Psi_{\rm LT}$ in the low-temperature regime in order to account for the physics of gapped systems, i.e. systems whose entropy vanishes exponentially with temperature, $S \sim e^{-\Delta/T}$ where Δ is an energy gap.

For illustration let us consider the simple case of non-interacting bosons in three dimensions. The free energy reads [41]

$$F = TV \int \frac{d^3k}{(2\pi)^3} \log\left(1 - e^{-\beta(\epsilon_{\mathbf{k}}-\mu)}\right) = -T\frac{V}{\lambda_T^3} g_{5/2}(z)\,. \tag{A.1}$$

where V is the volume. We introduced the thermal wavelength $\lambda_T = \sqrt{2\pi/(mT)}$, the fugacity $z = e^{\mu/T}$ and the function g_a,

$$g_a(z) = \sum_{n=1}^{\infty} \frac{z^n}{n^a}\,, \tag{A.2}$$

which has the convenient property $z g_a'(z) = g_{a-1}(z)$. Moreover, we used a quadratic dispersion for the bosons $\epsilon_{\mathbf{k}} = \mathbf{k}^2/(2m)$. In writing (A.1) we confined ourselves to the disordered side, $z < 1$, where the bosons are not condensed yet. Bose-Einstein condensation takes place when the (negative) chemical potential reaches zero. The chemical potential can therefore be identified with the control parameter of the quantum critical point. Taking the derivative with respect to temperature we obtain the entropy,

$$S = \frac{V}{\lambda_T^3}\left(\frac{5}{2} g_{5/2}(z) - g_{3/2}(z)\log z\right)\,. \tag{A.3}$$

Comparing this expression with the scaling form of the entropy in the quantum critical regime introduced in (1.23) we can conclude that the critical exponents are given by (applying hyperscaling $\phi = d + z$ and using $d = 3$),

$$z = 2 \qquad \text{and} \qquad \nu = 1/2\,. \tag{A.4}$$

Furthermore, for the sake of comparison with section 1.3.3 we introduce the non-universal temperature scale $T_0 = 2\pi/(mV^{2/3})$ and the control parameter $r = \mu/T_0 < 0$. We can identify the scaling functions to be

$$\Psi_{\rm QCR}(x) = \frac{5}{2} g_{5/2}\left(e^x\right) - x\, g_{3/2}\left(e^x\right) \tag{A.5}$$

$$\Psi^-_{\rm LT}(x) = x^{3/2}\, \Psi_{\rm QCR}(-1/x) \tag{A.6}$$

Since we restricted ourselves from the beginning to the uncondensed phase, $\mu < 0$, the scaling function $\Psi^+_{\rm LT}$ for positive values of the control parameter is beyond this simple approach. We can explicitly evaluate the limits for small arguments $x \to 0$,

$$\Psi_{\rm QCR}(x) = \frac{5}{2}\zeta\left(\frac{5}{2}\right) + \frac{3}{2}\zeta\left(\frac{3}{2}\right) x + \mathcal{O}(x^2) \tag{A.7}$$

$$\Psi^-_{\rm LT}(x) = x^{1/2}\, e^{-1/x} + \mathcal{O}\left(x^{3/2} e^{-1/x}\right) . \tag{A.8}$$

The scaling function in the quantum critical regime $\Psi_{\rm QCR}$ is analytic as assumed in (1.24). The Grüneisen parameter in the quantum critical regime can be read off from (1.28) to be

$$\Gamma_{{\rm QCR},cr} = -\frac{2\,\zeta(3/2)}{5\,\zeta(5/2)} \left(\frac{T}{T_0}\right)^{-1} . \tag{A.9}$$

On the other hand, the scaling function $\Psi^-_{\rm LT}$ is non-analytic! In particular, the entropy does not decay algebraically as assumed in (1.25) but falls off exponentially. The exponential decay of the entropy represents an Arrhenius factor $e^{-|\mu|/T}$ describing the thermal excitations across the gap of the excitation spectrum of size μ! In general, all gapped systems have an entropy decaying exponentially at low temperatures, and they are therefore not captured by the expansion Ansatz (1.24).

For gapped system the scaling function $\Psi_{\rm LT}$ is rather expected to behave as

$$\Psi_{\rm LT}(x) = \mathcal{C}_1\, x^a e^{-\mathcal{C}_2/x} + \ldots \qquad \text{for} \quad x \to 0 \tag{A.10}$$

where $\mathcal{C}_1$ and $\mathcal{C}_2$ are some positive constants and a is a positive or negative exponent. In particular, for the non-interacting Bose gas we have $\mathcal{C}_1 = \mathcal{C}_2 = 1$ and $a = 1/2$. Repeating the analysis of section 1.3.3 for the modified expansion (A.10) we obtain for the leading contribution of the specific heat and the thermal expansion in the low-temperature regime

$$T\frac{\partial S}{\partial T} \approx \mathcal{C}_1\mathcal{C}_2\, |r|^{\nu(\phi-z)} \left(\frac{T}{T_0}|r|^{-\nu z}\right)^{a-1} e^{-\mathcal{C}_2 |r|^{\nu z} T_0/T} \tag{A.11}$$

$$\frac{\partial S}{\partial r} \approx -\mathcal{C}_1\mathcal{C}_2\, \nu z\, |r|^{\nu(\phi-z)} \frac{1}{r} \left(\frac{T}{T_0}|r|^{-\nu z}\right)^{a-1} e^{-\mathcal{C}_2 |r|^{\nu z} T_0/T} . \tag{A.12}$$

This yields the universal Grüneisen parameter for gapped systems in the low-temperature regime

$$\boxed{\Gamma_{cr} = \frac{\nu z}{r} \qquad \text{for} \quad |r|\,(T/T_0)^{-\frac{1}{\nu z}} \gg 1\,.} \tag{A.13}$$

Interestingly, one would have obtained this result from expression (1.28) by just taking naively the limit of the specific heat exponent $y_0 \to \infty$.

In particular, for the non-interacting Bose gas we have

$$\Gamma_{\mu,cr} \equiv -\frac{(\partial S/\partial\mu)}{T(\partial S/\partial T)} = \begin{cases} -\dfrac{2\,\zeta(3/2)}{5\,\zeta(5/2)}\,\dfrac{1}{T} & \text{for} \quad 0 < -\mu \ll T \\ \dfrac{1}{\mu} & \text{for} \quad -\mu \gg T\,. \end{cases} \tag{A.14}$$

A.2 Lindhard function

In this section we evaluate the Lindhard function (2.14) and determine its form in the limit of small momentum and frequency. Let us consider the Lindhard function as a function of the complex frequency variable z,

$$\chi_0(z,\mathbf{k}) = -\frac{1}{\beta V}\sum_{\Omega_m,\mathbf{q}} \frac{1}{(-i\Omega_n+\xi_{\mathbf{q}})\,(-i\Omega_n - z + \xi_{\mathbf{q}+\mathbf{k}})} = -\frac{1}{V}\sum_{\mathbf{q}} \frac{f(\xi_{\mathbf{q}}) - f(\xi_{\mathbf{q}+\mathbf{k}})}{\xi_{\mathbf{q}} - \xi_{\mathbf{q}+\mathbf{k}} + z}\,, \quad \text{(A.15)}$$

where f is the Fermi function and the Matsubara sum has been evaluated by standard methods. The physical (retarded) response function, the dynamical suszeptibility, is given in the limit as we approach the real frequency axis from above

$$\chi_0(\omega + i0^+, \mathbf{k}) = \chi_0'(\omega,\mathbf{k}) + i\chi_0''(\omega,\mathbf{k})\,. \quad \text{(A.16)}$$

The imaginary part χ_0'' describes the dissipation due to the excitations of virtual electron–hole pairs out of the Fermi sea usually known as Landau damping,

$$\chi_0''(\omega,\mathbf{k}) = \pi \int \frac{d\mathbf{q}}{(2\pi)^3}\,(f(\xi_{\mathbf{q}}) - f(\xi_{\mathbf{q}+\mathbf{k}}))\,\delta\,(\xi_{\mathbf{q}} - \xi_{\mathbf{q}+\mathbf{k}} + \omega)\,. \quad \text{(A.17)}$$

The Lindhard function can be evaluated explicitely in the free electron model, i.e. by assuming a simple quadratic dispersion relation $\xi_{\mathbf{k}} = \mathbf{k}^2/(2m^*) - \mu$ [see section 5.1 of [26]]. A discussion of the low–momentum, low–frequency properties in the general case can be found in [42]. At small frequencies we can expand the second Fermi function and the expression simplifies at zero temperature to an integral over a surface region in momentum space

$$\begin{aligned} \chi_0''(\omega,\mathbf{k}) &\approx \pi\,\omega \int \frac{d\mathbf{q}}{(2\pi)^3}\left(-\frac{\partial f(\xi_{\mathbf{q}})}{\partial \xi_{\mathbf{q}}}\right)\delta\,(\xi_{\mathbf{q}} - \xi_{\mathbf{q}+\mathbf{k}} + \omega) \\ &= \pi\,\mathcal{N}_{\mathrm{F}}\,\omega \int \frac{d\Omega_{\mathbf{q}}}{4\pi}\delta\,(\epsilon_{\mathbf{q}} - \epsilon_{\mathbf{q}+\mathbf{k}} + \omega)\Big|_{\epsilon_{\mathbf{q}}=\epsilon_{\mathrm{F}}}\,. \end{aligned} \quad \text{(A.18)}$$

ferromagnetic instability

If the spin–density wave instability is of a ferromagnetic nature, i.e. if the instability occurs at $\mathbf{k} = 0$, the above expression can be simplified further. Expanding the energy $\epsilon_{\mathbf{q}+\mathbf{k}}$ inside the delta function for small $\mathbf{k}$ and assuming an isotropic Fermi surface the angular integral can be evaluated and yields for the

$$\text{ferromagnetic instability:} \qquad \chi_0''(\omega,\mathbf{k}) \approx \frac{\pi}{2}\mathcal{N}_{\mathrm{F}}\frac{\omega}{\mathrm{v}_{\mathrm{F}}k}\Theta(\mathrm{v}_{\mathrm{F}}{}^2k^2 - \omega^2)\,. \quad \text{(A.19)}$$

The frequencies $\omega > \mathrm{v}_{\mathrm{F}}k$ are lying outside the particle–hole continuum and the Landau damping vanishes in this frequency range. The momentum $\mathrm{v}_{\mathrm{F}}k$ therefore provides a natural cutoff for Landau damping. The dispersive part, χ_0', is an even function of frequency and momentum. Its value at zero frequency and zero momentum is easily evaluated to give the density of states at the Fermi energy $\mathcal{N}_{\mathrm{F}}$. The corrections to it will start quadratically in frequency and momentum.

antiferromagnetic instability

In the case of an antiferromagnetic instability the Lindhard function has a maximum at a finite wavevector $\mathbf{k} = \mathrm{Q}_0$. The critical behaviour is then dominated by the small fluctuations $\delta\mathbf{k} = \mathbf{k} - \mathrm{Q}_0$ around this value. It turns out that in contrast to the ferromagnetic case the leading contribution to the dissipative part does not depend on the momentum. Setting $\mathbf{k} = \mathrm{Q}_0$ in (A.18) the remaining integral over the momentum surface is expected to give a finite value which will however depend on the specific energy–momentum relation. That means the leading contribution to the dissipative part reads for an

$$\text{antiferromagnetic instability:} \qquad \chi_0''(\omega, \mathrm{Q}_0) \sim \omega\,. \tag{A.20}$$

The dispersive part, χ_0', will also depend on the specific band structure. The important observation is that the leading corrections in the momentum fluctuations $\delta\mathbf{k}$ starts quadratically since $\chi_0(\mathbf{k}, 0)$ has a maximum at $\mathbf{k} = \mathrm{Q}_0$.

A.3 Linked cluster expansion

Here we cite explicitly the contributions of all diagrams of the linked cluster expansion up to second order in the quartic coupling u in the Hertz' theory (2.23). The corrections to the Gaussian part of the free energy are given by the linked cluster diagrams,

$$F - F_{\text{Gaussian}} = -\frac{1}{\beta}\left\langle \exp\left[-S^{(4)}\right]\right\rangle_{\text{connected}} \tag{A.21}$$

where the average has to be taken with respect to the quadratic part $S^{(2)}$ of (2.23). The following diagrams contribute,

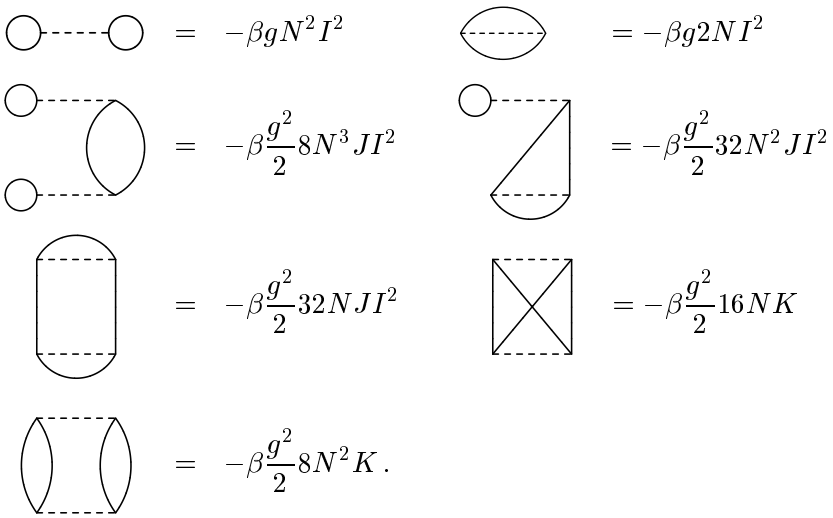

(A.22)

We introduced the quantities

$$
\begin{aligned}
I =& \frac{1}{\beta V} \sum_{\omega_n, \mathbf{k}} \chi_0(i\omega_n, \mathbf{k}) \,, \qquad J = -\frac{1}{\beta V} \sum_{\omega_n, \mathbf{k}} \chi_0(i\omega_n, \mathbf{k}) \chi_0(-i\omega_n, -\mathbf{k}) \,, \\
K =& -\frac{1}{(\beta V)^4} \sum_{\substack{\omega_{nj}, \mathbf{k}_j \\ j=1,2,3,4}} V \delta \left(\sum_{i=1}^{4} \mathbf{k}_i \right) \beta \delta \left(\sum_{i=1}^{4} \omega_{in} \right) \\
& \times \chi_0(i\omega_{1n}, \mathbf{k}_1) \chi_0(i\omega_{2n}, \mathbf{k}_2) \chi_0(i\omega_{3n}, \mathbf{k}_3) \chi_0(i\omega_{4n}, \mathbf{k}_4) \,.
\end{aligned}
\tag{A.23}
$$

where χ_0 is the Hertz propagator (2.27). This results in the free energy,

$$
F = F_G + gN(N+2)I^2 + \frac{g^2}{2!} \left[8N(N+2)^2 I^2 J + 8N(N+2)K \right] \,. \tag{A.24}
$$

Part II

Coupled Impurities

Chapter 5

Introduction

5.1 Motivation: disorder effects in heavy fermions

The unusual properties of heavy fermion materials [43], for example the unconventional, i.e., non-Fermi liquid magnetic susceptibility and (weakly divergent) specific heat are still lacking a complete theoretical understanding. In some of these materials disorder seems to be an essential ingredient of the physics observed and at the origin of the non-Fermi liquid behavior. The role of disorder in these systems can be multifarious.

Many experimental results can be described within the rather simple Kondo disorder model (KDM) [44, 45]. It assumes that each magnetic moment of the rare-earth ions couples independently to the spins of the conduction electrons via an exchange interaction J. However, the exchange couplings between the local moments, e.g. the RKKY interaction mediated indirectly by the conduction electrons, are neglected. In the simplest version of the KDM the influence of disorder is only taken into account in the form of a spatial variation of the coupling $J(\mathbf{R})$. This exchange interaction enters physical quantities only in the form of the Kondo temperature T_{K} that depends exponentially on $J(\mathbf{R})$, namely $T_{\mathrm{K}} \sim e^{-1/(2J(\mathbf{R})\nu)}$ where ν is the density of states of the conduction electrons. Due to this exponential dependence a modest variation of the exchange coupling, $J(\mathbf{R})$, can lead to a broad distribution of Kondo temperatures and, consequently, to a dramatic effect on the low temperature properties.

However, many heavy fermion systems are located near a magnetic instability where the physics is more complicated. The conduction electrons are collectively bound to the rare-earth ions, screening their local moments. The binding energy is the Kondo temperature T_{K}. Near the magnetic stability this Kondo effect competes with the RKKY interaction between the local moments that is struggling to align them and thus to establish long range order [46]. Which mechanism prevails depends on how the associated energy scales, T_K and T_{RKKY}, compare with each other [46]. (Magnetic instabilities in clean metals and the associated quantum phase transitions formed the subject of the first part of this work.) The presence of disorder will possibly alter the physical picture completely. A general scaling argument in the case of "bond-disorder", i.e. statistical variation of the coupling between the local moments, states that disorder cannot be neglected if the correlation length exponent of the clean system, ν, and the spatial dimension d fulfill the so-called Harris criterion [2]:

$$\nu < \frac{2}{d}\,. \tag{5.1}$$

Disorder is then a relevant perturbation to the clean theory, ultimately leading eventually

to new fixed points. In particular, the Harris criterion is fulfilled and randomness has to be taken into account in two and three dimensions for the Hertz–Millis theory presented in Chapter 2 where we have $\nu = 1/2$. Beyond the knowledge of its relevance, however, the role of disorder in quantum critical systems is only poorly understood [2].

An effect which may result from the presence of disorder is the generation of magnetic "droplets", locally confined condensation of the magnetization order parameter surrounded by an otherwise on average unordered medium. Due to disorder fluctuations of the interactions there are small regions in space where the RKKY interaction locally dominates over the Kondo effect leading to the formation of small magnetic domains. These magnetic droplets will dominate, for example, the susceptibility, resulting in so-called "Griffith–McCoy" singularities [2].

In a series of papers A. H. Castro Neto and B. A. Jones [47, 48, 49] considered the dynamics of such a single magnetic droplet and gave qualitative arguments proposing that it should behave as an effective spin coupled to an electron liquid undergoing a "cluster Kondo effect". Properties like the cluster Kondo temperature depend on the number of local moments of which the cluster is formed. The statistics of cluster sizes is reflected in a distribution of cluster Kondo temperatures leading to anomalous thermodynamic behavior in the spirit of the KDM. This viewpoint was challenged by A. J. Millis, D. K. Morr and J. Schmalian [50, 51] suggesting that the dissipative bath of electrons suppresses the tunneling between the cluster configurations for larger droplets destroying the cluster Kondo effect. In another letter N. Shah and A. J. Millis [52] studied an extended magnetic nanostructure and found that the quantum fluctuations within the cluster, which had been previously ignored, have a dramatic effect on the low temperature behavior. Griffith–McCoy phases near quantum critical points remain to be a contentious issue and further work is required to fully understand their complicated nature.

5.2 Model of a magnetic mini-domain

In the following chapters we would like to contribute to the understanding of the physics of magnetic clusters by considering the dynamics of the smallest possible magnetic droplet: an antiferromagnetically ordered domain which consists of just two strongly coupled localized spin-$\frac{1}{2}$,

$$H_{\mathrm{MD}} = K^{ij}\, S^i(\mathbf{R}/2)\, S^j(-\mathbf{R}/2)\,, \tag{5.2}$$

located at positions $\mathbf{R}/2$ and $-\mathbf{R}/2$. In heavy fermion materials the spin-orbit interactions are quite strong due to the heavy masses of the rare-earth ions and spin rotation invariance is destroyed. We assume that this leads to a preferred easy axis in the material along which the moments tend to order. We will take this into account with a strongly anisotropic Ising-like exchange coupling,

$$(K^{ij}) = \mathrm{diag}\{K_\perp, K_\perp, K_z\} \quad \text{where} \quad |K_\perp| \ll K_z\,. \tag{5.3}$$

The disorder fluctuations favor the coupling between the two selected local moments giving rise to a tiny magnetic droplet. We assume that the coupling between the moments is much stronger than their coupling to the remaining f-electron system, so that the latter can be neglected. Furthermore, the gas of magnetic droplets is so dilute that the interaction between droplets is also negligible. The local physics is therefore governed by the Hamiltonian (5.2)

in combination with the interaction of the local moments to the conduction electron system, to be described below.

In the limit of a large Ising coupling, $K_z \gg K_\perp$, the local moments tend to form what we call in the following an antiferromagnetic mini-domain, Fig. 5.2. The four energy levels of the Hamiltonian (5.2) are well separated into two pairs, see Fig. 5.1. This should be contrasted with the case of an SU(2)-symmetric coupling where the eigenstates are given by a singlet and a degenerate triplet. For an antiferromagnetic coupling $K_z > 0$ the degenerate ferromagnetic configurations have a much higher energy. If K_z is the largest energy scale involved the Hilbert space can be confined to the two lowest-lying levels in the low-temperature limit. Their eigenstates correspond to the even and odd combinations of the two antiferromagnetic configurations shown in Fig. 5.2,

$$|+\rangle = \frac{1}{\sqrt{2}}\left(|\uparrow\downarrow\rangle + |\downarrow\uparrow\rangle\right) ,$$
$$|-\rangle = \frac{1}{\sqrt{2}}\left(|\uparrow\downarrow\rangle - |\downarrow\uparrow\rangle\right) . \tag{5.4}$$

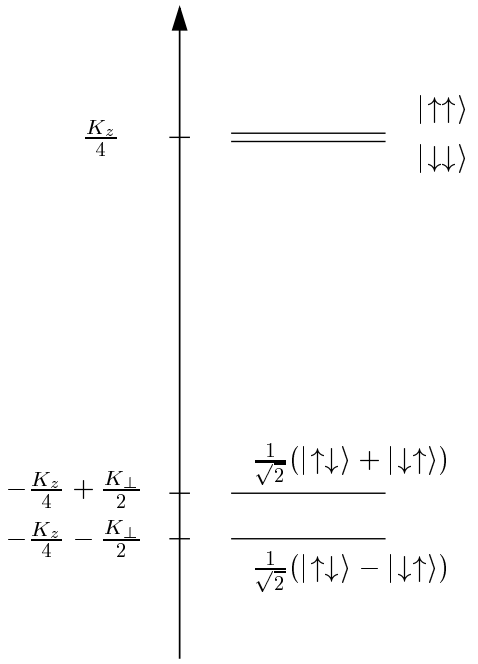

Figure 5.1: *Energy levels of the mini-domain Hamiltonian $H_{\rm MD}$ of equation (5.2). Due to the anisotropic coupling the antiferromagnetic configurations are much lower in energy than the ferromagnetic ones.*

This effective two level system — the mini-domain — may be represented by a pseudospin $\vec{\tau}$, where τ^i, $i = 1, 2, 3$, are the usual Pauli-matrices. The small energy difference of $\pm K_\perp/2$ between the two states $|+\rangle$ and $|-\rangle$ then corresponds to a "pseudo-magnetic" Zeeman splitting and the low-temperature Hamiltonian $\mathcal{H}_{\rm MD}$ can be expressed as

$$\mathcal{H}_{\rm MD} = \frac{K_\perp}{2}\,\tau^3 . \tag{5.5}$$

When the mini-domain is coupled to the conduction electrons quantum fluctuations between the two configurations of the mini-domain are induced, which will eventually lead to non-trivial dynamics. We model the interaction between the mini-domain and the conduction

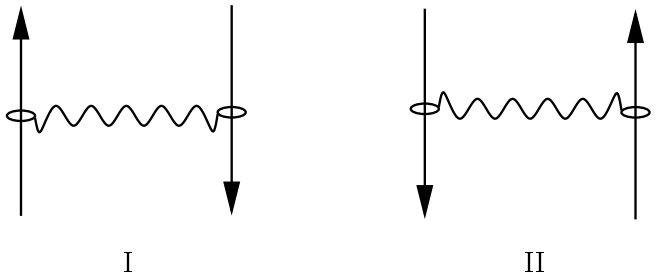

Figure 5.2: *Two configurations of the antiferromagnetic mini-domain. The wiggly lines indicate the strong Ising-coupling K_z between the localized spins.*

electrons by a Kondo coupling of each spin to the Fermi sea,

$$\begin{aligned} H_{\rm K} &= 2J^{ij}\left(s^i(\mathbf{R}/2)\,S^j(\mathbf{R}/2)+s^i(-\mathbf{R}/2)\,S^j(-\mathbf{R}/2)\right) \qquad (5.6)\\ &= J^{ij}\sum_{\mathbf{kq}}\left(e^{i(\mathbf{k}-\mathbf{q})\mathbf{R}/2}\,c^\dagger_{\mathbf{k}\alpha}\sigma^i_{\alpha\beta}c_{\mathbf{q}\beta}\,S^j(\mathbf{R}/2)+e^{-i(\mathbf{k}-\mathbf{q})\mathbf{R}/2}\,c^\dagger_{\mathbf{k}\alpha}\sigma^i_{\alpha\beta}c_{\mathbf{q}\beta}\,S^j(-\mathbf{R}/2)\right). \end{aligned}$$

The coupling J^{ij} is assumed to be the same for both impurity spins, thus preserving parity symmetry of the Hamiltonian H_K. However, it will in general be anisotropic, i.e.,

$$(J^{ij}) = \mathrm{diag}\{J_\perp, J_\perp, J_z\}\,. \qquad (5.7)$$

The electrons, $c_{\mathbf{k}\sigma}$, are assumed to belong to a featureless band with the kinetic part $H_0 = \sum_{\mathbf{k}\sigma}(\epsilon_{\mathbf{k}\sigma}-\mu)c^\dagger_{\mathbf{k}\sigma}c_{\mathbf{k}\sigma}$. The model Hamiltonian whose analysis will occupy the following chapters reads

$$H = H_0 + H_{\rm MD} + H_K\,. \qquad (5.8)$$

We will be mainly interested in the dynamics of the model in the parameter regime where the energy scale K_z responsible for the formation of the mini-domain is predominant. In Chapter 6 we derive the corrections to the low-energy Hamiltonian (5.5) by treating the Kondo coupling J as a perturbation. Through second-order processes, the Kondo coupling J will induce transitions between the states (5.4) of the low-temperature Hilbert space via virtual excitations of the ferromagnetic states, $|\uparrow\uparrow\rangle$ and $|\downarrow\downarrow\rangle$. This will result in an effective pseudospin–Kondo Hamiltonian.

In Chapter 7 we will restrict the model in the sense that we assume that (a) the perpendicular coupling between the spins vanishes identically, $K_\perp = 0$, and (b) the electronic bath at the respective impurity sites are not correlated with each other. Although these simplifications might appear artificial in the context of Kondo impurities in heavy fermions it is not only helps understand the various mechanisms competing with each other but also has a natural realization in double-quantum dot systems. As we will explain the two assumptions (a) and (b) allow for a quantum phase transition: As a function of the couplings K_z, J_z and $J_\perp$ the mini-domain either freezes in one of its two configurations or is screened in a "cluster Kondo effect". The theory describing the phase transition is indeed an effective Kondo model. In experimental realizations of the reduced mini-domain model in terms of quantum dots this transition leads to a universal jump in the conductance or to a characteristic zero-bias anomaly depending on the experimental set-up.

5.3 Overview: two-impurity Kondo model

The Hamiltonian (5.8) is a variant of the two-impurity Kondo model, which has been studied already for over twenty years. In its original formulation — in contrast to (5.8) — it assumes an SU(2)-symmetric exchange coupling, $K_{\shortparallel} = K_\perp = K$. In the following we will give a short overview of its main characteristics.

The two-impurity Kondo model was introduced by C. Jayaprakash, H. R. Krishna-murthy and J. W. Wilkins in Ref. [53], where they identified the different ground states existing in its parameter space. There are two different energy scales to be compared: the coupling K and the single-impurity Kondo temperature T_K. If the coupling is small, $|K| \ll T_K$, each impurity is separately screened by the conduction electrons and the coupling K plays a

minor role. For large antiferromagnetic coupling, $K \gg T_K$, the two impurities form a singlet and are decoupled from the low-energy dynamics of the conduction electrons. Finally, for large ferromagnetic coupling, $-K \gg T_K$, the model maps onto a two-channel spin-1 Kondo Hamiltonian. A generic channel anisotropy leads to the so-called two-stage Kondo effect: upon lowering the temperature the stronger coupled channel screens half a unit of the spin-1 impurity. At even lower temperatures the remaining spin-$\frac{1}{2}$ is quenched by the other channel leaving a local Fermi liquid. This early picture was subsequently confirmed by numerical renormalization group calculations (NRG) [54, 55] and Monte Carlo studies [56].

Generically, there is a smooth crossover between the different regimes, e.g. the susceptibility shows a smooth transition from the Kondo regime, $|K| \ll T_K$, to the strong coupling regime, $|K| \gg T_K$. That means that there is no quantum phase transition separating the regimes in the generic case. However, the situation changes drastically in the presence of a certain type of particle–hole symmetry. This can be rationalized by a phase-shift argument given in Ref. [57]. When the coupling K is varied the phase shift is expected to change continuously from the unitary-limit value $\pi/2$ in the Kondo phase to zero in the strong coupling phase. However, in the presence of particle–hole symmetry this cannot happen since a well-defined zero-energy phase-shift can only be 0 or $\pi/2$. As a consequence, there must be a point in the phase diagram which does not belong to either phase, but corresponds to some kind of phase transition. In the case of a first order transition the phase shift would jump from one value to the other. However, NRG calculations [58, 59] indicated that the transition is continuous. A conformal-field theory approach by I. Affleck *et al.* [59] and a Abelian bosonization analysis by J. Gan [60, 61, 62] identified the critical theory to be indeed of non-Fermi liquid type and therefore not characterizable in terms of a well-defined phase shift. The critical theory was shown to be a two-channel Kondo model [63]: only a single Majorana fermion couples to the impurity spins, which is ensured by a hidden SO(7) symmetry [59, 60, 61, 62].

Chapter 6

Magnetic Mini-Domain in a Metal

In this chapter we analyze the mini-domain model (5.8) in the limit of strong coupling where the energy scale K_z that holds the mini-domain together is much larger than any other scale involved in the problem. To zeroth order in the Kondo couplings, J_z and $J_\perp$, the effective Hamiltonian is just given by $\mathcal{H}_{\rm MD}$, defined in equation (5.5). It was obtained by truncating the Hilbert space taking into account only the low-lying antiferromagnetic states, $|\downarrow\uparrow\rangle$ and $|\uparrow\downarrow\rangle$, which can be described by an effective pseudospin, see Fig. 5.1. In this chapter we consider the modifications of the effective low-energy Hamiltonian due to the couplings of the local moments to the electrons. We will find that the conduction electrons induce transition between the two antiferromagnetic configurations. Taking these pseudospin flips into account the effective Hamiltonian has the form of an effective Kondo Hamiltonian in a pseudo-magnetic field. Moreover, we will show that it is of a two-channel type.

In Fig. 6.1 the specific heat of $CeCu_{6-x}Au_x$ is shown. This heavy fermion compound orders antiferromagnetically for doping levels larger than the critical value of $x = 0.1$. The logarithmic divergence of the specific heat coefficient directly at the critical doping can be understood in the framework of the the Hertz–Millis theory presented in Chapter 2 under the assumption that the spin fluctuations are dominantly two dimensional [7]. However, even for a doping level of fifteen and twenty percent of gold, i.e. far away from the zero temperature magnetic instability $x = 0.1$, the specific heat coefficient does not saturate at lowest temperatures as it is expected of a Fermi liquid. Instead, the peculiar increase persists which suggests that the system still possesses a substantial amount of residual entropy.

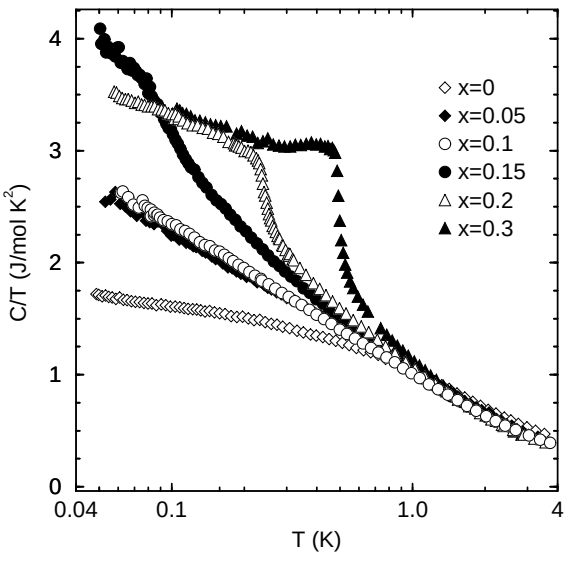

Figure 6.1: *Specific heat of $CeCu_{6-x}Au_x$ from Ref. [37], see main text.*

The residual entropy may be explained by the presence of almost degenerate two-level

systems like the mini-domain that is the subject of this chapter. Moreover, the characteristic feature of the effective two-channel Kondo model, which governs the dynamics of the strongly coupled mini-domain, are non-Fermi liquid signatures, for example, a logarithmically diverging specific heat coefficient [64, 12, 63]. One might speculate that the similar signatures observed in $CeCu_{6-x}Au_x$ are due to the formation of a dilute gas of small magnetic mini-domains, each generically undergoing two-channel Kondo type physics. However, as we will explain in detail in the following sections, the effective Hamiltonian always includes a pseudo-magnetic field. Pronounced non-Fermi liquid behavior is only expected if this field is sufficiently small compared to the effective Kondo temperature. Thus whether or not the two-channel Kondo effect develops depends on the microscopic details.

We will start in Section 6.1 by analyzing the symmetries of the model (5.8). In Section 6.2 we introduce the pseudospin notation for the conduction electrons. By applying a Schrieffer–Wolff transformation we will derive the effective Hamiltonian in the strong coupling limit, $K_z \to \infty$. Finally, in Section 6.5 this effective Hamiltonian is treated within a poor man's renormalization group treatment to investigate its low-energy behavior.

6.1 Symmetries

6.1.1 Conservation of the z-component of total spin

It will turn out to be crucial that the z-component of spin of the mini-domain is conserved. The restricted low-energy Hilbert space consists of the two antiferromagnetic states $|\uparrow\downarrow\rangle$ and $|\downarrow\uparrow\rangle$, which are eigenstates of the operator $S^z(\mathbf{R}/2) + S^z(-\mathbf{R}/2)$ with eigenvalue zero. The corresponding pseudospin of the mini-domain thus carries a zero z-component of spin. In particular, if the pseudospin is flipped, e.g. from $|\uparrow\downarrow\rangle$ to $|\downarrow\uparrow\rangle$, the spin of the mini-domain does not change. Moreover, since the Kondo coupling of the electrons to the mini-domain, (5.6), conserves spin, it follows that an electron cannot transfer spin to the mini-domain in pseudospin-flip processes. We at once conclude that for symmetry reasons the up- and down-spin electrons have to couple separately to the mini-domain at low temperatures leading to two different channels. The conservation of the z-component of total spin,

$$S^z_{\mathrm{tot}} = S^z(\mathbf{R}/2) + S^z(-\mathbf{R}/2) + \frac{1}{2}\sum_{\mathbf{k}} c^\dagger_{\mathbf{k}\alpha}\sigma^z_{\alpha\beta}c_{\mathbf{k}\beta} \tag{6.1}$$

in the model Hamiltonian (5.8) is the underlying reason for the degeneracy of these two channels.

At this point we should remark on the physical justification of this symmetry. The model was motivated by the physics of heavy fermions which are characterized by strong spin-orbit coupling arising from their heavy rare-earth ions. In fact, the strong spin-orbit coupling is the driving force which eventually leads to the pronounced anisotropy of the direct coupling K between the two impurity spins (5.2). All the spins of our model should therefore rather be regarded as effective spins arising, e.g., from the lowest-lying two-level systems of a multiplet of the total angular momentum that is split by crystal fields. In order to have a preserved spin z-component, a residual axial symmetry has to be present. The pictures I and II of the mini-domain Fig. 5.2 do not take this into account and are therefore misleading. One should rather think of the mini-domain as consisting of the configurations shown in Fig. 6.2.

However, we will continue to ignore the subtleties arising from the modifications of the band structure due to spin-orbit scattering and maintain the momentum label on the kinetic energy of the conduction electrons, $\epsilon_{\mathbf{k}\sigma}$.

6.1.2 Parity

Generally, a parity transformation reverses position $\mathbf{r}$ and momentum $\mathbf{p}$ and leaves the spin $\mathbf{s}$ unchanged,

$$\begin{aligned} \mathbf{r} &\longrightarrow -\mathbf{r}\,, \\ \mathbf{p} &\longrightarrow -\mathbf{p}\,, \\ \mathbf{s} &\longrightarrow \mathbf{s}\,. \end{aligned} \tag{6.2}$$

In particular, the spin field given by the two localized impurity spins transforms as

$$S^i(\pm\mathbf{R}/2) \longrightarrow S^i(\mp\mathbf{R}/2)\,. \tag{6.3}$$

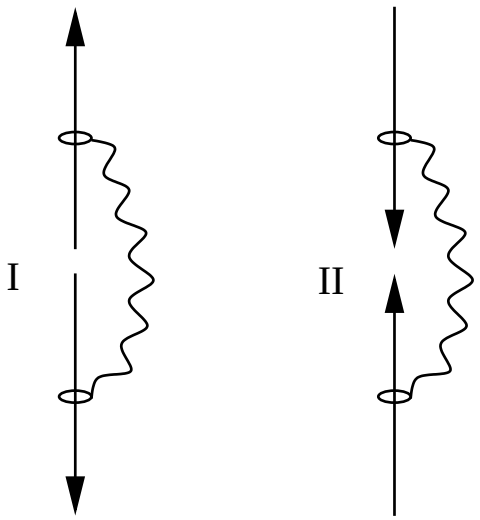

Figure 6.2: *Two configuration of the mini-domain with a axial symmetry. The wiggly lines indicate the strong coupling K_z between the spins.*

Under parity the configuration I shown in Fig. 5.2 or in Fig. 6.2 transforms to configuration II and vice versa, i.e. the eigenstates of the low-energy Hilbert space (5.4), $|+\rangle$ and $|-\rangle$, have even and odd parity, respectively. Since they are eigenstates of the pseudospin operator τ^3 introduced in (5.5), this pseudospin component can be identified as the parity operator $\mathcal{P}$ in pseudospin-space. In particular, the pseudospin $\vec{\tau}$ itself transforms as

$$\vec{\tau} \longrightarrow \tau^3\,\vec{\tau}\,\tau^3 = \begin{pmatrix} -\tau^1 \\ -\tau^2 \\ \tau^3 \end{pmatrix} \quad \text{under } \mathcal{P}\,. \tag{6.4}$$

We will demand invariance of the model under parity transformation, which implies that the dispersion relation satisfies $\epsilon_{\mathbf{k}\sigma} = \epsilon_{-\mathbf{k}\sigma}$.

6.1.3 Time-reversal symmetry

A time-reversal operation $\mathcal{T}$ leaves the position $\mathbf{r}$ unchanged and reverses momentum $\mathbf{p}$ and the spin $\mathbf{s}$,

$$\begin{aligned} \mathbf{r} &\longrightarrow \mathbf{r}\,, \\ \mathbf{p} &\longrightarrow -\mathbf{p}\,, \\ \mathbf{s} &\longrightarrow -\mathbf{s}\,. \end{aligned} \tag{6.5}$$

The spin field transforms accordingly as

$$S^i(\pm\mathbf{R}/2) \longrightarrow -S^i(\pm\mathbf{R}/2)\,. \tag{6.6}$$

As in the case of parity the states $|+\rangle$ and $|-\rangle$ therefore also have a definite signature under time-reversal. The time-reversal operator in pseudospin-space is given by $\tau^3\mathcal{C}$ where $\mathcal{C}$ is the

complex-conjugation operator,

$$\vec{\tau} \longrightarrow \tau^3 \, \mathcal{C} \vec{\tau} \, \left(\tau^3 \mathcal{C}\right)^{-1} = \begin{pmatrix} -\tau^1 \\ \tau^2 \\ \tau^3 \end{pmatrix} \quad \text{under } \mathcal{T}. \tag{6.7}$$

We will assume that the model (5.8) is also invariant under time-reversal, leading to the requirement $\epsilon_{\mathbf{k}\sigma} = \epsilon_{-\mathbf{k},-\sigma}$.

6.2 Pseudospin notation

The Kondo coupling (5.6) interchanges pseudospin, i.e., parity between the minidomain and the electrons. It is therefore convenient to introduce an explicit pseudospin index for the electrons. This is easily done with the new operators [54]

$$\begin{aligned} \Psi_{q\sigma+} &= \frac{q}{\pi} \left(1 + \frac{\sin qR}{qR}\right)^{-1/2} \int \frac{\mathrm{d}\Omega}{4\pi} \cos\left(\frac{\mathbf{qR}}{2}\right) c_{\mathbf{q}\sigma} \\ \Psi_{q\sigma-} &= \frac{q}{\pi} \left(1 - \frac{\sin qR}{qR}\right)^{-1/2} \int \frac{\mathrm{d}\Omega}{4\pi} \sin\left(\frac{\mathbf{qR}}{2}\right) c_{\mathbf{q}\sigma} \,, \end{aligned} \tag{6.8}$$

which fulfill the commutation relations

$$\{\Psi^\dagger_{q\sigma\chi}, \Psi_{q'\sigma'\chi'}\} = \delta(q-q')\delta_{\sigma\sigma'}\delta_{\chi\chi'} \,. \tag{6.9}$$

Only these modes $\Psi_{q\sigma\pm}$ are important in the two-impurity Kondo problem (5.6); all other modes decouple from the impurities. The new operators transform under parity as

$$\mathcal{P}\, \Psi_{q\sigma\pm}\, \mathcal{P}^\dagger = \frac{q}{\pi} \left(1 \pm \frac{\sin qR}{qR}\right)^{-1/2} \int \frac{\mathrm{d}\Omega}{4\pi} \begin{Bmatrix} \cos\left(\frac{\mathbf{qR}}{2}\right) \\ \sin\left(\frac{\mathbf{qR}}{2}\right) \end{Bmatrix} c_{-\mathbf{q}\sigma} = \pm \Psi_{q\sigma\pm} \,. \tag{6.10}$$

The third index therefore represents parity and can be identified as the pseudospin index of the electrons. It will couple to the pseudospin of the mini-domain in interchanging processes. The Kondo Hamiltonian (5.6) can now be reformulated in terms of the operators (6.8):

$$H_K = \frac{1}{\sqrt{2}} \, J^{ij} \sum_{\chi=+,-} \Theta^i_\chi S^j_\chi \,. \tag{6.11}$$

We have introduced the even/odd combination of the impurity spins

$$\begin{pmatrix} S_+ \\ S_- \end{pmatrix} = U \begin{pmatrix} S(\mathbf{R}/2) \\ S(-\mathbf{R}/2) \end{pmatrix}, \tag{6.12}$$

where the transformation is given by

$$U = U^{-1} = U^\top = \frac{1}{\sqrt{2}} \begin{pmatrix} 1 & 1 \\ 1 & -1 \end{pmatrix}. \tag{6.13}$$

Furthermore, Θ is defined as

$$\Theta^i_\chi = \sum_{kq} \sum_{\mu=+,-} \mu \, g_{k,(\mu\chi)} \, g_{q\mu} \, \Psi^\dagger_{k,\alpha,(\mu\chi)} \, \sigma^i_{\alpha\beta} \, \Psi_{q\beta\mu} \,, \tag{6.14}$$

where $\chi = \pm$ and the sum over momenta is to be understood as the integral $\sum_{kq} \equiv \int_0^\infty dk\, dq$. The couplings g,

$$\begin{aligned} g_{k+} &= \frac{4\pi^2}{(2\pi)^3}\, k \sqrt{1 + \frac{\sin kR}{kR}}\,, \\ g_{k-} &= i\,\frac{4\pi^2}{(2\pi)^3}\, k \sqrt{1 - \frac{\sin kR}{kR}}\,, \end{aligned} \tag{6.15}$$

originate essentially from the normalization of the operators (6.8).

6.3 Effective mini-domain Hamiltonian

The form (6.11) for the Kondo Hamiltonians is well suited to deriving the effective low-energy Hamiltonian. We will apply a Schrieffer–Wolff transformation treating the Kondo couplings J_z and $J_\perp$ as perturbations. We expand the wave function $|\Psi\rangle$ of the mini-domain in the basis $\{|\uparrow\uparrow\rangle, |\uparrow\downarrow\rangle, |\downarrow\uparrow\rangle, |\downarrow\downarrow\rangle\}$ where $S(\mathbf{R}/2)$ and $S(-\mathbf{R}/2)$ act on the first and second entry, respectively,

$$|\Psi\rangle = \psi_{\uparrow\uparrow}|\uparrow\uparrow\rangle + \psi_{\uparrow\downarrow}|\uparrow\downarrow\rangle + \psi_{\downarrow\uparrow}|\downarrow\uparrow\rangle + \psi_{\downarrow\downarrow}|\downarrow\downarrow\rangle\,. \tag{6.16}$$

The stationary Schrödinger equation can be expressed as[1]

$$H \begin{pmatrix} \psi_{\uparrow\uparrow} \\ \psi_{\uparrow\downarrow} \\ \psi_{\downarrow\uparrow} \\ \psi_{\downarrow\downarrow} \end{pmatrix} = E \begin{pmatrix} \psi_{\uparrow\uparrow} \\ \psi_{\uparrow\downarrow} \\ \psi_{\downarrow\uparrow} \\ \psi_{\downarrow\downarrow} \end{pmatrix}. \tag{6.17}$$

In this representation the direct impurity-spin coupling $H_{\rm MD}$ of the model Hamiltonian H takes the form

$$H_{MD} = \frac{1}{4} \begin{pmatrix} K_z & & & \\ & -K_z & 2\,K_\perp & \\ & 2\,K_\perp & -K_z & \\ & & & K_z \end{pmatrix}. \tag{6.18}$$

As already indicated in Fig. 5.1 this matrix has the eigenvalues $-K_z/4 \pm K_\perp/2$ which live in the low-energy sub-space spanned by the states $|\uparrow\downarrow\rangle$ and $|\downarrow\uparrow\rangle$, and the doubly degenerate

[1] In the chosen basis the impurity spins have the matrix representations

$$S^x(\mathbf{R}/2) = \tfrac{1}{2}\begin{pmatrix} & & 1 & \\ & & & 1 \\ 1 & & & \\ & 1 & & \end{pmatrix}, \qquad S^x(-\mathbf{R}/2) = \tfrac{1}{2}\begin{pmatrix} & 1 & & \\ 1 & & & \\ & & & 1 \\ & & 1 & \end{pmatrix},$$

$$S^y(\mathbf{R}/2) = \tfrac{1}{2}\begin{pmatrix} & & -i & \\ & & & -i \\ i & & & \\ & i & & \end{pmatrix}, \qquad S^y(-\mathbf{R}/2) = \tfrac{1}{2}\begin{pmatrix} & -i & & \\ i & & & \\ & & & -i \\ & & i & \end{pmatrix},$$

$$S^z(\mathbf{R}/2) = \tfrac{1}{2}\begin{pmatrix} 1 & & & \\ & 1 & & \\ & & -1 & \\ & & & -1 \end{pmatrix}, \qquad S^z(-\mathbf{R}/2) = \tfrac{1}{2}\begin{pmatrix} 1 & & & \\ & -1 & & \\ & & 1 & \\ & & & -1 \end{pmatrix}.$$

high energy value $K_z/4$.[2] The Kondo Hamiltonian H_K (6.11) is given in this basis by

$$H_K = \frac{1}{2}\begin{pmatrix} 2\,J_z\Theta^z_+ & J_\perp\left(\Theta^-_+ - \Theta^-_-\right) & J_\perp\left(\Theta^-_+ + \Theta^-_-\right) & 0 \\ J_\perp\left(\Theta^+_+ - \Theta^+_-\right) & 2\,J_z\Theta^z_- & 0 & J_\perp\left(\Theta^-_+ + \Theta^-_-\right) \\ J_\perp\left(\Theta^+_+ + \Theta^+_-\right) & 0 & -2\,J_z\Theta^z_- & J_\perp\left(\Theta^-_+ - \Theta^-_-\right) \\ 0 & J_\perp\left(\Theta^+_+ + \Theta^+_-\right) & J_\perp\left(\Theta^+_+ - \Theta^+_-\right) & -2\,J_z\Theta^z_+ \end{pmatrix}, \tag{6.19}$$

where the standard notation $\Theta^\pm_\chi = \Theta^x_\chi \pm i\Theta^y_\chi$ has been used. The effective low-energy Hamiltonian is obtained by restricting the Hamiltonian to the sub-space given by the states $\{|\uparrow\downarrow\rangle, |\downarrow\uparrow\rangle\}$,

$$\widetilde{\mathcal{H}} = \begin{pmatrix} H_{22} + H_{21}\,G_{11}\,H_{12} + H_{24}\,G_{44}\,H_{42} & H_{23} + H_{21}\,G_{11}\,H_{13} + H_{24}\,G_{44}\,H_{43} \\ H_{32} + H_{31}\,G_{11}\,H_{12} + H_{34}\,G_{44}\,H_{42} & H_{33} + H_{31}\,G_{11}\,H_{13} + H_{34}\,G_{44}\,H_{43} \end{pmatrix}, \tag{6.20}$$

with the Green function

$$G_{ij} = (E - H_{ij})^{-1}. \tag{6.21}$$

In the restricted Hilbert space the Schrödinger equation reduces to

$$\widetilde{\mathcal{H}}\begin{pmatrix} \psi_{\uparrow\downarrow} \\ \psi_{\downarrow\uparrow} \end{pmatrix} = E\begin{pmatrix} \psi_{\uparrow\downarrow} \\ \psi_{\downarrow\uparrow} \end{pmatrix}. \tag{6.22}$$

Equation (6.22) is so far still exact, but at this stage $\widetilde{\mathcal{H}}$ depends implicitly through the Green function on the energy E. This implicit energy dependence will now successively be eliminated by expanding $\widetilde{\mathcal{H}}$ in the small parameters $K_\perp$, J_z and $J_\perp$. The zeroth and first oder contributions are

$$\widetilde{\mathcal{H}}^{(0)} = \begin{pmatrix} H_0 - K_z/4 & \\ & H_0 - K_z/4 \end{pmatrix}, \tag{6.23}$$

$$\widetilde{\mathcal{H}}^{(1)} = \begin{pmatrix} J_z\Theta^z_- & K_\perp/2 \\ K_\perp/2 & -J_z\Theta^z_- \end{pmatrix}, \tag{6.24}$$

respectively. For the second order contribution one needs the Green functions to zeroth order

$$G_{11} = G + \mathcal{O}(J) = G_{44} \tag{6.25}$$

$$G = (E - H_0 - K_z/4)^{-1}. \tag{6.26}$$

The second order term of the effective Hamiltonian then reads

$$\widetilde{\mathcal{H}}^{(2)} = \frac{1}{2}J_\perp^2\begin{pmatrix} \Theta^+_L\,G\,\Theta^-_L + \Theta^-_R\,G\,\Theta^+_R & \Theta^+_L\,G\,\Theta^-_R + \Theta^-_R\,G\,\Theta^+_L \\ \Theta^+_R\,G\,\Theta^-_L + \Theta^-_L\,G\,\Theta^+_R & \Theta^+_R\,G\,\Theta^-_R + \Theta^-_L\,G\,\Theta^+_L \end{pmatrix}, \tag{6.27}$$

where we introduced

$$\begin{pmatrix} \Theta^i_R \\ \Theta^i_L \end{pmatrix} = U\begin{pmatrix} \Theta^i_+ \\ \Theta^i_- \end{pmatrix} \tag{6.28}$$

with the transformation U defined in (6.13). The four entries of $\widetilde{\mathcal{H}}^{(2)}$ can be interpreted as virtual excitations of the mini-domain to the ferromagnetic part of the Hilbert space. The off-diagonal entries thereby induce transitions between the states $|\uparrow\downarrow\rangle$ and $|\downarrow\uparrow\rangle$. The implicit

[2] In the case of isotropic coupling $K_z = K_\perp$, which is not considered here, the matrix H_{MD} has the usual three degenerate levels that form the spin 1 triplet and a single level, the singlet.

energy dependence of $\widetilde{\mathcal{H}}^{(2)}$ still has to be removed. Before doing so, however, we would like to transform the Hamiltonian $\widetilde{\mathcal{H}}$ to the proper pseudospin basis given by $\{|+\rangle, |-\rangle\}$,

$$\begin{pmatrix} |+\rangle \\ |-\rangle \end{pmatrix} = U \begin{pmatrix} |\uparrow\downarrow\rangle \\ |\downarrow\uparrow\rangle \end{pmatrix} \tag{6.29}$$

$$\bar{\mathcal{H}} = U\,\widetilde{\mathcal{H}}\,U = W_n \tau^n\,, \tag{6.30}$$

where we introduced the operators W_n by expanding the Hamiltonian in Pauli matrices. The sum goes from $n = 0$ to 3 and τ^0 is defined as the identity matrix.[3] By construction the components τ^1, τ^2 and τ^3 comprise the pseudospin of the antiferromagnetic mini-domain. The non-vanishing components of W of zeroth, first and second order are[4]

$$W_0^{(0)} = H_0 - K_z/4\,, \tag{6.31}$$

$$W_1^{(1)} = J_z \Theta_-^z\,, \tag{6.32}$$

$$W_3^{(1)} = K_\perp/2\,, \tag{6.33}$$

$$W_0^{(2)} = \frac{1}{2}\left(\widetilde{\mathcal{H}}_{11}^{(2)} + \widetilde{\mathcal{H}}_{22}^{(2)}\right) = \frac{1}{4} J_\perp^2 \sum_\chi \left(\Theta_\chi^+ G\, \Theta_\chi^- + \Theta_\chi^- G\, \Theta_\chi^+\right)\,, \tag{6.34}$$

$$W_1^{(2)} = \frac{1}{2}\left(\widetilde{\mathcal{H}}_{11}^{(2)} - \widetilde{\mathcal{H}}_{22}^{(2)}\right) = \frac{1}{4} J_\perp^2 \sum_\chi \left(-\Theta_\chi^+ G\, \Theta_{-\chi}^- + \Theta_\chi^- G\, \Theta_{-\chi}^+\right)\,, \tag{6.35}$$

$$W_2^{(2)} = -\frac{i}{2}\left(\widetilde{\mathcal{H}}_{12}^{(2)} - \widetilde{\mathcal{H}}_{21}^{(2)}\right) = -\frac{i}{4} J_\perp^2 \sum_\chi \left(\chi\, \Theta_\chi^+ G\, \Theta_{-\chi}^- - \chi\, \Theta_\chi^- G\, \Theta_{-\chi}^+\right)\,, \tag{6.36}$$

$$W_3^{(2)} = \frac{1}{2}\left(\widetilde{\mathcal{H}}_{12}^{(2)} + \widetilde{\mathcal{H}}_{21}^{(2)}\right) = \frac{1}{4} J_\perp^2 \sum_\chi \left(\chi\, \Theta_\chi^+ G\, \Theta_\chi^- + \chi\, \Theta_\chi^- G\, \Theta_\chi^+\right)\,. \tag{6.37}$$

The term $W_3^{(1)}$ is the previously mentioned pseudo-magnetic field stemming from the Hamiltonian (5.2) that leads to a pseudo-magnetic Zeeman splitting. We now eliminate the dependence of $W_n^{(2)}$ on the energy E by expanding it perturbatively in J. To this end consider the operator which appears in $W_n^{(2)}$

$$\Theta_\chi^i\, G\, \Theta_{\chi'}^j = \sum_{kk'qq'} \sum_{\mu\mu'} \mu\mu'\, g_{\,k(\mu\chi)}\, g_{\,k'(\mu'\chi')}\, g_{\,q\mu} g_{\,q'\mu'}\, \sigma^i_{\alpha\beta}\, \sigma^j_{\alpha'\beta'} \times \Psi^\dagger_{k\alpha(\mu\chi)} \Psi_{q\beta\mu}\, G\, \Psi^\dagger_{k'\alpha'(\mu'\chi')} \Psi_{q'\beta'\mu'}\,. \tag{6.38}$$

When we commute the Green function G either to the right or to the left of all the Ψ operators, the energy dependence of G can be removed by using the Schrödinger equation in zeroth order. In order to keep the formulae simple we will make an additional simplification: we will assume that the electron energies $\epsilon_{\mathbf{q}\sigma}$ only depend on the absolute value of the momentum, $\epsilon_{|\mathbf{q}|} = \epsilon_q$. The spin dependence has already dropped out since we have assumed that our

[3] The matrices τ^n are

$$\tau^0 = \begin{pmatrix} 1 & 0 \\ 0 & 1 \end{pmatrix}, \quad \tau^1 = \begin{pmatrix} 0 & 1 \\ 1 & 0 \end{pmatrix}, \quad \tau^2 = \begin{pmatrix} 0 & -i \\ i & 0 \end{pmatrix}, \quad \tau^3 = \begin{pmatrix} 1 & 0 \\ 0 & -1 \end{pmatrix}.$$

[4] The components of W can be easily obtained by using the properties of the Pauli matrices, $W^n = \frac{1}{2}\mathrm{tr}\{\mathcal{H}\tau^n\}$.

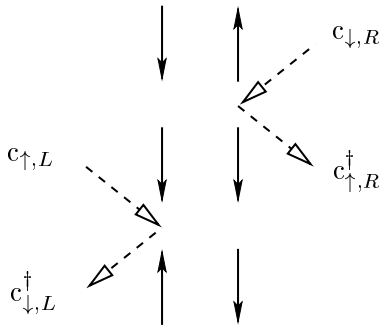

Figure 6.3: *Second order process in the Kondo coupling, J, which leads to a flip in the configuration of the mini-domain (see main text).*

model is invariant under time-reversal and parity symmetry. Beyond that, we now suppose the Fermi surface to be isotropic. This is not an essential assumption, but it keeps the formulae manageable. For an isotropic Fermi surface the electron operators $\Psi_{q\sigma\mu}$ have a simple commutation relation with the kinetic part of the Hamiltonian,

$$[\Psi_{q\sigma\mu}, H_0] = (\epsilon_q - \mu)\Psi_{q\sigma\mu}\,. \tag{6.39}$$

Using the Schrödinger equation in zeroth order one obtains to within order of $\mathcal{O}(J)$

$$\begin{aligned}
&\Psi^\dagger_{k\alpha(\mu\chi)}\Psi_{q\beta\mu}\,G\,\Psi^\dagger_{k'\alpha'(\mu'\chi')}\Psi_{q'\beta'\mu'} \\
&\quad\approx\quad (-K_z/2+\epsilon_k-\epsilon_q)^{-1}\,\Psi^\dagger_{k\alpha(\mu\chi)}\Psi_{q\beta\mu}\,\Psi^\dagger_{k'\alpha'(\mu'\chi')}\Psi_{q'\beta'\mu'} \\
&\quad\approx\quad \Psi^\dagger_{k\alpha(\mu\chi)}\Psi_{q\beta\mu}\,\Psi^\dagger_{k'\alpha'(\mu'\chi')}\Psi_{q'\beta'\mu'}\,(-K_z/2-\epsilon_{k'}+\epsilon_{q'})^{-1}\,.
\end{aligned} \tag{6.40}$$

Only the symmetrized form of the approximated Green function yields a hermitian expression. So we finally obtain

$$\begin{aligned}
\Theta^i_\chi\,G\,\Theta^j_{\chi'} = \sum_{kk'qq'}\sum_{\mu\mu'}\quad &\frac{\mu\mu'\,g_{\,k(\mu\chi)}\,g_{\,k'(\mu'\chi')}\,g_{\,q\mu}g_{\,q'\mu'}}{\frac{1}{2}\left(\epsilon_k-\epsilon_q-\epsilon_{k'}+\epsilon_{q'}\right)-K_z/2} \\
&\times\sigma^i_{\alpha\beta}\,\sigma^j_{\alpha'\beta'}\,\Psi^\dagger_{k\alpha(\mu\chi)}\Psi_{q\beta\mu}\,\Psi^\dagger_{k'\alpha'(\mu'\chi')}\Psi_{q'\beta'\mu'}\,.
\end{aligned} \tag{6.41}$$

The second order processes involve four electron operators. After normal ordering we will retain from this expression only the parts that are most relevant in the RG sense and discard the irrelevant fluctuations. Using

$$\sigma^i_{\alpha\beta}\,\sigma^j_{\alpha'\beta'}\,\Psi^\dagger_{k\alpha(\mu\chi)}\Psi_{q\beta\mu}\,\Psi^\dagger_{k'\alpha'(\mu'\chi')}\Psi_{q'\beta'\mu'} = \sigma^i_{\alpha\beta}\,\sigma^j_{\alpha'\beta'}\,\Psi^\dagger_{k\alpha(\mu\chi)}\Psi_{q'\beta'\mu'}\,\Psi_{q\beta\mu}\Psi^\dagger_{k'\alpha'(\mu'\chi')}\,, \tag{6.42}$$

this leads to the approximation

$$\begin{aligned}
\Psi^\dagger_{k\alpha(\mu\chi)}\Psi_{q'\beta'\mu'}\,\Psi_{q\beta\mu}\Psi^\dagger_{k'\alpha'(\mu'\chi')} \quad\longrightarrow\quad &:\Psi^\dagger_{k\alpha(\mu\chi)}\Psi_{q'\beta'\mu'}:\,\langle\Psi_{q\beta\mu}\,\Psi^\dagger_{k'\alpha'(\mu'\chi')}\rangle \\
&-\langle\Psi^\dagger_{k\alpha(\mu\chi)}\Psi_{q'\beta'\mu'}\rangle\,:\Psi_{q\beta\mu}\,\Psi^\dagger_{k'\alpha'(\mu'\chi')}: + \langle\Psi^\dagger_{k\alpha(\mu\chi)}\Psi_{q'\beta'\mu'}\rangle\langle\Psi_{q\beta\mu}\,\Psi^\dagger_{k'\alpha'(\mu'\chi')}\rangle
\end{aligned} \tag{6.43}$$

$$\begin{aligned}
= \quad &(1-f_q)\,\delta_{q,k'}\delta_{\beta,\alpha'}\delta_{\mu,\mu'\chi'}\,:\Psi^\dagger_{k\alpha(\mu\chi)}\Psi_{q'\beta'\mu'}: - f_{q'}\delta_{q',k}\delta_{\beta',\alpha}\delta_{\mu',\mu\chi}\,:\Psi^\dagger_{k'\alpha'(\mu'\chi')}\Psi_{q\beta\mu}: \\
&+(1-f_q)\delta_{q,k'}\delta_{\beta,\alpha'}\delta_{\mu,\mu'\chi'}f_{q'}\delta_{q',k}\delta_{\beta',\alpha}\delta_{\mu',\mu\chi}\,,
\end{aligned}$$

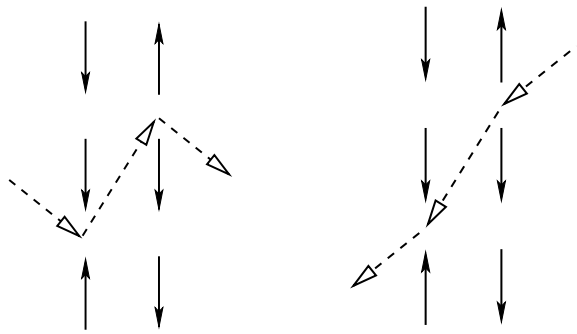

$-\langle \mathrm{c}^\dagger_{\downarrow,L}\mathrm{c}_{\downarrow,R}\rangle : \mathrm{c}_{\uparrow,L}\,\mathrm{c}^\dagger_{\uparrow,R} :$ $\quad \langle \mathrm{c}_{\uparrow,L}\mathrm{c}^\dagger_{\uparrow,R}\rangle : \mathrm{c}^\dagger_{\downarrow,L}\mathrm{c}_{\downarrow,R} :$ $\quad \langle \mathrm{c}^\dagger_{\downarrow,L}\mathrm{c}_{\downarrow,R}\rangle\langle \mathrm{c}_{\uparrow,L}\,\mathrm{c}^\dagger_{\uparrow,R}\rangle$

Figure 6.4: *Contributions of the process shown in Fig. 6.3 which are taken into account in the approximation made in (6.44).*

where the colons indicate normal ordering.[5] Effectively, only the exchange processes remain. Due to the spin structure the direct processes do not contribute. Inserting this expression into (6.41) finally results in

$$\begin{aligned}\Theta^i_\chi\, G\, \Theta^j_{\chi'} \;\longrightarrow\; & \sum_{kq}\sum_{k'\mu}\left(\frac{\chi' g^2_{k'\mu}\,(1-f_{k'})}{\frac{1}{2}\,(\epsilon_k+\epsilon_q-2\epsilon_{k'})-K_z/2}\,\big(\sigma^i\sigma^j\big)_{\alpha\beta}\right. \\ & \left.-\frac{\chi\, g^2_{k'(\mu\chi'\chi)} f_{k'}}{\frac{1}{2}\,(2\epsilon_{k'}-\epsilon_q-\epsilon_k)-K_z/2}\,\big(\sigma^j\sigma^i\big)_{\alpha\beta}\right) g_{\,k(\mu\chi)}\, g_{q(\mu\chi')}\; :\Psi^\dagger_{k\alpha(\mu\chi)}\,\Psi_{q\beta(\mu\chi')}: \\ & +\delta_{\chi\chi'}\sum_{kq}\sum_{\mu}\frac{\chi\, g^2_{k(\mu\chi)}\, g^2_{q\mu}\mathrm{tr}\{\sigma^i\,\sigma^j\}\,(1-f_q)f_k}{\epsilon_k-\epsilon_q-K_z/2}\,,\end{aligned} \tag{6.44}$$

where the indices i and j are either $+$ or $-$. In order to interpret the three terms obtained above we would like to visualize them diagrammatically. We switch back from the proper pseudospin basis $\{|+\rangle,|-\rangle|\}$ to the basis given by $\{|\uparrow\downarrow\rangle,|\downarrow\uparrow\rangle\}$, whose states correspond to the settings of the two impurity spins located at different positions in space. As an example we consider the contribution from the operator $\Theta^-_L\, G\,\Theta^+_R$, which already appeared as an off-diagonal entry in (6.27). Here the index L refers to the position $-\mathbf{R}/2$ and the index R to the position $\mathbf{R}/2$. This operator contains the following combination of the usual Fermi operators: $\mathrm{c}^\dagger_\downarrow(-\mathbf{R}/2)\mathrm{c}_\uparrow(-\mathbf{R}/2)\,\mathrm{c}^\dagger_\uparrow(\mathbf{R}/2)\mathrm{c}_\downarrow(\mathbf{R}/2) \equiv \mathrm{c}^\dagger_{\downarrow,L}\mathrm{c}_{\uparrow,L}\,\mathrm{c}^\dagger_{\uparrow,R}\mathrm{c}_{\downarrow,R}$. The spin of the electron on the right-hand side is flipped from down to up and the spin of the electron on the left-hand side is flipped from up to down. Since the Kondo coupling conserves spin the impurities at the respective locations have to reverse their spins in the opposite way. This is depicted in Fig. 6.3, which should be read from top to bottom. The domain starts in the $|\downarrow\uparrow\rangle$ configuration. An incoming electron flips the mini-domain into the high-energy ferromagnetic state $|\downarrow\downarrow\rangle$. A further electron scattering off the domain brings it back to the low-energy state $|\uparrow\downarrow\rangle$. Effectively, this process of second order in the Kondo coupling J changes the state of the mini-domain from $|\downarrow\uparrow\rangle$ to the $|\uparrow\downarrow\rangle$-configuration.

[5] Normal ordering of fermionic operators is defined as $:\Psi^\dagger_n\Psi_m: \equiv \Psi^\dagger_n\Psi_m - \langle\Psi^\dagger_n\Psi_m\rangle = \langle\Psi_m\Psi^\dagger_n\rangle - \Psi_m\Psi^\dagger_n$, where the indices n and m represent the appropriate set of quantum numbers.

The approximation we made above in neglecting the fluctuation amounts to connecting outgoing electron lines with incoming ones, see Fig. 6.4. If this is done with lines corresponding to operators at the same position, i.e. either $\mathbf{R}/2$ or $-\mathbf{R}/2$, it will lead to a direct process which vanishes after summing over all possible orientations of spin. There are three remaining terms which correspond to exchange processes and are shown in Fig. 6.4. They are analogous to the terms obtained in (6.44). From the diagrams it is apparent that the electrons mediate an effective coupling between the two states $|\uparrow\downarrow\rangle$ and $|\downarrow\uparrow\rangle$.

Now we would like to proceed in evaluating the operators $W_n^{(2)}$ further. It will be helpful to define

$$\mathcal{G}^{\pm}_{kq,k'} \equiv \frac{1-f_{k'}}{\frac{1}{2}(\epsilon_k+\epsilon_q)-\epsilon_{k'}-K_z/2} \pm \frac{f_{k'}}{\epsilon_{k'}-\frac{1}{2}(\epsilon_k+\epsilon_q)-K_z/2}\,. \tag{6.45}$$

Putting the above result for the operator $\Theta^i_\chi\, G\, \Theta^j_{\chi'}$ into the expressions for $W_n^{(2)}$ we get

$$\begin{aligned}
W_0^{(2)} &= J_\perp^2 \sum_{kq\chi}\left(\sum_{k'\mu}\mu\, g^2_{k'\mu}\,\mathcal{G}^-_{kq,k'}\right)\chi\, g_{k\chi}\, g_{q\chi}\,:\Psi^\dagger_{k\alpha\chi}\,\delta_{\alpha\beta}\,\Psi_{q\beta\chi}: \qquad (6.46)\\
&\quad + 2\,J_\perp^2 \sum_{kq}\sum_{\mu\chi}\frac{\mu\chi\, g^2_{k\mu}\, g^2_{q\chi}\, f_k(1-f_q)}{\epsilon_k-\epsilon_q-K_z/2}\,,\\
W_1^{(2)} &= J_\perp^2 \sum_{kq\chi}\left(\sum_{k'\mu}\mu\, g^2_{k'\mu}\,\mathcal{G}^+_{kq,k'}\right)\chi\, g_{k\chi}\, g_{q,-\chi}\,:\Psi^\dagger_{k\alpha\chi}\,\sigma^3_{\alpha\beta}\,\Psi_{q\beta,-\chi}:, \qquad (6.47)\\
W_2^{(2)} &= i\,J_\perp^2 \sum_{kq\chi}\left(\sum_{k'\mu} g^2_{k'\mu}\,\mathcal{G}^-_{kq,k'}\right) g_{k\chi}\, g_{q,-\chi}\,:\Psi^\dagger_{k\alpha\chi}\,\sigma^3_{\alpha\beta}\,\Psi_{q\beta,-\chi}:, \qquad (6.48)\\
W_3^{(2)} &= J_\perp^2 \sum_{kq\chi}\left(\sum_{k'\mu} g^2_{k'\mu}\,\mathcal{G}^-_{kq,k'}\right) g_{k\chi}\, g_{q\chi}\,:\Psi^\dagger_{k\alpha\chi}\,\delta_{\alpha\beta}\,\Psi_{q\beta\chi}: \qquad (6.49)\\
&\quad + 2\,J_\perp^2 \sum_{kq}\sum_{\mu\chi}\frac{g^2_{k\mu}\, g^2_{q\chi}\, f_k(1-f_q)}{\epsilon_k-\epsilon_q-K_z/2}\,.
\end{aligned}$$

As anticipated in the introduction the above operators conserve the spin of the electrons since the above expressions are diagonal with respect to the electron spin. That means that the spin-up and -down electrons couple separately to the pseudospin of the mini-domain leading to two channels. Introducing generalized Pauli-matrices κ^m, $m=0,\ldots,3$, for the parity index of the electron operators, cf. footnote on page 103, the effective Hamiltonian up to second order can be written as

$$\bar{\mathcal{H}} = H_0 + \sum_{kq}\mathcal{J}^i_{mn}(k,q)\,:\Psi^\dagger_{k\alpha\chi}\,\sigma^i_{\alpha\beta}\,\kappa^m_{\chi\mu}\,\Psi_{q\beta\mu}:\,\frac{\tau^n}{2} + (K_\perp+h_\perp)\,\frac{\tau^3}{2} \tag{6.50}$$

where we have discarded the constant $-K_z/4$ and the constant contribution from $W_0^{(2)}$. As already mentioned the sum over momenta is to be understood as the integral $\sum_{kq} \equiv \int_0^\infty dk\,dq$. The first term is the usual diagonal part of the electrons, the second term contains a pseudospin–Kondo coupling and the third term is a pseudospin–Zeeman splitting. The

non-vanishing entries of the coupling matrix $\mathcal{J}$ are

$$\begin{aligned}
\begin{pmatrix} \mathcal{J}^0_{00}(k,q) & \mathcal{J}^0_{03}(k,q) \\ \mathcal{J}^0_{30}(k,q) & \mathcal{J}^0_{33}(k,q) \end{pmatrix} &= J_\perp^2 \sum_{k'\mu\chi} \mathcal{G}^-_{kq,k'}\, g^2_{k'\mu}\, g_{k\chi}\, g_{q\chi} \begin{pmatrix} \mu\chi & 1 \\ \mu & \chi \end{pmatrix}, \\
\begin{pmatrix} \mathcal{J}^3_{11}(k,q) & \mathcal{J}^3_{12}(k,q) \\ \mathcal{J}^3_{21}(k,q) & \mathcal{J}^3_{22}(k,q) \end{pmatrix} &= -J_z \sum_{\chi} g_{k\chi}\, g_{q,-\chi} \begin{pmatrix} \chi & 0 \\ i & 0 \end{pmatrix} \\
&\quad + J_\perp^2 \sum_{k'\mu\chi} g^2_{k'\mu}\, g_{k\chi}\, g_{q,-\chi} \begin{pmatrix} \mu\chi\, \mathcal{G}^+_{kq,k'} & i\, \mathcal{G}^-_{kq,k'} \\ i\,\mu\, \mathcal{G}^+_{kq,k'} & -\chi\, \mathcal{G}^-_{kq,k'} \end{pmatrix}.
\end{aligned} \tag{6.51}$$

In the notation of generalized Pauli matrices, the component $\mathcal{J}^0_{00}(k,q)$ corresponds to a potential scattering term. The component $\mathcal{J}^0_{03}(k,q)$ describes the fluctuations around the pseudo-magnetic field generated by the electrons and acts on the pseudospin. The component $\mathcal{J}^0_{30}(k,q)$, on the other hand, is the pseudo-magnetic field generated by the mini-domain and acting on the electrons. All the other components comprise the actual pseudospin Kondo coupling matrix.

The components in the 1-2–pseudospin space given by the second matrix of (6.51) couple to the σ^3-part of the conduction electron spin, so the spin-up and the spin-down channel have a relative minus sign in these components. However, this relative minus sign can be eliminated by a rotation by π of the spin-down components of the electrons around the z-axis of the pseudospin. This rotation is given by the unitary operator

$$D = \exp\{\, i\, \frac{\pi}{2} \sum_k \Psi^\dagger_{k\downarrow\chi}\, \kappa^3_{\chi\mu}\, \Psi_{k\downarrow\mu} \}\,. \tag{6.52}$$

As is shown in Appendix B.1, this rotation applied to the effective Hamiltonian (6.50), $\mathcal{H} = D\,\bar{\mathcal{H}}\,D^\dagger$, yields

$$\boxed{\mathcal{H} = H_0 + \sum_{kq} \sum_{\alpha=\uparrow,\downarrow} \mathcal{J}_{mn}(k,q)\ :\Psi^\dagger_{k\alpha\chi}\, \kappa^m_{\chi\mu}\, \Psi_{q\alpha\mu}: \frac{\tau^n}{2} + (K_\perp + h_\perp)\, \frac{\tau^3}{2}} \tag{6.53}$$

The coupling matrix is given by $\mathcal{J}_{mn}(k,q) = \mathcal{J}^0_{mn}(k,q) + \mathcal{J}^3_{mn}(k,q)$. The restrictions imposed by symmetry on the coupling matrix $\mathcal{J}_{mn}(k,q)$ are analyzed in Appendix B.2.

The pseudo-magnetic field $h_\perp$ generated in second order is the RKKY interaction [65] between the two impurity spins mediated by the electrons

$$\begin{aligned}
h_\perp &= 4\, J_\perp^2 \sum_{kq} \sum_{\mu\chi} \frac{g^2_{k\mu}\, g^2_{q\chi}\, f_k(1-f_q)}{\epsilon_k - \epsilon_q - K_z/2} \\
&= 4\, J_\perp^2 \int \frac{\mathrm{d}^3\mathbf{k}}{(2\pi)^3} \frac{\mathrm{d}^3\mathbf{q}}{(2\pi)^3} \frac{f_k(1-f_q)}{\epsilon_k - \epsilon_q - K_z/2}\, \cos(\mathbf{kR}) \cos(\mathbf{qR})\,.
\end{aligned} \tag{6.54}$$

In the second line we introduced again the three-dimensional integrals. In contrast to the usual discussion of the RKKY interaction an additional energy difference of $K_z/2$ appears in the denominator. This is due to the fact that the second order process underlying $h_\perp$ involves virtual excitations to the ferromagnetic states which have an energy $K_z/2$ higher than the antiferromagnetic ones of the restricted Hilbert space. Usually, one considers the RKKY

interaction in the complete Hilbert space of the two impurity spins and it has the form of the Hamiltonian (5.2) but with K replaced by the RKKY coupling. The pseudo-magnetic field $h_\perp$ and the transverse coupling $K_\perp$ appear therefore in the effective Hamiltonian on an equal footing. In the restricted Hilbert space, however, only the x- and y-, i.e., the perpendicular components of the direct K-coupling and of the generated RKKY interaction affect the low-energy states of the mini-domain. The z-component of the generated RKKY-interaction just yields the constant energy shift $W_0^{(2)}$ that we discarded.

6.4 Parameters of the effective Hamiltonian

In the following the effective parameters are evaluated in the limits when the microscopic parameter $k_\mathrm{F}R$ is either much smaller or larger than one. In these limits the Kondo coupling $\mathcal{J}$ and the pseudo-magnetic field $h_\perp$ can be obtained without knowing the exact dispersion relation, ϵ_q, of the conduction electrons. In the following we set temperature $T = 0$.

6.4.1 Pseudo-magnetic field

We give here the results for the limits small and large $k_\mathrm{F}R$ at temperature $T = 0$. The details of the calculations are found in Appendix B.3.

- $k_\mathrm{F}R \ll 1$

$$h_\perp \sim -4(J_\perp\rho)^2 \min\left\{D, \frac{D^2}{K_\perp}\right\} \tag{6.55}$$

  where D is a band cut-off and ρ the density of states per spin at the Fermi energy.

- $k_\mathrm{F}R \gg 1$

$$h_\perp \approx (J_\perp\rho)^2 \frac{2\mathrm{v_F}k_\mathrm{F}}{(k_\mathrm{F}R)^3} \begin{cases} \dfrac{2\cos^2(k_\mathrm{F}R)}{\alpha} + \mathcal{O}(\alpha^{-3}) & \text{for} \quad \alpha \gg 1 \\ \dfrac{\pi}{2}\cos(2k_\mathrm{F}R) + 2\,\alpha\log\alpha\,\cos^2(k_\mathrm{F}R) + \mathcal{O}(\alpha) & \text{for} \quad \alpha \ll 1 \end{cases} \tag{6.56}$$

  where $\alpha = RK_z/(2\mathrm{v_F})$, $\mathrm{v_F} = \mathrm{d}\epsilon(k_\mathrm{F})/\mathrm{d}k$ is the Fermi velocity and $\rho = k_\mathrm{F}^2/(2\pi^2\mathrm{v_F})$.

The result for large $k_\mathrm{F}R$ depends on an additional parameter α, which is given by the ratio of two energy scales. The energy $K_z/2$ is the separation between the antiferromagnetic and the ferromagnetic states, cf. Fig. 5.1, and thus originates from the direct interaction (5.2) between the two impurity spins forming the mini-domain. The other energy scale $\mathrm{v_F}/R$ corresponds to the inverse time the electrons need to travel ballistically from one impurity to another. So there exist two forms of communications between the impurities, one is given by the direct interaction and the other is mediated by the conduction electrons. These two forms of communications compete with each other. The electronic way of communication is more efficient if the time $R/\mathrm{v_F}$ is shorter than the time given by $2/K_z$, i.e. if α is smaller than one. In this case $h_\perp$ exhibits the known $\cos(2k_\mathrm{F}R)$ oscillations of the RKKY-interaction. However, if α is larger than one the direct interaction dominates over the electrons and the $\cos(2k_\mathrm{F}R)$ oscillations change into $\cos^2(k_\mathrm{F}R)$ oscillations.

Besides the pseudo-magnetic field that splits the pseudospin levels of the mini-domain, there exist the pseudo-magnetic field $\mathcal{J}_{30}(k,q)$ that acts on the pseudospin of the electrons. The latter will renormalize the former and we obtain a correction that can be estimated as

$$h_\perp \longrightarrow h_\perp + \mathcal{J}^0_{33}\, h_\perp\, \chi = h_\perp + \mathcal{O}(J_\perp \rho)^4, \tag{6.57}$$

where χ is the susceptibility of the electrons. The renormalization is of higher order in the coupling $J_\perp$ and will be neglected in the following. The axial symmetry present in our model forbids that different components of the pseudo-magnetic field in the x- and y-direction will be generated.

6.4.2 Pseudospin Kondo coupling

In this section we simplify the expressions for the coupling matrix $\mathcal{J}$ (6.51). In the RG sense the momentum dependence of $\mathcal{J}(k,q)$ is irrelevant and we will henceforth set the momenta equal to the Fermi momentum. We cite here only the leading order contributions in the limits $k_\mathrm{F}R$ small and large. The details can be found in the Appendix B.3.

- $k_\mathrm{F}R \ll 1$

$$\begin{aligned}
\begin{pmatrix} \mathcal{J}_{00} & \mathcal{J}_{03} \\ \mathcal{J}_{30} & \mathcal{J}_{33} \end{pmatrix} &= -2\mathrm{v_F}(J_\perp\rho)^2 \begin{pmatrix} A & A+\mathcal{O}\left(k_\mathrm{F}R\right)^2 \\ A\left(1+\mathcal{O}\left(k_\mathrm{F}R\right)^2\right) & A+\mathcal{O}\left(k_\mathrm{F}R\right)^2 \end{pmatrix} \\
\begin{pmatrix} \mathcal{J}_{11} & \mathcal{J}_{12} \\ \mathcal{J}_{21} & \mathcal{J}_{22} \end{pmatrix} &= \mathrm{v_F}(J_z\rho)\frac{k_\mathrm{F}R}{\sqrt{3}} \begin{pmatrix} 0 & 0 \\ 1+\mathcal{O}\left(k_\mathrm{F}R\right)^2 & 0 \end{pmatrix} \\
&\quad + 2\mathrm{v_F}(J_\perp\rho)^2\,\frac{k_\mathrm{F}R}{\sqrt{3}} \begin{pmatrix} 0 & A+\mathcal{O}\left(k_\mathrm{F}R\right)^2 \\ S\left(1+\mathcal{O}\left(k_\mathrm{F}R\right)^2\right) & 0 \end{pmatrix}
\end{aligned} \tag{6.58}$$

  where $\mathrm{v_F}$ is the Fermi velocity and $\rho = k_\mathrm{F}^2/(2\pi^2\mathrm{v_F})$ is the density of states per spin at the Fermi energy. The coefficients A and S depend on the band cut-off D and are defined in (B.37) and (B.36), respectively. The coefficient A is particle–hole asymmetric and S is particle–hole symmetric.

- $k_\mathrm{F}R \gg 1$

$$\begin{aligned}
\begin{pmatrix} \mathcal{J}_{00} & \mathcal{J}_{03} \\ \mathcal{J}_{30} & \mathcal{J}_{33} \end{pmatrix} &\approx -2\mathrm{v_F}\,(J_\perp\rho)^2 \begin{pmatrix} A & \dfrac{\sin(k_\mathrm{F}R)\cos(k_\mathrm{F}R)}{(k_\mathrm{F}R)^2}\,\mathcal{F}(\alpha) \\ A\,\dfrac{\sin(k_\mathrm{F}R)}{k_\mathrm{F}R} & \dfrac{\cos(k_\mathrm{F}R)}{k_\mathrm{F}R}\,\mathcal{F}(\alpha) \end{pmatrix} \\
\begin{pmatrix} \mathcal{J}_{11} & \mathcal{J}_{12} \\ \mathcal{J}_{21} & \mathcal{J}_{22} \end{pmatrix} &\approx \mathrm{v_F}\,(J_z\rho) \begin{pmatrix} 0 & 0 \\ 1 & 0 \end{pmatrix} + 2\mathrm{v_F}\,(J_\perp\rho)^2 \begin{pmatrix} 0 & \dfrac{\cos(k_\mathrm{F}R)}{k_\mathrm{F}R}\,\mathcal{F}(\alpha) \\ S & 0 \end{pmatrix}
\end{aligned} \tag{6.59}$$

  where $\alpha = RK_z/(2\mathrm{v_F})$ and the function $\mathcal{F}$ is defined in (B.31).

In the case of a particle–hole symmetric model the potential scattering terms $\mathcal{J}_{00}$ and $\mathcal{J}_{30}$ vanish identically irrespective of the value $k_{\mathrm{F}}R$. This is analogous to the usual Anderson model in the local moment regime; in addition to the Kondo couplings the Schrieffer–Wolff transformation generally yields a potential scattering term which, however, vanishes in the case of particle–hole symmetry [66].

6.5 Poor man's scaling analysis

We have seen in the last section that the effective low-energy Hamiltonian is given by the two-channel pseudospin Kondo model with a pseudo-magnetic Zeeman splitting. The two-channel Kondo model in zero (pseudo-)magnetic field exhibits non-Fermi liquid physics below the characteristic temperature scale T_K, which is the Kondo temperature [12, 64]. However, the non-Fermi liquid features can be destroyed by either a (pseudo-)magnetic field, that acts on the effective impurity, or a channel anisotropy. These two types of operators are relevant with respect to the two-channel non-Fermi liquid fixed point and drive the systems towards a stable Fermi liquid at low temperatures [67]. The channel isotropy in our case is secured due to the conservation of total spin (6.1). The total pseudo-magnetic field $K_\perp + h_\perp$ on the other hand will destroy the non-Fermi signatures. It has been shown [68, 12] that the temperature scale associated with the run-away flow from the non-Fermi liquid fixed point is given by $T_{\mathrm{FL}} = (K_T + h_T)^2/T_K$. In order for a pronounced non-Fermi liquid regime to exist this temperature scale must be much smaller than the Kondo temperature T_K, see Fig. 6.5. Since we have introduced the coupling constant $K_\perp$ as a bare parameter of our model we adopt the point of view that it can be used to tune the effective pseudo-magnetic field to zero, $K_\perp + h_\perp = 0$. The coupling $K_\perp$ thus plays the role of a control parameter that determines the temperature width of the $\log\sqrt{2}$ plateau of the entropy in Fig. 6.5, which is the characteristic signature of the two-channel Kondo fixed point. Besides, the question remains whether the microscopic parameters allow for a sizeable Kondo temperature or not.

The Kondo temperature can be obtained via the poor man's scaling treatment [69, 66]. As usual, its scaling equations describe the flow of the effective coupling constants while the band cut-off D is reduced. The scaling equations are

$$\frac{\partial \mathcal{J}_{mn}}{\partial \log D} = -\zeta\, \varepsilon_{klm}\, \varepsilon_{pjn}\, \mathcal{J}_{kp}\, \mathcal{J}_{lj}\,, \tag{6.60}$$

where all indices now run from 1 to 3. We have introduced $\zeta = 1/\mathrm{v_F}$ and ε_{pjn} is the totally antisymmetric tensor with the normalization $\varepsilon_{123} = 1$. All the other parameters, e.g. the potential scattering term $\mathcal{J}_{00}$ or the pseudo-magnetic field, are scale invariant in lowest order. Taking into account only the non-vanishing entries these equations reduce to

$$\frac{\partial \mathcal{J}_{12}}{\partial \log D} = 2\,\zeta\, \mathcal{J}_{21}\, \mathcal{J}_{33} \tag{6.61}$$

$$\frac{\partial \mathcal{J}_{21}}{\partial \log D} = 2\,\zeta\, \mathcal{J}_{12}\, \mathcal{J}_{33} \tag{6.62}$$

$$\frac{\partial \mathcal{J}_{33}}{\partial \log D} = 2\,\zeta\, \mathcal{J}_{12}\, \mathcal{J}_{21}\,. \tag{6.63}$$

All components grow in absolute value towards strong coupling upon lowering the cutoff D if the condition $\mathrm{sign}\{\mathcal{J}_{12}\mathcal{J}_{21}\mathcal{J}_{33}\} = -1$ is fulfilled. Dividing equation (6.61) by equation (6.62)

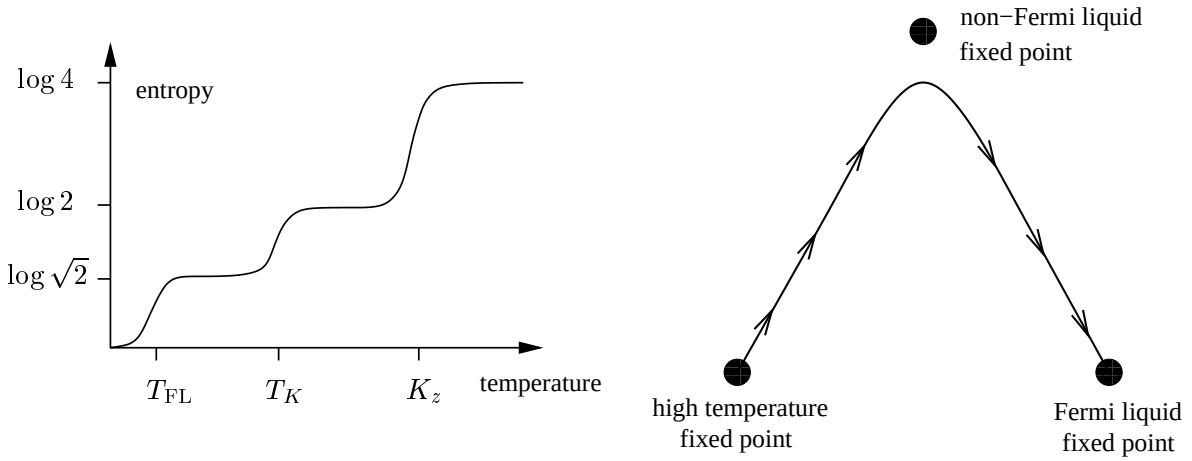

Figure 6.5: *The left panel shows the evolution of the entropy of the mini-domain coupled by a strong Ising-like coupling K_z. For high temperatures the mini-domain entropy is given by log 4. At a temperature scale of the order of the Ising coupling the mini-domain forms and the high-energy ferromagnetic states are frozen out, see Fig. 5.1. At the Kondo temperature T_K the entropy is further lowered by half to the typical two-channel Kondo value of* $\log\sqrt{2}$. *Finally, at the crossover scale $T_{\rm FL} = (K_\perp + h_\perp)^2/T_K$ the Zeeman splitting destroys the non-Fermi liquid signatures, and the system is driven towards a stable Fermi liquid phase. The corresponding RG flow is sketched in the right panel.*

and (6.61) by (6.63) lead to the so-called scaling trajectories

$$(\mathcal{J}_{12})^2 - (\mathcal{J}_{21})^2 = \text{const}\,, \tag{6.64}$$
$$(\mathcal{J}_{33})^2 - (\mathcal{J}_{12})^2 = \text{const}'\,., \tag{6.65}$$

A set of trajectories is shown in Fig. 6.6. Using the trajectories the scaling equation can be solved analytically. In the case where the couplings grow with decreasing band-width we can extract the energy scale T_K at which the couplings have scaled to a value of order $\mathcal{O}(1)$. In the following we would like to solve the scaling equations in the limits $k_{\rm F}R$ large and small. Using the estimates derived in the previous section we will obtain an expression for the Kondo temperature T_K.

6.5.1 Limit $k_{\rm F}R \ll 1$

Consider first the limit $k_{\rm F}R \ll 1$. From the estimate (6.58) in this regime we have

$$|\mathcal{J}_{33}| \gg |\mathcal{J}_{12}| \qquad \text{if} \qquad k_{\rm F}R \ll 1\,. \tag{6.66}$$

The relationship between the other pairs of couplings can in principle be arbitrary, so we will limit ourselves to certain special cases. In the limit $k_{\rm F}R \ll 1$ the relationship $\text{sign}(\mathcal{J}_{33}\mathcal{J}_{12}) = -1$ holds and the condition for a flow towards strong coupling becomes $\mathcal{J}_{21} > 0$, i.e. $J_z\rho > 0$.

1. **Large particle–hole asymmetry**
   The first case we consider is representative for a large particle–hole asymmetry. We assume the particle–hole asymmetry parameter A to be of order $\mathcal{O}(1)$, while the remaining small parameters are of the same order $\mathcal{O}(k_{\rm F}R) \sim \mathcal{O}(J_z\rho) \sim \mathcal{O}(J_\perp\rho)$. According to

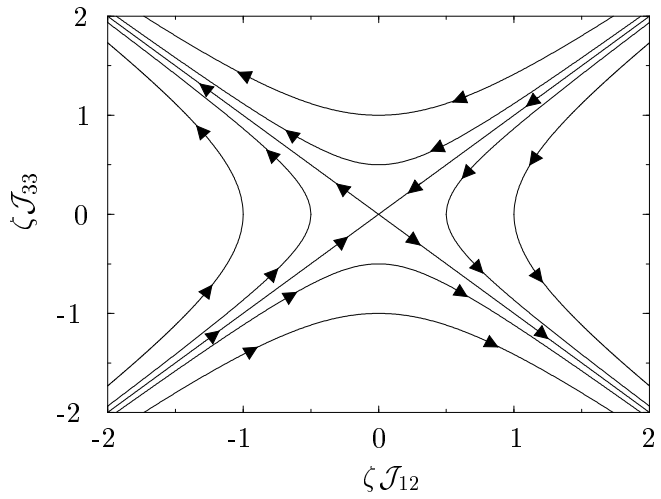

Figure 6.6: *Flow of the effective coupling constants $\mathcal{J}_{12}$ and $\mathcal{J}_{33}$ in the case of positive $\mathcal{J}_{21}$. The solid lines correspond to the scaling trajectories and the arrows indicate the direction of the flow. The flow is towards strong coupling if* $\mathrm{sign}\{\mathcal{J}_{33}\mathcal{J}_{12}\} = -1$.

(6.58) the two components $\mathcal{J}_{33}$ and $\mathcal{J}_{21}$ are of second order in these small parameters whereas the component $\mathcal{J}_{12}$ is of third order. So in this case we have the following hierarchy among the Kondo couplings

$$|\mathcal{J}_{33}| \sim |\mathcal{J}_{21}| \gg |\mathcal{J}_{12}| \,. \tag{6.67}$$

After integrating the scaling equations and expanding in the small coupling $\mathcal{J}_{12}$ we find for the Kondo temperature

$$T_K \sim D\, e^{-\frac{\pi}{4\,\zeta\,\mathcal{J}_{21}}} = D\, e^{-\frac{\sqrt{3}\,\pi}{4\,J_z\rho\,k_{\mathrm{F}}R}} \,. \tag{6.68}$$

2. **Small particle–hole asymmetry**
   Now we would like to assume that the particle-hole asymmetry is of the same order as the other small parameters $\mathcal{O}(A) \sim \mathcal{O}(k_{\mathrm{F}}R, J_z\rho, J_\perp\rho)$. We obtain according to (6.58) the following hierarchy for the couplings

$$|\mathcal{J}_{21}| \gg |\mathcal{J}_{33}| \gg |\mathcal{J}_{12}| \,. \tag{6.69}$$

   Integrating the scaling equations and expanding according to this hierarchy results in the Kondo temperature

$$T_K \sim D \left| \frac{\sqrt{8}\mathcal{J}_{21}}{\mathcal{J}_{33}} \right|^{-\frac{1}{2\,\zeta\,\mathcal{J}_{21}}} = D \left| \frac{\sqrt{2}J_z\rho\,k_{\mathrm{F}}R}{\sqrt{3}\,(J_\perp\rho)^2\,A} \right|^{-\frac{\sqrt{3}}{2\,J_z\rho\,k_{\mathrm{F}}R}} \,. \tag{6.70}$$

We can summarize that in the limit $k_{\mathrm{F}}R \ll 1$ the Kondo temperature is suppressed by $k_{\mathrm{F}}R$ in the denominator of the exponent.

6.5.2 Limit $k_{\rm F}R \gg 1$

In the opposite limit $k_{\rm F}R \gg 1$ the estimates (6.59) yield the hierarchy

$$|\mathcal{J}_{21}| \gg |\mathcal{J}_{33}| = |\mathcal{J}_{12}| \qquad \text{for} \qquad k_{\rm F}R \gg 1\,. \tag{6.71}$$

Again we have the relationship $\mathrm{sign}\{\mathcal{J}_{33}\mathcal{J}_{12}\} = -1$ leading to the condition $\mathcal{J}_{21} > 0$, i.e. $J_z\rho > 0$, for a flow to strong coupling. Integrating the scaling equation and expanding in the small couplings gives the Kondo temperature

$$T_K \sim D \left|\frac{\mathcal{J}_{12}}{2\mathcal{J}_{21}}\right|^{\frac{1}{2\zeta\,\mathcal{J}_{21}}} = D \left|\frac{(J_\perp\rho)^2}{J_z\rho}\,\frac{\cos(k_{\rm F}R)}{k_{\rm F}R}\,\mathcal{F}(\alpha)\right|^{\frac{1}{2\,J_z\rho}}\,. \tag{6.72}$$

where $\alpha = RK_z/(2\mathrm{v_F})$ and the function $\mathcal{F}$ is defined in (B.31).

6.6 Discussion

In this chapter we have considered a simple model of a magnetic droplet consisting of two local moments (5.8). We have shown that for strong Ising-like coupling of the two local moments the effective theory is given by a two-channel Kondo Hamiltonian with a Zeeman splitting (6.53). The degeneracy of the two channels is ensured by the assumption that an axial symmetry of the droplet is present, see Fig. 6.2. We estimated the couplings of the effective Kondo model in terms of the parameters of the high energy theory, neglecting the effect of spin–orbit coupling on the band structure of the conduction electrons; we expect that its inclusion will not qualitatively alter the results. We found that the development of non-Fermi liquid physics in the effective model requires fine-tuning in order to eliminate the Zeeman splitting, which would otherwise drive the system to a stable Fermi liquid phase. We determined the Kondo temperature of the effective model in different parameter regimes with the help of a poor man's scaling analysis. We found that for small separation of the local moments, $k_{\rm F}R \ll 1$, the Kondo temperature is suppressed whereas in the other limit it is sizable.

We can conclude that the scenario of a dilute gas of magnetic droplets, each independently exhibiting a two-channel Kondo effect is not expected to be generic in heavy fermion compounds because it requires fine-tuning. It therefore remains speculative that the observed non-Fermi liquid behavior of these materials can be attributed to the dynamics of magnetic droplets.

Chapter 7

Mini-Domains in Quantum Dots

In this chapter we consider a special case of the mini-domain model (5.8). We assume (a) that the transverse direct coupling $K_\perp$ vanishes identically and (b) that the conduction electrons at the respective impurity sites are uncorrelated, i.e. the conduction electrons at each impurity site belong to two independent baths. To be definite the Hamiltonian that is considered in this chapter reads

$$H = K_z S_L^z S_R^z + \sum_{j=L,R} H_j^K \,, \tag{7.1}$$

where the index L and R labels the left and right impurities and electron baths. H_j^K describes the coupling of the j^{th} bath to the j^{th} impurity via an anisotropic Kondo Hamiltonian,

$$H_j^K = H_0[c_{\mathbf{k}\sigma j}] + \sum_{n\alpha\beta} J_n S_j^n c_{\alpha j}^\dagger \sigma_{\alpha\beta}^n c_{\beta j} \,. \tag{7.2}$$

The electron operators of each bath are $c_{\sigma j} = \sum_{\mathbf{k}} c_{\mathbf{k}\sigma j}$ and the kinetic part of the Hamiltonian is $H_0[c_{\mathbf{k}\sigma j}] = \sum_{\mathbf{k}\sigma} (\epsilon_{\mathbf{k}} - \mu) c_{\mathbf{k}\sigma j}^\dagger c_{\mathbf{k}\sigma j}$. The Kondo coupling is assumed to be the same for each impurity and has the anisotropic form $(J_n) = (J_\perp, J_\perp, J_z)$. A schematic representation of the model is shown in Fig. 7.1.

Whereas we confined ourselves in Chapter 6 to the strong coupling limit only, $K_z \gg |J_n|$, the two assumptions (a) and (b) simplify the model dramatically so that we will be able to analyze its properties in the whole parameter space. We will show that the physics in the strong coupling limit, $K_z \gg |J_n|$, is *qualitatively* different. Due to the absence of a transverse direct coupling, $K_\perp$, the two antiferromagnetic configurations of the mini-domain are degenerate (compare Fig. 5.1). This results in a strong-coupling phase characterized by

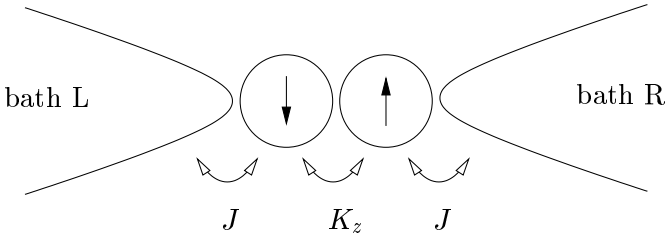

Figure 7.1: *Schematic representation of the mini-domain model Hamiltonian (7.1).*

a non-zero residual entropy of log 2. This is in contrast to the strong-coupling phase of the general model (5.8) described by an effective two-channel Kondo model with a "pseudo-magnetic" field (6.53) derived in Chapter 6. Here, due to the generic channel anisotropy the strong coupling phase is characterized by a local Fermi-liquid fixed point with vanishing residual entropy. The degeneracy of the ground state of the mini-domain leading to the residual entropy log 2 is also the underlying reason why the model (7.1) shows a quantum phase transition usually absent in the generic two-impurity Kondo model (without particle–hole symmetry; compare Section 5.3). That a phase transition has to exist in parameter space can be understood by comparing with the weak coupling limit, $K_z = 0$: The two impurities are decoupled and will be separately screened by their respective electron baths. Each impurity spin then forms a composite singlet with the electronic spins, resulting in a local Fermi liquid with a residual entropy of log 1. The ground states in the weak and strong coupling limits thus differ in their residual entropy and therefore have to be separated by a phase transition.

The existence of the phase transition in the mini-domain model (7.1) was first realized by N. Andrei, G. T. Zimányi and G. Schön [9]. They considered the same Hamiltonian as a model of two coupled quantum dots. It was conjectured that the quantum phase transition is continuous in nature and qualitative arguments were given for how the conductance through the double dot system should behave at low temperatures. We were able to solve this issue. It will be shown in the following sections that the quantum phase transition belongs to the Kosterlitz–Thouless universality class [70]. The conductance at the phase transition has a peculiar zero-bias anomaly and we will determine its characteristic exponent.

This chapter is organized as follows. We will start in Section 7.1 with an analysis of the model in the limit of strong Ising coupling, K_z. We will determine the scaling dimension of the least irrelevant operator and derive a criterion for where the strong coupling phase should become unstable. In Section 7.2 this criterion is borne out by a suitable mapping of the mini-domain model (7.1) to a certain generalized Anderson model which we then analyze. With the help of a Schrieffer–Wolff transformation we show that the effective theory near the phase transition is a Kondo model with the two antiferromagnetic configurations of the mini-domain, see Fig. 5.2, playing the role of the pseudospin. As a consequence, the phase transition between the strong coupling phase and the Kondo-screened phase belongs to the Kosterlitz–Thouless universality class as explained in detail in Section 7.3. In Section 7.4 the results are compared with numerical renormalization group (NRG) calculations by M. Vojta and T. Pruschke and physically interpreted. The robustness of our results is discussed in Section 7.5. Finally, in Section 7.6 we present predictions for two experiments described by the mini-domain model where the quantum phase transition shows itself either in a universal jump in the conductance or in a characteristic zero-bias anomaly.

The work of this chapter is published in Ref. [11].

7.1 Strong coupling analysis

In the strong coupling limit, $K_z \gg |J_n|$, the two impurity spins form an antiferromagnetic mini-domain with the configurations $|\uparrow\downarrow\rangle$ and $|\downarrow\uparrow\rangle$, see Fig. 5.2. In zeroth order in the Kondo coupling, J_n, these two configurations form a degenerate doublet, see Fig. 5.1, since according to assumption (a) the transverse coupling is identically zero, $K_\perp = 0$. This degenerate doublet will eventually lead to a residual entropy of log 2 in the strong coupling phase. As in

Chapter 6 we would like to derive an effective Hamiltonian by performing a Schrieffer–Wolff transformation that takes into account the fluctuation induced by the Kondo coupling J_n. Due to the fact that the impurities couple to different electron baths the effective Hamiltonian is easily derived and has the form

$$\mathcal{H} = \mathcal{H}_0 + \mathcal{H}_{\text{flip}} \qquad \text{where} \qquad \mathcal{H}_0 = \sum_{j=L,R} \left[H_0[c_{\mathbf{k}\sigma j}] + \sum_{\alpha\beta} J_z S^z_j c^\dagger_{\alpha j} \sigma^z_{\alpha\beta} c_{\beta j} \right] . \tag{7.3}$$

The z-component of the Kondo coupling leaves the low-energy Hilbert space of the mini-domain invariant. It represents a scattering potential for the conduction electrons of size J_z, the sign of which depends however on the configuration of the mini-domain. The leading term of the induced mini-domain flips in a perturbative expansion in $J_\perp$ is of order $\mathcal{O}(J_\perp^2/K_z)$,

$$\mathcal{H}_{\text{flip}} = \frac{4J_\perp^2}{K_z} \left(S^+_L S^-_R c^\dagger_{\downarrow L} c_{\uparrow L} c^\dagger_{\uparrow R} c_{\downarrow R} + \text{h.c.} \right) . \tag{7.4}$$

A process described by $\mathcal{H}_{\text{flip}}$ has already been depicted in Fig. 6.3. However, in contrast to the discussion following Fig. 6.3 in Chapter 6 the electron operators in (7.4) cannot be contracted since they belong to different Fermi seas. This is a consequence of assumption (b), that the electrons coupled to the respective impurities belong to different baths and are therefore uncorrelated. In particular, no RKKY interaction is generated. That means that the doublet forming the mini-domain remains degenerate and will not be split by a generated "pseudo-magnetic" field as in Chapter 6. In this sense the doublet represents a perfect pseudospin.

What is the ground state of the strong coupling Hamiltonian (7.3)? The part $\mathcal{H}_{\text{flip}}$ is the only term in (7.3) which couples the different configurations of the pseudospin, $|\uparrow\downarrow\rangle$ and $|\downarrow\uparrow\rangle$. In its absence the mini-domain is "frozen" in either of these configurations and the ground state therefore has a residual entropy of log 2. The flip term $\mathcal{H}_{\text{flip}}$ comprises four electron operators and at first sight it seems to be irrelevant in the RG sense[1]. Since each electron operator carries a scaling dimension of 1/2, its bare scaling dimension is $\dim[H_{\text{flip}}]_{\text{bare}} = 2$ and the log 2 fixed point seems to be stable. However, this conclusion is only valid for small coupling J_z as we will explain in the following. Due to the presence of the spin-flip operators in (7.4) the term $\mathcal{H}_{\text{flip}}$ acquires an anomalous dimension. When the pseudospin of the mini-domain is flipped once by $\mathcal{H}_{\text{flip}}$ the conduction electrons experience an instantaneous sign change in the scattering potential J_z. This whirls up both Fermi seas, leaving a foam of an infinite number of excited particle–hole pairs. It takes an unusually long time until the seas have calmed down again. This phenomenon is known as Anderson's orthogonality catastrophe [71, 72]. In the presence of a sharp Fermi edge the unusual long-time response results in a so-called x-ray edge singularity which manifests itself in an anomalous scaling dimension of the flip operator $\mathcal{H}_{\text{flip}}$.

In the following we will determine this scaling dimension using Hopfield's rule of thumb [73]. To adjust the Fermi sea to a new ground state after the mini-domain has flipped once, a certain amount of spin Δn has to flow to infinity away from the impurity sites. Hopfield noticed

[1] We will use the convention that the scaling dimension of an operator $\mathcal{O}$ derives from its correlation function in the following way:

$$\langle \mathcal{O}(t)\mathcal{O}(0)\rangle \sim t^{-2\dim[\mathcal{O}]} .$$

For example the scaling dimension of the kinetic Hamiltonian $H_0[c_{\mathbf{k}\sigma j}]$ is 1. Contributions to the Hamiltonian with a scaling dimension 1 are dubbed marginal, whereas contributions with scaling dimensions smaller or larger than 1 are called relevant or irrelevant, respectively.

that the collective response of a Fermi sea depends only on Δn in the long-time limit: the corresponding correlation function decays as $t^{-(\Delta n)^2}$. In our problem, we will have to consider four different Fermi seas ($j = L, R$, $\sigma = \uparrow, \downarrow$) each contributing independently. A single mini-domain flip occurs when the flip operator $\mathcal{H}_{\text{flip}}$ acts once on the Fermi seas. In the *absence* of any further flips the long-time limit of the correlation function is given according to Hopfield's rule by

$$\langle \mathcal{H}_{\text{flip}}(t)\mathcal{H}_{\text{flip}}(0)\rangle_{\mathcal{H}_0} \sim t^{-\sum\limits_{\substack{j=L,R;\\ \sigma=\uparrow,\downarrow}} (\Delta n_{\sigma,j})^2} . \tag{7.5}$$

The index on the correlator indicates that it is to be calculated with respect to the Hamiltonian $\mathcal{H}_0$. The transfered spins are easily obtained by the use of the Friedel sum rule [66]. Consider the mini-domain flip process shown in Fig. 6.3, which involves the operator $S_L^+ S_R^- c_{\downarrow L}^\dagger c_{\uparrow L} c_{\uparrow R}^\dagger c_{\downarrow R}$. Let us start with the Fermi sea of the spin up electrons in the right-hand bath. The creation operator $c_{\uparrow R}^\dagger$ adds one spin up. Moreover, due to the spin flip operator S_R^- the scattering potential seen by these electrons changes suddenly from $+J_z$ to $-J_z$ accompanied by a change in the associated phase shift from δ_{J_z} to $-\delta_{J_z}$. According to Friedel's sum rule the change in the phase shifts leads to a transfer of spin $-2\delta_{J_z}/\pi$. Altogether, the Fermi sea of the up electrons in the right bath have to rearrange a spin of magnitude $\Delta n_{\uparrow,R} = 1 - 2\delta_{J_z}/\pi$. Similar arguments yield for the other Fermi seas $\Delta n_{\downarrow R} = -\Delta n_{\downarrow L} = \Delta n_{\uparrow L} = -\Delta n_{\uparrow R}$. The scaling dimension of the flip operator $\mathcal{H}_{\text{flip}}$ with respect to the "frozen mini-domain" phase of residual entropy log 2 represented by $\mathcal{H}_0$ can thus be read off to be

$$\dim\left[\mathcal{H}_{\text{flip}}\right] = \frac{1}{2}\sum_{\substack{j=L,R;\\ \sigma=\uparrow,\downarrow}} (\Delta n_{\sigma,j})^2 = 2\left(1 - \frac{2\delta_{J_z}}{\pi}\right)^2 . \tag{7.6}$$

This result is verified in Appendix B.4 with the bosonization technique following K. D. Schotte and U. Schotte [74]. Indeed, in the absence of the scatterer, $\delta_{J_z} = 0$, the scaling dimension is 2 as naively guessed in the beginning. For small phase shifts, i.e. small J_z, the "frozen mini-domain" fixed point is stable with respect to the flip term $\mathcal{H}_{\text{flip}}$ since it is irrelevant. However, mini-domain flips are relevant if the phase shift is larger than a critical value $\delta_{J_z} > \delta_T$,

$$\delta_T = \frac{\pi}{2}\left(1 - \frac{1}{\sqrt{2}}\right) . \tag{7.7}$$

Beyond this critical value fluctuations of the mini-domain grow towards low energies giving rise to a new phase. The "frozen" mini-domain fixed point and the associated log 2 entropy phase becomes unstable.

It turns out that the special value of the phase shift, δ_T, is well known as the Toulouse point of the single-impurity anisotropic Kondo model [66]. In the next section we will exploit the special properties of the Toulouse point which enables us to identify the quantum phase transition taking place at δ_T.

7.2 Bosonization: generalized Anderson model

At the Toulouse point the single-impurity anisotropic Kondo model is exactly solvable in closed form. This becomes especially apparent in the framework of bosonization [75]. In this section we will bosonize the mini-domain Hamiltonian (7.1). After performing a unitary

transformation and subsequent refermionization we will show that the model takes the form of a generalized Anderson model. We will repeat the strong coupling analysis which is especially revealing in this new formulation since at the Toulouse point the generalized Anderson model simplifies to the usual single-impurity Anderson model [66] as was noticed before by S. Kehrein and M. Vojta [10].

In bosonizing the mini-domain Hamiltonian we closely follow Ref. [68]. We stick mostly to the conventions outlined in the introductory tutorial on bosonization by J. von Delft and H. Schöller [76]; the sole exception will be a different normalization of the electron Green function from that in Ref. [76] which can be accounted for by replacing all fermionic operators by $c_{\text{von Delft, Schöller}} \to \sqrt{2\pi}\, c$, such that $\{c_n^\dagger(x), c_{n'}(x')\} = \delta_{nn'}\delta(x-x')$.

The Kondo interaction (7.2) is local in space. It therefore involves only the s-wave electrons; the other electrons are decoupled from the impurity spins. The s-wave electrons form an effective one-dimensional system that is amenable to the bosonization technique. For this purpose they are described by one-dimensional so-called chiral fields,

$$c_{\sigma j}(x) = \sum_k e^{-ikx} c_{k\sigma j}, \qquad x \in (-\infty, \infty)\,, \tag{7.8}$$

where $k \equiv p - p_{\rm F}$ is the radial momentum relative to the Fermi momentum. The $x > 0$ and $x < 0$ portions of the chiral field are associated with the incoming and outgoing scattering states, respectively. We will also need the density of states per spin of incoming or outgoing electrons, i.e. of an electron living on a half-line, $\rho = 1/(2\pi \mathrm{v_F})$. The central ingredient in the following treatment is the bosonization identity

$$c_{\sigma j}(x) = \frac{1}{\sqrt{2\pi a}} F_{\sigma j}\ \mathrm{e}^{-i\phi_{\sigma j}(x)}\,, \tag{7.9}$$

where a is a short distance cutoff, $F_{\sigma j}$ is an anticommuting Klein factor, $\{F_{\sigma j}^\dagger, F_{\sigma' j'}\} = 2\delta_{\sigma\sigma'}\delta_{jj'}$, and $\phi_{\sigma j}$ is the corresponding bosonic field which obeys the commutation relation

$$[\phi_{\sigma j}(x), \partial_{x'}\phi_{\sigma' j'}(x')] = 2\pi i \delta(x-x')\delta_{jj'}\delta_{\sigma\sigma'}\,. \tag{7.10}$$

Transforming to bosonic charge and spin fields $\phi_{s/c,j} = \frac{1}{\sqrt{2}}\left(\phi_{\uparrow j} \pm \phi_{\downarrow j}\right)$, the bosonized version of the Hamiltonian H_j^K (7.2) is given by [75, 68]

$$H_j^K = H_0[\phi_{cj}] + H_0[\phi_{sj}] + \frac{J_z}{\sqrt{2}\pi} S_j^z \partial_x \phi_{sj}(0) + \frac{J_\perp}{2\pi a}\left(\mathrm{e}^{-i\sqrt{2}\phi_{sj}(0)} S_j^+ F_{\downarrow j}^\dagger F_{\uparrow j} + \text{h.c.}\right). \tag{7.11}$$

Assuming a linear dispersion $\epsilon_k = \mathrm{v_F} k$ the kinetic parts are

$$H_0[\phi] = \mathrm{v_F} \int \frac{dx}{2\pi}\frac{1}{2} : (\partial_x \phi(x))^2 : \,. \tag{7.12}$$

The bosonization treatment shows explicitly that the charge degrees of freedom represented by the field ϕ_{cj} decouple from the spin dynamics in the Kondo model. The charge field ϕ_{cj} will be omitted in the following. Applying a general Emery–Kivelson transformation [63] with the "boundary condition changing operator" [74, 77]

$$U_\gamma = \exp\left[i\gamma \sum_{j=R,L} S_{zj}\phi_{sj}(0)\right], \tag{7.13}$$

parametrized by γ, the Hamiltonian H_j^K transforms into $\tilde{H}_j^K = U_\gamma H_j^K U_\gamma^\dagger$ with

$$\tilde{H}_j^K = H_0[\phi_{sj}] + \left(\frac{J_z}{\sqrt{2}\pi} - \gamma v_{\rm F}\right) S_j^z \partial_x \phi_{sj}(0) + \frac{J_\perp}{2\pi a}\left(\mathrm{e}^{-i(\sqrt{2}-\gamma)\phi_{sj}(0)} S_j^+ F_{\downarrow j}^\dagger F_{\uparrow j} + \text{h.c.}\right) . \quad (7.14)$$

The important thing to note is that the Ising coupling of the mini-domain, $K_z S_L^z S_R^z$, is *invariant* under this transformation.

For the special value $\gamma = \sqrt{2} - 1$ the exponentials appearing in expression (7.14) have the same form as in the bosonization identity (7.9). For this special value the Kondo Hamiltonian can be refermionized upon introducing a new pseudo-fermion field Ψ_j representing *solitonic* spin excitations of the original conduction electrons. (There exists another interesting value $\gamma = \sqrt{2}$ where the model collapses to two coupled spin-boson models, see Appendix B.5.) We will further represent the spin operators S_j^η in terms of fermion operators d_j, e.g. $S_j^z = d_j^\dagger d_j - \frac{1}{2}$. For details, in particular how to ensure proper anticommutation relations among the fermions, see, e.g., Appendix D of Ref. [68]. The refermionized mini-domain Hamiltonian (7.1) takes the form of a generalized Anderson model,

$$\boxed{\begin{aligned} H_{GA} = \quad & K_z\left(d_R^\dagger d_R - \tfrac{1}{2}\right)\left(d_L^\dagger d_L - \tfrac{1}{2}\right) + \\ & \sum_{j=R,L}\left[H_0[\Psi_j] + V\left(d_j^\dagger \Psi_j(0) + \text{h.c.}\right) + W\left(d_j^\dagger d_j - \tfrac{1}{2}\right) : \Psi_j^\dagger(0)\Psi_j(0) :\right] , \end{aligned}} \quad (7.15)$$

where the colons indicate normal ordering. The new coupling constants V and W are defined in terms of the Kondo couplings,

$$V = \frac{J_\perp}{\sqrt{2\pi a}} \qquad \text{and} \qquad W\rho = \sqrt{2} J_z \rho - (\sqrt{2} - 1) . \quad (7.16)$$

As promised above, the special properties of the Toulouse point emerge here naturally. At the Toulouse point the coupling W vanishes, which implies $J_z\rho = 1 - 1/\sqrt{2}$ as explained in detail in the following section.

7.2.1 Phase shift relationship

Before making the connection with the strong coupling analysis of Section 7.1 we have to spend some time on the subtleties of how the results depend on the applied cutoff scheme. Generally, the cutoff scheme strongly influences the meaning of the coupling constants of the Hamiltonian. In the original formulation of the mini-domain model (7.1) the Kondo interaction was point-like and the conduction electrons belonged to a band with a finite width, i.e. cutoff, D. On the other hand, the bosonization procedure relies on extending the band to infinity: the sum over radial momenta k in (7.8) extends from minus to plus infinity. The cutoff was reintroduced with the short distance cutoff a in the bosonization identity (7.9). This effectively corresponds to a Kondo interaction with a finite range in space. A thorough discussion of this issue can be found in Appendix A of Ref. [68].

The application of different cutoff procedures in the two formulations implies that one has to be very careful in identifying the couplings of the generalized Anderson model, W and V, with the Kondo couplings, J_z and $J_\perp$, in the original formulation (7.1). The identification (7.16) is only valid within the bosonization cutoff scheme. A way out of this dilemma is provided by the calculation of certain physical observables which are independent of the

cutoff scheme applied, i.e. which describe measurable low-energy properties of the model. One such quantity is the phase shift. After the phase shift is calculated within the different cutoff schemes the identification of the coupling constants can be made by comparing the results. The phase shift of the original mini-domain model (7.1) as well as of the generalized Anderson model (7.15) can be easily calculated for $J_\perp = 0$ and $V = 0$. For a

$$\text{finite band cutoff scheme} \qquad \begin{aligned} \delta_{J_z} &= \arctan \frac{(-J_z/2)\,\mathrm{Im}\, g_c(0)}{1-(-J_z/2)\,\mathrm{Re}\, g_c(0)} &&= \arctan\left[\frac{\pi J_z \rho_{\mathrm{F}}}{2}\right] \\ \delta_W &= \arctan \frac{(-W/2)\,\mathrm{Im}\, g_\Psi(0)}{1-(-W/2)\,\mathrm{Re}\, g_\Psi(0)} &&= \arctan\left[\frac{\pi W \rho_{\mathrm{SF}}}{2}\right] \end{aligned} \tag{7.17}$$

the phase shifts associated with the interactions J_z and W are given in terms of the Green function of the conduction electrons, c, and the *solitonic* fermions, Ψ, respectively. The last equality is only valid in the case of particle–hole symmetry when the local Green function, $g(\omega) = \sum_k (\omega - \epsilon_k + i0^+)^{-1}$, in each case reduce to $g_c(0) = -i\pi\rho_{\mathrm{F}}$ and $g_\Psi(0) = -i\pi\rho_{\mathrm{SF}}$, respectively, where ρ_{F} and ρ_{SF} are the density of states of the respective fermions. On the other hand, the phase shifts read within the

$$\text{bosonization cutoff scheme} \qquad \begin{aligned} \delta_{J_z} &= \frac{\pi J_z \rho}{2} \\ \delta_W &= \frac{\pi W \rho}{2}\,. \end{aligned} \tag{7.18}$$

Loosely speaking, the Born approximation of the phase shifts in the finite band cutoff scheme, i.e. the expansion of expression (7.17) to first order in the coupling constants, yields the exact result in the bosonization cutoff scheme provided the respective densities of states are identified with each other.

Now we are in a position to establish a universal relationship between the mini-domain Hamiltonian (7.1) to the generalized Anderson model (7.15) in the limit $V, J_\perp \to 0$. Replacing the coupling constants in (7.16) by the phase shifts (7.18) derived within the bosonization cutoff scheme we obtain

$$\frac{2\delta_W}{\pi} = \sqrt{2}\left(\frac{2\delta_{J_z}}{\pi} - \left(1 - \frac{1}{\sqrt{2}}\right)\right) = \sqrt{2}\left(\frac{2\delta_{J_z}}{\pi} - \frac{2\delta_T}{\pi}\right) \qquad \text{for} \quad V = J_\perp = 0\,. \tag{7.19}$$

In the strong coupling analysis of Section 7.1 we found that the mini-domain starts to fluctuate when the phase shift δ_{J_z} exceeds a critical value δ_T (7.7) identified as the Toulouse point. We can easily verify that the associated critical value for the phase shift δ_W is zero. We summarize that exactly at the Toulouse point, where the quantum phase transition is supposed to happen, the coupling W in the generalized Anderson model (7.15) vanishes.

7.2.2 On the Toulouse line

As S. Kehrein and M. Vojta [10] have pointed out, for $W = 0$ the generalized Anderson model simplifies to the conventional (particle–hole symmetric) single-impurity Anderson model. The Ising interaction K_z plays the role of the local Coulomb repulsion and V is the hybridization between the solitonic fermions, Ψ, and the pseudo-fermions, d, on the effective Anderson impurity. The bath index, j, can be identified with a pseudospin, $R \equiv \Uparrow$ and $L \equiv \Downarrow$,

$$H_A = K_z\left(d^\dagger_\Uparrow d_\Uparrow - \frac{1}{2}\right)\left(d^\dagger_\Downarrow d_\Downarrow - \frac{1}{2}\right) + \sum_{\sigma=\Uparrow,\Downarrow}\left[H_0[\Psi_\sigma] + V\left(d^\dagger_\sigma \Psi_\sigma(0) + \text{h.c.}\right)\right]. \tag{7.20}$$

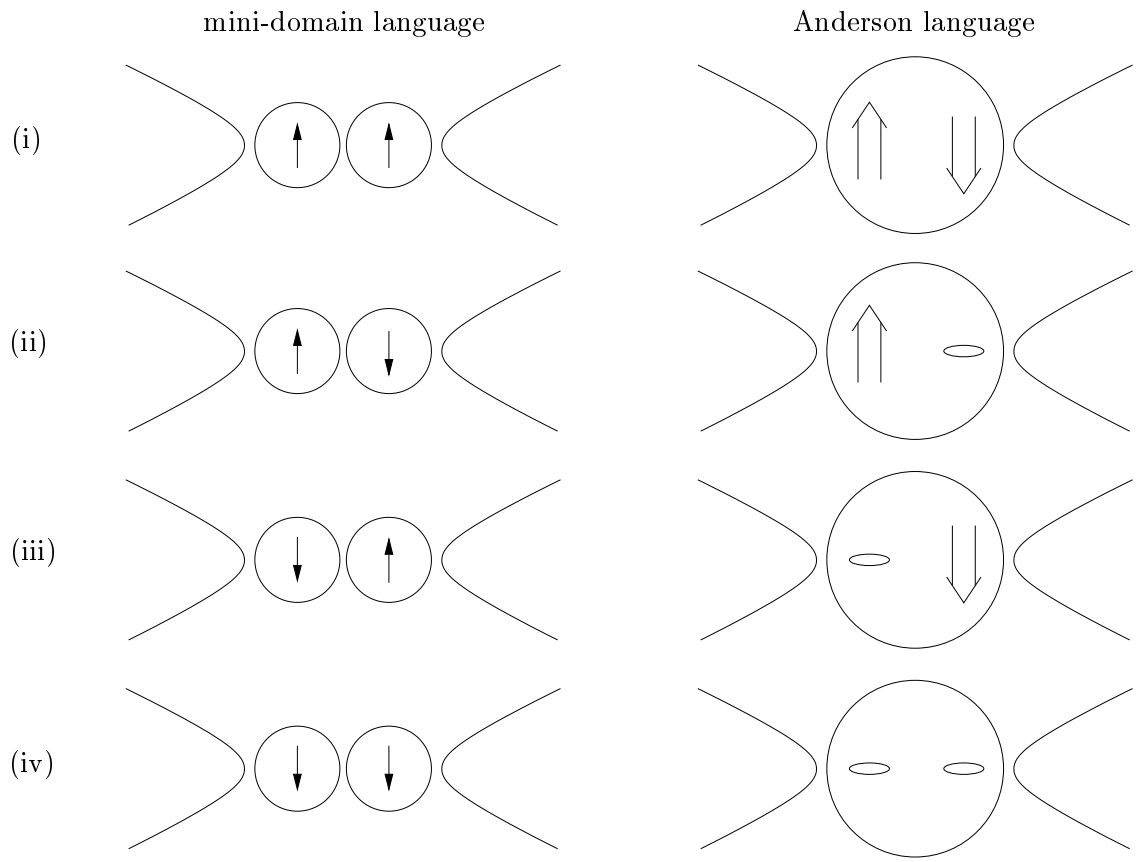

Figure 7.2: *Correspondence between the configurations of the impurity spins forming the mini-domain and the effective single impurity described by the Anderson model. The antiferromagnetic configurations of the mini-domain, (ii) and (iii), can be attributed to a singly occupied Anderson impurity with a well-defined pseudospin of either* $\Uparrow$ *or* $\Downarrow$.

The pseudospin is indeed exactly the one already introduced in Chapter 6. In Fig. 7.2 the correspondence between the configurations of the original two impurity spins and the effective single Anderson impurity is illustrated. The antiferromagnetic mini-domain, (ii) and (iii) of Fig. 7.2, forms in the strong coupling limit $K_z \gg \rho_{\rm SF} V^2$, where $\rho_{\rm SF}$ is the density of states of the solitonic fermions. In the language of the Anderson model this is the so-called local moment regime where the Anderson impurity is singly occupied and has a definite pseudospin of either $\Uparrow$ or $\Downarrow$. The pseudospin is thus in one-to-one correspondence with the two antiferromagnetic configurations of the mini-domain already depicted in Fig. 5.2.

When the coupling K_z is reduced the pseudocharge fluctuations of the Anderson model, i.e. the excitations of the doubly occupied state(i) and the empty state (iv), grow in importance. The Anderson impurity cannot be associated with a well-defined pseudospin any more; it is said to enter a mixed valence regime. The transition from the local moment to the mixed valence regime is known to be a crossover: the Anderson model does not exhibit a quantum phase transition! The phase transition in the generalized Anderson model is thus to be found not along the Toulouse line, $W = 0$, but rather perpendicular to it, i.e. by considering its behavior in the presence of a finite coupling W.

Let us consider the Anderson model (7.20) in its local moment regime, $K_z \gg \rho_{\rm SF} V^2$, and

investigate how a small coupling W affects its behavior. After applying a Schrieffer–Wolff transformation, which treats the hybridization V perturbatively, the Anderson model reduces in the local moment regime to an effective *isotropic* Kondo model [66],

$$\mathcal{H}_A = \sum_{\sigma=\Uparrow,\Downarrow} H_0[\Psi_\sigma] + \frac{4V^2}{K_z} \sum_{\alpha,\beta=\Uparrow,\Downarrow} \vec{\mathfrak{S}}\, \Psi^\dagger_\alpha(0)\vec{\sigma}_{\alpha\beta}\Psi_\beta(0) \tag{7.21}$$

where the pseudospin of the Anderson impurity is represented by the spin-$\frac{1}{2}$ operator $\vec{\mathfrak{S}} = \frac{1}{2}\sum_{\alpha,\beta=\Uparrow,\Downarrow} d^\dagger_\alpha \vec{\sigma}_{\alpha\beta} d_\beta$ and the coupling constant is $4V^2/K_z$. Note that no potential scatterer is generated since the Anderson model (7.20) is particle–hole symmetric. Equation (7.21) is in itself an important result. It states explicitly that the two antiferromagnetic configurations, i.e. the pseudospin of the mini-domain are governed by a Kondo Hamiltonian in the strong coupling regime, $K_z \gg \rho_{\rm SF} V^2$, at least on the Toulouse line $W = 0$. Let us perturb this effective Kondo model by switching on a small coupling W. The corresponding interaction in (7.15) can be separated into two parts,

$$\begin{aligned} & W \sum_{\sigma=\Uparrow,\Downarrow} \left(d^\dagger_\sigma d_\sigma - \frac{1}{2} \right) : \Psi^\dagger_\sigma(0)\Psi_\sigma(0) : \qquad (7.22) \\ &= W \sum_{\alpha,\beta} \mathfrak{S}^z\, \Psi^\dagger_\alpha(0)\sigma^z_{\alpha\beta}\Psi_\beta(0) + \frac{W}{2}\left(d^\dagger_\Uparrow d_\Uparrow + d^\dagger_\Downarrow d_\Downarrow - 1 \right) \left(: \Psi^\dagger_\Uparrow(0)\Psi_\Uparrow(0) : + : \Psi^\dagger_\Downarrow(0)\Psi_\Downarrow(0) : \right) . \end{aligned}$$

The first part describes the pseudospin fluctuations and acts only on the low-energy Hilbert space of the Anderson impurity, i.e. states (ii) and (iii) in Fig. 7.2. The second part represents the pseudocharge fluctuations and affects the high-energy states, (i) and (iv). In the local moment regime the charge fluctuations are frozen out and a small coupling W modifies the strong coupling Kondo Hamiltonian (7.21) only with the contribution involving the pseudospin degree of freedom,

$$\delta\mathcal{H} = W \sum_{\alpha,\beta} \mathfrak{S}^z\, \Psi^\dagger_\alpha(0)\sigma^z_{\alpha\beta}\Psi_\beta(0)\,. \tag{7.23}$$

A small interaction W thus shifts the z-component of the Kondo coupling in the strong coupling Hamiltonian (7.21) leading to an effective *anisotropic* Kondo model, $\mathcal{H}_A + \delta\mathcal{H}$, with coupling constants (compare with (7.2)),

$$\mathcal{J}_z = W + \frac{4V^2}{K_z} \qquad \text{and} \qquad \mathcal{J}_\perp = \frac{4V^2}{K_z}\,. \tag{7.24}$$

Before analyzing this effective Kondo model we would, however, like to extend the strong coupling analysis away from the Toulouse line.

7.2.3 Strong coupling analysis

In the last section we considered the strong coupling limit, $K_z \gg \rho_{\rm SF} V^2$, of the generalized Anderson model (7.15) on the Toulouse line $W = 0$ which after a Schrieffer–Wolff transformation lead to an effective Kondo model. Afterwards we perturbed this effective Kondo model with the small interaction W. In doing so we neglected the effect of the interaction W on the Schrieffer–Wolff transformation itself. In the present section we would like to remedy this shortcoming by performing a Schrieffer–Wolff transformation of the generalized Anderson

model (7.15) in the presence of a *finite* interaction W. We will show that the resulting effective theory is still described by a Kondo Hamiltonian but with power-law renormalizations of the effective Kondo couplings. These renormalizations arise from a x-ray edge singularity associated with the virtual excited high-energy states. As long as the Anderson impurity is fixed in a certain configuration the interaction W just acts as a potential scatterer. If, however, a pseudo-fermion hops onto or off the impurity this potential scatterer changes its sign instantly, leading to a long-time response of the associated (solitonic) Fermi seas in a similar manner to that discussed in Section 7.1.

In order to derive the effective Hamiltonian of the generalized Anderson model in the strong coupling limit the usual Schrieffer–Wolff transformation has to be modified. Instead of working in frequency space we will prefer the time domain in which the physics is easier to understand. The following calculation was strongly inspired by a re-derivation of the Anderson–Yuval–Hamann scaling equations [78] of the anisotropic Kondo model in the framework of bosonization, which is presented in Appendix B.6.

Consider the generalized Anderson model (7.15) in its bosonized version. The interaction W can be formally eliminated by applying the Emery–Kivelson transformation (7.13) with $\gamma^* = W\rho$,

$$U_{\gamma^*} H_{GA} U_{\gamma^*}^\dagger = K_z \left(d_R^\dagger d_R - \frac{1}{2} \right) \left(d_L^\dagger d_L - \frac{1}{2} \right) + \sum_{\sigma=\Uparrow,\Downarrow} H_0[\phi_\sigma] + H_{\rm int} \,. \tag{7.25}$$

Now W enters only the hybridization term

$$H_{\rm int} = \frac{V}{\sqrt{2\pi a}} \sum_{\sigma=\Uparrow,\Downarrow} \left(d_\sigma^\dagger \mathrm{e}^{-i(1-W\rho)\phi_\sigma(0)} F_\sigma + \text{h.c.} \right) \,. \tag{7.26}$$

In the strong coupling regime, $K_z \gg \rho_{\rm SF} V^2$, the Anderson impurity is only singly occupied. The low-energy Hilbert space consists of the two states $|\Uparrow\rangle$ and $|\Downarrow\rangle$ which have an associated local moment, i.e. pseudospin, and are separated from the doubly occupied and empty state by an energy $K_z/2$. The hybridization V will induce virtual excitations to the high energy states whose dynamics will lead to the effective low-energy Hamiltonian. In order to derive it we consider the S-matrix projected onto the low-energy Hilbert space perturbatively expanded in the hybridization V,

$$\mathcal{P}\,\mathcal{T}\mathrm{e}^{-i\int_{-\infty}^{\infty} d\tau H_{\rm int}(t)}\mathcal{P} = \sum_{n=0}^{\infty} \int_{-\infty}^{\infty} \underset{t_{2n}>\cdots>t_1}{dt_{2n}\ldots dt_1}\, \mathcal{P}\, iH_{\rm int}(t_{2n})\ldots iH_{\rm int}(t_1)\mathcal{P} \,. \tag{7.27}$$

where $\mathcal{T}$ is the time-ordering operator. The projection operator is given by $\mathcal{P} = \sum_{\sigma=\Uparrow,\Downarrow} |\sigma\rangle\langle\sigma|$. Since the interaction Hamiltonian $H_{\rm int}$ communicates between the high- and low-energy sectors only even powers of $H_{\rm int}$ survive after projection. The products of $2n$ $H_{\rm int}$ operators can be divided into n virtual excitations each consisting of a consecutive application of two interaction Hamiltonians $H_{\rm int}$. Each of these will leave the low-energy subspace invariant. If the hybridization V is small the virtual excitations are rare and well separated in time, see Fig. 7.3. They will eventually comprise the effective low-energy Hamiltonian. Consider one

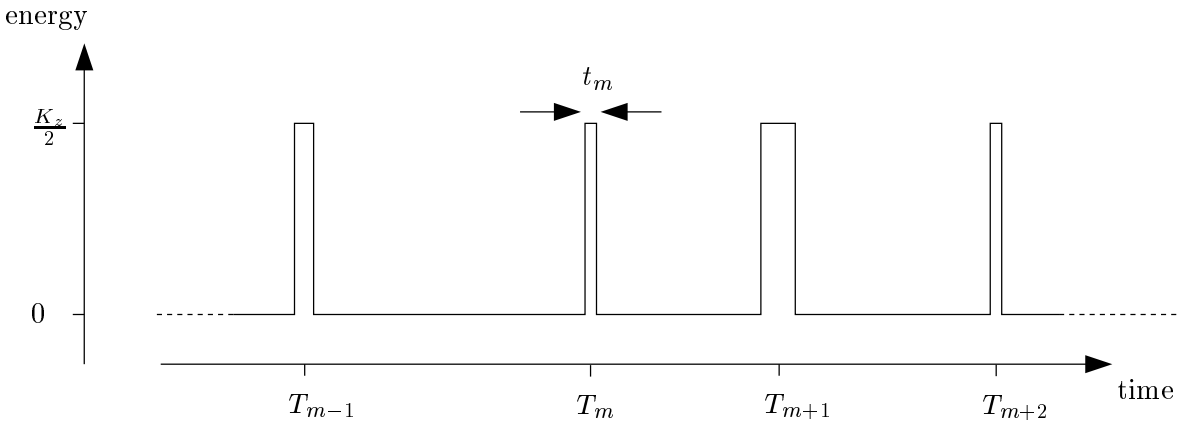

Figure 7.3: *Visualization of a particular time evolution of the Anderson impurity in the strong coupling regime, $K_z \gg \rho_{\rm SF} V^2$, as described by the scattering matrix (7.27). At times T_j the high-energy Hilbert space is visited via virtual excitations. These are well separated due to the smallness of the hybridization V, and their extension in time, t_j, is confined since the Ising coupling K_z is large.*

pair of interaction Hamiltonians forming a virtual excitation

$$\int_{-\infty}^{t_{2m+1}} dt_{2m} \int_{-\infty}^{t_{2m}} dt_{2m-1} i H_{\rm int}(t_{2m}) i H_{\rm int}(t_{2m-1}) \approx -i \int_{-\infty}^{T_{m+1}} \mathcal{H}_{\rm int}(T_m)\,, \tag{7.28}$$

$$\text{with} \qquad \mathcal{H}_{\rm int}(T_m) = -i \int_0^\infty dt\, H_{\rm int}(T_m + t/2) H_{\rm int}(T_m - t/2)\,,$$

where we have introduced the center-of-time and relative coordinates. We have extended the upper limit of the integral over the relative time t to infinity and replaced the upper limit of the integral over the center-of-time T_m by the one of the following pair, T_{m+1}. We have thereby neglected the interaction between adjacent virtual excitations. In the following we would like to integrate over t. Introducing the spin notation $\mathfrak{S}^z = \frac{1}{2}\sum_{\sigma=\Uparrow,\Downarrow} \sigma d_\sigma^\dagger d_\sigma$ and $\mathfrak{S}^+ = d_\Uparrow^\dagger d_\Downarrow$ to represent the two states of the low-energy Hilbert space we get

$$\begin{aligned}\mathcal{H}_{\rm int}(T_m) \;=\; & -i\frac{V^2}{2\pi a}\int_0^\infty dt\, {\rm e}^{-iK_z t/2} \sum_{\sigma=\Uparrow,\Downarrow} \Big[{\rm e}^{-i2\mathfrak{S}^z \sigma(1-W\rho)\phi_\sigma(T_m+t/2)} {\rm e}^{i2\mathfrak{S}^z\sigma(1-W\rho)\phi_\sigma(T_m-t/2)} \\ & + \Big(\mathfrak{S}^+ F_\uparrow F_\downarrow^\dagger {\rm e}^{-i\sigma(1-W\rho)\phi_\sigma(T_m+t/2)} {\rm e}^{i\sigma(1-W\rho)\phi_{-\sigma}(T_m-t/2)} + {\rm h.c.}\Big)\Big]\,.\end{aligned}$$

The oscillating factor $e^{-iK_z t/2}$ guarantees that the virtual excitations are only short-lived so that we can expand the term in the bracket in the small relative time t. To this end we apply the operator product expansion (compare Ref. [76])

$${\rm e}^{i\lambda\phi_\sigma(t)} {\rm e}^{-i\lambda\phi_\sigma(t')} = (1 + i(t-t')/a)^{-\lambda^2} + \lambda a (1 + i(t-t')/a)^{1-\lambda^2} \partial_{t'}\phi_\sigma(t') + \ldots \tag{7.29}$$

to the first term and integrate over the relative time t using the integral

$$\int_0^\infty {\rm e}^{-iK_z t/2} (1 + it/a)^{-\alpha} = -i \frac{2\,\Gamma(1-\alpha)}{K_z} (aK_z/2)^\alpha\,. \tag{7.30}$$

After introducing the pseudospin field $\phi = \frac{1}{\sqrt{2}} \sum_{\sigma=\Uparrow,\Downarrow} \sigma \phi_\sigma$, we obtain in leading order for large K_z

$$\begin{aligned} \mathcal{H}_{\rm int} &= \frac{4V^2}{K_z\sqrt{2}\pi}(1-W\rho)\,\Gamma\left[2-(1-W\rho)^2\right]\left(\frac{aK_z}{2}\right)^{(1-W\rho)^2-1} \mathfrak{S}^z\,\partial_x\phi(0) \\ &\quad + \frac{4V^2}{K_z 2\pi a}\left(\mathfrak{S}^+ \mathrm{e}^{-i\sqrt{2}(1-W\rho)\phi(0)} F^\dagger_\Downarrow F_\Uparrow + \mathrm{h.c.}\right). \end{aligned} \tag{7.31}$$

Before identifying the coupling constants of the effective low-energy Hamiltonian we have to address a subtle point. In integrating out the virtual excitations on the time-scale of order $1/K_z$ we effectively reduced the short distance cutoff from a to a_K, where the new cutoff is of order $a_K \sim 1/K_z$. This has to be accounted for in the implicit cutoff dependence of the vertex operators appearing in the pseudospin-flip term in (7.31). This is similar to the origin of renormalization of the perpendicular Kondo coupling in the Anderson–Yuval–Hamann RG as outlined in Appendix B.6. The implicit cutoff dependence of the vertex operator becomes apparent after normal ordering,

$$e^{i\lambda\phi} = \left(\frac{2\pi a}{L}\right)^{\frac{\lambda^2}{2}} :e^{i\lambda\phi}: = \left(\frac{a}{a_K}\right)^{\frac{\lambda^2}{2}} \left(\frac{2\pi a_K}{L}\right)^{\frac{\lambda^2}{2}} :e^{i\lambda\phi}: = \left(\frac{a}{a_K}\right)^{\frac{\lambda^2}{2}} e^{i\lambda\bar{\phi}}, \tag{7.32}$$

where $\bar{\phi}$ denotes the field defined with respect to the new cutoff a_K. This effectively leads to the substitution

$$\frac{4V^2}{K_z 2\pi a} \to \frac{4V^2}{K_z 2\pi a_K}\left(\frac{a}{a_K}\right)^{(1-W\rho)^2-1} \tag{7.33}$$

in the second term of (7.31). In a final step we undo the Emery-Kivelson transformation leading to an effective Kondo model in its bosonized form.

7.3 Effective Kondo model: fluctuating mini-domain

The low-energy degrees of freedom of the generalized Anderson model (7.15) in the limit of strong coupling, $K_z \gg \rho_{\rm SF} V^2$, are described by an effective Kondo model (compare (7.11)),

$$\mathcal{H}_{GA} = H_0[\bar{\phi}] + \frac{\mathcal{J}_z}{\sqrt{2}\pi}\mathfrak{S}^z\partial_x\bar{\phi}(0) + \frac{\mathcal{J}_\perp}{2\pi a_K}\left(\mathrm{e}^{-i\sqrt{2}\bar{\phi}(0)}\mathfrak{S}^+ F^\dagger_\Downarrow F_\Uparrow + \mathrm{h.c.}\right), \tag{7.34}$$

where the pseudocharge field, $\phi_c = \frac{1}{\sqrt{2}}\sum_{\sigma=\Uparrow,\Downarrow}\phi_\sigma$, has been omitted since it decouples from the pseudospin. The Kondo couplings are given in terms of the hybridization V, Ising coupling K_z, interaction W and the short distance cutoff a:

$$\begin{aligned} \mathcal{J}_z &= W + \frac{4V^2}{K_z}\mathcal{C}_z(W)\left(\frac{aK_z}{2}\right)^{(1-W\rho)^2-1} \\ \mathcal{J}_\perp &= \frac{4V^2}{K_z}\mathcal{C}_\perp(W)\left(\frac{aK_z}{2}\right)^{(1-W\rho)^2-1} \end{aligned} \tag{7.35}$$

where $\mathcal{C}_z(W) \equiv (1-W\rho)\Gamma[2-(1-W\rho)^2]$ and we have further introduced the function $\mathcal{C}_\perp(W) \equiv (2/(a_K K_z))^{(1-W\rho)^2-1}$. The arguments given in Section 7.2.3 suggest that $\mathcal{C}_\perp$ is a

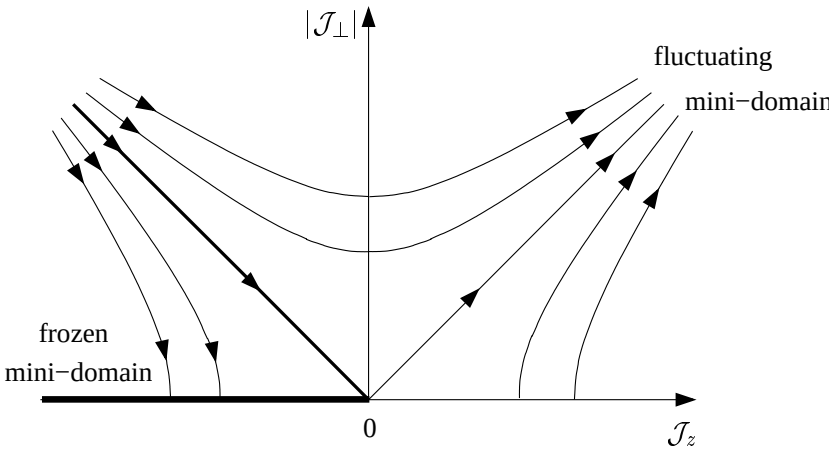

Figure 7.4: *Kosterlitz–Thouless flow diagram representing the RG equations (7.37). For $\mathcal{J}_z < -|\mathcal{J}_\perp|$ the couplings flow towards a* line *of fixed point associated with the "frozen mini-domain" phase. For parameters $\mathcal{J}_z > -|\mathcal{J}_\perp|$ the coupling are determined by a* single *fixed point describing the "fluctuating mini-domain" phase.*

function of W only and is of order one. The derivation presented does not yield a functional relationship between $\mathcal{C}_\perp$ and W, and it remains in general an unknown prefactor. However, both functions have the important property

$$\lim_{W\to 0} \mathcal{C}_z(W) = \mathcal{C}_z(0) = 1 \qquad \text{and} \qquad \lim_{W\to 0} \mathcal{C}_\perp(W) = \mathcal{C}_\perp(0) = 1\,. \tag{7.36}$$

The effective Kondo couplings (7.24) derived on the Toulouse line $W \to 0$ are modified by power-law renormalizations dependent on K_z due to x-ray edge singularities induced by a finite interaction W. They are indeed recovered from (7.35) in the limit $W \to 0$.

Now we are finally in a position to address the question of the quantum phase transition in the mini-domain model posed in Section 7.1. It is the same phase transition that the anisotropic Kondo model exhibits when the coupling $\mathcal{J}_z$ is increased from negative values towards zero. According to the poor man's scaling equations [69], (B.74),

$$\begin{aligned} \frac{d(\mathcal{J}_z\rho)}{d\log a} &= 2\,(\mathcal{J}_\perp\rho)^2\,, \\ \frac{d(\mathcal{J}_\perp\rho)}{d\log a} &= 2(\mathcal{J}_z\rho)(\mathcal{J}_\perp\rho)\,, \end{aligned} \tag{7.37}$$

and the associated RG flow depicted in Fig. 7.4, the separatrix, which separates the RG flows to weak and strong coupling, is given by the condition $\mathcal{J}_z = -|\mathcal{J}_\perp|$. For $\mathcal{J}_z < -|\mathcal{J}_\perp|$ the ferromagnetic phase of the Kondo model is stable with a residual entropy of log 2. This is apparently the "frozen mini-domain" phase: the domain flips between configurations (ii) and (iii) in Fig. 7.2 are frozen out. Its degeneracy leads to the finite residual entropy. For couplings $\mathcal{J}_z > -|\mathcal{J}_\perp|$ the Kondo coupling flows to the strong-coupling Fermi liquid fixed point with an entropy of log 1. The pseudospin of the Anderson impurity is bound into a singlet with the pseudospin of the solitonic fermions. The antiferromagnetic mini-domain is still well-defined, but due to the coupling to the conduction electron it fluctuates so strongly that it eventually gets quenched. Correspondingly, we will dub it the "fluctuating mini-domain" phase. The

quantum phase transition that happens at $\mathcal{J}_z = -|\mathcal{J}_\perp|$ is governed by the scaling equations (7.37) which are characteristic of the so-called Kosterlitz–Thouless universality class [70, 79].

7.3.1 Phase boundary

The criterion $\mathcal{J}_z = -|\mathcal{J}_\perp|$ yields for the critical coupling K_z^{cr} separating the frozen and fluctuating mini-domain phases

$$W = -4\,2^{1-(1-W\rho)^2}\left(\mathcal{C}_z(W)+\mathcal{C}_\perp(W)\right)\frac{V^2 a^{(1-W\rho)^2-1}}{{K_z^{cr}}^{2-(1-W\rho)^2}}\,, \tag{7.38}$$

or equivalently

$$\begin{aligned} &K_z^{cr}\,(-W)^{(2-(1-W\rho)^2)^{-1}} = \\ &\left[4\,2^{1-(1-W\rho)^2}\left(\mathcal{C}_z(W)+\mathcal{C}_\perp(W)\right)\right]^{(2-(1-W\rho)^2)^{-1}}\left(V^2 a^{(1-W\rho)^2-1}\right)^{(2-(1-W\rho)^2)^{-1}}. \end{aligned} \tag{7.39}$$

In the vicinity of the Toulouse point we can expand in the small coupling W and we obtain

$$\boxed{W = -\frac{8}{K_z^{cr}}\left(V^2 a^{(1-W\rho)^2-1}\right)^{(2-(1-W\rho)^2)^{-1}}\,.} \tag{7.40}$$

It is apparent that the critical coupling $K_z^{cr} > 0$ depends crucially on how the phase transition is approached in the parameter space spanned by W and V,

$$K_z^{cr} \sim \begin{cases} -8\,W^{-1}V^2 & \longrightarrow \infty \quad \text{for} \quad W \to 0^- \\ -8\,W^{-1}\left(V^2 a^{(1-W\rho)^2-1}\right)^{(2-(1-W\rho)^2)^{-1}} & \longrightarrow 0 \quad \text{for} \quad V \to 0\,. \end{cases} \tag{7.41}$$

In the limit $W \to 0^-$ for a finite hybridization V the critical coupling diverges. This order of limits corresponds to the regime accessible by the simple strong coupling analysis on the Toulouse line of Section 7.2.2. The reverse order of limits, however, is exclusively the realm of the considerations of Section 7.2.3, since here the critical Ising coupling vanishes (while maintaining $K_z \gg \rho V^2$) and the interaction $W < 0$ has to be considered as a large scale in the strong coupling limit. In this region of parameter space the x-ray edge like power-law renormalizations induced by the interaction W are an important result of the physics taking place.

The power-law renormalizations of the effective Kondo couplings (7.35) are accompanied by an explicit dependence on the short distance cutoff a. Indeed this explicit cutoff dependence is necessary in order to recover universality as we will explain in the following. The effective Kondo model (7.34) was derived in such a way that in the end it had its own short distance cutoff a_K. In particular, this was achieved by accounting for the implicit cutoff dependence of the vertex operator (7.32). As a consequence, the effective couplings $\mathcal{J}_\perp$ and $\mathcal{J}_z$ are supposed to be invariant upon a rescaling of the *old* cutoff a of the underlying generalized Anderson model. Whereas the Ising interaction K_z has a zero scaling dimension (and the scaling dimension of W can be neglected to lowest order in $J_\perp$), the hybridization V is not invariant upon rescaling a. However, the combination $V^2 a^{(1-W\rho)^2-1}$ is! This can be shown within the Anderson–Yuval–Hamann RG approach to the Kondo model [78] (see Appendix B.6). The scaling dimension of the hybridization V results from the scaling dimension of the original

perpendicular interaction $J_\perp$ of the Kondo Hamiltonian (7.2) that coupled the single spins of the mini-domain to their baths. The RG equation for the perpendicular coupling (derived within the bosonization cutoff scheme) reads (B.72)

$$\frac{d\log J_\perp}{d\log a} = 1-(1-J_z\rho)^2 \ . \tag{7.42}$$

Using the relationships (7.16) between the Kondo couplings and the interactions W and V this translates into

$$\frac{d\log V^2}{d\log a} = 1-(1-W\rho)^2 \ , \tag{7.43}$$

which confirms that the combination $V^2 a^{(1-W\rho)^2-1}$ is scale invariant. Its scale invariance ensures that it can be expressed in terms of universal quantities. Indeed it is directly related to the Kondo temperature T_K of a *single* Kondo Hamiltonian (7.2). If the UV cutoff $1/a$ is rescaled to this characteristic temperature scale the non-perturbative character of Kondo physics becomes apparent: the perpendicular Kondo coupling, $J_\perp = V\sqrt{2\pi a}$, has rescaled to a value of order one,

$$\left(V^2 a^{(1-W\rho)^2-1}\right)^{(2-(1-W\rho)^2)^{-1}} \sim a^{-1} J_\perp^{(1-(1-W\rho)^2/2)^{-1}} \sim T_K \, . \tag{7.44}$$

The combination $V^2 a^{(1-W\rho)^2-1}$ in the effective couplings (7.35) can therefore be replaced by the Kondo temperature and, consequently, the dependence on the cutoff a of the high-energy theory be removed. The scale invariance thus eventually ensures the universality of the effective Kondo theory describing the fluctuating mini-domain.

The combination on the left-hand side of (7.44) is just the one appearing in the expression for the critical coupling (7.40). The important point to note is that it is proportional to the Kondo temperature T_K, irrespective of the relative values of the small interactions W and V. In the following we would like to fix the prefactor in expression (7.44). To this end the definition of the Kondo temperature has to be specified. We will identify the Kondo temperature using the value the impurity specific heat coefficient attains in the limit of low temperature, $\gamma = \lim_{T\to 0} C_{\rm imp}/T$,

$$T_K \equiv w\frac{\pi^2}{3}\gamma^{-1} \tag{7.45}$$

where $w = 0.41071...$ is the Wilson number [66]. The specific heat coefficient can easily be calculated *on* the Toulouse line, i.e. for $W = 0$, $\gamma = 1/(3\rho_{\rm SF}V^2)$, where $\rho_{\rm SF}$ is the density of states of the solitonic fermions. This yields the universal asymptotic behavior of the phase boundary near the Toulouse point,

$$\rho_{\rm SF} W_{cr} = -\frac{8}{w\pi^2}\frac{T_K}{K_z^{cr}} \approx -1.974\frac{T_K}{K_z^{cr}} \, . \tag{7.46}$$

In general, universality is expected in the so-called scaling limit when all characteristic energy scales are much smaller than the energy cutoff scale. For example, in our problem the scaling limit can be reached by sending the short distance cutoff a to zero while holding both the Kondo temperature T_K and the Ising coupling K_z fixed. From equation (7.44) it follows that in the scaling limit the perpendicular Kondo coupling vanishes, $J_\perp \to 0$. This then means

that the critical ratio T_K/K_z^{cr} just depends on J_z. Using the relationship (7.17) and (7.19) we obtain in the

$$\boxed{\text{scaling limit:} \qquad \frac{T_K}{K_z^{cr}} = -\frac{w\pi^2\sqrt{2}\sin^2\left(\frac{\pi}{2\sqrt{2}}\right)}{8}\rho_{\rm F}\left(J_z^{cr}-J_z\right) \approx 0.575\rho_{\rm F}\left(J_z^{cr}-J_z\right)\,.} \tag{7.47}$$

The critical coupling J_z^{cr} is given by $\rho_{\rm F}J_z^{cr} = 2/\pi\,\tan\delta_T \approx 0.315$.

7.3.2 Characteristic energy scales near the transition

Close to the quantum phase transition on both sides of the phase boundary there exists a characteristic energy scale. Far away from the Toulouse point, the distance to the phase transition is measured by the RG invariant

$$\mathcal{C} \equiv (\mathcal{J}_\perp\rho)^2 - (\mathcal{J}_z\rho)^2\,. \tag{7.48}$$

The RG invariant $\mathcal{C}$ vanishes on the separatrix, i.e. at the phase transition. Consider the rescaled coupling $\mathcal{J}_z(T)$ after scaling the cutoff of the effective Kondo model K_z to the temperature T,

$$\log\frac{T}{K_z} = -\frac{1}{2}\int\limits_{\mathcal{J}_z\rho}^{\mathcal{J}_z(T)\rho}\frac{d(\mathcal{J}_z'\rho)}{\mathcal{C}+(\mathcal{J}_z'\rho)^2}\,. \tag{7.49}$$

In the fluctuating mini-domain phase the coupling between the pseudospin of solitonic spin excitations and the pseudospin of the mini-domain grows under renormalization and a energy scale T^* is dynamically generated, the collective Kondo temperature of the effective low-energy theory (7.34). It can be estimated by sending the rescaled coupling to infinity $\mathcal{J}_z(T)\to\infty$,

$$T^* \sim K_z\, e^{\frac{1}{2|\mathcal{J}_z\rho|}} e^{-\frac{\pi}{2\sqrt{\mathcal{C}}}} \sim e^{-\frac{\pi}{2\sqrt{\mathcal{C}}}}\,. \tag{7.50}$$

We have used the fact that close to the phase transition the bare coupling $\mathcal{J}_z$ is necessarily negative. In the frozen mini-domain phase on the other hand, where $\mathcal{C}<0$, the couplings flow to zero. Nevertheless, we can distinguish an energy scale associated here with the change of the scaling behavior of, for example, the perpendicular coupling $\mathcal{J}_\perp(T)$,

$$\log\frac{T}{K_z} = \int\limits_{\mathcal{J}_\perp\rho}^{\mathcal{J}_\perp(T)\rho}\frac{d(\mathcal{J}_\perp'\rho)}{2\mathcal{J}_\perp'\rho\sqrt{(\mathcal{J}_\perp'\rho)^2+|\mathcal{C}|}} = \begin{cases} \dfrac{1}{2\sqrt{|\mathcal{C}|}}\log\dfrac{\mathcal{J}_\perp(T)}{\mathcal{J}_\perp} & \text{for} \quad |\mathcal{J}_\perp\rho| \ll \sqrt{|\mathcal{C}|} \\ \dfrac{1}{2|\mathcal{J}_\perp\rho|} - \dfrac{1}{2|\mathcal{J}_\perp(T)\rho|} & \text{for} \quad |\mathcal{J}_\perp(T)\rho| \gg \sqrt{|\mathcal{C}|}\,, \end{cases} \tag{7.51}$$

i.e. it scales either algebraically or exponentially with temperature. The crossover temperature $T_{\rm cross}$ where $|\mathcal{J}_\perp(T)\rho| \simeq \sqrt{|\mathcal{C}|}$ can be determined to be

$$T_{\rm cross} \sim K_z\, e^{\frac{1}{2|\mathcal{J}_\perp\rho|}}\, e^{-\frac{\log(1+\sqrt{2})}{2\sqrt{|\mathcal{C}|}}}\,. \tag{7.52}$$

When the phase transition is approached, for example by varying the Ising coupling K_z, $\mathcal{C}\propto |K_z-K_z^{cr}|\to 0$, the crossover temperature $T_{\rm cross}$ as well as the collective Kondo temperature T^* vanish exponentially.

7.4 Phase diagram: comparison with NRG

The treatment of the preceding section allowed us to determine the phase boundary (7.47) in the vicinity of the Toulouse point. We established that here the quantum phase transition belongs to the Kosterlitz–Thouless universality class. The Toulouse point corresponds to the extreme anisotropic limit of single-impurity Kondo couplings, $J_\perp \ll J_z$, and the question remains how the phase transition changes away from the Toulouse point. Continuity suggests that it evolves continuously towards the isotropic point of Kondo couplings $J_\perp \approx J_z$. But one can *a priori* not exclude that another fixed point might intervene in between. The questions can be answered with the help of the numerical renormalization group (NRG) [66]. An NRG study of the generalized Anderson model (7.15) was performed by M. Vojta and T. Pruschke, and it is explained in detail in Ref. [11]. In the present section we will outline the main results. This will complement the picture of the phase diagram.

For an NRG treatment the generalized Anderson model (7.15) has certain advantages over the original two-impurity model (7.1). The two bands of spinful fermions of the two-impurity model are computationally demanding. The generalized Anderson model on the other hand already takes into account the fact that the respective charge sectors of the two fermionic bands decouple from the impurities, and therefore features only a single band of (pseudo-)spinful fermions allowing for high-accuracy numerical simulations down to lowest energy scales and temperatures. According to the relationship (7.19) between the phase shifts of the two formulations of the mini-domain model and the expression (7.17) the following range of values for J_z can be covered by varying the interaction W (for small $J_\perp$ and V, respectively)

$$\begin{aligned} \rho_{\mathrm{SF}} W \qquad &\longmapsto \quad \rho_{\mathrm{F}} J_z = \frac{2}{\pi} \tan\left[\frac{1}{\sqrt{2}} \arctan\left(\frac{\pi}{2}\rho_{\mathrm{SF}} W\right) + \delta_T\right] , \\ (-\infty, \infty) \qquad &\longrightarrow \quad \left[\frac{2}{\pi}\tan\left(\frac{\pi}{2}(1-\sqrt{2})\right), \frac{2}{\pi}\tan\frac{\pi}{2}\right) = [-0.485, \infty) . \end{aligned} \tag{7.53}$$

Importantly, this includes the isotropic point $J_z \approx J_\perp \ll 1$. In particular, a vanishing Kondo coupling, $J_z = 0$, maps onto $W\rho_{\mathrm{SF}} = (2/\pi)\tan[\pi(1-\sqrt{2})/2] \approx -0.485$. The Toulouse point, $W = 0$, corresponds to the Kondo coupling $\rho_{\mathrm{F}} J_z = 2/\pi \tan\delta_T \approx 0.315$.

7.4.1 NRG flow and entropy

In the left panel of Fig. 7.5 NRG flow diagrams are shown displaying the energies of a few low-lying many-body eigenstates as function of the number of NRG steps N. The data in the upper graph a) clearly shows that for small values of K_z the same fixed point is reached for various V and W — this fixed point can be identified with the Fermi-liquid phase with a residual entropy $S_0 = 0$. In particular, it is also reached for $K_z = 0$, the limit where the two impurity spins are separately Kondo screened by their respective fermionic baths. This proves that the Fermi-liquid of two separately Kondo-screened impurities is adiabatically connected to the "fluctuating mini-domain" regime which can be characterized by pseudospin screening below the collective Kondo temperature T^* (7.50). In the lower graph b) flow diagrams for larger values of K_z are shown. The fixed points reached at low energies are very similar for different parameter sets, but not identical. This is consistent with the notion of a line of fixed points expected from the Kosterlitz–Thouless RG flow of Fig. 7.4. Further evidence that the quantum phase transition belongs to the Kosterlitz–Thouless universality class is provided

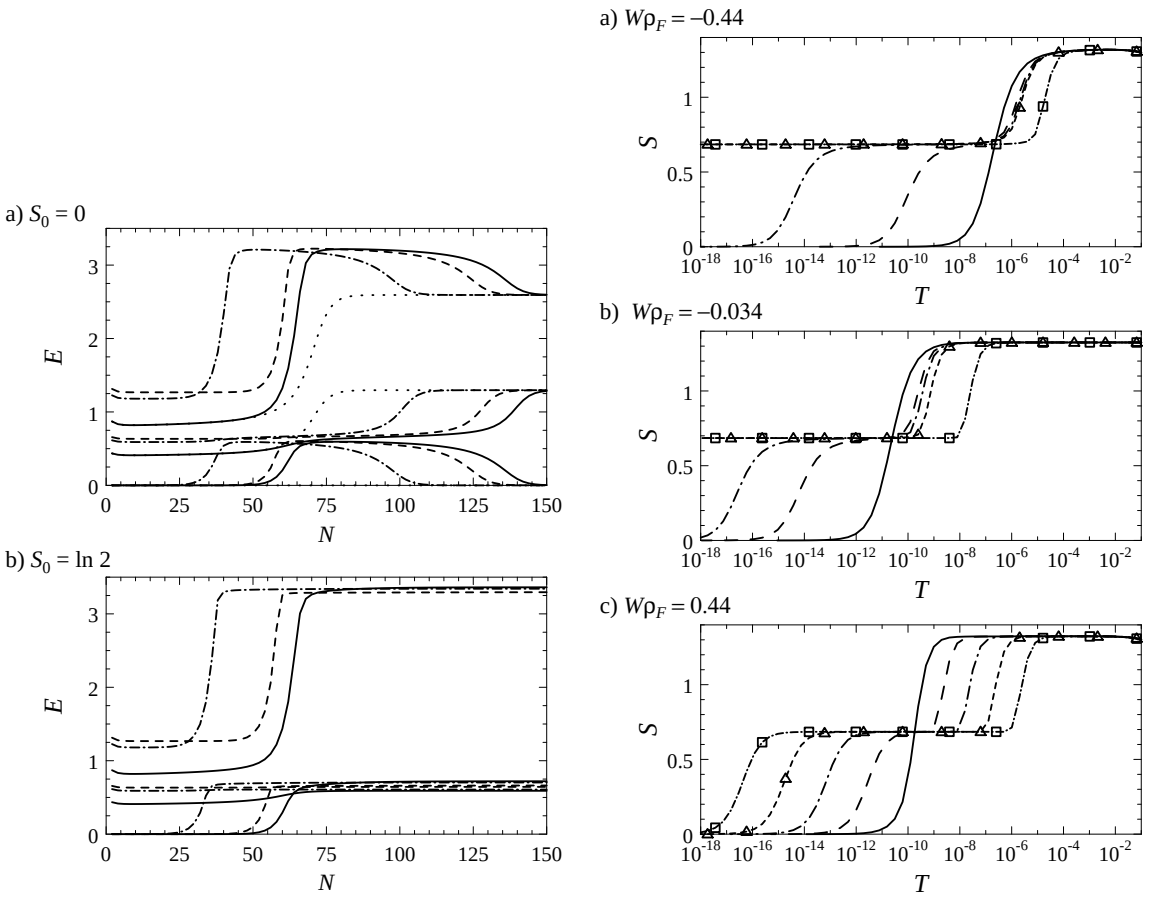

Figure 7.5: *Left panel: NRG flow diagram for the generalized single-impurity Anderson model (7.15), for parameter values belonging to a) the Fermi-liquid phase with $S_0 = 0$, b) the frozen mini-domain phase with $S_0 = \ln 2$. Solid: $W\rho_F = -0.44$, $V = 0.075$ ($K_z^{cr} = 7.9 \times 10^{-10}$), Dash-dot: $W\rho_F = -0.10$, $V = 1.5 \times 10^{-3}$ ($K_z^{cr} = 3.6 \times 10^{-6}$), Dashed: $W\rho_F = -0.034$, $V = 1.5 \times 10^{-5}$ ($K_z^{cr} = 5.6 \times 10^{-9}$). In a) and b), K_z has been chosen slightly below and above the critical value, respectively. For all parameters, the system is in an $S = \ln 4$ regime at high temperatures (small N), in a) it flows to the $S = 0$ state by passing through a regime with $S = \ln 2$. In a), the additional dotted curves show the flow for $W\rho_F = -0.44$, $V = 0.075$, and $K_z = 0$. The $W\rho_F$ values span a large range of anisotropies; nevertheless, the $S = 0$ fixed point is unique, and the finite-temperature crossover is universal for the curves close to K_z^{cr}. Panel b) nicely shows that $S = \ln 2$ actually corresponds to a line of fixed points.*

Right panel: Temperature evolution of the impurity entropy calculated by NRG for different anisotropies of the Kondo coupling. In the "frozen mini-domain" phase the residual entropy is $\ln 2$ *while it vanishes for $K_z < K_z^{cr}$. For $T_K \gg K_z$ (solid curves), the high-temperature* $\ln 4$ *entropy is quenched in a single step, whereas two-stage screening occurs for $T_K < K_z < K_z^{cr}$. a) $W\rho_F = -0.44$, $V = 0.15$ ($K_z^{cr} = 1.5 \times 10^{-5}$), close to isotropic Kondo coupling. K_z is: solid 0, long-dash 10^{-5}, long-dash-dot 1.3×10^{-5}, short-dash 1.5×10^{-5}, short-dash-dot 10^{-4}. b) $W\rho_F = -0.034$, $V = 1.5 \times 10^{-5}$ ($K_z^{cr} = 5.6 \times 10^{-9}$), i.e., close to the Toulouse point of the individual Kondo impurities. The K_z values are: solid 0, long-dash 10^{-9}, long-dash-dot 1.5×10^{-9}, short-dash 3×10^{-9}, short-dash-dot 10^{-7}. c) $W\rho_F = 0.44$, $V = 1.5 \times 10^{-7}$, no phase transition occurs as function of K_z. K_z is: solid 0, long-dash 10^{-8}, long-dash-dot 10^{-7}, short-dash 10^{-6}, short-dash-dot 10^{-5}.*

by the fact that no additional fixed point is observed for $K_z \approx K_z^{cr}$, which could possibly correspond to an (unstable) critical fixed point.

In the right panel of Fig. 7.5 the impurity entropy $S(T)$ is plotted as a function of temperature. At high temperatures the two single impurities occupy a total of four states, resulting in an entropy of log 4. Upon lowering the temperature this high temperature value gets quenched. However, this quenching process depends crucially on the values of the Ising coupling K_z and the Kondo temperature T_K of a single impurity. In the parameter regime $K_z \ll T_K$ the individual Kondo screening of the two impurity spins by their respective electron bath is so overwhelming that the log 4 entropy is reduced in a single step to zero, resulting in two local Fermi liquids. In the other regime $K_z \gg T_K$ the energy scale given by the Ising interaction is detected, leading to a quenching of only half the high energy entropy to log 2 at a temperature $T \sim K_z$. This corresponds to a reduction of the Hilbert space to the low-energy states depicted in Fig. 5.2, giving rise to an effective pseudospin: the mini-domain is born. Below a temperature $T < K_z$ the physics is hence dominated by the fluctuating mini-domain. Its fate depends on the Kondo coupling J_z, or equivalently on the interaction W, giving rise to a critical value for the Ising interaction K_z^{cr}. Above the critical value $K_z > K_z^{cr}$ the fluctuations of the mini-domain are frozen out leaving a non-zero residual entropy of log 2: this is the frozen mini-domain phase. For couplings $T_K < K_z < K_z^{cr}$ on the other hand the remaining log 2 entropy gets quenched at a temperature of the order of a collective energy scale T^* (7.50) attributed to the effective low-energy theory describing the mini-domain physics. For sufficiently large couplings J_z and W the fluctuating mini-domain is always screened, giving a vanishing residual entropy as shown in graph c) in the right panel of Fig. 7.5.

7.4.2 Phase diagram

In Section 7.3 we were able to determine the nature of the quantum phase transition and the dependence of the phase boundary (7.47) in the vicinity of the Toulouse point. The NRG study showed that this phase transition also extends to the isotropic limit of Kondo couplings, $J_z \approx J_\perp$, and that it is governed throughout by the Kosterlitz–Thouless universality class. In particular, there is no fixed point of a different nature interfering. With this result from the NRG the following picture of a phase diagram emerges (Fig. 7.6).

In the regime $K_z \ll T_K$ each impurity is separately Kondo-screened by its respective electronic bath and mini-domain physics does not play any role. This is the regime where the high-energy entropy log 4 is quenched in a single step to zero, cf. Fig. 7.5. Only below the dashed line in Fig. 7.6 do we find the regime where the low-energy physics is dominated by a well-defined mini-domain.

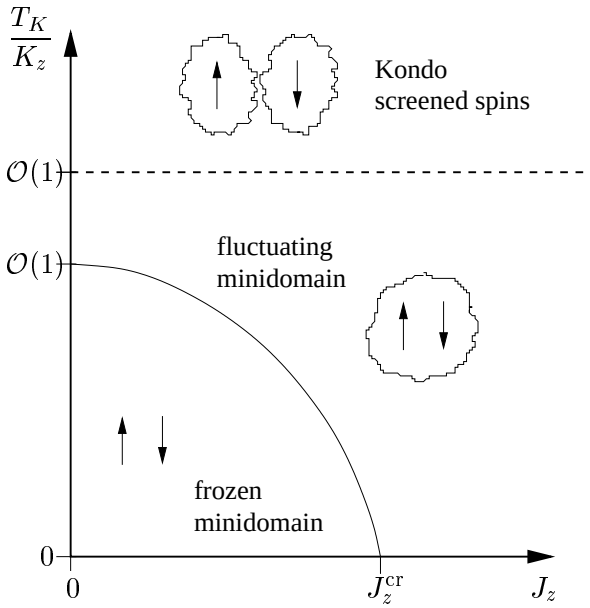

Figure 7.6: *Schematic phase diagram of the mini-domain model (7.1), see text.*

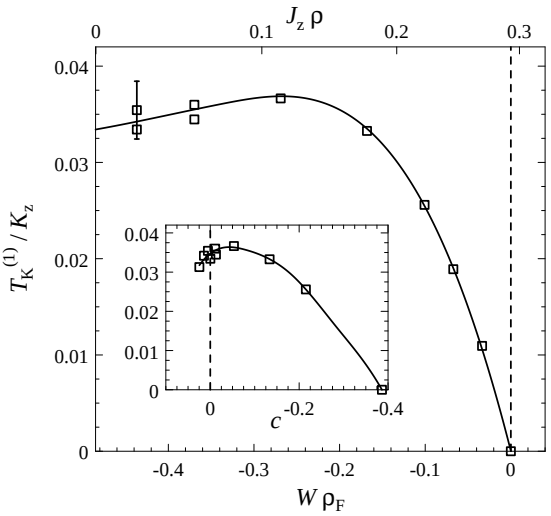

Figure 7.7: *Phase diagram of the generalized single-impurity Anderson model (7.15) deduced from NRG calculations for NRG discretization parameter $\Lambda = 2$. The vertical dashed line shows the Toulouse point of the individual Kondo impurities. Small values of V have been used to reach the universal regime $T_K \ll D$. The upper horizontal axis shows the corresponding values of J_z in the bosonization cutoff scheme. The error bar shows the typical uncertainty in the numerical determination of T_K/K_z^{cr}. The inset shows the same data for T_K/K_z^{cr}, now plotted as function of the RG invariant c of the single-impurity model (7.54) — this plot covers the range of positive as well as negative J_z (here $c > 0$). The lines are a guide to the eye only.*

The Ising interaction K_z is strong enough to bind the two impurity spins into an antiferromagnetic configuration. The two ferromagnetic impurity states decouple from the low-energy physics giving rise to a log 2 plateau in the temperature dependence of the entropy, see right panel of Fig. 7.5. The fate of the mini-domain depends on its coupling to the conduction electrons. If the coupling strength is sufficiently strong a non-perturbative energy scale T^* is dynamically generated below which the conduction electrons are collectively bound to the mini-domain, quenching the remaining degree of freedom. This is the phase of the fluctuating mini-domain. At a critical coupling strength however the fluctuations of the mini-domain are frozen out. The mini-domain is frozen in one of the two antiferromagnetic configurations leading to a residual entropy of log 2. This is accompanied by a quantum phase transition of the Kosterlitz–Thouless universality class indicated by the solid line in Fig. 7.6.

The phase boundary determined by NRG [11] is shown in Fig. 7.7. As already mentioned in Section 7.3 in the scaling limit near the Toulouse point the critical value of the ratio T_K/K_z can just be labeled by the z-component of the Kondo coupling J_z. This is done in the main panel of Fig. 7.7 where the horizontal axis is labeled by J_z and W. However, a proper label for the horizontal axis would actually be an RG invariant $\mathcal{C}$ of the single-impurity Kondo model, as in the inset of Fig. 7.7. This is especially important near the isotropic limit $J_z \approx J_\perp$, as we will explain in the following. According to the Anderson–Yuval–Hamann RG [78] approach (see Appendix B.6), which is applicable for arbitrary J_z in the limit of small perpendicular

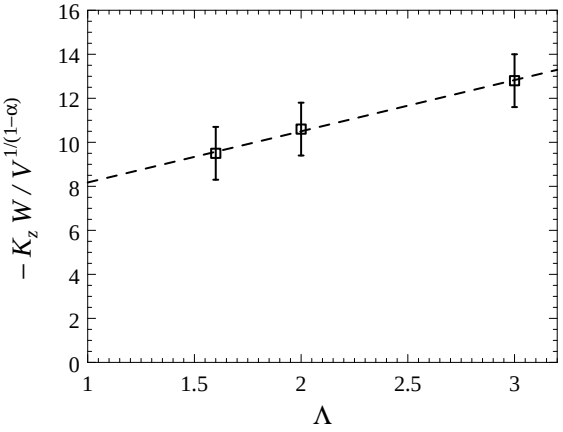

Figure 7.8: *Dependence of the slope of the phase boundary near the Toulouse point on the NRG discretization parameter Λ defining the logarithmic discretization of the conduction band. The dashed line is a linear fit. Each data point involves an extrapolation of the numerical results at finite negative W to $W \to 0^-$.*

coupling $J_\perp$, such an RG invariant is given by

$$c \;=\; 2(J_\perp\rho)^2 + \left[1 - \left(1 - \frac{2\delta_{J_z}}{\pi}\right)^2\right] + 2\ln\left(1 - \frac{2\delta_{J_z}}{\pi}\right) . \tag{7.54}$$

Identical low-energy behavior is expected even for different values of interaction parameters as long as they can be attributed to the same RG invariant c. Near the Toulouse point the contribution of $J_\perp$ to the RG invariant can be neglected and c is unambiguously given by J_z, recovering the label of the main panel. For small values of both J_z and $J_\perp$, however, the expression for c can be expanded and reduces to the poor man's version already encountered in (7.48),

$$c \approx 2\,\mathcal{C} = 2(J_\perp\rho)^2 - 2(J_z\rho)^2 . \tag{7.55}$$

The limit of isotropic Kondo couplings, $J_\perp = J_z$, corresponds therefore to a vanishing RG invariant, $c = 0$, and the contribution of $J_\perp$ cannot be neglected any more. In particular, this means that near the limit of isotropic Kondo coupling the RG invariant is the proper label for the horizontal axis of the phase diagram.

It turned out that some NRG results show a relatively strong dependence on the NRG discretization parameter Λ [11]. Fig. 7.7 shows the phase diagram for $\Lambda = 2$; results for other Λ values are similar, but the critical ratio T_K/K_z^{cr} was found to differ by 50% or more. Therefore, an extrapolation to $\Lambda \to 1$ was performed for a few important quantities. A sample extrapolation is shown in Fig. 7.8 for the slope of the phase boundary near the Toulouse point, which was determined analytically in Section 7.3. The extrapolated value of $K_z W/V^{\frac{1}{1-\alpha}} \approx 8$, with $2\alpha = (1 - 2\delta_W/\pi)^2$, is consistent with the exact result (7.40).

The maximum value of the ratio T_K/K_z^{cr} of the phase boundary shown in Fig. 7.7 occurring near $J_z = 0$ was also analyzed for different discretization parameters and was found to extrapolate to $(T_K/K_z^{cr})_{\max} = 0.1 \pm 0.03$.

Alternatively, one can draw a quantum phase diagram in the plane where the temperature T is plotted versus Ising coupling K_z for a fixed Kondo temperature T_K, see

Fig. 7.9. For $T = 0$ there is a quantum phase transition at the critical coupling $K_z = K_z^{cr}$ from a Fermi liquid with residual entropy $S_0 = 0$ to the "frozen mini-domain" phase with $S_0 = \log 2$. At $T > 0$ only smooth crossovers occur, indicated by the dashed and dotted lines. At the dashed lines, the entropy S changes by log 2. For small K_z there is a single crossover at the single-impurity Kondo temperature T_K where the log 4 entropy is quenched in a single step to zero. This crossover splits into two when K_z approaches values of order T_K — then the two-stage quenching of the entropy described above is observed. In this regime the upper crossover temperature, T_0, is associated with the formation of the magnetic mini-domain where relative fluctuations of the two impurity spins are frozen out. The lower crossover temperature is the collective energy scale T^* below which the pseudospin of the mini-domain is screened. Generally, for a Kosterlitz–Thouless transition this energy scale vanishes exponentially upon approaching the phase transition,

$$T^* \sim T_0 \, e^{-\mathcal{A}/\sqrt{|K_z^{cr} - K_z|}} \qquad (7.56)$$

where $\mathcal{A}$ is a function of T_K. For $K_z \geq K_z^{cr}$ another crossover happens at a temperature scale $T_{\rm cross}$ (7.52), which however has much weaker signatures. Here the character of the leading corrections to the entropy and other quantities changes. For a more detailed discussion of these corrections we refer the reader to Section 7.6. This crossover scale $T_{\rm cross}$ also vanishes exponentially near the critical coupling K_z^{cr}. For large K_z the entropy change from log 4 to log 2 occurs around $T \sim K_z$, and therefore T_0 approaches K_z in this limit.

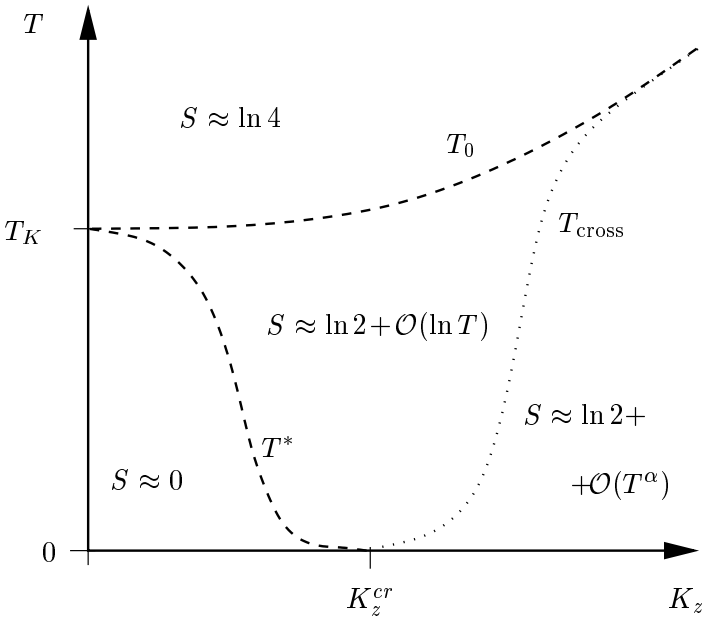

Figure 7.9: *Quantum phase diagram in the K_z–T plane.*

7.5 Symmetries and perturbations

To what extent do the results presented in the previous sections depend on the details of the models under consideration? To answer this question we will investigate whether and how (small) perturbations of (7.1) qualitatively change the physics. Fermi-liquid phases with vanishing residual entropy are stable against small perturbations, but this is not necessarily the case for our "frozen mini-domain" characterized by a residual entropy of log 2. The existence of this log 2 phase is a fundamental feature of the mini-domain model (7.1), giving rise to a quantum phase transition. Indeed the general mini-domain model (5.8) was suitably reduced in this chapter with the two assumptions mentioned in the introduction — (a) $K_\perp = 0$ and (b) uncorrelated electronic baths — in order to achieve exactly this stability. In the following we will discuss the necessary conditions for these assumptions to hold.

Let us start by considering the effect of a magnetic field in the z-direction acting on the impurity spins. A staggered magnetic field, $h_s(S_L^z - S_R^z)$, will directly destroy the degeneracy of the two antiferromagnetic configurations, $|\uparrow\downarrow\rangle$ and $|\downarrow\uparrow\rangle$. A homogeneous magnetic field $h(S_L^z + S_R^z)$, on the other hand, will not destroy the log 2 phase. It is interesting how these terms modify the generalized Anderson model (7.15). The magnetic field h results in a term $h\sum_{\sigma=\Uparrow,\Downarrow} d_\sigma^\dagger d_\sigma$ which breaks particle–hole symmetry in the generalized Anderson model and therefore modifies only the position of the phase boundary. However, the staggered magnetic field h_s leads to a term $h_s\sum_{\sigma=\Uparrow,\Downarrow}\sigma d_\sigma^\dagger d_\sigma$ which corresponds to a (pseudo-)magnetic field acting on the pseudospin of the Anderson model. Only the staggered magnetic field is a relevant perturbation destroying the log 2 phase.

Apart from these magnetic fields in the z-direction there are other relevant terms which lift the two-fold degeneracy and which have the forms:

$$S_j^+ \qquad j = L, R, \tag{7.57}$$

$$S_L^+ S_R^-\,, \tag{7.58}$$

$$S_L^+ S_R^- \Psi_{i\sigma}^\dagger \Psi_{j\sigma} \qquad i, j = L, R, \tag{7.59}$$

$$S_L^+ S_R^- \Psi_{i\alpha}^\dagger \boldsymbol{\sigma}_{\alpha\beta} \Psi_{j\beta} \qquad i, j = L, R \tag{7.60}$$

and their hermitian conjugates. It turns out that all these operators are forbidden if we impose the following two symmetry conditions: the model should be invariant under the two *separate* spin rotations of each impurity and its electronic bath about an angle of π, i.e., under the transformation

$$U_j = \mathrm{e}^{i\pi I_j^z} \tag{7.61}$$

with $j = L, R$. I_j^z is the z-component of total spin of sub-system j, $I_j^z = S_j^z + \sum_k c_{k\alpha j}^\dagger \frac{1}{2}\sigma_{\alpha\beta}^z c_{k\beta j}$. In the presence of these π-rotation symmetries, U_j, the terms (7.57) – (7.60) are absent and the frozen mini-domain phase survives. The quantum phase transition from the frozen mini-domain with residual entropy log 2 to the phase of Kondo screened impurities therefore just relies on the symmetries U_L and U_R (in the absence of a staggered magnetic field).

The model (7.1) considered here possesses by construction symmetries beyond U_j. They are not necessary for the stability of the log 2 phase. For example, the two baths are assumed to have the same Kondo coupling J_n. This parity symmetry can be relaxed without destroying the frozen mini-domain phase. Furthermore, the z-component of spin of each system, I_j^z, is conserved in our model since we chose $J_x = J_y = J_\perp$. This symmetry can also be perturbed without lifting the two-fold degeneracy. Moreover, the frozen mini-domain phase is stable against breaking of the particle-hole symmetry which we implicitly assumed in the bosonization treatment when we linearized the dispersion relation of the conduction electrons. In all these situations, we therefore expect that all of the *qualitative* results, i.e., the structure of the phase diagram and the nature of the quantum phase transition, are unaffected.

However, any perturbation which breaks either U_L or U_R (or both) will generically generate one of the relevant couplings (7.57–7.60) which all destroy the log 2 phase. In the following we briefly discuss two such cases which are likely to occur in experimental realizations.

Let us relax assumption (a), i.e. consider a situation where a small spin-flip coupling (7.58) is added on top of the large Ising interaction of the spins,

$$\delta H_{LR}^\perp = K_\perp \left(S_L^x S_R^x + S_L^y S_R^y\right)\,. \tag{7.62}$$

In realizations of our model based on spins and strongly anisotropic spin-orbit interactions — as we originally had in mind, see Section 5.1 — such a term will always be present. A small $K_\perp$ will immediately lead to a tunneling between the two pseudospin configurations of the mini-domain: their degeneracy is lifted, the two spins form a singlet and the log 2 residual entropy is quenched completely.

Two-impurity Kondo models with $K_\perp = K_z$ have been widely studied — see the short review in Section 5.3. As argued in Refs. [57, 59] the resulting phase diagram depends on the presence or absence of particle–hole symmetry (which, however, does *not* modify the phase diagram for $K_\perp = 0$ as pointed out above). In the absence of particle–hole symmetry the phase transition at $K_\perp = 0$ is replaced by a smooth crossover. However, in the presence of particle–hole symmetry, the scattering phase shifts of the electrons can only take the values 0 or $\pi/2$. As the Kondo-screened phase and the inter-impurity singlet phase have different phase shifts, there has to be a phase transition in between. This transition is *not* of Kosterlitz–Thouless type, but is characterized [59, 60, 61, 62] by a critical fixed point associated with a residual entropy of $\log\sqrt{2}$. Nevertheless, this transition will merge with ours in the limit $K_\perp \to 0$, as an infinitesimal $K_\perp$ does not affect the Kondo-screened phase but leads immediately to the formation of an inter-impurity singlet in the frozen mini-domain phase.

Now let us dispense with assumption (b), which means allowing for a coupling between the two Fermi seas, e.g., by tunneling between the two leads

$$\delta H_{LR}^{\text{tunneling}} = \sum_{k,k',\alpha} \left(t_{kk'} : c^\dagger_{k\alpha L} c_{k'\alpha R} : + \text{h.c.} \right) . \tag{7.63}$$

While this term is not relevant by power counting, it will induce an RKKY interaction between the spins and therefore generate the relevant coupling (7.59) and (7.58) or (7.62). As such a term also breaks particle–hole symmetry, the quantum phase transition will be replaced by a smooth crossover.

7.6 Experimental implications: transport

In this section we discuss how the phase diagram and, more importantly, the corresponding quantum phase transition can be revealed in transport experiments. What is the most characteristic signature of the Kosterlitz–Thouless quantum phase transition which we found happens in the mini-domain model (7.1)?

The most famous example of a Kosterlitz–Thouless transition is probably the vortex binding–unbinding transition in superfluid ^{4}He films [79]. This transition is governed by the same RG flow, see Fig. 7.10. When a path is taken in parameter space similar to the one shown by the dashed line in Fig. 7.10 a vortex binding–unbinding transition takes place. Starting on the left hand side the RG flow is towards a *line* of fixed points corresponding to a superfluid with a certain value of the superfluid density ρ_s/T depending on the initial conditions. Directly at the phase transition indicated by the black dot the parameter flow is towards a critical, universal value [13] of the superfluid density ρ_s^{cr}/T_c before it vanishes becoming a normal fluid. The vortex binding–unbinding transition is therefore characterized by a universal jump of the superfluid density at the phase transition from ρ_s^{cr}/T_c to zero. This is impressively confirmed by experiments as shown in the left panel of Fig. 7.10.

Interestingly, the analogue of the superfluid density in the mini-domain model is the scattering phase shift δ of the conduction electrons, and the arguments for a universal jump in

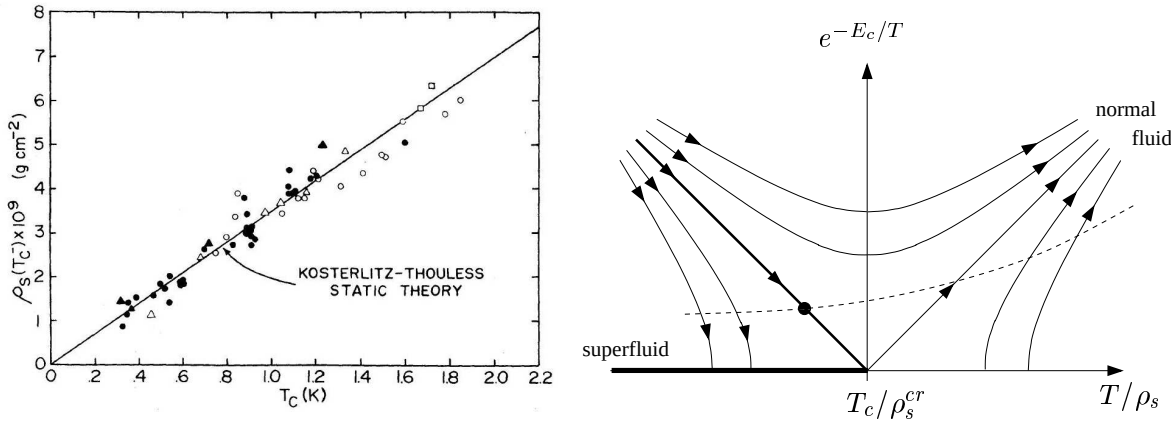

Figure 7.10: *Left panel: Jump discontinuities in the superfluid density versus critical temperature for over 70 different experiments on ^{4}He films for different substrates and film thickness [80]. Right panel: Kosterlitz–Thouless flow governing the vortex binding–unbinding transition in ^{4}He films. E_c is the core energy of a vortex. The dashed line represents a possible path in parameter space; the quantum phase transition occurs at the black dot. At the transition the superfluid density jumps from the critical value $\rho_s^{cr}/T_c = 3.491 \times 10^{-9}$ g cm^{-2} K^{-1} to zero giving rise to the universal slope in the graph of the left panel.*

the superfluid density carry over to a universal jump in δ. Let us recall the analysis of the effective low-energy theory in Section 7.3, especially its RG flow diagram Fig. 7.4. In the "frozen mini-domain" phase the system flows towards a *line* of fixed points and the fixed point value of the Kondo coupling J_z and the associated phase shift δ increase continuously upon approaching the phase boundary. Directly at the phase transition the fixed point value of the phase shift acquires the Toulouse value $\delta_T = \pi/2(1 - 1/\sqrt{2})$. After crossing the phase boundary, however, the physics is controlled by a *single* strong coupling fixed point which corresponds to the unitary limit $\delta = \pi/2$. At the Kosterlitz–Thouless quantum phase transition the phase shift therefore undergoes the universal jump from δ_T to $\pi/2$! The analysis presented in Section 7.3 was confined to the vicinity of the Toulouse point. However, universality demands that the phase shift, which is a measurable low-energy property of the model, jumps by the same value along the whole phase boundary of the phase diagram, Fig. 7.6, given that no further fixed point is intervening. That the latter does not happen was shown by the NRG calculations.

We shall show in the following that depending on the type of experiment the universal jump of the phase shift results in either a universal fractional critical conductance or a characteristic zero-bias anomaly.

7.6.1 Universal conductance of Ising-coupled quantum dots

Consider first the experimental set-up sketched in the left panel of Fig. 7.11 where the conductance through the left dot is measured. The linear conductance can be obtained from the Kubo formula [81],

$$G = \lim_{\omega \to 0} \frac{e^2}{\hbar} \frac{1}{\omega} \int_0^\infty dt\, e^{i\omega t} \langle [j(t), j(0)] \rangle \,, \tag{7.64}$$

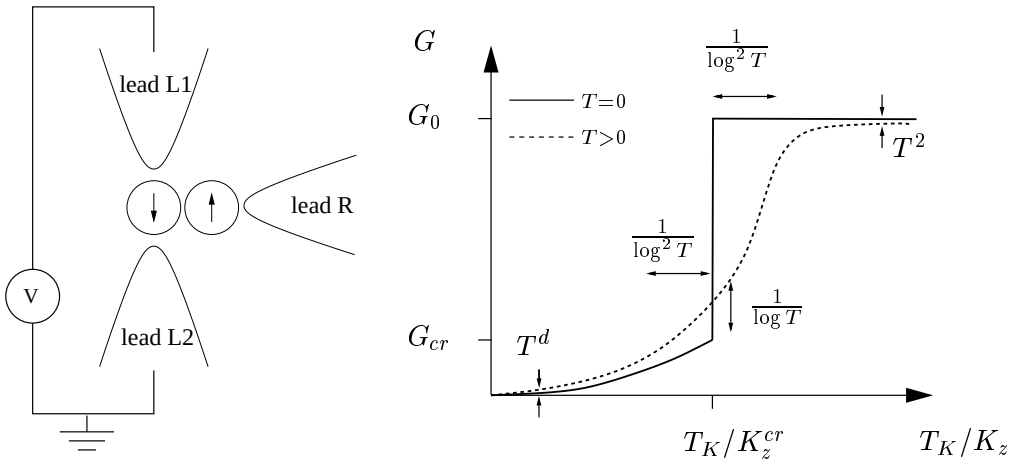

Figure 7.11: *Left panel: Experimental set-up to measure the conductance through a single dot. Right panel: At T=0 (solid line), the conductance takes the universal value* $G_{cr} = G_0 \cos^2 \frac{\pi}{2\sqrt{2}}$*, (7.66), at the quantum phase transition. Dashed line: schematic plot of the conductance at finite* T*. Corrections to the* $T = 0$ *result are logarithmic at the transition. The exponent* $d \equiv 2\dim[\mathcal{H}_{\rm eff}^{\rm flip}] - 2 = 8(\frac{2\delta}{\pi} - \frac{2\delta_T}{\pi})^2 - 8(\frac{2\delta}{\pi} - \frac{2\delta_T}{\pi})$ *is given by the dimension of the domain flip term (7.4).*

where the current operator is given by $j(t) = \frac{d}{dt}\frac{1}{2}\left(\hat{N}_{L1} - \hat{N}_{L2}\right)$. The operator $\hat{N}_{Lj}$ counts the total number of electrons in the upper (L1) and lower (L2) left lead. The linear conductance through the left dot is given exclusively in terms of the electron degrees of freedom which are coupled to the local moment on the dot, i.e. which participate in the Kondo effect [81]. If Kondo screening prevails, (in the case of a symmetric coupling of the leads to the dot) the conductance for $T \to 0$ will be given by the conductance quantum $G_0 = 2e^2/(2\pi\hbar)$ [81]. In the frozen mini-domain phase on the other side of the phase diagram, spin flips are completely suppressed for $T \to 0$ and therefore we can assume a *static* spin configuration to calculate $G(T = 0)$. For such a potential scattering problem, the conductance is given by [81]

$$G(T = 0) = G_0 \sin^2 \delta \,. \tag{7.65}$$

Directly at the quantum phase transition, the conductance therefore takes the universal value

$$G_{cr}(T = 0) = G_0 \sin^2 \delta_T = G_0 \cos^2 \left[\frac{\pi}{2\sqrt{2}}\right] \approx 0.197\, G_0 \,, \tag{7.66}$$

and it jumps to the Kondo value G_0 upon entering the Kondo-screened phase. This universal fractional conductance at the quantum phase transition is one of the remarkable features of the mini-domain model (7.1).

It is interesting to compare this to the well-known result for the usual Kondo effect, where the conductance jumps from 0 to G_0 when the exchange coupling J is tuned from ferromagnetic to antiferromagnetic. In Section 7.2.3 we found that the effective theory describing the quantum phase transition is just such a Kondo model, but the fermionic degrees of freedom in this effective Kondo model (7.34) are complicated *solitonic* excitations in terms of the original fermions. While the phase shift of these solitons vanishes at the quantum phase transition, the phase shift of the *physical* electrons takes the fractional value δ_T leading to a fractional conductance.

In the right panel of Fig. 7.11 the zero-temperature conductance close to the phase transition is shown. At any finite temperatures, the jump in the conductance is strongly smeared as sketched schematically in the figure. There are different crossover scales which we have already discussed in the context of the temperature dependence of the entropy, see Fig. 7.9. The T-dependence at lowest temperature is determined by the dimension of the leading irrelevant operators. In the Kondo-screened phase, $\delta \gg \delta_T$, the leading corrections for $T \to 0$ to the Kondo conductance G_0 are Fermi-liquid like and of order $(T/T^*)^2$ for $T \ll T^*$. Here T^* is the solitonic Kondo temperature (7.50) and is exponentially small close to the quantum phase transition. However, at a temperature of order T^*,

$$T \sim T^* \simeq \mathcal{A} \exp\left[-\frac{\mathcal{B}}{\sqrt{\frac{T_K}{K_z} - \frac{T_K}{K_z^{cr}}}}\right] \qquad \Rightarrow \qquad \frac{T_K}{K_z} - \frac{T_K}{K_z^{cr}} \sim \frac{\mathcal{B}^2}{\log^2 \mathcal{A}/T}\,, \tag{7.67}$$

logarithmic temperature corrections take over. (The quantities $\mathcal{A}$ and $\mathcal{B}$ depend on the Ising coupling K_z and on the single impurity Kondo temperature T_K.) According to the poor man's scaling equations (7.37) the strong coupling limit, $\mathcal{J}\rho \sim 1$, is only reached when the energy cutoff has rescaled to a value of the order of T^*. If, however, the RG flow is stopped at a temperature $T > T^*$. Then the effective couplings are rather of order

$$\mathcal{J}(T)\rho \sim \frac{1}{\log T/T^*}\,. \tag{7.68}$$

This leads to a correction of the phase shift δ and, as consequence, a temperature correction to the conductance of order $\frac{1}{\log T/T^*}$. The same holds true in the frozen mini-domain phase near the transition where the correction is of order $\frac{1}{\log T/T_{\rm cross}}$ with the crossover temperature $T_{\rm cross}$ defined in (7.52). On the other hand, deep in the frozen mini-domain phase the current operator j can be calculated perturbatively in the single-impurity Kondo couplings. The leading contribution stems from the collective mini-domain flip and is of order $j \sim \mathcal{O}(J_\perp^2)$ and therefore carries the same scaling dimension as the domain flip operator $\mathcal{H}_{\rm eff}^{\rm flip}$ (7.4). Putting this into the Kubo formula we obtain the scaling dimension of the associated conductance $\dim[G] = 2\dim[j] - 2 = 2\dim[\mathcal{H}_{\rm eff}^{\rm flip}] - 2$. Hence, the temperature correction deep in the frozen mini-domain phase is given by

$$G(T) \propto T^{2\dim[\mathcal{H}_{\rm eff}^{\rm flip}]-2} = T^{8(\frac{2\delta}{\pi} - \frac{2\delta_T}{\pi})^2 - 8(\frac{2\delta}{\pi} - \frac{2\delta_T}{\pi})}\,. \tag{7.69}$$

In the set-up considered here, Fig. 7.11, the mini-domain consists of real spins and a perpendicular direct coupling, $K_\perp$, will always be present in contrast to the assumptions on which the mini-domain model (7.1) is based. All the above considerations are therefore only valid for temperatures large enough that the splitting of the antiferromagnetic doublet, Fig. 5.1, is not yet resolved. This might appear too academic. Nevertheless, the Kosterlitz–Thouless phase transition gives rise to a remarkable universal fractional conductance in this experiment and this may serve as an illustration that a quantum phase transition might be a possible mechanism for the generation of non-integer conductance features in nanostructures, such as the infamous 0.7 conductance anomaly [82] observed in quantum point contacts.

7.6.2 Zero-bias anomaly of capacitively coupled quantum dots

The model is probably most easily experimentally realized in a system of two capacitively coupled quantum dots. The electron–electron interaction has a dramatic effect on small

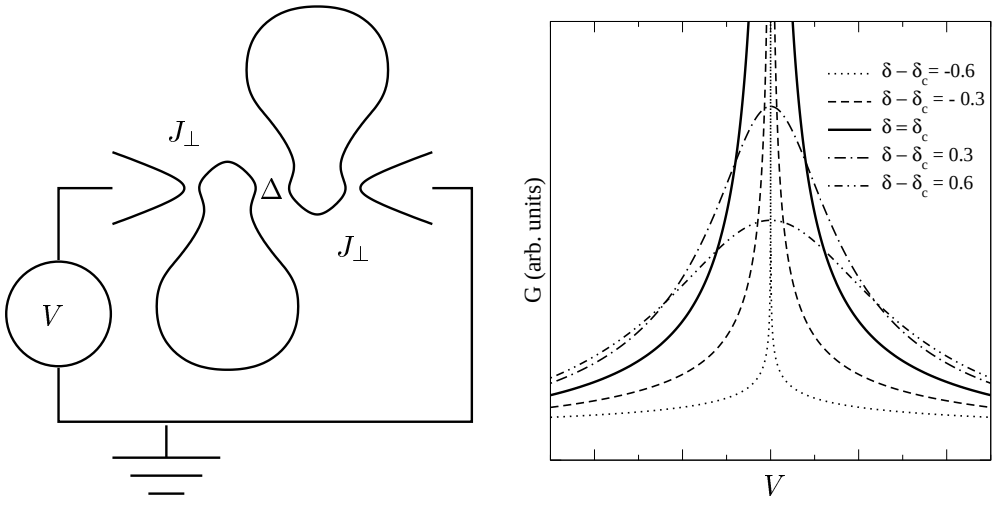

Figure 7.12: *Left panel: Experimental set-up to measure the tunneling conductance between two charge coupled quantum dots. To observe the conductance anomaly the contacts have to be sufficiently close. Right panel: Schematic plot of the zero bias anomaly of the conductance at $T = 0$. In the "frozen mini-domain" phase, $\delta < \delta_c$, the conductance diverges algebraically according to (7.73). At the quantum phase transition, $\delta = \delta_c$, the exponent takes the universal value $-2(\sqrt{2} - 1)$ according to (7.74). In the Kondo screened phase, $\delta > \delta_c$, the conductance is finite for $V \to 0$.*

quantum dots. It manifests itself in a charging energy $E_Q = (Q - CV_G)^2/(2C)$, where C is the capacitance and Q the charge of a dot and V_G is the gate voltage. The number of electrons in the ground state of a quantum dot can be controlled by the gate voltage V_G. For $CV_G = n + 1/2$ the two ground states with n and $n + 1$ electrons on the dot are degenerate, and at such a degeneracy point the ground state of each dot can be described by an effective pseudospin S. It was realized by Matveev [83, 84] that an additional coupling of a dot to a lead at the degeneracy point leads to an effective anisotropic Kondo model in the case of spinless fermions. The electrons carry pseudospin up if they belong to the lead, and pseudospin down if they are located on the dot. Electrons can be considered as spinless if for example the dot is placed in a sufficiently strong magnetic field so that one spin component decouples from the low-energy physics of the problem, or, alternatively, strong spin-orbit scattering mixes the spin channels separating energetically one effective channel by the spin-orbit energy scale. We would now like to consider two such dot–lead systems both tuned to their respective degeneracy points. If the two dots are capacitively coupled this interaction takes the form of pure Ising interaction in the language of pseudospins, S_L and S_R. The capacitatively coupled charge boxes are just described by the mini-domain model (7.1). This experimental realization has already been suggested by N. Andrei *et al.* [9].

In this realization using *charge* states the conductance is not easily measured. We propose instead another experiment, sketched in Fig. 7.12. We assume that in addition to the strong capacitive coupling K_z the two dots are coupled by weak tunneling Δ. In the Matveev language this tunneling term takes the form

$$H_{\rm tun} = \Delta\, S_L^+ S_R^- c_{\downarrow L}^\dagger c_{\downarrow R} + \text{h.c.} \tag{7.70}$$

It will be crucial in the following that the tunneling is into the electronic degrees of freedom,

$c_{\sigma i}$, which also participate in the single-impurity Kondo effect (7.2). For this to be the case the distance between the contacts has to be sufficiently small, as indicated in Fig. 7.12.

We calculate the conductance in perturbation theory in the inter-dot tunneling Δ. We first consider the "frozen mini-domain" phase. Following the arguments given in Section 7.1, the dimension of the tunneling term (or equivalently of the current operator) with respect to the "frozen mini-domain" fixed point is given by

$$\dim[H_{\rm tun}] = \left(\frac{2\delta}{\pi}\right)^2 + \left(1 - \frac{2\delta}{\pi}\right)^2 . \tag{7.71}$$

This is smaller than 1, i.e. it is a *relevant* perturbation to the mini-domain Hamiltonian. At this stage it is essential that the electrons involved in tunneling also participate in the single-impurity Kondo effect. If this were not the case the scaling dimension would rather be $\dim[H_{\rm tun}] = 2(\frac{2\delta}{\pi})^2 + 1$ missing the composite character between impurity spin and conduction electrons rendering the tunneling perturbation irrelevant.

Similar arguments to those in the previous section yield for the conductance

$$G(T) \sim \Delta^2\, T^{2\dim[H_{\rm tun}]-2} = \Delta^2\, T^{-4\frac{2\delta}{\pi}\left(1-\frac{2\delta}{\pi}\right)} . \tag{7.72}$$

This divergence of the conductance arises because the tunneling is a *relevant* perturbation which will finally destroy the "frozen mini-domain" phase and quench its residual entropy $\log 2$ below some small energy scale. Eq. (7.72) is therefore only valid for sufficiently small Δ, when this energy scale is smaller than the temperature T. Furthermore, a finite domain-flip rate induced by (7.4) is required to obtain a finite current. Above we implicitly assumed that Δ is so small that it determines the bottleneck for charge transport.

At finite voltage $V \gg T$, T in (7.72) can be replaced by V and we expect a zero-bias anomaly characterized by a pronounced peak in the conductance:

$$G(V) \sim |V|^{-4\frac{2\delta}{\pi}\left(1-\frac{2\delta}{\pi}\right)} . \tag{7.73}$$

As the quantum phase transition is approached, the divergence increases and at the Kosterlitz–Thouless transition it takes the universal form

$$G_{cr}(T) \sim T^{-2(\sqrt{2}-1)} \approx T^{-0.83} , \tag{7.74}$$

$$G_{cr}(V) \sim |V|^{-2(\sqrt{2}-1)} \approx |V|^{-0.83} \tag{7.75}$$

up to logarithmic corrections.

In the Kondo-screened Fermi liquid phase, the scaling dimension of the tunneling Hamiltonian (7.70) will be marginal, leading to a constant contribution to the conductance below the characteristic temperature scale T^*

$$G(V) \approx G(T) \approx \text{const.} \tag{7.76}$$

In Fig. 7.12 we show schematically the nonlinear conductance as a function of voltage, V, in the vicinity of the quantum phase transition.

In contrast to (7.72) and (7.76), N. Andrei *et al.* [9] obtained an exponentially small conductance in the "frozen mini-domain" phase and $G \sim T^4$ in the Fermi liquid phase, which we believe are incorrect.

7.7 Discussion

We have considered the model (7.1) of two local moments coupled by an Ising interaction K_z, where each local moment is in addition coupled to its own fermionic bath via a Kondo interaction with the associated energy scale T_K. This model exhibits a quantum phase transition.

We have derived the effective theory near the phase transition, which turned out to be an effective Kondo model. As a consequence, we were able to conclude that the quantum phase transition belongs to the Kosterlitz–Thouless universality class. In deriving the effective model we made use of a special point in parameter space known as the Toulouse point which turned out to be part of the phase boundary. We applied a Schrieffer–Wolff transformation in the time domain to capture power-law renormalizations of the effective Kondo couplings arising from an orthogonality catastrophe in the high-energy sector. This was necessary in order to obtain a universal effective Kondo theory independent of the cutoff structure of the original high-energy theory (7.1). The Kondo pseudospin degree of freedom was shown to correspond to the degenerate configurations of a magnetic mini-domain. Interestingly, the fermionic degrees of freedom of the effective Kondo model are solitonic spin excitations of the conduction electrons.

The following physical picture of the quantum phase transition emerged. For energies larger than the Ising interaction K_z the two local moments fluctuate independently. At an energy scale of order of K_z a well-defined mini-domain forms. Consequently, for lower energies the two local moments fluctuate in a correlated fashion. This dynamics is described by the above mentioned effective Kondo model. The quantum phase transition is now associated with the fate of this fluctuating mini-domain. The control parameter is the ratio of the Ising interaction K_z and the Kondo temperature T_K of a single impurity. For $T_K \ll K_z$ the fluctuations freeze out at lowest energies and the mini-domain is locked in one of the two degenerate configurations, giving rise to a residual entropy of log 2. For $T_K \gg K_z$, however, the mini-domain undergoes a cluster Kondo effect, being screened by collective spin excitations of the two conduction Fermi seas.

Due to the solitonic nature of the fermionic degrees of freedom involved in the collective Kondo effect the phase shift of the conduction electrons jumps at the phase transition from $\pi/2(1-1/\sqrt{2})$ to $\pi/2$. This universal jump in the phase shift is the analogue of the universal jump in the superfluid densities at the vortex binding–unbinding transition in superfluid ^{4}He films. The universal jump in the phase shift would give rise to characteristic signatures in transport experiments, such as a universal jump in the conductance or a characteristic zero-bias anomaly.

Appendix B

B.1 Unitary transformation: absorption of a minus sign

In this appendix it will be shown explicitly that the Hamiltonian (6.50) can be transformed to (6.53) by the unitary transformation

$$D \equiv e^A = \exp\{\, i\, \frac{\pi}{2} \sum_{k'} \Psi^\dagger_{k'\alpha'\chi'}\, \frac{1}{2}(1-\sigma^3_{\alpha'\beta'})\kappa^3_{\chi'\mu'}\, \Psi_{k'\beta'\mu'}\}\,. \tag{B.1}$$

The diagonal part H_0 and the pseudospin-Zeeman splitting in (6.50) remain invariant under the rotation D. Only the term containing the pseudospin-Kondo coupling will be affected by D. Due to the structure of the coupling matrix $\mathcal{J}^i_{mn}(k,q)$, cf. (6.51), the pseudospin-Kondo coupling consists only of the following operators

$$\Psi^\dagger_{k\alpha\chi}\, \kappa^m_{\chi\mu}\, \Psi_{q\alpha\mu} \qquad \text{where} \quad m = 0 \text{ or } 3\,, \tag{B.2}$$

$$\Psi^\dagger_{k\alpha\chi}\, \sigma^3_{\alpha\beta}\, \kappa^m_{\chi\mu}\, \Psi_{q\beta\mu} \qquad \text{where} \quad m = 1 \text{ or } 2\,, \tag{B.3}$$

where a summation over the spin and pseudospin indices is implied, however not over the momenta. To evaluate the transformation of these operators we will use the Baker-Haussdorff formula which reads

$$DBD^\dagger = e^A\, B\, e^{-A} = \sum_{n=0}^{\infty} \frac{1}{n!}\, [A,B]_n\ , \tag{B.4}$$

where $[A,B]_{n+1} = [A,[A,B]_n]$ and $[A,B]_0 = B$. The operator B is one of the two operators, (B.2) or (B.3). First we calculate the required commutators.

1. $B = \Psi^\dagger_{k\alpha\chi}\, \kappa^m_{\chi\mu}\, \Psi_{q\alpha\mu}$
   In this case the commutator of A and B vanishes for $m = 0$ or 3,

   $$[A,B] = [A, \Psi^\dagger_{k\alpha\chi}\, \kappa^m_{\chi\mu}\, \Psi_{q\alpha\mu}] = 0 \qquad \text{if} \quad m = 0 \text{ or } 3\,, \tag{B.5}$$

   so that B remains invariant under D.

2. $B = \Psi^\dagger_{k\alpha\chi}\, \sigma^3_{\alpha\beta}\, \kappa^m_{\chi\mu}\, \Psi_{q\beta\mu}$
   The index m is understood to be either 1 or 2. In this case the commutators read

   $$[A,B]_1 \;=\; -\pi\ \Psi^\dagger_{k\alpha\chi}\, \frac{1}{2}(1-\sigma^3_{\alpha\beta})\epsilon^{m3l}\kappa^l_{\chi\mu}\, \Psi_{q\beta\mu} \tag{B.6}$$

   $$[A,B]_2 \;=\; \pi^2\ \Psi^\dagger_{k\alpha\chi}\, \frac{1}{2}(1-\sigma^3_{\alpha\beta})\kappa^m_{\chi\mu}\, \Psi_{q\beta\mu} \tag{B.7}$$

   $$[A,B]_{n+2} \;=\; -\pi^2\ [A,B]_n \tag{B.8}$$

Inserted into the Baker–Hausdorff formula this gives

$$DBD^\dagger = B + \sum_{n=1}^{\infty} \frac{1}{(2n)!} [A,B]_{2n} + \sum_{n=0}^{\infty} \frac{1}{(2n+1)!} [A,B]_{2n+1} \tag{B.9}$$

$$= B + \sum_{n=1}^{\infty} \frac{1}{(2n)!} (-\pi^2)^{n-1} [A,B]_2 + \sum_{n=0}^{\infty} \frac{1}{(2n+1)!} (-\pi^2)^n [A,B]_1 \tag{B.10}$$

$$= B + 2\,\pi^{-2}\ [A,B]_2 = \Psi^\dagger_{k\alpha\chi}\, \kappa^m_{\chi\mu}\, \Psi_{q\alpha\mu} \tag{B.11}$$

With the transformation D we can therefore eliminate the coupling to the σ^3 component. Consequently, the relative minus sign between the spin-up and spin-down components is removed and we end up with the effective Hamiltonian (6.53).

B.2 Symmetries of the effective mini-domain Hamiltonian

We would like to consider which kind of constraints on the parameters of the effective Hamiltonian (6.53) are posed by symmetries. However, in order to avoid a discussion of the symmetry properties of the rotation operator D, (6.52), which was applied to obtain the effective Hamiltonian, we will rather consider the preliminary effective Hamiltonian (6.50)

$$\bar{\mathcal{H}} = H_0 + \sum_{kq} \mathcal{J}^i_{mn}(k,q)\ :\Psi^\dagger_{k\alpha\chi}\, \sigma^i_{\alpha\beta}\, \kappa^m_{\chi\mu}\, \Psi_{q\beta\mu}: \frac{\tau^n}{2} + (K_\perp + h_\perp)\, \frac{\tau^3}{2}\,. \tag{B.12}$$

As explained in the text the symmetry properties of the coupling matrix of the effective Hamiltonian $\mathcal{J}_{mn}(k,q)$ follow straightforwardly from the those of $\mathcal{J}^i_{mn}(k,q)$.

1. **Hermiticity**
   From the condition that the Hamiltonian must be hermitian it follows that

   $$(\mathcal{J}^i_{mn})^*(k,q) = \mathcal{J}^i_{mn}(q,k)\,. \tag{B.13}$$

   In particular, if one neglects the momentum dependence the coupling matrix will be real.

2. **Conservation of the z-component of the total spin**
   The basis of our model was the assumption that the z-component of the total spin, $S^z(\mathbf{R}/2) + S^z(-\mathbf{R}/2) + \frac{1}{2}\sum_{\mathbf{k}\sigma} c^\dagger_{\mathbf{k}\alpha}\, \sigma^z_{\alpha\beta}\, c_{\mathbf{k}\beta}$, is conserved. The pseudospin of the mini-domain τ commutes with $S^z(\mathbf{R}/2) + S^z(-\mathbf{R}/2)$ by construction, so the conservation of the z-component of spin reduces to the condition

   $$[\bar{\mathcal{H}}, \sum_{\mathbf{k}\sigma} c^\dagger_{\mathbf{k}\alpha}\, \sigma^z_{\alpha\beta}\, c_{\mathbf{k}\beta}] = 0\,, \tag{B.14}$$

   from which one derives the condition on the coupling

   $$\mathcal{J}^i_{mn}(k,q) = 0 \qquad \text{for} \quad i = 1,2\,. \tag{B.15}$$

3. **Parity**
   According to (6.4) the pseudospin τ^n, $n = 0, 1, 2, 3$, transforms under parity as

$$\tau^n \longrightarrow (1 - 2\delta^{n1})(1 - 2\delta^{n2})\tau^n \,, \tag{B.16}$$

   where in this case no summation over the index n is implied. The electron operators transform under parity as (6.10)

$$\Psi_{q\alpha\mu} \longrightarrow \mu\Psi_{q\alpha\mu} \,. \tag{B.17}$$

   Invariance under parity yield the following condition on the coupling

$$\mathcal{J}^i_{mn}(k,q) = (1 - 2\delta^{n1})(1 - 2\delta^{n2})(1 - 2\delta^{m1})(1 - 2\delta^{m2})\mathcal{J}^i_{mn}(k,q) \,. \tag{B.18}$$

4. **Time-reversal symmetry**
   Using the transformation properties of the pseudospin (6.7) and of the electron operators under time-reversal,

$$\Psi_{q\alpha\mu} \longrightarrow i\mu\sigma^2_{\alpha\beta}\Psi_{q\beta\mu} \,, \tag{B.19}$$

   we obtain the condition on the coupling

$$(\mathcal{J}^i_{mn})^*(k,q) = (1 - 2\delta^{n1})(1 - 2\delta^{m1})(2\delta^{i0} - 1)J^i_{mn}(k,q) \,. \tag{B.20}$$

The coupling matrix at the Fermi momentum, $\mathcal{J}^i_{mn} \equiv \mathcal{J}^i_{mn}(k_\mathrm{F}, k_\mathrm{F})$, plays a special role in the analysis of the effective Hamiltonian since the deviations from it are irrelevant in the RG sense. From the requirement of hermiticity it follows that the coupling $\mathcal{J}^i_{mn}$ will be real. Moreover, spin conservation, parity and time-reversal symmetry demand that only the coefficients $\mathcal{J}^0_{11}, \mathcal{J}^0_{00}, \mathcal{J}^0_{03}, \mathcal{J}^0_{30}, \mathcal{J}^0_{33}$ and $\mathcal{J}^3_{12}, \mathcal{J}^3_{21}$ are non-vanishing. As outlined in Section 6.4 all these couplings except $\mathcal{J}^0_{11}$ are generated in the Schrieffer-Wolff transformation.

B.3 Effective parameters of the mini-domain Hamiltonian

B.3.1 Pseudomagnetic field

For $T = 0$ the pseudomagnetic field (6.54) reads

$$h_\perp = \frac{1}{\pi^4}\frac{J_\perp^2}{R^2}\int_0^{k_\mathrm{F}} \mathrm{dk} \int_{k_\mathrm{F}}^{\infty} \mathrm{dq} \frac{k\,q}{\epsilon_k - \epsilon_q - K_z/2} \sin(kR)\,\sin(qR) \,. \tag{B.21}$$

We will start by considering the case $k_\mathrm{F}R \ll 1$. To obtain the leading order in this limit we neglect the oscillatory part altogether. Furthermore, we introduce the density of states per spin

$$\rho(\epsilon - \epsilon_\mathrm{F}) = \frac{4\pi k^2}{(2\pi)^3}\frac{\mathrm{d}k}{\mathrm{d}(\epsilon - \epsilon_\mathrm{F})}. \tag{B.22}$$

and assume the density of states to be constant

$$\rho(\omega) = \rho\,\Theta(D^2 - \omega^2) \,, \tag{B.23}$$

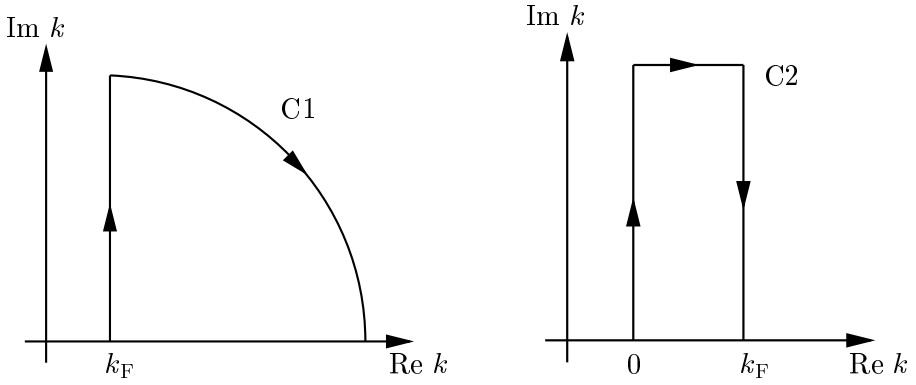

Figure B.1: *Stationary-phase integration contours. C1 is used for the integral I_1 and C2 for the integral I_2.*

where D is the cut-off of the band. We obtain the following estimate for the pseudomagnetic field

$$\begin{aligned}
h_\perp &\approx 4J_\perp^2 \int_{-\epsilon_\mathrm{F}}^{0} \mathrm{d}\omega_1 \int_{0}^{\infty} \mathrm{d}\omega_2 \frac{\rho(\omega_1)\rho(\omega_2)}{\omega_1 - \omega_2 - K_z/2} \\
&\approx 4(J_\perp \rho)^2 \int_{-D}^{0} \mathrm{d}\omega_1 \int_{0}^{D} \mathrm{d}\omega_2 \frac{1}{\omega_1 - \omega_2 - K_z/2} \\
&= -4(J_\perp \rho)^2 \left(K_z \log\left(\frac{K_z/2}{K_z/2 + D} \right) + (K_z + 4D) \log\left(\frac{K_z + 4D}{K_z + 2D} \right) \right) \\
&\approx -8(J_\perp \rho)^2 \begin{cases} D \log 2 & \text{if} \quad D \gg K_z \\ \frac{D^2}{K_z} & \text{if} \quad D \ll K_z \end{cases} \\
&\sim -8(J_\perp \rho)^2 \min\left\{ D, \frac{D^2}{K_z} \right\} \qquad \text{if} \quad k_\mathrm{F} R \ll 1 \,. \qquad \text{(B.24)}
\end{aligned}$$

The derivation in the limit $k_\mathrm{F} R \gg 1$ is more elaborate. We will use the method of steepest descent [85], for which we first have to deform the integration contours of the integrals in (B.21) to stationary phase contours. As a first step consider the integral

$$I_1 = \int_{k_\mathrm{F}}^{\infty} \mathrm{dq} \frac{q}{\epsilon_k - \epsilon_q - K_z/2} \sin(qR) = \frac{1}{2\,i} \int_{k_\mathrm{F}}^{\infty} \mathrm{dq} \frac{q}{\epsilon_k - \epsilon_q - K_z/2} \left(e^{iqR} - e^{-iqR} \right) \qquad \text{(B.25)}$$

The stationary-phase integration contour we use for this integral is shown in Fig. B.1. The contour C1 is needed for the first term of I_1 with the positive imaginary part in the exponent. For the second term with the negative imaginary part in the exponent we use the contour C1 reflected in the real axis. These contours together with the real axis do not enclose any singularity. Furthermore, the part over the quarter circle vanishes at infinity in each case and the integral I_1 becomes

$$I_1 = \frac{k_\mathrm{F}}{2} \int_{0}^{\infty} \mathrm{d}t \, e^{-k_\mathrm{F} R t} \left(\frac{k_\mathrm{F}(1+it)}{\epsilon_k - \epsilon_{k_\mathrm{F}(1+it)} - K_z/2} e^{ik_\mathrm{F} R} + \frac{k_\mathrm{F}(1-it)}{\epsilon_k - \epsilon_{k_\mathrm{F}(1-it)} - K_z/2} e^{-ik_\mathrm{F} R} \right) . \qquad \text{(B.26)}$$

We proceed analogously with the second integral. Consider

$$I_2 = \int_0^{k_\mathrm{F}} \mathrm{dk} \frac{k}{\epsilon_k - \epsilon_q - K_z/2} \sin(kR) = \frac{1}{2\,i} \int_0^{k_\mathrm{F}} \mathrm{dk} \frac{k}{\epsilon_k - \epsilon_q - K_z/2} \left(e^{ikR} - e^{-ikR} \right) . \tag{B.27}$$

We deform the integration along the contour C2 shown in Fig. B.1, and again for the negative imaginary exponent we use the contour reflected in the real axis. These contours do not surround any singularity, and the integral over the horizontal part vanishes at infinity. We are left with

$$\begin{aligned} I_2 &= \frac{k_\mathrm{F}}{2} \int_0^\infty \mathrm{d}u\, e^{-k_\mathrm{F} R u} \left(\left[\frac{i k_\mathrm{F} u}{\epsilon_{k_\mathrm{F} i u} - \epsilon_q - K_z/2} - \frac{k_\mathrm{F}(1+iu)}{\epsilon_{k_\mathrm{F}(1+iu)} - \epsilon_q - K_z/2} e^{i k_\mathrm{F} R} \right] \right. \\ &\quad \left. - \left[\frac{i k_\mathrm{F} u}{\epsilon_{-k_\mathrm{F} i u} - \epsilon_q - K_z/2} + \frac{k_\mathrm{F}(1-iu)}{\epsilon_{k_\mathrm{F}(1-iu)} - \epsilon_q - K_z/2} e^{-i k_\mathrm{F} R} \right] \right) . \end{aligned} \tag{B.28}$$

The electron energy, ϵ_k, is an even function of k which is ensured by the symmetries of our model, time-reversal invariance and parity symmetry, so the first and third term cancel each other.

Combining the results of both integrals we can rewrite the expression for the pseudomagnetic field (B.21). We obtain

$$\begin{aligned} h_\perp = -\frac{1}{2\pi^4} \frac{J_\perp^2 k_\mathrm{F}^4}{R^2} \mathrm{Re} \left\{ \int_0^\infty \mathrm{d}u\, \mathrm{d}t\, e^{-k_\mathrm{F} R(u+t)} \right. \\ \left. \times \left[\frac{(1+iu)(1+it)}{\epsilon_{k_\mathrm{F}(1+iu)} - \epsilon_{k_\mathrm{F}(1+it)} - K_z/2} e^{-i2k_\mathrm{F} R} + \frac{(1+iu)(1-it)}{\epsilon_{k_\mathrm{F}(1+iu)} - \epsilon_{k_\mathrm{F}(1-it)} - K_z/2} \right] \right\} \end{aligned} \tag{B.29}$$

So far we have not made use of any approximations. However, we have put the expression for $h_\perp$ into a form suitable for the application of the method of steepest descent in the limit $k_\mathrm{F} R \gg 1$. This will be done in the following. The exponential factor with the large $k_\mathrm{F} R$ in the exponent ensures that the term in the square brackets contributes only for small $(u+t)$. Since both integration variables, u and t, are positive it follows that the contribution is appreciable only if both u and t are small. So in order to obtain the leading contribution in $(k_\mathrm{F} R)^{-1}$ we expand the term in the square bracket in u and t simultaneously. It reads

$$\begin{aligned} h_\perp &\approx -\frac{1}{2\pi^4} \frac{J_\perp^2 k_\mathrm{F}^4}{R^2} \mathrm{Re} \left\{ \int_0^\infty \mathrm{du}\ \mathrm{dt}\, e^{-k_\mathrm{F} R(u+t)} \right. \\ &\quad \left. \times \left[\frac{1}{\mathrm{v_F} k_\mathrm{F} i(u-t) - K_z/2} e^{-i2k_\mathrm{F} R} + \frac{1}{\mathrm{v_F} k_\mathrm{F} i(u+t) - K_z/2} \right] \right\} \\ &= \frac{1}{2\pi^4} \frac{J_\perp^2 k_\mathrm{F}^2}{\mathrm{v_F} R^3} \mathrm{Re} \left\{ \int_0^\infty \mathrm{du}\ \mathrm{dt}\, e^{-(u+t)} \int_0^\infty \mathrm{d}\phi\, e^{-\frac{RK_z}{2\mathrm{v_F}}\phi} \left(e^{i(2k_\mathrm{F} R + (u-t)\phi)} + e^{i(u+t)\phi} \right) \right\} \\ &= (J_\perp \rho)^2 \frac{2\mathrm{v_F} k_\mathrm{F}}{(k_\mathrm{F} R)^3} \left(\cos(2k_\mathrm{F} R) - \alpha \frac{\partial}{\partial \alpha} \right) \mathcal{F}(\alpha) \Big|_{\alpha = \frac{RK_z}{2\mathrm{v_F}}} , \end{aligned} \tag{B.30}$$

where we have introduced the Fermi velocity $\mathrm{v_F} = d\epsilon(k_\mathrm{F})/dk$ and the density of states per spin at the Fermi energy $\rho = k_\mathrm{F}^2/(2\pi^2 \mathrm{v_F})$. Furthermore, the function $\mathcal{F}$ is defined as

$$\mathcal{F}(\alpha) = \int_0^\infty \mathrm{d}\phi \, e^{-\alpha\phi} \frac{1}{1+\phi^2} \,. \tag{B.31}$$

Due to the energy $K_z/2$ in the denominator, which is the energy difference between the antiferromagnetic and the ferromagnetic states, the result is dependent on the parameter $\alpha = RK_z/(2\mathrm{v_F})$. For small and large α the function $\mathcal{F}$ is approximately

$$\mathcal{F}(\alpha) = \begin{cases} \dfrac{1}{\alpha} - \dfrac{2}{\alpha^3} + \mathcal{O}(\dfrac{1}{\alpha^5}) \\ \dfrac{\pi}{2} + (\gamma - 1)\alpha + \alpha \log \alpha + \mathcal{O}(\alpha^2) \end{cases} \tag{B.32}$$

where $\gamma = 0.5772\ldots$ is the Euler constant. So we obtain finally for $h_\perp$ the leading contribution in $(k_\mathrm{F}R)^{-1}$ for small and large $\alpha = RK_z/(2\mathrm{v_F})$,

$$h_\perp \approx (J_\perp \rho)^2 \, \frac{2\mathrm{v_F} k_\mathrm{F}}{(k_\mathrm{F}R)^3} \begin{cases} \dfrac{2\cos^2(k_\mathrm{F}R)}{\alpha} + \mathcal{O}(\alpha^{-3}) \\ (\dfrac{\pi}{2} - \alpha)\cos(2k_\mathrm{F}R) + 2\,\alpha(\gamma + \log\alpha)\,\cos^2(k_\mathrm{F}R) + \mathcal{O}(\alpha^2) \end{cases} \tag{B.33}$$

It is interesting to note that the limit $\alpha \ll 1$ recovers the usual expression for the RKKY interaction. For large α the $\cos(2k_\mathrm{F}R)$ oscillation change into $\cos^2(k_\mathrm{F}R)$ oscillations.

B.3.2 Pseudospin Kondo coupling

Setting the momenta of the coupling matrix $\mathcal{J}(k,q)$ (6.51) equal to the Fermi momentum yields for the finite components

$$\begin{pmatrix} \mathcal{J}_{00} & \mathcal{J}_{03} \\ \mathcal{J}_{30} & \mathcal{J}_{33} \end{pmatrix} = \frac{4}{(2\pi)^4} J_\perp^2 \, k_\mathrm{F}^2 \sum_k k^2 \, \mathcal{G}^-_{k_\mathrm{F}k_\mathrm{F},k} \begin{pmatrix} 1 & \dfrac{\sin(k_\mathrm{F}R)}{k_\mathrm{F}R}\dfrac{\sin(kR)}{kR} \\ \dfrac{\sin(k_\mathrm{F}R)}{k_\mathrm{F}R} & \dfrac{\sin(kR)}{kR} \end{pmatrix} \tag{B.34}$$

$$\begin{aligned} \begin{pmatrix} \mathcal{J}_{11} & \mathcal{J}_{12} \\ \mathcal{J}_{21} & \mathcal{J}_{22} \end{pmatrix} =& \frac{1}{2\pi^2} J_z \, k_\mathrm{F}^2 \sqrt{1 - \left(\frac{\sin(k_\mathrm{F}R)}{k_\mathrm{F}R}\right)^2} \begin{pmatrix} 0 & 0 \\ 1 & 0 \end{pmatrix} \\ &+ \frac{4}{(2\pi)^4} J_\perp^2 \, k_\mathrm{F}^2 \sqrt{1 - \left(\frac{\sin(k_\mathrm{F}R)}{k_\mathrm{F}R}\right)^2} \sum_k k^2 \begin{pmatrix} 0 & -\dfrac{\sin(kR)}{kR}\mathcal{G}^-_{k_\mathrm{F}k_\mathrm{F},k} \\ -\mathcal{G}^+_{k_\mathrm{F}k_\mathrm{F},k} & 0 \end{pmatrix} \end{aligned} \tag{B.35}$$

It will be convenient to introduce the quantities S and A, which are essentially the integrals over $\mathcal{G}^+_{k_\mathrm{F}k_\mathrm{F},k}$ and $\mathcal{G}^-_{k_\mathrm{F}k_\mathrm{F},k}$ respectively. Therefore, S is particle–hole symmetric and A particle–

hole antisymmetric. At zero temperature we obtain the estimates

$$\begin{aligned} S &\equiv -\frac{1}{2\rho}\frac{4\pi}{(2\pi)^3}\int_0^\infty \mathrm{d}k\, k^2\, \mathcal{G}^+_{k_\mathrm{F}k_\mathrm{F},k} = -\frac{1}{2\rho}\int_{-\epsilon_\mathrm{F}}^\infty \mathrm{d}\omega\, \rho(\omega)\, \left(\frac{1-f(\omega)}{-\omega-K_z/2}+\frac{f(\omega)}{\omega-K_z/2}\right) \\ &\approx \int_{-\infty}^\infty \mathrm{d}\omega\, \frac{\rho(-\omega)+\rho(\omega)}{2\rho}\,\frac{f(\omega)}{K_z/2-\omega} \\ &\sim \int_{-D}^D \mathrm{d}\omega\, \frac{f(\omega)}{K_z/2-\omega} = \log\left(1+\frac{D}{K_z/2}\right) \end{aligned} \tag{B.36}$$

and

$$\begin{aligned} A &\equiv -\frac{1}{2\rho}\frac{4\pi}{(2\pi)^3}\int_0^\infty \mathrm{d}k\, k^2\, \mathcal{G}^-_{k_\mathrm{F}k_\mathrm{F},k} = \int_{-\epsilon_\mathrm{F}}^\infty \mathrm{d}\omega\, \frac{\rho(\omega)}{2\rho}\, \left(\frac{f(\omega)}{\omega-K_z/2}-\frac{1-f(\omega)}{-\omega-K_z/2}\right) \\ &\approx \int_{-\infty}^\infty \mathrm{d}\omega\, \frac{\rho(-\omega)-\rho(\omega)}{2\rho}\,\frac{f(\omega)}{K_z/2-\omega} \\ &\sim \frac{\rho'}{\rho}\int_{-D}^0 \mathrm{d}\omega\, \frac{\omega}{\omega-K_z/2} = \frac{\rho' D}{\rho}\left(1+\frac{K_z/2}{D}\log\left(\frac{K_z/2}{K_z/2+D}\right)\right) \\ &\approx \begin{cases} \frac{\rho' D}{\rho}\left(1+\frac{K_z}{2D}\log\left(\frac{K_z}{2D}\right)\right) & \text{if} \quad D \gg K_z \\ \frac{\rho'}{\rho}\frac{D^2}{K_z} & \text{if} \quad D \ll K_z\,. \end{cases} \end{aligned} \tag{B.37}$$

In the line indicated by $\sim$ we have assumed the density of states per spin to be

$$\rho(\omega) = (\rho + \rho'\,\omega)\,\Theta(D^2-\omega^2)\,, \tag{B.38}$$

where $\rho = k_\mathrm{F}^2/(2\pi^2 \mathrm{v}_\mathrm{F})$ is the density at the Fermi energy. Irrespective of the value of $k_\mathrm{F}R$ the components $\mathcal{J}_{00}$ and $\mathcal{J}_{30}$ are always proportional to A and therefore vanish exactly in the case of particle–hole symmetry.

To obtain an estimate in the limit of small $k_\mathrm{F}R$ we again neglect the oscillatory terms in the integrals. For $k_\mathrm{F}R \ll 1$ the leading order contribution reads

$$\begin{aligned} \begin{pmatrix} \mathcal{J}_{00} & \mathcal{J}_{03} \\ \mathcal{J}_{30} & \mathcal{J}_{33} \end{pmatrix} &= -\,2\mathrm{v}_\mathrm{F}(J_\perp\rho)^2 \begin{pmatrix} A & A+\mathcal{O}\left(k_\mathrm{F}R\right)^2 \\ A\left(1+\mathcal{O}\left(k_\mathrm{F}R\right)^2\right) & A+\mathcal{O}\left(k_\mathrm{F}R\right)^2 \end{pmatrix} \\ \begin{pmatrix} \mathcal{J}_{11} & \mathcal{J}_{12} \\ \mathcal{J}_{21} & \mathcal{J}_{22} \end{pmatrix} &= \mathrm{v}_\mathrm{F}(J_z\rho)\frac{k_\mathrm{F}R}{\sqrt{3}} \begin{pmatrix} 0 & 0 \\ 1+\mathcal{O}\left(k_\mathrm{F}R\right)^2 & 0 \end{pmatrix} \\ &\quad + 2\mathrm{v}_\mathrm{F}(J_\perp\rho)^2\,\frac{k_\mathrm{F}R}{\sqrt{3}} \begin{pmatrix} 0 & A+\mathcal{O}\left(k_\mathrm{F}R\right)^2 \\ S\left(1+\mathcal{O}\left(k_\mathrm{F}R\right)^2\right) & 0 \end{pmatrix}. \end{aligned} \tag{B.39}$$

In the other limit of large $k_\mathrm{F}R$ we again use the method of steepest descent analogous to the evaluation of $h_\perp$. Consider for example the component $\mathcal{J}_{33}$. Using the stationary-phase

integration contours of Fig. B.1 this integral can be rewritten as

$$\mathcal{J}_{33} = \frac{4}{(2\pi)^4} J_\perp^2 \, k_{\rm F}^2 \int\limits_0^\infty {\rm d}k \, k^2 \, \mathcal{G}^-_{k_{\rm F} k_{\rm F}, k} \frac{\sin(kR)}{kR} \tag{B.40}$$

$$= \frac{4}{(2\pi)^4} \frac{J_\perp^2 \, k_{\rm F}^5}{k_{\rm F} R} {\rm Re} \left\{ \int\limits_0^\infty {\rm d}u \, e^{-k_{\rm F} R \, u} \, e^{i k_{\rm F} R} \left(\frac{1+iu}{\epsilon_{\rm F} - \epsilon_{k_{\rm F}\,(1+iu)} - K_z/2} + \frac{1+iu}{\epsilon_{k_{\rm F}\,(1+iu)} - \epsilon_{\rm F} - K_z/2} \right) \right\} .$$

The leading contribution in $(k_{\rm F} R)^{-1}$ is obtained when the term in the brackets is expanded for small u:

$$\begin{aligned} \mathcal{J}_{33} &\approx \frac{4}{(2\pi)^4} \frac{J_\perp^2 \, k_{\rm F}^5}{k_{\rm F} R} {\rm Re} \left\{ \int\limits_0^\infty {\rm d}u \, e^{-k_{\rm F} R \, u} \, e^{i k_{\rm F} R} \left(\frac{1}{-{\rm v}_{\rm F} k_{\rm F} \, iu - K_z/2} + \frac{1}{{\rm v}_{\rm F} k_{\rm F} \, iu - K_z/2} \right) \right\} \\ &= -2{\rm v}_{\rm F} \, (J_\perp \rho)^2 \, \frac{\cos(k_{\rm F} R)}{k_{\rm F} R} \, \mathcal{F}(\alpha) \Big|_{\alpha \, = \, \frac{RK_z}{2{\rm v}_{\rm F}}} , \end{aligned} \tag{B.41}$$

where we again used the function $\mathcal{F}$ defined in (B.31) and $\rho = k_{\rm F}^2/(2\pi^2 {\rm v}_{\rm F})$ is the density of states at the Fermi energy. The other coupling components can be derived similarly and we get

$$\begin{pmatrix} \mathcal{J}_{00} & \mathcal{J}_{03} \\ \mathcal{J}_{30} & \mathcal{J}_{33} \end{pmatrix} \approx -2{\rm v}_{\rm F} \, (J_\perp \rho)^2 \begin{pmatrix} A & \frac{\sin(k_{\rm F} R)\cos(k_{\rm F} R)}{(k_{\rm F} R)^2} \mathcal{F}\left(\frac{RK_z}{2{\rm v}_{\rm F}}\right) \\ A \, \frac{\sin(k_{\rm F} R)}{k_{\rm F} R} & \frac{\cos(k_{\rm F} R)}{k_{\rm F} R} \mathcal{F}\left(\frac{RK_z}{2{\rm v}_{\rm F}}\right) \end{pmatrix} \tag{B.42}$$

$$\begin{pmatrix} \mathcal{J}_{11} & \mathcal{J}_{12} \\ \mathcal{J}_{21} & \mathcal{J}_{22} \end{pmatrix} \approx {\rm v}_{\rm F} \, (J_z \rho) \begin{pmatrix} 0 & 0 \\ 1 & 0 \end{pmatrix} + 2{\rm v}_{\rm F} \, (J_\perp \rho)^2 \begin{pmatrix} 0 & \frac{\cos(k_{\rm F} R)}{k_{\rm F} R} \mathcal{F}\left(\frac{RK_z}{2{\rm v}_{\rm F}}\right) \\ S & 0 \end{pmatrix} .$$

The components of the effective Kondo coupling are ordered in the following hierarchy

$$|\mathcal{J}_{21}| > |\mathcal{J}_{33}| = |\mathcal{J}_{12}| \qquad \text{if} \qquad k_{\rm F} R \gg 1 \, . \tag{B.43}$$

B.4 Scaling dimension of the leading irrelevant operator

In the strong coupling analysis of the mini-domain model (7.1) in Section 7.1 the scaling dimension of the flip operator $\mathcal{H}_{\rm flip}$ (7.4) was determined using Hopfield's rule of thumb. In this appendix the result obtained is verified with the help of the bosonization technique along the lines of the treatment of the x-ray edge singularity by K. D. Schotte and U. Schotte [74].

We would like to obtain the scaling dimension with respect to the unperturbed Hamiltonian $\mathcal{H}_0$ of (7.3). Let $|0_L, 0_R, \sigma_L, \sigma_R\rangle$ be the ground state of $\mathcal{H}_0$ where $\sigma_L, \sigma_R = \uparrow, \downarrow$ indicates the spin of the left and right impurity and $|0_j\rangle$, with $j = L, R$, represents the ground state of the conduction electrons in the left and right lead, respectively. Since we assume that the two impurities are frozen into the antiferromagnetic configurations we have $\sigma_L = -\sigma_R$. The

correlator (7.5) whose time dependence determines the sought-after scaling dimension then reads

$$\langle \mathcal{H}_{\rm flip}(t)\mathcal{H}_{\rm flip}(0)\rangle_{\mathcal{H}_0} = \sum_{\sigma=\uparrow,\downarrow} \langle 0_L, 0_R, \sigma, -\sigma | \mathcal{H}_{\rm flip}(t)\mathcal{H}_{\rm flip}(0) | 0_L, 0_R, \sigma, -\sigma\rangle$$

$$= \left(\frac{4J_\perp^2}{K_z}\right)^2 \Big[\langle 0_L, 0_R, \downarrow, \uparrow | \left[S_R^+ S_L^- c_{\downarrow R}^\dagger c_{\uparrow R} c_{\uparrow L}^\dagger c_{\downarrow L}\right]_t \left[S_L^+ S_R^- c_{\downarrow L}^\dagger c_{\uparrow L} c_{\uparrow R}^\dagger c_{\downarrow R}\right]_{t=0} |0_L, 0_R, \downarrow, \uparrow\rangle \tag{B.44}$$

$$+ \langle 0_L, 0_R, \uparrow, \downarrow | \left[S_L^+ S_R^- c_{\downarrow L}^\dagger c_{\uparrow L} c_{\uparrow R}^\dagger c_{\downarrow R}\right]_t \left[S_R^+ S_L^- c_{\downarrow R}^\dagger c_{\uparrow R} c_{\uparrow L}^\dagger c_{\downarrow L}\right]_{t=0} |0_L, 0_R, \uparrow, \downarrow\rangle \Big] \ .$$

Since the left and right sub-systems are not coupled by the Hamiltonian $\mathcal{H}_0$ the matrix elements factorize into products of matrix elements involving only degrees of freedom of a single sub-system. Moreover, we assume the left and right sub-systems to be symmetric so that we can drop the index R/L altogether yielding

$$2\left(\frac{4J_\perp^2}{K_z}\right)^2 \langle 0, \downarrow | \left[S^- c_\uparrow^\dagger c_\downarrow\right]_t \left[S^+ c_\downarrow^\dagger c_\uparrow\right]_{t=0} |0, \downarrow\rangle \langle 0, \uparrow | \left[S^+ c_\downarrow^\dagger c_\uparrow\right]_t \left[S^- c_\uparrow^\dagger c_\downarrow\right]_{t=0} |0, \uparrow\rangle \, . \tag{B.45}$$

Realizing that the remaining product consists of matrix elements that are time-reversed to each other we are finally left with

$$\langle \mathcal{H}_{\rm flip}(t)\mathcal{H}_{\rm flip}(0)\rangle_{\mathcal{H}_0} = 2\left(\frac{4J_\perp^2}{K_z}\right)^2 M(t) M^*(-t) \tag{B.46}$$

where the matrix element is given by

$$M(t) = \langle 0, \downarrow | S^-(t) c_\uparrow^\dagger(t) c_\downarrow(t) S^+(0) c_\downarrow^\dagger(0) c_\uparrow(0) | 0, \downarrow\rangle \, . \tag{B.47}$$

The time-dependence of the operators stems from using the interaction representation,

$$\mathcal{O}(t) = e^{i\mathcal{H}_0^{(1)} t} \mathcal{O} e^{-i\mathcal{H}_0^{(1)} t} \, , \tag{B.48}$$

and the Hamiltonian $\mathcal{H}_0^{(1)}$ describes a single sub-system only, $\mathcal{H}_0^{(1)} = H_0[\phi] + \frac{J_z}{\sqrt{2}\pi} S^z \partial_x \phi(0)$. The correlator (B.47) is easily evaluated within bosonization, compare section 7.2. Applying the bosonization identity (7.9) it becomes

$$M(t) = \frac{1}{(2\pi a)^2} \langle 0, \downarrow | e^{i\mathcal{H}_0^{(1)} t} S^- F_\uparrow^\dagger e^{i\phi_\uparrow(0)} F_\downarrow e^{-i\phi_\downarrow(0)} e^{-i\mathcal{H}_0^{(1)} t} S^+ F_\downarrow^\dagger e^{i\phi_\downarrow(0)} F_\uparrow e^{-i\phi_\uparrow(0)} | 0, \downarrow\rangle \tag{B.49}$$

The Klein factors cancel each other, $F_\sigma^\dagger F_\sigma = 1$, and can be omitted. (Their time dependence can be neglected in the limit of large system size.) The essential step will be the application of a general Emery–Kivelson transformation (7.13) with $\gamma = \sqrt{2} J_z \rho$, where $\rho = 1/(2\pi v_{\rm F})$, which transforms the bosonized Hamiltonian into a diagonal form,

$$U_\gamma \mathcal{H}_0^{(1)} U_\gamma^\dagger = \sum_{\sigma=\uparrow,\downarrow} H_0[\phi_\sigma] \tag{B.50}$$

where $H_0[\phi_\sigma]$ is given by (7.12). Introducing the transformed vacuum $U_\gamma |0\rangle = |\hat{0}\rangle$ and the spin field $\phi_s = \frac{1}{\sqrt{2}} (\phi_\uparrow - \phi_\downarrow)$ the correlator reduces to

$$M(t) = \frac{1}{(2\pi a)^2} \langle \hat{0} | e^{i\sqrt{2}(1 - J_z\rho)\phi_s(t)} e^{-i\sqrt{2}(1 - J_z\rho)\phi_s(0)} | \hat{0}\rangle \, . \tag{B.51}$$

The actual attractiveness of the bosonization approach is that the remaining correlator of bosonic fields can be evaluated [76],

$$M(t) = \frac{1}{(2\pi a)^2} \left(1 + it/a\right)^{-2(1-J_z\rho)^2} . \tag{B.52}$$

Correspondingly, the correlator behaves in the long-time limit as

$$\langle \mathcal{H}_{\rm flip}(t)\mathcal{H}_{\rm flip}(0)\rangle_{\mathcal{H}_0} \sim 2\left(\frac{4J_\perp^2}{K_z}\right)^2 \frac{1}{(2\pi a)^4} \left(it/a\right)^{-4(1-J_z\rho)^2} , \tag{B.53}$$

implying a scaling dimension of the flip operator in agreement with the result of Section 7.1

$$\dim\left[\mathcal{H}_{\rm flip}\right] = 2\left(1 - J_z\rho\right)^2 = 2\left(1 - \frac{2\delta_{J_z}}{\pi}\right)^2 . \tag{B.54}$$

In the last step we made use of the relationship between the coupling constant J_z and the phase shift in the bosonization cutoff scheme, compare (7.18).

B.5 Spin–Boson model representation

In the mapping of the mini-domain model (7.1) onto the generalized Anderson model (7.15) in Section 7.2 we made use of the Emery–Kivelson transformation (7.13) with the value $\gamma = \sqrt{2} - 1$. In this appendix we are going to show that for another value the mini-domain model can be put into the form of two coupled spin–boson models [86]. For the particular value $\gamma = \sqrt{2}$ the bosonic fields decouple from the spin flip operator in expression (7.14). Introducing the Fourier components for the derivative of the bosonic spin fields,

$$\partial_x \phi_{sj}(x) = \sum_{k>0} \sqrt{\frac{2\pi k}{L}} \left(b_{kj} e^{-ikx} + b_{kj}^\dagger e^{ikx}\right) e^{-ak/2} , \tag{B.55}$$

the kinetic Hamiltonian (7.12) can be rewritten as

$$H_0[\phi_{sj}] = \mathrm{v_F} \int \frac{dx}{2\pi} \frac{1}{2} : \left(\partial_x \phi_{sj}(x)\right)^2 := \sum_{k>0} \omega_k \; b_{kj}^\dagger b_{kj} \equiv H_0[b_{kj}] , \tag{B.56}$$

with $\omega_k = \mathrm{v_F} k$. Each single-impurity Kondo model reduces to a so-called spin–boson model and the mini-domain model then takes the form

$$H_{\rm CSB} = K_z S_L^z S_R^z + \sum_{j=L,R} \left(H_0[b_{kj}] + \Delta \; S_j^x + \sum_{k>0} \lambda_k \; S_j^z \left(b_{kj}^\dagger + b_{kj}\right)\right) , \tag{B.57}$$

where the parameters are given in terms of the Kondo couplings by

$$\Delta = \frac{J_\perp}{\pi a} \qquad \text{and} \qquad \lambda_k = \sqrt{\frac{2\pi k}{L}} \left(\frac{J_z}{\sqrt{2}\pi} - \sqrt{2}\mathrm{v_F}\right) e^{-ak/2} . \tag{B.58}$$

The properties of the spin–boson model are completely parametrized by the spectral function

$$J(\omega) \equiv \sum_{k>0} \lambda_k^2 \, \delta(\omega - \omega_k) = 2\alpha \, \omega \, e^{-\omega/\omega_c} . \tag{B.59}$$

The last equality defines the Ohmic form of the spectral function characterized by the strength α, and ω_c is a cutoff. From the mapping it follows that $\alpha = (J_z\rho - 1)^2$ with $\rho = 1/(2\pi \mathrm{v_F})$ and $\omega_c = \mathrm{v_F}/a$.

B.6 Anderson–Yuval–Hamann RG

In this section we rederive in the bosonoziation approach the scaling equations of the Kondo model found by P.W. Anderson, G. Yuval and D.R. Hamann (AYH) [78]. We find that in the language of bosonization the AYH RG can be reinterpreted as a sequence of infinitesimal unitary transformations. We will perform the RG on a Hamiltonian level by considering the imaginary time $\mathcal{S}$-matrix instead of its average, the partition function, as was done by AYH. We start from the bosonized version of the Kondo Hamiltonian (compare Section 7.2):

$$H_K \;=\; H_0[\phi] + \frac{J_z}{\sqrt{2}\pi} S_z \partial_x \phi(0) + \frac{J_\perp}{2\pi a}\left(S^+ F e^{-i\sqrt{2}\phi(0)} + \text{h.c.}\right) . \tag{B.60}$$

The J_z term can be absorbed into the scaling dimension of the vertex operator appearing in the spin-flip term by applying the "boundary condition changing operator" [74, 77]

$$U_\gamma \equiv e^{i\gamma S_z \phi(0)} , \tag{B.61}$$

with $\gamma = \sqrt{2} J_z \rho$ and the density of states $\rho = 1/(2\pi \mathrm{v_F})$. The transformed Hamiltonian becomes $U_\gamma H_K U_\gamma^\dagger = H_0 + H_{\text{int}}$ with the interaction Hamiltonian

$$H_{\text{int}} = \frac{J_\perp}{2\pi a}\left(S^+ F e^{-i\lambda\phi(0)} + \text{h.c.}\right) \qquad \text{where} \quad \lambda = \sqrt{2}\,(1 - J_z\rho) . \tag{B.62}$$

The imaginary time $\mathcal{S}$-matrix is

$$\mathcal{S} = \mathcal{T}\exp\left[-\int_0^\beta d\tau H_{\text{int}}(\tau)\right] = \sum_{n=0}^{\infty} (-1)^n \int_0^\beta d\tau_n \int_0^{\tau_n} d\tau_{n-1} \ldots \int_0^{\tau_2} d\tau_1 H_{\text{int}}(\tau_n)\ldots H_{\text{int}}(\tau_1) . \tag{B.63}$$

In an RG-step we are going to integrate out short time scales and absorb the generated terms into a renormalization of the coupling constants. Formally this is achieved by separating from each time integral an on-shell part

$$\int_0^{\tau_{m+1}} d\tau_m = \int_0^{\tau_{m+1}-d\tau} d\tau_m + \int_{\tau_{m+1}-d\tau}^{\tau_{m+1}} d\tau_m , \tag{B.64}$$

where $d\tau > 0$ is infinitesimally small. First let us consider the effect of the on-shell part of the m^{th} integral only. We get

$$\begin{aligned}
&\ldots \int_0^{\tau_{m+3}} d\tau_{m+2} \int_0^{\tau_{m+2}} d\tau_{m+1} \int_{\tau_{m+1}-d\tau}^{\tau_{m+1}} d\tau_m \int_0^{\tau_m} d\tau_{m-1} H_{\text{int}}(\tau_{m+2}) H_{\text{int}}(\tau_{m+1}) H_{\text{int}}(\tau_m) H_{\text{int}}(\tau_{m-1}) \ldots \\
&\qquad = \ldots \int_0^{\tau_{m+3}} d\tau_{m+2} \int_0^{\tau_{m+1}} d\tau_{m-1} H_{\text{int}}(\tau_{m+2}) \\
&\qquad \times \left(\int_{\tau_{m-1}}^{\tau_{m+2}} d\tau_{m+1} \int_{\tau_{m+1}-d\tau}^{\tau_{m+1}} d\tau_m H_{\text{int}}(\tau_{m+1}) H_{\text{int}}(\tau_m) \right) H_{\text{int}}(\tau_{m-1}) \cdots + \mathcal{O}(d\tau^2) .
\end{aligned}$$

On the right-hand side of the equation we replaced the upper limit τ_m of the $(m-1)^{\text{th}}$ time integral by τ_{m+1} inducing an error of order $d\tau^2$. However, this enables us to absorb the m^{th} and $(m+1)^{\text{th}}$ spin flips into a renormalized interaction between adjacent flips. These are the "close pairs" of AYH which effectively "will change the mean magnetization slightly". Doing this for all time integrals the $\mathcal{S}$-matrix can be put into the form

$$\mathcal{S} = \sum_{n=0}^{\infty} (-1)^n \int_0^{\beta-d\tau} d\tau_n \int_0^{\tau_n-d\tau} d\tau_{n-1} \ldots \int_0^{\tau_2-d\tau} d\tau_1 V(\beta,\tau_n) H_{\text{int}}(\tau_n) V(\tau_n,\tau_{n-1}) \tag{B.65}$$
$$H_{\text{int}}(\tau_{n-1}) V(\tau_{n-1},\tau_{n-2}) \ldots H_{\text{int}}(\tau_2) V(\tau_2,\tau_1) H_{\text{int}}(\tau_1) V(\tau_1,0)\,,$$

where

$$V(\tau_{m+1},\tau_m) = 1 + \int_{\tau_m}^{\tau_{m+1}} d\tau' \int_{\tau'-d\tau}^{\tau'} d\tau'' H_{\text{int}}(\tau') H_{\text{int}}(\tau'') + \mathcal{O}(d\tau^2)\,. \tag{B.66}$$

In the following we are going to simplify the expression for V further. Since the time arguments τ' and τ'' are separated at most by the small time $d\tau$ we can apply an operator product expansion [76] to the integrand. Always neglecting contributions of order $d\tau^2$ we get (in the limit of zero temperature)

$$\begin{aligned} V(\tau_{m+1},\tau_m) &\approx 1 + \left(\frac{J_\perp}{2\pi a}\right)^2 \int_{\tau_m}^{\tau_{m+1}} d\tau' \int_{\tau'-d\tau}^{\tau'} d\tau'' \left(S^+ F e^{-i\lambda\phi(\tau')} + \text{h.c.}\right) \left(S^+ F e^{-i\lambda\phi(\tau'')} + \text{h.c.}\right) \\ &= 1 + \left(\frac{J_\perp}{2\pi a}\right)^2 \int_{\tau_m}^{\tau_{m+1}} d\tau' \int_{\tau'-d\tau}^{\tau'} d\tau'' e^{-i2S_z\lambda\phi(\tau')} e^{i2S_z\lambda\phi(\tau'')} \\ &\approx 1 + d\tau \left(\frac{J_\perp}{2\pi a}\right)^2 \int_{\tau_m}^{\tau_{m+1}} d\tau' \left(1 - i2S_z\lambda a \partial_{\tau'}\phi(\tau')\right)\,. \end{aligned} \tag{B.67}$$

This is the right moment to pause for a bit and to spend some words on the cutoff procedure we have chosen. We have applied a sharp cutoff scheme and separated a fixed time slice $d\tau$ as the on-shell part of the time integral. We could equally well have chosen a multiplicative renormalization of the upper limits of all time integrals in the $\mathcal{S}$-matrix, $\tau_m \to \tau_m e^{dl}$, with an infinitesimal dl. This however would have led us to a time slice $d\tau = \tau' - \tau' e^{-dl} \approx \tau' dl$ dependent on τ' in the integrand of the expression for V. The renormalization of the interaction between spin flips V and all resulting scaling equations therefore depend on the precise form of the cutoff scheme (cf. also the appendix of AYH). In particular, the remaining integral in expression (B.67) can be most easily performed with the additive on-shell separation chosen here,

$$\begin{aligned} V(\tau_{m+1},\tau_m) &\approx 1 + \left(\frac{J_\perp}{2\pi a}\right)^2 d\tau \left(\tau_{m+1} - \tau_m - i2S_z\lambda a \left(\phi(\tau_{m+1}) - \phi(\tau_m)\right)\right) \\ &\approx \exp\left[\left(\frac{J_\perp}{2\pi a}\right)^2 d\tau \left(\tau_{m+1} - \tau_m - i2S_z\lambda a \left(\phi(\tau_{m+1}) - \phi(\tau_m)\right)\right)\right] \\ &\approx \exp\left[\left(\frac{J_\perp}{2\pi a}\right)^2 d\tau \left(\tau_{m+1} - \tau_m\right)\right] U_{d\lambda}(\tau_{m+1}) U_{d\lambda}^\dagger(\tau_m) \end{aligned} \tag{B.68}$$

where U is the "boundary condition changing operator" (B.61) in the interaction representation with $d\lambda = -d\tau (J_\perp/(2\pi a))^2\, 2\lambda a$. Putting this result into the expression for the $\mathcal{S}$-matrix we get

$$\begin{aligned} \mathcal{S} &= \exp\left[\left(\frac{J_\perp}{2\pi a}\right)^2 \beta d\tau\right] \\ &\quad \times U_{d\lambda} \sum_{n=0}^{\infty} (-1)^n \int_0^{\beta - d\tau} d\tau_n \int_0^{\tau_n - d\tau} d\tau_{n-1} \ldots \int_0^{\tau_2 - d\tau} d\tau_1 H'_{\rm int}(\tau_n) \ldots H'_{\rm int}(\tau_1)\, U^\dagger_{d\lambda}\,, \end{aligned} \tag{B.69}$$

where we have used $U^\dagger_{d\lambda}(0) = U^\dagger_{d\lambda}(\beta) = U^\dagger_{d\lambda}$ since for bosons $\phi(\beta) = \phi(0)$. This expression for the $\mathcal{S}$-matrix should be compared to equation (15) of AYH [78]. The renormalized interaction Hamiltonian is given by an infinitesimal unitary transformation of the bare interaction Hamiltonian,

$$H'_{\rm int} = U^\dagger_{d\lambda} H_{\rm int} U_{d\lambda} = \frac{J_\perp}{2\pi a}\left(S^+ F e^{-i\lambda'\phi(0)} + \text{h.c.}\right) \qquad \text{where} \quad \lambda' = \lambda + d\lambda\,. \tag{B.70}$$

The displacement of the upper limits of all time integrals by the slice $d\tau$ leads effectively to a renormalization of the short distance cutoff $a \to a' = a + \mathrm{v_F} d\tau$. Hence, before identifying the renormalized coupling constants, we have to take into account the implicit cutoff dependence of the bosonic field in the vertex operator of the interaction Hamiltonian. This is easily done if we normal order it since in this form the cutoff dependence becomes explicit,

$$e^{-i\lambda'\phi(0)} = \left(\frac{2\pi a}{L}\right)^{\lambda'^2/2} :\! e^{-i\lambda'\phi(0)} \!: \,. \tag{B.71}$$

Now we have arrived at the final stage of this derivation. Comparing the parameters of the renormalized interaction Hamiltonian $H'_{\rm int}$ with the original version $H_{\rm int}$ we can read off the renormalizations of the coupling constants,

$$\begin{aligned} a &\longrightarrow a' = a + \mathrm{v_F} d\tau \\ H_{\rm int} &\longrightarrow H'_{\rm int} \\ J_\perp a^{-1+\lambda^2/2} &\longrightarrow J'_\perp a'^{-1+\lambda'^2/2} = J_\perp a^{-1+\lambda'^2/2} \\ \lambda &\longrightarrow \lambda' = \lambda + d\lambda\,. \end{aligned}$$

In its differential form the AYH scaling equations for the Kondo model therefore reads

$$\frac{d\log\lambda}{d\log a} = -2\,(J_\perp\rho)^2 \tag{B.72}$$

$$\frac{d\log J_\perp\rho}{d\log a} = 1 - \frac{\lambda^2}{2} \tag{B.73}$$

with $\lambda = \sqrt{2}(1 - J_z\rho)$. In the limit of small J_z the AYH scaling equations reduce to the famous poor man's scaling equations of the Kondo model

$$\begin{aligned} \frac{d(J_z\rho)}{d\log a} &= 2\,(J_\perp\rho)^2 \\ \frac{d(J_\perp\rho)}{d\log a} &= 2(J_z\nu)(J_\perp\rho)\,. \end{aligned} \tag{B.74}$$

Acknowledgements

First of all I would like to thank Prof. P. Wölfle for giving me the opportunity to do my PhD at the Insitut für Theorie der Kondensierten Materie.

I am deeply indebted to my supervisor and teacher Dr. A. Rosch. The time and patience he spent on me have been unlimited, and the care I received was such as a PhD student can only wish for. I was even in the fortunate position of sharing an office with him for most of the time I was working on my PhD. This not only allowed me to witness and profit directly from the immense intuition with which he approaches physical problems, but also left me infected with his contagious enthusiasm for physics.

I also would like to thank Prof. M. Vojta for the many discussions and his knowledgeable advice. In particular, I enjoyed the collaboration with him on the subject of Chapter 7 which stimulated many interesting ideas. He also deserves my thanks for accepting the Korreferat.

I thank Dr. P. Howell. It was a pleasure to share numerous hours together and I am especially grateful for his helpful advice and criticism. This thesis also profited enormously from his careful proof-reading.

Finally, I thank all members of the Institut für Theorie der Kondensierten Materie for the scientifically inspiring and friendly atmosphere. In particular, discussions with T. Costi, F. Evers, I. Fischer, L. Fritz, K. Haule, S. Kirchner and G. Sellier are gratefully acknowledged.

Bibliography

[1] M. Vojta, cond-mat/0309604.

[2] S. Sachdev, *Quantum Phase Transitions* (Cambridge University Press, Cambridge, 1999).

[3] L. Zhu, M. Garst, A. Rosch, and Q. Si, Phys. Rev. Lett. **91**, 066404 (2003).

[4] J. A. Hertz, Phys. Rev. B **14**, 1165 (1976).

[5] A. J. Millis, Phys. Rev. B **48**, 7183 (1993).

[6] U. Zülicke and A. J. Millis, Phys. Rev. B **51**, 8996 (1995).

[7] A. Rosch, A. Schröder, O. Stockert, and H. von Löhneysen, Phys. Rev. Lett. **79**, 159 (1997).

[8] O. Stockert *et al.*, Phys. Rev. Lett. **80**, 5627 (1998).

[9] N. Andrei, G. T. Zimanyi, and G. Schön, Phys. Rev. B **60**, R5125 (1999).

[10] S. Kehrein and M. Vojta, cond-mat/0208390.

[11] M. Garst *et al.*, cond-mat/0310222.

[12] D. L. Cox and A. Zawadowski, Adv. Phys. **47**, 599 (1998).

[13] D. R. Nelson and J. M. Kosterlitz, Phys. Rev. Lett. **39**, 1201 (1977).

[14] N. D. Mermin and H. Wagner, Phys. Rev. Lett. **17**, 1133 (1966).

[15] E. Grüneisen, Ann. Phys. (Leipzig) **39**, 257 (1912).

[16] L. D. Landau and E. M. Lifshitz, *Statistical Physics* (Butterworth–Heinemann, Oxford, 1997).

[17] S.-K. Ma, *Modern Theory of Critical Phenomena* (W. A. Benjamin, Inc., Massachusetts, 1976).

[18] N. Goldenfeld, *Lectures on phase transitions and the renormalization group* (Addison–Wesley, Boston, 1992).

[19] D. Belitz, T. R. Kirkpatrick, M. T. Mercaldo, and S. L. Sessions, Phys. Rev. B **63**, 174427 (2001).

[20] Q. Si, S. Rabello, K. Ingersent, and L. Smith, Nature **413**, 804 (2001).

[21] J.-X. Zhu, D. R. Grempel, and Q. Si, Phys. Rev. Lett. **91**, 156404 (2003).

[22] R. Küchler *et al.*, Phys. Rev. Lett. **91**, 066405 (2003).

[23] R. Küchler, private communication.

[24] O. Trovarelli *et al.*, Phys. Rev. Lett. **85**, 626 (2000).

[25] D. V. Schroeder and M. E. Peskin, *An Introduction to Quantum Field Theory* (Addison–Wesley, Cambridge, 1999).

[26] G. D. Mahan, *Many-Particle Physics* (Plenum Press, New York, 1990).

[27] J. Wilson, K. G.and Kogut, Phys. Rep. C **12**, 75 (1974).

[28] D. Belitz, T. R. Kirkpatrick, and T. Vojta, Phys. Rev. B **55**, 9452 (1997).

[29] D. Belitz, T. R. Kirkpatrick, A. J. Millis, and T. Vojta, Phys. Rev. B **58**, 14155 (1998).

[30] G. Y. Chitov and A. J. Millis, Phys. Rev. Lett. **86**, 5337 (2001).

[31] A. J. Millis, A. J. Schofield, G. G. Lonzarich, and S. A. Grigera, Phys. Rev. Lett. **88**, 217204 (2002).

[32] D. Belitz, T. R. Kirkpatrick, and T. Vojta, Phys. Rev. B **65**, 165112 (2002).

[33] S. Sachdev, Phys. Rev. B **55**, 142 (1997).

[34] D. R. Nelson, Phys. Rev. B **11**, 3504 (1975).

[35] K. Wilson and M. Fisher, Phys. Rev. Lett. **28**, 240 (1972).

[36] J. Zinn-Justin, *Quantum Field Theory and Critical Phenomena* (Oxford University Press, Oxford, 2002).

[37] H. von Löhneysen, J. Phys. Cond. Matt. **8**, 9689 (1996).

[38] A. Schröder *et al.*, Phys. Rev. Lett. **80**, 5623 (1998).

[39] D. Finsterbusch *et al.*, Physica B **223**, 329 (1996).

[40] B. Lüthi, private communication.

[41] L. E. Reichl, *A modern course in statistical physics* (John Wiley & Sons, Inc., New York, 1998).

[42] T. Moriya, Phys. Rev. Lett. **24**, 1433 (1970).

[43] G. R. Stewart, Rev. Mod. Phys. **73**, 797 (2001).

[44] O. O. Bernal, D. E. MacLaughlin, H. G. Lukefaahr, and B. Andraka, Phys. Rev. Lett. **75**, 2023 (1995).

[45] E. Miranda, V. Dobrosavljević, and G. Kotliar, Phys. Rev. Lett. **79**, 290 (1997).

[46] S. Doniach, Physica B **91**, 231 (1977).

[47] A. H. Castro Neto, G. Castilla, and B. A. Jones, Phys. Rev. Lett. **81**, 3531 (1998).

[48] A. H. Castro Neto and B. A. Jones, Phys. Rev. B **62**, 14975 (2000).

[49] A. H. Castro Neto and B. A. Jones, cond-mat/0106176.

[50] A. J. Millis, D. K. Morr, and J. Schmalian, Phys. Rev. Lett. **87**, 167202 (2001).

[51] A. J. Millis, D. K. Morr, and J. Schmalian, Phys. Rev. B **66**, 174433 (2002).

[52] N. Shah and A. J. Millis, Phys. Rev. Lett. **91**, 147204 (2003).

[53] C. Jayaprakash, H. R. Krishna-murthy, and J. W. Wilkins, Phys. Rev. Lett. **37**, 737 (1981).

[54] B. A. Jones and C. M. Varma, Phys. Rev. Lett. **58**, 843 (1987).

[55] J. B. Silve *et al.*, Phys. Rev. Lett. **76**, 275 (1996).

[56] R. M. Fye, J. E. Hirsch, and D. J. Scalapino, Phys. Rev. B **35**, 4901 (1987).

[57] A. J. Millis, B. G. Kotliar, and B. A. Jones, in *Field Theories in Condensed Matter Physics*, edited by Z. Tesanovic (Addison–Wesley, Redwood City, CA, 1990), pp. 159–166.

[58] B. A. Jones, C. M. Varma, and J. W. Wilkins, Phys. Rev. Lett. **61**, 125 (1988).

[59] I. Affleck, A. W. W. Ludwig, and B. A. Jones, Phys. Rev. B **52**, 9528 (1995).

[60] J. Gan, Phys. Rev. Lett. **74**, 2583 (1995).

[61] J. Gan, Phys. Rev. Lett. **74**, 5287 (1995).

[62] J. Gan, Phys. Rev. B **51**, 8287 (1995).

[63] V. J. Emery and S. Kivelson, Phys. Rev. B **46**, 10812 (1992).

[64] P. D. Sacramento and P. Schlottmann, Phys. Rev. B **43**, 13294 (1991).

[65] M. A. Ruderman and C. Kittel, Phys. Rev. **96**, 99 (1954).

[66] A. C. Hewson, *The Kondo Problem to Heavy Fermions* (Cambridge University Press, Cambridge, 1997).

[67] J. von Delft, private communication.

[68] G. Zaránd and J. von Delft, Phys. Rev. B **61**, 6918 (2000), cond-mat/9812182.

[69] P. W. Anderson, J. Phys. C **3**, 2436 (1970).

[70] J. M. Kosterlitz and D. J. Thouless, J. Phys. C **6**, 1181 (1973).

[71] P. W. Anderson, Phys. Rev. Lett. **18**, 1049 (1967).

[72] P. W. Anderson, Phys. Rev. **164**, 352 (1967).

[73] J. J. Hopfield, Comments Solid State Phys. **2**, 40 (1969).

[74] K. D. Schotte and U. Schotte, Phys. Rev. **182**, 479 (1969).

[75] A. O. Gogolin, A. A. Nersesyan, and A. M. Tsvelik, *Bosonization and Strongly Correlated Systems* (Cambridge University Press, Cambridge, 1998).

[76] J. von Delft and H. Schöller, Ann. Physik (Leipzig) **7**, 225 (1998).

[77] I. Affleck and A. W. W. Ludwig, J. Phys. A **27**, 5375 (1994).

[78] P. W. Anderson, G. Yuval, and D. R. Hamann, Phys. Rev. B **1**, 4464 (1970).

[79] D. R. Nelson, *Defects and Geometry in Condensed Matter Physics* (Cambridge University Press, Cambridge, 2002).

[80] D. J. Bishop and J. D. Reppy, Phys. Rev. Lett. **40**, 1727 (1978).

[81] L. I. Glazman and M. Pustilnik, in *Proceedings "New Directions in Mesoscopic Physics"* (NATO-ASI, Erice, 2002), cond-mat/0302159.

[82] K. J. Thomas *et al.*, Phys. Rev. Lett. **77**, 135 (1996).

[83] K. A. Matveev, Sov. Phys. JETP **72**, 892 (1991).

[84] K. A. Matveev, Phys. Rev. B **51**, 1743 (1995).

[85] C. M. Bender and S. A. Orszag, *Advanced Mathematical Methods for Scientists and Engineers* (McGraw-Hill, New York, 1978).

[86] U. Weiss, *Quantum Dissipative Systems* (World Scientific, Singapore, 1999).